# $GABA_A$ plasticity during persistent inflammation in male and female rats

by

Karen Jill Tonsfeldt

A DISSERTATION

Presented to the Neuroscience Graduate Program and the Oregon Health & Science University in partial fulfillment of the degree requirements for the degree of Doctor of Philosophy

August 2014

# Contents

# List of Figures

# List of Tables

# List of Abbreviations

| | |
|---|---|
| aCSF | Artificial cerebrospinal fluid |
| AMPA | α-Amino-3-hydroxy-5-methyl-4-isoxazolepropionic acid |
| ANOVA | Analysis of variance |
| BIC | Bicuculline |
| CFA | Complete Freund's adjuvant |
| CI | Confidence interval |
| CNS | Central nervous system |
| dlPAG | Dorsolateral periaqueductal gray |
| DMSO | Dimethyl sulfoxide |
| DNQX | 6,7-dinitroquinoxaline-2,3-dione |
| DOPr | Delta opioid receptor |
| dPAG | Dorsal periaqueductal gray |
| DS2 | 4-Chloro-N-[2-(2-thienyl)imidazo[1,2-a]pyridin-3-yl]benzamide |
| EAA | Excitatory amino acids |
| ED50 | Half-maximal dose |
| eIPSC | Evoked inhibitory postsynaptic current |
| ER | Estrogen receptor |

| | |
|---|---|
| FM | Fibromyalgia |
| GABA | Gamma-aminobutyric acid |
| GBZ | Gabazine (SR-95531) |
| GIRK | G protein-coupled inwardly-rectifying potassium channels |
| HC | Healthy control |
| HP | Hindpaw |
| IPSC | Inhibitory postsynaptic current |
| KOPr | Kappa opioid receptor |
| MIA | Sodium iodoacetate |
| mRNA | Messenger RNA |
| NMDA | N-methyl-D-aspartate |
| OA | Osteoarthritis |
| PAG | Periaqueductal gray |
| PIC | Picrotoxin |
| PND | Postnatal day |
| PNS | Peripheral nervous system |
| qRT-PCR | Quantitative reverse-transcription polymerase chain reaction |
| RVM | Rostral ventromedial medulla |
| SEM | Standard error of the mean |
| THIP | 4,5,6,7-Tetrahydroisoxazolo[5,4-c]pyridin-3-ol hydrochloride |
| TPMPA | (1,2,5,6-Tetrahydropyridin-4-yl)methylphosphinic acid |
| vlPAG | Ventrolateral periaqueductal gray |

# Acknowledgements

First and foremost, I would like to thank my advisor, Susan Ingram. You are an incredible role model. Thank you for sitting at the rig and joking with me. Thank you for giving me autonomy and trusting my ability. Thank you for letting me contribute my interest in female physiology and molecular biology to the lab and this thesis, to make it something truly mine.

I also thank my lab mates, Katie Suchland and Minghua Li, for being so wonderful. I will miss you.

Thank you to my committee: Chuck Allen, Julie Saugstad, John Williams, and Beth Habecker. I appreciate the time you have invested in to helping me become a better scientist. Chuck, I especially appreciate your friendship and advice, and will remember our shared SfN fame fondly. I would also like to thank Mary Heinricher, for helping me navigate graduate school.

I would like to thank Oline Rønnekleiv and Martin Kelly for their mentorship. Thanks to them both for teaching me how to conduct neuroendocrine research, and how to integrate molecular and electrophysiological data. The technical tools I gained will serve me for years to come. I must also thank Martha Bosch, for giving me a shoulder to cry on over failed experiments or failed quilting projects.

Graduate school has been a rich source of wonderful friends. Thank you to Barb and Phil Silver and ARCS for their support. I have truly enjoyed forging a relationship with the you, and I am grateful for the perspective you give me on my research. Thank you to Carolina Borges Merjane for the best memories, on and off campus. And thank you for teaching me what a graduate school experience should be. Many thanks as well to Meredith Hartley, for making post-docing seem less terrifying. And, thank you to Ehow Chen and Obi, for never missing an opportunity to play board games.

I would like to extend a special thank my parents, Ward and Jean, and my brother, Eric, for their support. Dad, thank you for teaching me to look for zen in all things, be it fly fishing, pillow fighting, or electrophysiology. Mom, thank you for always making me feel like there wasn't anything I couldn't do. Awa, thank you for being the catalyst that launched me into scientific research. If only every day was as fun as our time together in the Van Winkle lab.

Finally, thank you a million times over to Daniel Cleary. You are such an excellent partner in all things, and this adventure would have been a lot harder without you.

In loving memory of Marjorie Danielson

# Abstract

At its core, the brain is an integrator of sensory information. It undergoes dynamic changes depending on stimuli and environment, both of which directly affect sensory perception. In nociception, these changes manifest as descending inhibition or facilitation of pain. While either mode of modulation can be beneficial to an organism, pathological modulation can also occur. As a result, chronic pain can arise from a loss of descending inhibition, or a gain of descending facilitation of pain. By understanding the mechanisms that underlie chronic pain, we can begin to identify specific proteins that can be targeted for the development of novel therapeutics for chronic pain disorders. Equally important is to focus the studies on both male and female populations. To date, most studies use male subjects exclusively even in light of overwhelming data that chronic pain conditions manifest predominately in females.

$GABA_A$ signaling in the ventrolateral periaqueductal gray (vlPAG) is critical to the descending pain modulatory circuit. In the vlPAG, GABA provides tonic inhibition that when relieved, as in the case of endogenous opioid release or exogenous administration of morphine, activates the output neurons from the vlPAG to the rostral ventromedial medulla (RVM) in the descending pain modulatory pathway to inhibit pain responses in the spinal cord. GABA activates both phasic signaling through synaptic $GABA_A$ receptors and tonic

signaling through extrasynaptic receptors. Extrasynaptic $GABA_A$ receptors have been identified in the vlPAG, but their role in chronic pain states has not been explored. The studies described show that the extrasynaptic $GABA_A$ receptor increases during chronic pain in females, and not males. Additional studies demonstrate differential regulation of genes between males and females during chronic inflammatory pain. These data identify GABAergic signaling in the vlPAG as sexually dimorphic, and these proteins may be a critical substrate for sex-based differences in nociception and chronic pain.

Central nervous system plasticity is suspected in chronic pain patients that do not have an obvious prior history of injury, but this has not been unequivocally demonstrated. A study herein presents the case that light may be used as a novel diagnostic test for measuring sensitization of central circuits in humans. Light produces pain in chronic pain patients that is not present in healthy controls. This is an important finding because light is a stimulus that is transmitted to the central nervous system without going through spinal pathways suggesting that central circuits are sensitized in chronic pain states. Further validation of light as a diagnostic tool will help in treatment decisions on a personal basis.

These findings contribute to our understanding of the central mechanisms underlying both chronic pain in general and the differential sensitivity of females to pain stimuli. The sexual dimorphism of chronic pain in the vlPAG between males and females indicates a critical role of the vlPAG in mediating the differences between chronic pain in the sexes. Future studies will examine how circulating estrogen affects the extrasynaptic $GABA_A$, as well as the contribution of regulated genes to the development and maintenance of chronic pain in males and females.

# Chapter 1

# Introduction

> *"Pain is a part of life. Sometimes it's a big part, and sometimes it isn't, but either way, it's part of the big puzzle, the deep music, the great game. Pain does two things: It teaches you, tells you you're alive. Then it passes away and leaves you changed. It leaves you wiser, sometimes. Sometimes it leaves you stronger. Either way, pain leaves its mark, and everything important that will ever happen to you in life is going to involve it in one degree or another."* Jim Butcher, White Night

---

Chronic pain is a major societal problem. It impacts over 20% of the population globally, and over 60% of the population will suffer from chronic pain at one point in their lives (Ruiz-Lopez, 1995). The mechanisms that lead to and support chronic pain are unknown, but targets from the periphery to the central nervous system have been identified. Laboratory work has revealed that plasticity occurring at multiple levels in the CNS leads to facilitation of pain, a process called central sensitization. Further, there is a stark lack of

female models in basic research, which is slowly becoming recognized by funding agencies. Pain patients are typically middle-aged women (Berkley, 1997), which provides a strong impetus for expanding pain research to females. However, little is known about whether the mechanisms of supraspinal control of chronic pain are different between males and females. This thesis examines sexually dimorphic effects of chronic pain, and identifies potential physiological contributors. I also identify and characterize changes in GABA signaling within the ventrolateral region of the periaqueductal gray during chronic pain, which may underlie the maintenance of chronic pain.

These mechanisms identified herein, and other modes of central nervous system plasticity, are hypothesized to initiate and maintain chronic pain. However, there are no methods to measure central sensitization in a human population. I present evidence that one mechanism of central sensitization identified in laboratory studies is present in a human chronic pain population.

## 1.1 Female physiology

Ovarian sex steroid hormones - estrogen and progesterone - undergo dramatic changes over the menstrual (human, 28-31 days) or estrous cycle (rodents, 4-5 days; Figure 1.1). Estrogen and progesterone receptors are both powerful transcription factors, and variance across the cycles can cause profound differences in gene expression in multiple tissue types. While both support reproductive organ function, they also have widespread CNS effects through their cognate receptors estrogen receptor $\alpha$ and $\beta$ (ER$\alpha$, ER$\beta$) and progesterone receptor. Signaling through either estrogen or progesterone receptors is defined as classical or nonclassical in nature. Classical signaling promotes transcription changes, where

the estrogen-bound receptor binds to estrogen response elements, which regulate the genomic effects of estrogen. Non-classical actions are membrane-initiated, and can rapidly signal through a variety of second messenger cascades including protein kinase C, protein kinase A, phosphatidylinositol-3 kinase, and mitogen-activated protein kinase (Roepke et al., 2011; Marino et al., 2006; Ellmann et al., 2009). The effects of steroid hormones can be broadly classified as "organizational" or "activational" (Phoenix et al., 1959). The organizational effects generally occur during a critical period during development and are irreversible in mammals. Activational effects, on the other hand, are acute, reversible, and can occur at any time (Arnold, 2009).

Estrogen levels are high at birth and 48 hours following, and then drop to a low constant level until the onset of puberty (Konkle and McCarthy, 2011; Montano, 1995). In rats, vaginal opening marks puberty, which is also the first day of ovulation (Parker, 1976). Vaginal opening occurs around 35 days post-natal in Sprague-Dawley rats (Lewis et al., 2002; Rivest, 1991). After puberty, cycling ovarian hormones stimulate the estrous cycles, but these are not regular until over 50 days of age (Zemunik et al., 2003). Males exhibit less overt signs of pubertal progression, but show linear increases in testosterone levels between 40-50 days (Zanato et al., 1994), and are considered pubertal at the time of spermatozoa development (50 days, (Robb et al., 1978)).

The rodent estrous cycle is divided into four sections, based on hormone levels (Figure 1.1). During the first day of diestrus, progesterone and estrogen levels are low, but rise throughout the day. On the second day of diestrus, progesterone levels fall while estrogen levels continue to rise. During proestrus, estrogen levels rise rapidly, followed by dramatic increases in progesterone, derived from the newly formed corpus luteum. The rapid increase in estrogen triggers ovulation at the end of proestrus, and the animal progresses

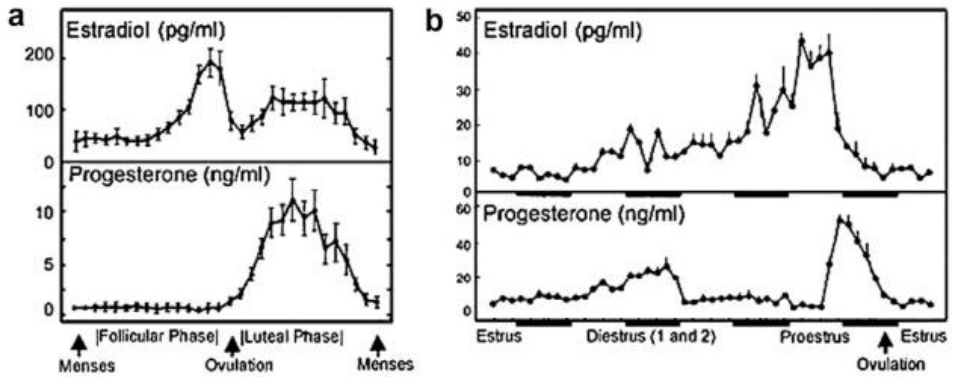


Figure 1.1: Hormone profiles throughout the menstrual or estrous cycle in humans and rodents
Levels of 17β-estradiol and progesterone through the menstrual cycle (a) and estrous cycle (b). Time in (a) is in days, and in (b) is in hours. Dark bars in (b) indicate dark period. In diestrus 2 in rats and the follicular phase in humans, there is an increase in estradiol while progesterone remains low. Ovulation is initiated by the increase in estrogen and progesterone is elevated after ovulation in both species. Because rodents do not have a luteal phase and the associated estrogen release, estrogen levels remain low after ovulation until the next cycle. In humans, estrogen is moderately elevated during this period.
Adapted from Becker et al., (2005). Strategies and methods for research on sex differences in brain and behavior. *Endocrinology* 2005;146:1650-1673.

into estrus as progesterone and estrogen fall. Staging is determined by vaginal cytology, which is obtained by vaginal gavage. The hormonal changes during the rodent estrous cycle are distinct from that of the human menstrual cycle because of the lack of a luteal (post-ovulatory) phase. Otherwise, the hormonal profiles between species are similar.

There is no broadly accepted method to account for the effects of ovarian hormones when utilizing female models. The International Association for the Study of Pain's Sex, Gender and Pain Special Interest Group has made the recent recommendation that "all pain researchers consider testing their hypotheses in both sexes, or if restricted by practical considerations, only in females" (Greenspan et al., 2007). In this publication, they advocate comparing gonadally intact adult male and females and only testing females at different

estrous or menstrual stages if there is evidence to suggest ovarian hormones may influence the results. These recommendations are supported by an in-depth statistical analysis of several pain assays from over 800 animals in one lab, which demonstrated that the amount of variability in female rats across estrous was no different than that of males (Mogil and Chanda, 2005). Thus, while ovarian hormones will affect some specific assays, it may be more important to demonstrate a rationale to study stage differences, rather than to not.

## 1.2 Pain

Pain is a supraspinal process, typically - although not always - resulting from activation of peripheral nociceptors. Pain is defined by the International Association for the Study of Pain as "an unpleasant sensory and emotional experience associated with actual or potential tissue damage, or described in terms of such damage" (Merskey and Bogduk, 1994). The emotional aspect of pain is critical to its distinction from nociception, as these emotional and cognitive states can influence the experience of pain. Furthermore, pain is not related to the degree of tissue damage, and therefore is highly subjective and difficult to quantify between individuals.

### 1.2.1 Nociception

Nociception is relayed to the brain through two classes of primary afferents. Primary afferent somas are localized to the dorsal root or the trigeminal ganglion, and send projections centrally and peripherally. The primary afferents that respond to high-intensity nociceptive stimulation are Aδ or C fibers. A range of noxious stimuli activates these afferents, which

innervate the skin, viscera, deep muscle, and joints. The Aδ afferents are thinly myelinated and conduct impulses faster than the unmyelinated C fibers. Activation of Aδ fibers produces sharp, localized pain from thermal or mechanical stimuli. Activation of C fibers produces dull, diffuse pain from polymodal pain sources (mechanical, chemical and thermal)(Basbaum and Jessell, 2013). The firing of these afferents is directly proportional to the intensity of a painful stimulus (Heinricher et al., 2009; Heinricher and Ingram, 2008). Primary afferents synapse on neurons in the dorsal horn, and this synapse is a major site of modulation of nociceptive information from supraspinal sites.

The number of ascending pathways of primary afferents reflects the supraspinal effect on pain. The information ascends primarily through the spinothalamic tract, but also the spinoreticular tract, spinomesencephalic tract, cervicothalamic tract, and spinohypothalamic tract (Basbaum and Jessell, 2013). The various targets of nociceptive information can then project back to the spine via the descending modulatory pathways. These efferents from the brain synapse directly on to dorsal horn neurons, and can thus directly facilitate or inhibit nociception.

### 1.2.2 Descending modulation

One of the supraspinal systems that can modulate pain is composed of a circuit from the periaqueductal gray (PAG) to the rostral ventromedial medulla (RVM) to the dorsal horn of the spinal cord (reviewed in Heinricher and Ingram (2008); Heinricher et al. (2009))(Figure 1.2). Importantly, the circuit is capable of producing both nociceptive inhibition and facilitation through direct action of the RVM on to the spinal cord. This concept is best illustrated by considering phenomenon that increase or decrease the perception of pain. For example, fear or stress can produce hypoalgesia, or pain inhibition. In contrast, illness or

inflammation can produce hyperalgesia, or pain facilitation. Thus, the salience of nociception can be modified depending on the situation, which requires signaling through the PAG and RVM (Fields, 2004). However, maladaptive nociceptive facilitation can lead to chronic pain, either through enhanced facilitation of pain or decreased inhibition of pain.

### 1.2.3 Chronic pain

Chronic pain is a prolonged pathological pain state, in which nociceptive signals outlast, or arise in absence of, tissue damage. Approximately one quarter of the global population – both developed and developing countries - report chronic pain (van Hecke et al., 2013; Breivik et al., 2006; Tsang et al., 2008; Goldberg and McGee, 2011; Ruiz-Lopez, 1995). Patients with chronic pain complain of allodynia and hyperalgesia. Allodynia is the phenomenon where non-painful stimuli, such as a light touch, become painful. Hyperalgesia describes the state in which noxious stimuli elicits an exaggerated pain response (Figure 1.3). Common chronic pain conditions include diabetic neuropathy, fibromyalgia, migraine headache, low back pain, arthritis, postherpetic neuralgia, multiple sclerosis, cancer pain, and neuropathic pain.

Chronic pain can arise from several sources, including hyperexcitability of primary afferents, ongoing tissue damage, and central sensitization. To illustrate, osteoarthritis (OA) is an easily definable peripheral inflammatory pain condition. It has a distinct source, arising from joint degeneration, and is characterized by deep, aching pain (Merskey and Bogduk, 1994). However, the pain experienced by OA patients does not correlate with degree of joint degradation (Phillips and Clauw, 2011). Furthermore, many of these patients experience hyperalgesia in areas distant from the affected joint (Kosek and Ordeberg, 2000b,a). The serotonin and norepinephrine reuptake inhibitors duloxetine and milnacipran, which

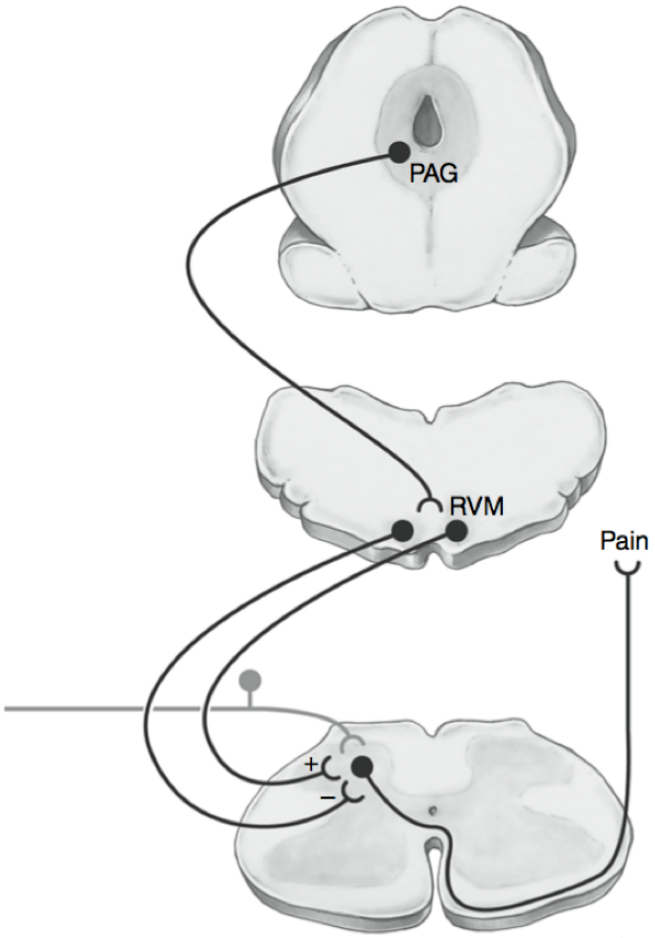


Figure 1.2: Descending modulation of pain
The functional organization of descending pain circuitry. Neurons from the ventrolateral periaqueductal gray (vlPAG) project to pain facilitory (+) or inhibitory (-) neurons in the rostral ventromedial medulla (RVM). These neurons then project to the spinal cord, where they can exert bidirectional control on the transduction of nociceptive information. Stimulation of the vlPAG predominately results in antinociception.
From Heinricher, M.M. and Ingram, S.L. (2008). The brainstem and nociceptive modulation. In *The Senses: a Comprehensive Reference* 5: 593-626.

act centrally, diminish pain in OA patients (Chappell et al., 2009; Burnham and Dickenson, 2013). These phenomena indicate central nervous system involvement in OA pain.

The CNS promotes chronic pain through pathologic pain modulation. An increase in descending facilitation, or a decrease in descending inhibition, via the descending modulatory pathway is strongly implicated in the development and maintenance of chronic pain (Vera-Portocarrero et al., 2006; Heinricher and Ingram, 2008; De Felice et al., 2011; Hahm et al., 2011). The exact mechanisms are unknown, but there is evidence that facilitation and inhibition from the RVM are separate functions (Basbaum and Fields, 1984; Fields, 2004). While the RVM exerts the direct effects on the spinal cord, the PAG influences RVM action. The PAG is best known to produce pain inhibition through analgesia (see Section 1.3.2). However, the PAG can also produce descending facilitation through a decrease in descending inhibition, which indicates a specific role of the PAG in chronic pain (Hahm et al., 2011; De Felice et al., 2011).

### 1.2.4 Central sensitization

Central sensitization causes hypersensitivity to nociception due to plasticity in the central nervous system areas that regulate pain, including the spinal cord and descending modulatory pathways. Central sensitization refers to the mechanisms that may drive increased nociception observed in chronic pain, and as such is confined to laboratory settings. In central sensitization, nociceptive neurons have increased responsiveness to afferent input (Merskey and Bogduk, 1994). These central neurons can become hypersensitive because of decreased descending inhibition or increased descending facilitation (Scholz and Woolf, 2002; Yunus, 2008; Kwon et al., 2013). In the absence of peripheral pathologies, central sensitization is believed to be the root cause of chronic pain. For example, patients with

fibromyalgia have no evidence of peripheral sensitization or tissue damage, but complain of chronic diffuse pain, hyperalgesia and allodynia (Figure 1.3). Diseases related to central sensitization, such as fibromyalgia, inflammatory bowel disease, and migraine, tend to cluster in patients, suggesting a common underlying mechanism (Yunus, 2008).

Central sensitization can only be described where increased descending facilitation can be directly examined, in animal models. In humans, there are methods to detect the outcomes of central sensitization, such as hyperalgesia and allodynia, but no way to directly investigate the function of descending pathways. Demonstrating central sensitization in humans would bridge a critical gap in animal and human research.

### 1.2.5 Animal models of pain

Pain is difficult to quantify and depends on emotional and physical status. These confounds, along with the limitations of clinical studies, necessitates animal models of pain. These animal models usually represent neuropathic (e.g., spinal nerve ligation) or inflammatory pain (e.g. osteoarthritis) and recreate the reproducible effects of chronic pain, including allodynia and hyperalgesia. This thesis is largely concerned with inflammatory pain, and will describe the two models used.

#### 1.2.5.1 Complete Freund's Adjuvant

Complete Freund's adjuvant (CFA) is inactivated and dried mycobacteria – usually *M. tuberculosis* - emulsified in mineral oil, and is used as a model of persistent inflammatory pain. Subcutaneous injection of CFA – usually into the plantar surface of the hindpaw - produces prolonged joint and thermal hyperalgesia, and mechanical allodynia (Ren and Dubner, 1993, 1999). The acute inflammatory response peaks 6-8 hours after injection, but

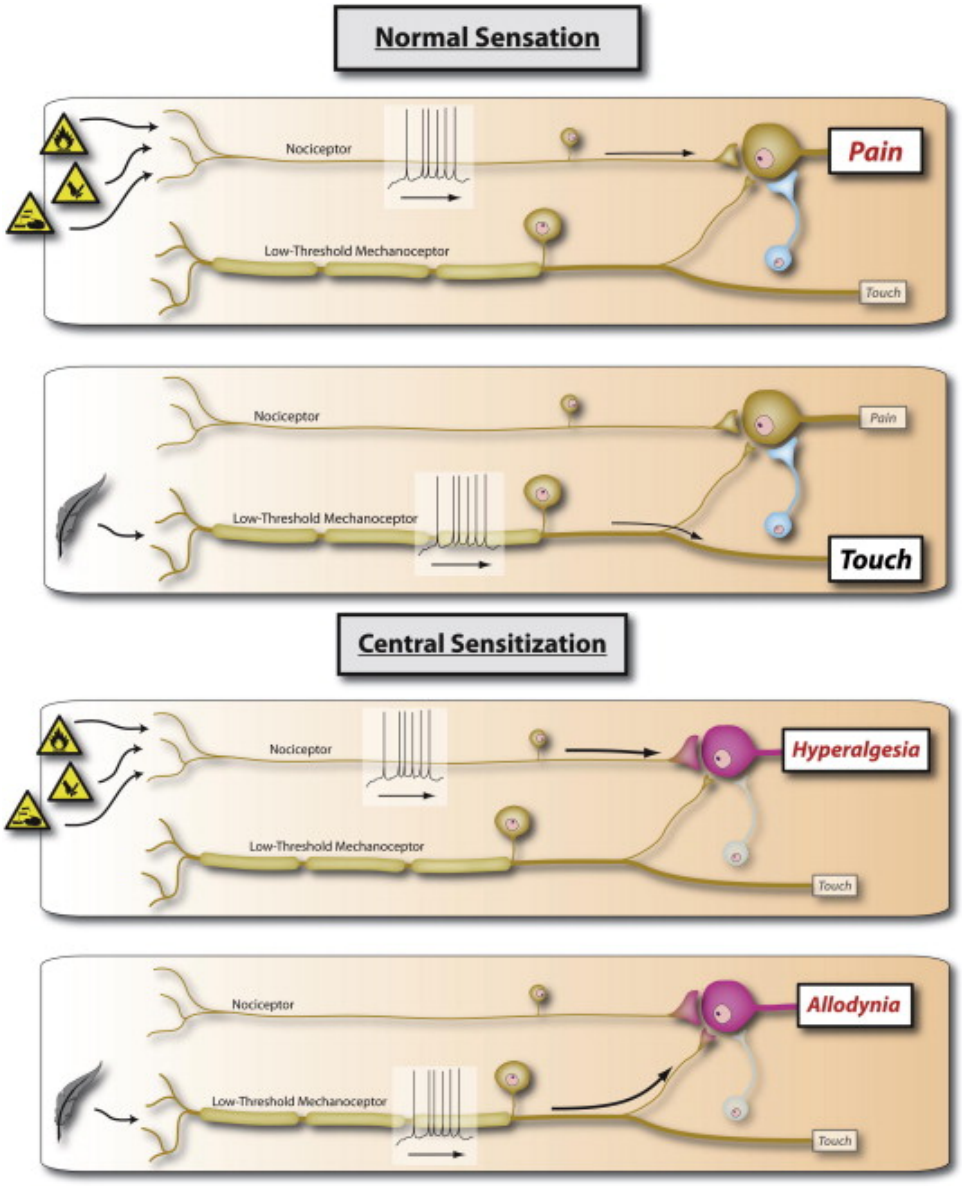


Figure 1.3: Central sensitization

In normal sensation, noxious stimuli activate nociceptors to produce pain. Non-noxious stimuli activate a different class of afferents, which lead to the sensation of touch. During central sensitization, the nociceptive signal is amplified and produces a disproportionate response, known as hyperalgesia. The previously non-noxious touch also produces pain, called allodynia. The increased sensitivity of the dorsal horn neurons can occur through a decrease in inhibitory circuits or an increase in excitatory circuits.

From Woolf, C. 2011. Central sensitization: Implications for the diagnosis and treatment of pain. *Pain* 152:3(S2-15).

hyperalgesia persists 4 or more weeks. (Ren and Dubner, 1993; Nagakura et al., 2003). During the period of inflammation, the paw swells and the affected rats show decreased rate of growth and mobility (Nagakura et al., 2003). CFA treatment is a popular model in inflammatory pain studies, and CFA has been demonstrated to alter gene expression and neuronal activity in RVM and PAG (Eidson and Murphy, 2013; Hu et al., 2009; Vera-Portocarrero et al., 2006; Gao and Ji, 2010; Hylden et al., 1989). While CFA does produce prolonged and painful inflammation in people (Gould, 2000), its utility as a model is has been questioned because it does not represent one distinct pain condition and instead generalized to persistent arthritic and tissue injury pain.

Persistent inflammation by CFA injection produces central sensitization. Following CFA treatment, there is an increase in excitability and receptive fields of nociceptive dorsal horn neurons (Wei et al., 1999; Hylden et al., 1989). There are also changes in the brain, specifically in regions associated with descending modulation. In the RVM, CFA pain increases AMPA and NMDA receptor mRNA and evoked excitatory postsynaptic current amplitude (Miki et al., 2002; Zhang and Hammond, 2009). CFA treatment increases release of aspartate and glutamate from the PAG, and increases the expression of the NMDA receptor NR2B and brain derived neurotrophic factor in male rats (Guo et al., 2006; Hu et al., 2009). The recruitment of central mechanisms in CFA pain makes it a useful model for studying the underpinnings of chronic pain, and not just inflammation. However, the majority of these studies have focused on the spinal cord and the RVM, and very few have examined changes to the PAG.

#### 1.2.5.2 Osteoarthritis

While CFA can be injected in to the knee to produce a model of osteoarthritis (OA), other models exemplify the human condition better. The sodium iodoacetate (MIA) model involves an intra-articular injection of MIA into the knee. MIA inhibits the Krebs Cycle, which kills chondrocytes in the knee following injection (Guingamp et al., 1997; Marker and Pomonis, 2012). This injection produces an acute pain phenotype for one week after injection, followed by a prolonged period of chronic pain. The rats reduce weight bearing on the affected limb, and cannot tolerate manual extension of the joint (Marker and Pomonis, 2012). OA animals develop mechanical hyperalgesia and allodynia (Combe et al., 2004; Pomonis et al., 2005), and demonstrate enhanced spinal nociceptive reflexes, indicating the presence of central involvement (Kelly et al., 2013; Lee et al., 2011). The OA model is advantageous in its similarity to the human condition, but less is known about how it affects the central nervous system.

### 1.2.6 Sex differences in nociception

In humans and rodents, females have lower nociceptive thresholds than males in all assays except in the hotplate thermal nociception test (Riley III et al., 1999; Bradshaw et al., 2000; Mogil, 2009; Mogil et al., 2000). These data indicate that pain is fundamentally and physiologically different between males and females, but the underlying mechanisms of this difference remain elusive.

The prevalence of chronic pain is greater in females than in males at all ages, including prepubertal (Berkley, 1997; Unruh, 1996; van Hecke et al., 2013; Tsang et al., 2008). The sex disparity can be attributed in part to some chronic pain conditions being specific to women (e.g. vulvodynia, endometriosis) or occurring more often in women than men (e.g.

fibromyalgia, migraine, irritable bowel syndrome). However, the predominance of women with chronic pain is primarily believed to be due to physiological differences in nociception and treatment response between sexes (Greenspan et al., 2007; Fillingim et al., 2009). The mechanisms underlying pain differences in males and females has received very little study, despite the predominance of women with chronic pain (Mogil and Chanda, 2005).

Differences in nociception persist following CFA treatment. Despite males exhibiting greater paw edema following CFA injection, females have significantly lower mechanical and thermal hyperalgesia thresholds (Bradshaw et al., 2000; Cook and Moore, 2006; Cook and Nickerson, 2005). The effect of ovarian steroid hormone milieu on pain is less clear. In CFA-treated and control animals, mechanical thresholds were greatest in diestrus 1 and diestrus 2 (Bradshaw et al., 2000; Cook and Nickerson, 2005). Still other investigators have observed that female rats stop cycling following CFA treatment, entering a period of prolonged diestrus (Rahn et al., 2014; Wang et al., 2006). While circulating ovarian hormones can alter pain perception in females, the persistence of decreased pain thresholds in rats that have stopped cycling indicates that these differences may arise from a developmental effect, rather than an acute effect of estrogen.

## 1.3 The periaqueductal gray

The periaqueductal gray (PAG) is a critical part of the descending modulatory pathway that is involved in chronic pain. It is named for its gray color, which arises from densely-packed neurons, and its location around the cerebral aqueduct. The PAG is a large structure that extends rostrally from the pericoerulear area of the pons to the opening of the third ventricle. The neurons within the PAG neurons are heterogenous in function, somatic size,

and dendritic arborization (Mantyh, 1982). It mediates opioid analgesia as well as reproductive behaviors, autonomic control, vocalization, and defense behaviors, which arise differentially from the functional division of the PAG in to columns (Heinricher et al., 2009; Bandler and Shipley, 1994)(Figure 1.4). Microinjections of excitatory amino acids (EAA) in to the PAG reveal specific, regional effects. Activation of the dorsolateral (dl) or lateral (l) PAG produces confrontational defensive behaviors in the rostral regions, whereas caudal regions promote a flight or escape response (Krieger and Graeff, 1985; Depaulis et al., 1992). Stimulation of either area can produce hypertension and tachycardia (Yardley and Hilton, 1986). In contrast, EAA injection into the ventrolateral PAG (vlPAG) produces quiescence, hypotension and bradycardia (Depaulis et al., 1992; Keay et al., 1997). While stimulation of the d, dl, or vlPAG can produce analgesia, only the vlPAG produces a robust, endogenous opioid-mediated analgesia (Morgan, 1991). The analgesic effect is mediated through direct projections to the RVM (Lovick, 1985), thereby contributing descending inhibition to the modulation of pain.

### 1.3.1 Connectivity of the PAG

The PAG receives inputs from many regions throughout the CNS, many of which have been demonstrated to affect descending modulation (Beitz, 1982). Projections from the anterior cingulate and the ventrolateral orbital cortex can elicit pain-related responses from the vlPAG (Pastoriza et al., 1996; Donahue et al., 2001; LaGraize et al., 2004). The hypothalamic afferents to the PAG, which are believed to inhibit pain during times of illness, arise from the lateral hypothalamus and the medial preoptic area (Semenenko and Lumb, 1992; Behbehani et al., 1990). Afferents from the central nucleus of the amygdala can facilitate pain (Burstein and Potrebic, 1993; Gauriau and Bernard, 2004). The RVM is also capable of

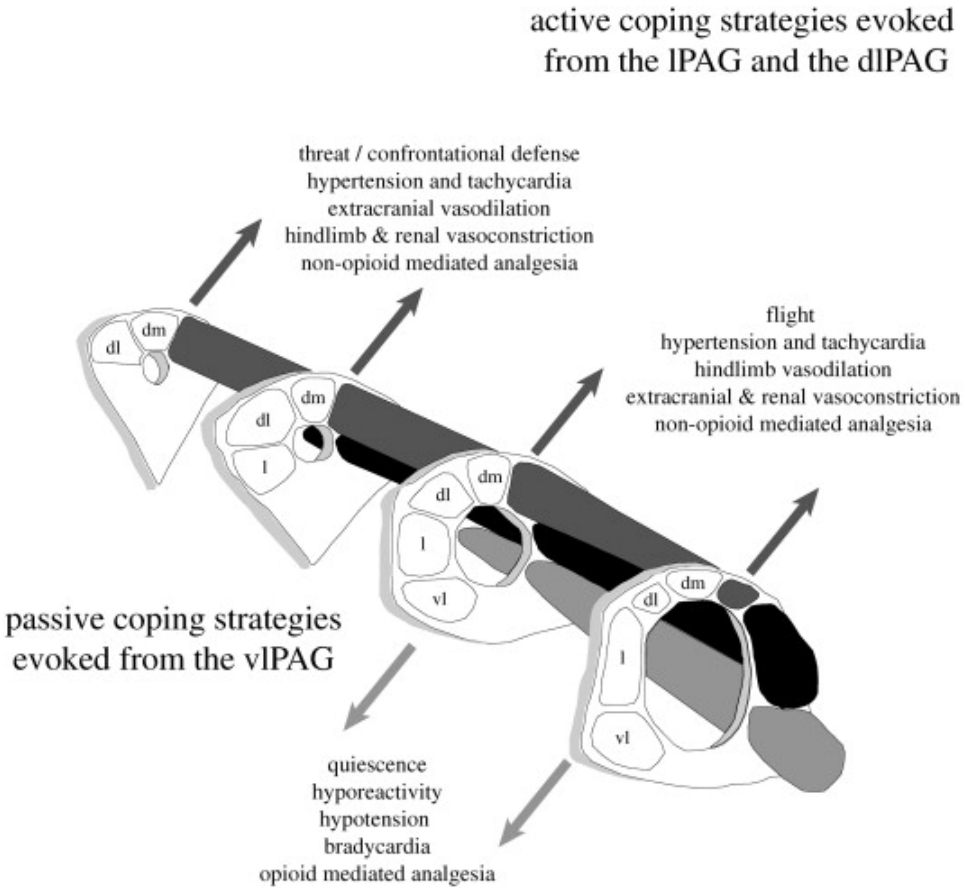


Figure 1.4: Columnar organization of the PAG

Distinct columns in the PAG that extend from rostral to caudal control different elements of physiological responses. Stimulation of the vlPAG evokes opioid analgesia, as bradycardia, hypotension, and immobility.

From Keay & Bandler (2001). Parallel circuits mediating distinct emotional coping reactions to different types of stress. *Neuroscience and Biobehavioral Reviews*. Dec;25(7-8):669:78.

projecting to the PAG, as are other brainstem regions such as the nucleus tractus solitaries, locus coeruleus, and pontine reticular formation (Burstein and Potrebic, 1993). The connectivity of the PAG is impressive, and reflects the position of the PAG as a "integration center" of cortical influences on brainstem functions.

The descending modulation of pain from the PAG is achieved primarily through a direct projection to the RVM, which is critical for analgesic effects from the PAG (Fields, 2004; Heinricher and Ingram, 2008). Both GABAergic and non-GABAergic PAG projections synapse on multiple cell types within the RVM, and approximately one-third of these RVM neurons project directly to the spinal cord (Morgan et al., 2008). The PAG also sends projections to the dorsolateral pontine tegmentum as well as sparse projections directly to the spinal cord (Heinricher and Ingram, 2008). However, the primary afferent of interest is that to the RVM for its well-defined role in descending modulation and analgesia.

### 1.3.2 Role of the PAG in descending modulation

The ability of the PAG to produce descending inhibition of pain was first discovered by the observation that midbrain electrolytic lesions in cats could produce profound analgesia, so that anesthetic was not necessary during *in vivo* recordings (Martin and Branch, 1958). Eventually, this observation was localized to the PAG in rats, where local stimulation produced analgesia strong enough for a laparotomy (Reynolds, 1969). These results were applied to humans, and PAG stimulation was used to treat chronic pain with relative success (Barbaro, 1988). However, due to the extra-analgesic roles of the PAG, these stimulations also evoked intense feelings of fear and discomfort and were poorly tolerated (Nashold et al., 1969). In animals, it was revealed that the mechanism of PAG analgesia was

to affect firing in nociceptive dorsal horn neurons through the RVM. This activation specifically inhibited pain transmitted by C fibers without affecting A-fiber nociception (Waters and Lumb, 1997; McMullan and Lumb, 2006; Leith et al., 2007), which is hypothesized to maintain the sensory component of nociception while blocking painful C-fiber input (Heinricher et al., 2009). Therefore, the PAG is capable of producing potent analgesia at the spinal cord through the descending modulatory pathway.

There is evidence to suggest the PAG is both necessary and sufficient for the manifestation of chronic pain. An increase in PAG activation, as measured by fMRI, is observed in patients suffering from chronic pain (Iannetti et al., 2005; Gwilym et al., 2009). Lesioning the vlPAG blocks the development of hyperalgesia following repeated foot shocks (McLemore et al., 1999), while injection of capsaicin or bradykinin into the vlPAG produce hyperalgesia (Burdin et al., 1992; McGaraughty et al., 2003). More directly, prostaglandin release in the vlPAG has been shown to recruit descending facilitation in the RVM (Heinricher and Neubert, 2004).

### 1.3.3 The disinhibition hypothesis

Descending inhibition from the vlPAG occurs via activation of PAG-RVM output neurons by opioids. Microinjections of μ-opioid receptor (MOPr) agonists into the vlPAG are analgesic, and act via RVM projections (Heinricher and Fields, 2003; Tortorici and Morgan, 2002). Opioids have both pre- and postsynaptic effects in vlPAG neurons. The postsynaptic effects of opioids are likely not the source of analgesia: only one-third of vlPAG neurons have a G-protein-coupled inwardly rectifying potassium (GIRK) conductance in response to opioids (Chieng and Christie, 1994a; Osborne et al., 1996). However, vlPAG neurons are under a constitutive GABAergic inhibition, which is inhibited by opioids. The presynaptic

MOPr couples to an arachadonic acid signaling pathway that couples to voltage-dependent potassium channels to inhibit GABA release onto vlPAG neurons (Chieng and Christie, 1994b; Vaughan and Christie, 1997; Vaughan et al., 1997). Therefore, it has been proposed that the analgesic action of opioids arises from disinhibition, or inhibition of presynaptic GABA inhibition (Basbaum and Fields, 1984). In support of this hypothesis, vlPAG microinjection of the $GABA_A$ antagonist bicuculline produces analgesia and decreases dorsal horn neuron responses to noxious stimuli, whereas the $GABA_A$ agonist muscimol attenuates morphine analgesia (Zambotti et al., 1982; Moreau and Fields, 1986; Sandkühler and Zimmermann, 1988). Thus the balance of $GABA_A$ signaling in the vlPAG is critical for descending modulation.

The analgesic actions of opioids in the vlPAG are mediated through the MOPr in the rat, based on evidence that agonists directed at either kappa or delta opioid receptors neither produce analgesia nor block presynaptic GABA release (Bodnar et al., 1988; Smith et al., 1988; Ossipov et al., 1995; Fang et al., 1989; Vaughan and Christie, 1997). Mice have kappa and delta opioid receptor effects in the vlPAG (Vaughan et al., 2003), but MOPr knockout mice show no morphine analgesia, further supporting the exclusive role of MOPr in antinociception (Kieffer, 1999).

While the original disinhibition hypothesis described inhibitory interneurons as the source of GABA on to vlPAG neurons, it is not clear if opioid inhibits GABA release from vlPAG interneurons. Although there are GABAergic neurons in the vlPAG (Morgan et al., 2008), paired recordings within the region have not revealed any indication of an inhibitory interneuron population (Lau, 2011). As described previously, there is a wealth of afferents to the vlPAG, some of which are known to be GABAergic. For example, the central nucleus of the amygdala is a major GABAergic projection to the vlPAG, (and interestingly,

MOPr agonists also have analgesic actions through GABA disinhibition in the amygdala (Finnegan et al., 2005)). The bed nucleus of the stria terminalis and ventral tegmental area are also major sources of GABA to the vlPAG (Kirouac et al., 2004). Therefore, vlPAG GABA may arise from inputs, rather than local inhibitory interneurons.

Excitation of the vlPAG through electrical stimulation or EAA microinjection at the vlPAG produces analgesia (Moreau and Fields, 1986), so opioid disinhibition should also excite vlPAG neurons. GABA and the $GABA_A$ agonists reduce firing in vlPAG neurons while the $GABA_A$ antagonist bicuculline increases firing (Ogawa et al., 1994). The excitatory effect of bicuculline on vlPAG neurons have been confirmed *in vivo* (Behbehani et al., 1990). Therefore, processes that alter the firing potential of vlPAG output neurons could attenuate its ability to produce descending inhibition.

### 1.3.4 Sex differences in vlPAG organization and analgesia

Loyd and Murphy have described organizational differences between the male and female vlPAG-RVM connection (2006). Their research found that females had almost double the number of RVM-projecting vlPAG neurons as males, but significantly fewer showed Fos activation following CFA inflammation. Despite this, morphine administration activates more vlPAG-RVM neurons in males than in females (Loyd et al., 2007). Males have more MOPr neurons in the vlPAG as measured by immunohistochemistry, and saporin-conjugated dermorphin injection into the vlPAG reduced morphine analgesia in males, but not females (Loyd et al., 2008). These data strongly indicate a different population or mechanism of morphine analgesia in females. These experiments were performed in intact female rats, so an acute effect of estrogen cannot be ruled out: approximately one-quarter of the vlPAG

neurons that project to the RVM express ER$\alpha$ (Loyd et al., 2008). However, CFA inflammation stopped estrous cycles in these rats, indicating that the the results may arise from developmental effects of estrogen

Morphine analgesia is significantly less potent and efficacious in females, revealing further differences in vlPAG physiology. Microinjections of morphine into the PAG also produce sex-dependent effects on the resulting analgesia, in which the half-maximal dose ($ED_{50}$) of females is at least twice as high as that in males (Krzanowska and Bodnar, 1999; Loyd et al., 2008; Bobeck et al., 2009). In one study, the vlPAG $ED_{50}$ of females was lethal to males (Loyd et al., 2008). vlPAG morphine is significantly less effective during proestrus and estrous (Krzanowska and Bodnar, 1999; Loyd et al., 2008; Krzanowska et al., 2002), indicating an acute effect of estrogen. However, the organizational effect of estrogen is clear: females gonadectomized and given testosterone immediately after birth and during the critical window for the developmental effects achieved similar levels of morphine analgesia as males (Krzanowska et al., 2002). Therefore, estrogen can exert an effect on analgesia both at an "organizational" (developmental) and "activational" (acute) level.

Humans also experience sexually dimorphic actions of morphine, but the data are from systemic administration and thus less clear. Males consume more morphine after surgery than females (Chia et al., 2002). However, adverse side effects of opioid use, such as dysphoria, headache, and nausea, are more severe in women than men, which may limit use in women (Fillingim et al., 2005). There is little agreement as to whether morphine produces more analgesia in males or females (Sarton et al., 2000; Cepeda and Carr, 2003; Fillingim et al., 2005). However, human data are confounded by the effects of morphine outside of the vlPAG.

It must be noted that there are no differences in morphine pharmacokinetics between sexes in either species. In rodents, morphine reaches the same concentrations in the brain and blood between sexes regardless of dose, and elimination occurs over the same time course (Cicero et al., 1997). Humans also show consistent pharmacokinetic profiles of morphine in men and women (Sarton et al., 2000). Therefore, the differences in male and female morphine analgesia, at least in rodents, are due in part to fundamental differences in the vlPAG.

## 1.4 $GABA_A$ signaling

vlPAG neurons are under tonic GABAergic inhibition that directly affects descending modulation. The $GABA_A$ receptor is a pentomeric ligand-gated ion channel that preferentially conducts chloride (Barnard and Seeburg, 1988; Farrant and Nusser, 2005). These receptors produce chloride currents that can produce phasic or tonic inhibition. The subunits that compose GABA receptors arise from eight families: $\alpha$(1-6), $\beta$(1-3), $\gamma$(1-3), $\delta$, $\varepsilon$, $\vartheta$, $\pi$, and $\rho$(1-3, formerly $GABA_C$)(Rudolph and Möhler, 2006; Sieghart, 2006). The $\gamma$2 subunit generally promotes postsynaptic clustering of the $GABA_A$ receptors, but localization can vary with subunit coexpression (Essrich et al., 1998; Glykys and Mody, 2006; Serwanski et al., 2006). Signaling through $GABA_A$ receptors can be tonic (extrasynaptic) or phasic (synaptic) in nature (Figure 1.5). The charge transfer of extrasynaptic $GABA_A$ signaling is over five times that of synaptic $GABA_A$ signaling, indicating a greater potential to influence neuronal excitability (Semyanov et al., 2003). The role of synaptic $GABA_A$ signaling in vlPAG neurons has been studied in the context of the disinhibition hypothesis, but little work has examined the function, if any, of an extrasynaptic current in these neurons.

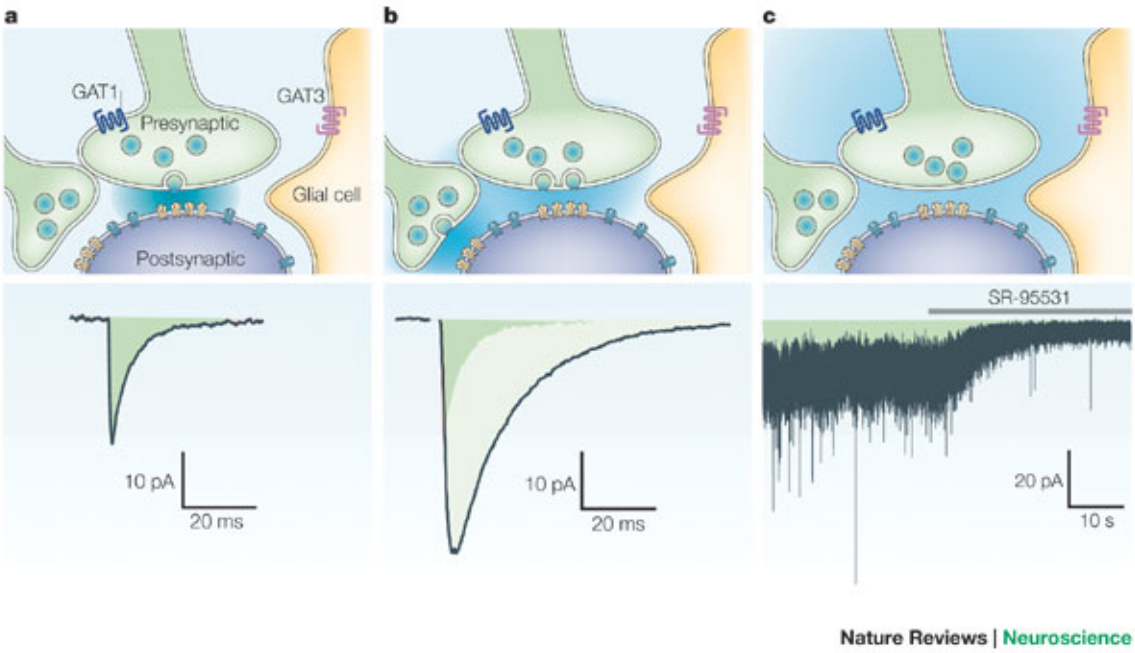


Figure 1.5: $GABA_A$ signaling

$GABA_A$signaling contributes to miniature inhibitory postsynaptic currents (mIPSCs, A), evoked inhibitory postsynaptic currents (eIPSCs, B), and tonic extrasynaptic currents (C). GABA concentration is shown in blue, and shaded green area beneath the traces represents charge transfer. In (A), spontaneous vesicle fusion produces a mIPSC in the postsynaptic cell through activation of synaptic $GABA_A$ receptors (yellow). In (B), concerted vesicle fusion achieved through electrical stimulation produces a large eIPSC (mIPSC area shown in dark green). In (C), extrasynaptic $GABA_A$ receptor activation by ambient GABA produces a change in holding potential, which is revealed by application of high concentrations of SR-95531 (Gabazine). This blocks both the synaptic events (visible in C) and the tonic current.

From Farrant, M. and Nusser, Z. (2005). Variation on an inhibitory theme: Phasic and tonic activation of $GABA_A$ receptors. *Nature Reviews Neuroscience* 6(3):215-29

### 1.4.1 The extrasynaptic $GABA_A$ current

The extrasynaptic $GABA_A$ current produces inhibition by hyperpolarization (via chloride influx) or by shunting (via reduction of membrane resistance)(Brickley and Mody, 2012; Farrant and Nusser, 2005). There are some exceptions, which depend on the chloride driving force. In neurons that do not express the chloride transporter KCC2, and therefore have high internal chloride concentrations, the extrasynaptic current is excitatory instead (Szabadics et al., 2006). However, even excitation by $GABA_A$ can become inhibitory, as shunting dominates when $GABA_A$ conductance is high (Pavlov et al., 2014; Song et al., 2012; Cope et al., 2005). In the vlPAG, there is no evidence to suggest that the extrasynaptic $GABA_A$ current would be excitatory.

Tonic currents are revealed by sustained reduction in holding current after application of $GABA_A$ antagonists. Certain pharmacological manipulations can aid in isolating and identifying the extrasynaptic $GABA_A$ current (Bright and Smart, 2013). Picrotoxin is a mixed $GABA_A$ receptor antagonist, which is believed to stabilize the $GABA_A$ receptor in a closed state (Smart and Constanti, 1982; Sedelnikova et al., 2006). Bicuculline is a competitive $GABA_A$ antagonist, but can also block $Ca^{2+}$-activated $K^+$ channels (Seutin and Johnson, 1999). Neither of these agents discriminate between extrasynaptic and synaptic currents. Gabazine, another competitive $GABA_A$ antagonist, can be used in low concentrations to selectively block synaptic $GABA_A$ currents (Stell and Mody, 2002; Park et al., 2007; Yamada et al., 2007). $Zn^{2+}$, $Cu^{2+}$, and $La^{3+}$ are able to produce some inhibition of receptors containing $\delta$ subunits (McGee et al., 2013; Krishek et al., 1998).

Enhancement of the extrasynaptic $GABA_A$ current is moderately more selective. 4,5,6,7-tetrahydoisoxazolo[5,4-c]pyridin-3(2H)-one (THIP) is a "super agonist" at $\alpha\beta\delta$ receptors, where it evokes a greater response than GABA (Krogsgaard-Larsen et al., 2002).

THIP is also a partial agonist at $\alpha\beta\gamma$ receptors, which requires careful interpretation of slice and *in vivo* data (Ebert et al., 1994; Mortensen et al., 2004). DS2 is a relatively new allosteric modulator of $GABA_A$ receptors that acts at the $\delta$ subunit. DS2 enhances holding currents and increases the IPSC decay in neurons with a $\delta$ subunit-mediated extrasynaptic current (Herd et al., 2013; Ye et al., 2013; Wafford et al., 1996; Jensen et al., 2013).

### 1.4.2 The extrasynaptic $GABA_A$ current in the vlPAG

As described, the extrasynaptic $GABA_A$ current can have profound effects on neuronal excitability in a number of brain regions. An extrasynaptic $GABA_A$ current has been identified functionally and histologically in the vlPAG, but it has not been well described. Lovick and colleagues (2005; 2005) reported expression of $\alpha 4$, $\beta 1$ and $\delta$ subunits in the vlPAG of male and female rats as measured by immunohistochemistry. Lau et al. (2014) have reported a tonic, THIP-sensitive $GABA_A$ current that is modulated by menthol in the vlPAG. These studies indicate that an extrasynaptic $GABA_A$ current is present in vlPAG neurons, but do not shed light on any effect of this current on descending modulation.

### 1.4.3 The extrasynaptic $GABA_A$ current and nociception

Bicuculline microinjection into the vlPAG is analgesic, but does not distinguish between extrasynaptic and synaptic actions (Zambotti et al., 1982; Bobeck et al., 2014). THIP microinjection into the vlPAG attenuates morphine antinociception, but has no effect on hot plate latency on its own (Depaulis et al., 1987). However, high concentrations of THIP can also act as a partial agonist at synaptic $GABA_A$ receptors (Mortensen et al., 2004), so it's difficult to ascribe those effects solely to extrasynaptic $GABA_A$ actions. $\delta$-subunit

knockout mice have increased pain behaviors, but this could be due to action of the δ subunit in the spinal cord: intrathecal THIP administration decreases nociception in mice, but has no effect in δ-subunit knockouts (Bonin et al., 2011). $GABA_A$ signaling and neuronal excitability in the vlPAG are critical components of antinociception. The extrasynaptic $GABA_A$ current is a compelling target for modulation during chronic pain, and may contribute to a decrease in descending inhibition.

### 1.4.4 vlPAG $GABA_A$ in females

Lovick et al. observed no overt differences in the amount of $GABA_A$ α4, β1 and δ subunit expression between males and females when the number of neurons that expressed each subunit was quantified by area (2005). Females do show an estrous stage-dependent change in expression of all the listed subunits, with the highest levels occurring in the second day of diestrus. These subunits were evaluated separately in the dorsal, dorsolateral, lateral and ventrolateral PAG, but combined for statistics. Therefore, it is difficult to determine if the δ subunits had a significant change in the vlPAG. The authors propose that the upregulation occurs on diestrus 2 due to the drop in progesterone. However, there is no evidence of progesterone receptors in the vlPAG (Lonstein and Blaustein, 2004; Quadros et al., 2008), so this effect may be directly mediated through estrogen. Systemic estrogen upregulates $GABA_A$δ subunit expression in some regions of the brain (Calza et al., 2010; Shen et al., 2005; Xu et al., 2008). Additionally, the $GABA_A$δ subunit has an estrogen response element, indicating that estrogen can increase its transcription (Bourdeau et al., 2004).

One study examined dorsal PAG neuronal excitability when $GABA_A$δ subunit expression was high (diestrus 2), operating under the hypothesis that the extrasynaptic $GABA_A$

current is expressed by inhibitory interneurons. In support of this hypothesis, an increase in δ subunit expression was associated with greater excitability and had greater increases in firing following bicuculline application (Brack and Lovick, 2007). While that may be the case in the dorsal PAG, the lack of evident inhibitory interneurons in the vlPAG may mean that the extrasynaptic $GABA_A$ current occurs postsynaptically, producing a direct inhibitory influence on PAG-RVM output.

## 1.5 Aims

This thesis focused on understanding the central mechanisms underlying chronic pain using models most relevant to clinical pain. These approaches used both male and female models to describe chronic pain conditions and vlPAG physiology.

$GABA_A$signaling in the vlPAG is an important component of the analgesic actions of the descending modulatory pathway. The extrasynaptic $GABA_A$ subunit has been identified in vlPAG neurons, but has not been characterized nor examined during chronic pain. Therefore, I identified specific alterations to synaptic and extrasynaptic $GABA_A$ signaling in the vlPAG between male and females in naïve and chronic pain conditions. GABA signaling was measured using whole-cell, patch clamp electrophysiology from vlPAG neurons from rats during CFA inflammation. I also measured mRNA expression of $GABA_A$ receptor subunits and associated genes in the vlPAG during CFA and OA treatment, and compared changes between treatment and sex.

One major clinical barrier to understanding the consequences of plasticity changes in descending modulation is the lack of a diagnostic test for central sensitization. Previous studies from the Heinricher lab have indicated that pain facilitating neurons in the RVM

increase activity in response to light, indicating that light may be able to be used to activate the descending modulatory pathway without involving the peripheral nervous system. We characterized light sensitivity as a marker of abnormal descending modulation in women with fibromyalgia.

# Chapter 2

**A tonic $GABA_A$ current in the periaqueductal gray is involved in persistent inflammation-induced plasticity in female, but not male rats**

Karen J. Tonsfeldt, Katherine L. Suchland, Susan L. Ingram

Department of Neurological Surgery, Oregon Health & Science University, Portland, OR 97239

Supported by NIH grants DA027625 (SLI) and T32 AG023477 (KJT).

## 2.1 Abstract

The ventrolateral periaqueductal gray (vlPAG) is a critical component of the descending pain modulatory circuit that inhibits incoming nociceptive signals in the spinal cord. The vlPAG output neurons are under tonic GABAergic inhibition by spontaneous GABA release and the presence of a tonic $GABA_A$-mediated current. The tonic current in the vlPAG is activated by THIP a selective agonist of $GABA_A$ receptors containing the $\delta$ subunit and blocked by picrotoxin and bicuculline but not low concentrations of gabazine indicating the presence of an extrasynaptic current mediated by GABAA $\delta$ receptors. The tonic current is differentially modulated in male and female rats by chronic inflammatory pain. Complete Freund's adjuvant (CFA) injections into the hindpaw induced persistent inflammation in both male and female rats. The tonic $GABA_A$ current, as well as $GABA_A$ $\delta$ subunit protein levels and $\delta$ subunit expression were significantly increased in female, but not male rats. Finally, we demonstrate that activation of the $GABA_A$ $\delta$ receptors *in vivo* using microinjections of the positive allosteric agonist of the $\delta$ subunit 4-chloro-N-[2-(2-thienyl)imidazo[1,2-a]pyridin-3-yl]benzamide (DS2) into the vlPAG attenuates morphine antinociception indicating a role of this current in descending pain modulation. Together, these data support a role of the $\delta$-subunit mediated extrasynaptic $GABA_A$ current in the development and maintenance of chronic pain in females.

## 2.2 Introduction

Chronic pain is a debilitating disease that affects over 100 million Americans and has an annual cost in the U.S. of over $500 billion dollars (Gaskin and Richard, 2012). Chronic pain is often initiated by tissue damage and lasts long after the initial insult heals; however, it can also appear in the absence of injury. The underlying mechanisms of the development and maintenance of chronic pain are poorly understood. It is now well-established that chronic pain is produced by sensitization of neuronal circuits (reviewed in Sandkühler (2009)). The primary supraspinal circuit that regulates the response to pain is the descending pain modulatory pathway which projects from the ventrolateral periaqueductal gray (vlPAG) to the rostral ventromedial medulla (RVM) and then to the spinal cord (reviewed in Heinricher and Ingram (2008)). Chronic inflammation sensitizes neuronal responses throughout the pathway that are thought to contribute to the development of chronic pain (Porreca et al., 2001; Guan et al., 2002; Ren and Dubner, 2002; Heinricher et al., 2009). PAG activation is readily observed in fMRI imaging of patients suffering from chronic pain or induced secondary hyperalgesia (Gwilym et al., 2009). Similarly, in animal models, chronic inflammation induced by Complete Freund's Adjuvant (CFA) modulates synaptic plasticity in the vlPAG (Hu et al., 2009). These data provide strong evidence of a role for the vlPAG in various chronic pain states. However, the cellular mechanisms that contribute to sensitization of vlPAG neurons and the descending pain pathway during chronic pain are not known.

Activity of the descending pain modulatory pathway is under tonic inhibition by GABA acting on $GABA_A$ receptors in the PAG. Analgesia mediated by the descending pain pathway occurs through disinhibition (or removal of $GABA_A$-mediated inhibition) of PAG output neurons that project to the RVM (Heinricher and Ingram, 2008). This hypothesis is

supported by many studies showing that opioid microinjection into vlPAG induces analgesia and *in vitro* studies showing opioid suppression of GABA release onto vlPAG neurons (Heinricher and Ingram, 2008; Vaughan and Christie, 1997). In addition, GABAA receptor inhibitors induce analgesia when microinjected into the vlPAG (Depaulis et al., 1987). Thus, $GABA_A$ signaling in the vlPAG is an important component regulating the descending modulation of pain, and may be an important target of modulation during chronic inflammatory pain. GABAA receptors are ion channels with pentomeric structure that consist of 5 subunits with the pore in the middle (reviewed in Barnard and Seeburg (1988); Farrant and Nusser (2005)). To date, there are 19 cloned $GABA_A$ receptor subunits, and there appears to be specificity in subunit composition depending on location within the cell. The most prevalent $GABA_A$ receptors are localized to synapses that generally contain 2 $\alpha$, 2 $\beta$ and a $\gamma$ subunit. The $\gamma$ subunit is necessary for trafficking to the synapse and these receptors are sensitive to bicuculline, picrotoxin and benzodiazepines (Arancibia-Cárcamo and Kittler, 2009). Extrasynaptic $GABA_A$ receptors primarily contain $\alpha$4 or $\alpha$6, $\beta$2 or $\beta$3, and a $\delta$ subunit. The $\delta$ subunit confers sensitivity to neurosteroids and ethanol and insensitivity to benzodiazepines. $GABA_A$ receptors containing $\alpha 4\beta 1\delta$ subunits are expressed in the PAG (Griffiths and Lovick, 2005; Lovick et al., 2005), where they may mediate tonic GABAergic tone. Tonic, extrasynaptic $GABA_A$ signaling produces a current that is critical for mediating excitability at the cell- and circuit-level in areas such as the thalamus, cerebellum, and cortex (reviewed in Brickley and Mody (2012)). In the vlPAG, synaptic $GABA_A$ signaling is well-characterized (Vaughan et al., 1997; Vaughan and Christie, 1997), but extrasynaptic $GABA_A$ signaling has only just been described (Lau et al., 2014).

In this study we sought to characterize the extrasynaptic $GABA_A$ current in vlPAG neurons both *in vivo* and *in vitro*, and to explore changes to this current during chronic

inflammatory pain. Given the documented differences in δ subunit expression in the vlPAG between males and females, we determined if there was a functional difference in the extrasynaptic current between males and females and whether $GABA_A$ receptors containing the δ subunit play a role in chronic inflammatory pain in the vlPAG.

## 2.3 Materials & Methods

### Animals

Female and male Sprague-Dawley rats were used for all experiments. Male rats were between 21-50 days postnatal (PND) at the time of experimentation. Female rats used for molecular and electrophysiological studies were 21-32 PND, and absence of vaginal opening was confirmed at time of sacrifice. Female rats (35-50 days PND) were used for behavioral experiments. Vaginal cytology in these females was performed by daily vaginal gavage for at least one week prior to experimentation. Lights were on a 12-h light and dark cycle, and food and water were provided ad libitum. All experiments were approved by the Animal Care and Use Committee at Oregon Health and Science University.

### Complete Freund's adjuvant treatment

Rats were lightly anesthetized with isoflurane and administered 100 μL of complete Freund's adjuvant (CFA, Sigma, St. Louis MO) into left or right hindpaw. Paw inflammation was measured at the time of sacrifice. CFA significantly increased paw diameter in males and females (data not shown).

### Electrophysiology

Rats were anesthetized with isoflurane and decaptitated. Brains were quickly removed

and immersed in ice-cold sucrose artificial cerebrospinal fluid (sCSF) containing (in mM): 75 NaCl, 2.5 KCl, 0.1 CaCl2, 6 MgSO4, 1.2 NaH2PO4, 25 NaHCO3, 2.5 D-Dextrose, 50 Sucrose. Coronal slices containing the vlPAG were cut 220 μm thick with a Vibratome (Leica Microsystems, Inc. Deerfield, IL). Slices were placed in a holding chamber with oxygenated with aCSF containing (in MM): 126 NaCl, 21.4 NaHC3, 11.1 Dextrose, 2.5 KCl, 2.4 CaCl2, 1.2 MgCl2, and 1.2 NaH2PO4, and equilibrated with 95% O2 / 5% CO2 at 32ºC until recording. Brain slices were placed into a recording chamber on an upright Zeiss Examiner Z1 and superfused with 32ºC aCSF. Neurons were visualized with infrared Nomarski optics. Cells were viewed with a water immersion 40X objective. Recordings were made with electrodes pulled to 2-5 MOhms resistance. Voltage clamp recordings were made using an internal solution containing (in mM) 130 CsCl, 10 HEPES, 1.1 EGTA, 10 KCl, 2 MgCl2, 0.1 CaCl2, 4 MgATP, and 1 NaGTP (pH 7.4 with CsOH). Current-voltage relationships were made using an internal solution containing (in mM) 128 KGluconate, 10 HEPES, 1 EGTA, 10 KCl, 1 MgCl2, 0.3 CaCl2, 4 MgATP, and 1 NaGTP (pH 7.4 with KOH). Series resistance (< 12 MOhms) was compensated by 80% and continuously monitored throughout the experiment. Liquid junction potentials of 5 mV (CsCl intracellular solution) or 15 mV (KGlu intracellular solution) were corrected.

**Western Blot**

Rats were injected with CFA in a hind paw or were naive to treatment. 5 days later, brains were removed and vlPAG tissue was collected and homogenized in M-PER Mammalian Protein Extraction Reagent (ThermoScientific, Rockford, IL) with protease inhibitors added. After incubating 30 min on ice, lysates were centrifuged at 13,000 RPM for 10 min and supernatant was collected. Protein concentration was determined by BCA

protein assay (ThermoScientific). Total protein was separated by electrophoresis on pre-cast NuPAGE 4-12% Bis-Tris gels (Life Technologies, Carlsbad, CA) and transferred to nitrocellulose membrane. Blots were blocked with 5% milk in TBS-T buffer (20 mM Tris, pH 7.6, 137 mM NaCl, 0.1% Tween 20) at room temperature for 1 h. Blots were then incubated with $GABA_A$ δ antibody (sc-25705, Santa Cruz Biotechnologies, Santa Cruz, CA; 1:200) in 1% milk in TBS-T for 36 hours at 4ºC. After thorough washing in TBS-T buffer, membranes were incubated in goat anti-rabbit secondary antibody for 1 h at room temperature (Life Technologies; 1:2000). Immunoreactivity was detected using SuperSignal West Pico Chemiluminescent Substrate (ThermoScientific). Chemiluminescence was captured with an Alpha Innotech FluorChem FC2 (San Leandro, CA) and analyzed using ImageJ software (National Institutes of Health, USA).

**qRT-PCR**

Following treatment, rats were anesthetized with isoflurane and rapidly decapitated. Brains were put in ice-cold PBS, and then 100 mm sections of the midbrain were made using a brain block. Sections containing the PAG were removed and placed on an RNAse-free, ice-cold surface. The vlPAG was carefully dissected from all relevant slices, and placed in a 1:1 solution of RNAse-free water and RNAlater (Invitrogen; Grand Island, NY). Tissue was stored for 24-48 hours at 4ºC until RNA isolation. RNAlater was removed from eppendorf tubes containing tissue, and replaced with 1 mL Trizol (Invitrogen). A phenol-chloroform extraction was performed, and the resulting RNA was processed with the Ambion PureLink kit (Life Technologies). Isolated RNA was then analyzed using a NanoDrop (ThermoScientific) for quantification and quality control.

qRT-PCR primers for the δ subunit were designed to bridge introns using Primer3 (Koressaar and Remm, 2007). $GABA_A$ δ subunit (Accession number NM_017289.1 F: TGGCCAGCTGATTTGAAGTTC; R: ACTGGCCCAGTTCACTATCACC. 200 bp) β-actin (Accession number NM_031144.3 F: CAGCCTTCCTTCCTGGGTATG; R: TAGAGCCACCAATCCACACAG. 247 bp). Standard curves were performed using serial dilutions of vlPAG tissue (1:20, 1:50, 1:100, 1:200, 1:400, 1:800, 1:1600, 1:3200, 1:6400). Primer efficiency was 100% for $GABA_A$ δ (slope: -3.36, r2: 0.99) and 97% for β-actin (slope: -3.39, r2: 0.99). Melting curves were examined after each experiment to insure only one product was formed.

2 μg isolated RNA was converted to cDNA using the High Capacity cDNA Reverse Transcription Kit (Life Technologies). Controls lacking reverse transcriptase (-RT) were also created. Reactions were performed using SYBR Select Master Mix on an ABI 7000 and were analyzed using SDS software (Applied Biosystems). Negative controls were performed without template cDNA as well as –RT samples.

Samples were run in triplicate ($GABA_A$ δ) or duplicate (β-actin), and Ct values were averaged from these. CFA and naïve animals were run on the same plate, separated by sex. To compare mRNA expression of $GABA_A$δ subunit, the ΔΔCt analysis was used. All data were normalized to the naïve group of the plate. Data are reported as a fold change in gene expression. T-test was used for statistical analysis.

**Microinjections**

Adult rats (250-350 g) were anaesthetized with a cocktail of ketamine, xylazine, acepromazine (37.5 mg/kg, 7.5 mg/kg, 1.5 mg/kg) and implanted with a guide cannula (23 gauge, 9 mm long) aimed at the vlPAG (AP: +1.7 mm, ML: -0.6 mm, DV: -4.6 mm from lambda) using stereotaxic techniques. The guide cannula was attached to two screws in the skull

by dental cement. After surgery, a stylet was inserted into the cannula and rats were maintained under a heat lamp until awake. Rats were housed singly for two days post-surgery and were then rehoused two per cage. Rats were handled daily and experiments were begun at least seven days after surgery.

Drugs were administered directly into the vlPAG through a 31-gauge injection cannula (0.25 mm OD and 0.127 mm ID) inserted into and extending 2 mm beyond the tip of the guide cannula. One day prior to testing, all rats received a sham injection in which the injection cannula was inserted into the guide cannula but no drug was administered. This procedure reduces responses resulting from mechanical stimulation of neurons during the experiment and habituates the animal to the microinjection procedure. Testing with drug administration began the next day. All drugs were injected at a rate of 0.1 μL per 10 s while the rat was gently restrained by hand. The injection cannula remained in place an additional 20 s to minimize backflow of drug back up the cannula track. Following the injection the rat was returned to its home cage.

**Testing of antinociceptive behavior**

All behavioral assessments were conducted using the hot plate test which consisted of measuring the latency of the rat to lick a hindpaw when placed on a hot plate at 52.5ºC. The rat was removed from the hot plate if no response occurred before the cut-off of 50 s. Any animal with baseline hot plate latency above 20 s was omitted from the study. Only rats with injection sites in or on the border of the vlPAG were included in data analyses (Paxinos and Watson, 2005). Female rats cycled normally for one week prior to cannula placement. After cannulation, all female rats transitioned to a prolonged diestrus state.

On test day, baseline hot plate nociception was assessed. Animals were pretreated with either a microinjection of 4-Chloro-N-[2-(2-thienyl)imidazo[1,2-a]pyridin-3-yl]benzamide

(DS2) (3 µg per 0.5 µL; Abcam Cambridge UK) or its vehicle, 100% DMSO (0.5 µL) 10 min prior to receiving microinjections of cumulative third-log doses of morphine (Males: 1, 2.2, 4.6, 10, and 22 ug/0.4 µl; Females: 2.2, 4.6, 10, 32 and 54 ug/0.4 µl) at 20 min intervals. Hot plate latencies were measured 15 min following each microinjection.

**Data analysis** Average holding current, variance and mIPSCs were analyzed using Axograph. mIPSCs were detected by selecting events that exceeded a preset threshold (set to 20 pA) and fit the criteria: 10-90% rise time (0 and 2 ms) and half-width (> 4 ms). Events were verified individually and ranked by amplitude and inter-event interval to determine cumulative probability. All distributions were tested for normality using the Shapiro-Wilk normality test. Frequency was determined over one or two minute epochs after equilibration of each drug. All data are expressed as mean ± SEM. Statistical significance was determined in two group comparisons by paired t-tests or Mann-Whitney U tests and in more than two group comparisons by one-way ANOVA or Kruskal-Wallis (nonparametric ANOVA) when appropriate ($p < 0.05$), followed by Bonferroni post-hoc tests or Dunn's multiple comparisons test (Graphpad Prism 4, La Jolla CA).

## 2.4 Results

**Characterization of $GABA_A$-mediated phasic and tonic currents in vlPAG** Whole-cell patch-clamp recordings from vlPAG neurons voltage-clamped at -70 mV revealed the presence of spontaneous $GABA_A$-mediated synaptic currents isolated in the presence of the AMPA and kainate receptor antagonist DNQX (20 µM) (Figure 2.1, A-C). Tonic currents were revealed with superfusion of $GABA_A$ antagonists as outward deflections of the holding current. GABAergic currents are typically inward at a holding potential of -70 mV

when using CsCl intracellular recording solutions because the equilibrium potential for chloride flux is approximately 0 mV. Nonselective GABAA antagonists, picrotoxin (PIC; 300 μM) and bicuculline (BIC; 20 μM), blocked both the spontaneous synaptic currents and a tonic GABAA current (Figure 2.1). The tonic current revealed by PIC (300 μM) was evident in a subpopulation of vlPAG neurons from male rats (8 out of 13 neurons; 10 ± 2 pA). A similar subpopulation of neurons (8 out of 14 neurons) had a GABAergic tonic current in female rats (10 ± 1 pA). Bicuculline (20 μM)-induced currents were smaller overall (5 ± 1 pA, n = 15 (males (n = 9) and females (n = 6) combined). In contrast to PIC and BIC, 1 uM GBZ had no effect on the holding current in any vlPAG neuron examined (Figure 1C). Low concentrations of gabazine (GBZ; 1 μM) are more selective for synaptic $GABA_A$ currents (Park et al., 2007; Yamada et al., 2007). Gabazine decreased spontaneous synaptic $GABA_A$ currents without decreasing the tonic current elicited by PIC. The variance of the noise at the holding current is another method to estimate the tonic current, because variance is proportional to the number of channels open (Bright and Smart, 2013). Both BIC and PIC significantly reduced the variance of the holding current (Figure 2.1E).

BIC has also been shown to inhibit SK channels (Seutin and Johnson, 1999), so we compared the reversal potential of the BIC-blocked tonic current using CsCl and KGluconate intracellular solutions to determine if the shift in reversal potential was predicted for a chloride ion flux according to the Goldman equation (1F). Using a CsCl internal solution ([Cl-]in 134.2 mM), the experimental reversal potential was -17 ± 7 mV (n = 5) that shifted to -67 ± 9 mV (n = 4) with a potassium gluconate internal solution (Figure 2.1F). The shift indicates that the primary ion conducted by the BIC-sensitive current is chloride.

**THIP dose-dependently increases the tonic $GABA_A$-mediated current** Tonic currents are often mediated by $GABA_A$ receptors that contain the δ subunit (Brickley and Mody,

2012). 4,5,6,7-Tetrahydroisoxazolo[5,4-c]pyridin-3-ol hydrochloride (THIP/ Gaboxadol) is a $GABA_A$ agonist that is selective for the $GABA_A$ δ subunit at low concentrations (Brown et al., 2002; Adkins et al., 2001). THIP activation of the tonic current has recently been demonstrated in the vlPAG of male rats (Lau et al., 2014) so we verified that THIP activated currents in female vlPAG neurons. Bath application of THIP (1 and 10 μM) increased the holding current by 5 ± 2 pA and 64 ± 6 pA, respectively (Figure 2.2B). The THIP-mediated currents were blocked by PIC (300 μM) and the current amplitude was measured as the difference between the holding current in the presence of THIP minus the holding current in the presence of THIP + PIC. The variance of the holding current was also dose-dependently changed by THIP application (Figure 2.2C) in female vlPAG neurons. For comparison between cells, the THIP variance was normalized to the PIC variance for each cell.

**Chronic inflammatory pain significantly increases the extrasynaptic $GABA_A$ current in vlPAG neurons in females, but not males.** To determine if the tonic $GABA_A$-mediated current is modulated in chronic pain states, chronic inflammatory pain was induced in male and female rats with hindpaw injections of CFA (100 μL). The injected paws were larger than the control paws in both female and male rats 5-6 days after the injection at the time of sacrifice for whole-cell recordings (data not shown). There was a significant effect of Treatment on the amplitude of the PIC (300 μM)-induced current ($F_{(1,27)} = 5.32$, $p < 0.05$) that was driven by the increase in PIC-induced currents in female (19 ± 5 pA, n = 7) compared to naïve rats (10 ± 1 pA, n = 8; Bonferroni's post-hoc, Figure 2.3A). In contrast, the PIC-induced current in CFA males (10 ± 2 pA, n = 8) is not significantly different from naive males (13 ± 2 pA, n = 8).

To determine if the changes in the extrasynaptic current were due to changes in $GABA_A$ δ subunit expression, we measured both the protein and mRNA levels of $GABA_A$ δ subunits in naive and CFA-treated males and females. There was a significant increase in band intensity on Western blots of CFA-treated compared to naïve females (Figure 2.3B and C) that was not detectable in vlPAG tissue from CFA-treated male rats (Figure 2.3C). Primers were made against the rat $GABA_A$ δ subunit subunit and β-actin, as described in methods. A standard curve generated by using serial dilutions of vlPAG tissue indicated that the efficiency of the primers were 100% and 98%, respectively (Figure 2.3D and E). These efficiencies are within the acceptable range to use for ΔΔCt analysis, which was performed independently for males and females. For both sexes, values were normalized to the naive animals, and are expressed as fold change compared to the average of naive. Females displayed a robust upregulation of the $GABA_A$ δ subunit (Figure 2.3E; t-test, $p<0.01$). Males showed no such significant change in $GABA_A$ δ subunit mRNA expression (Figure 2.3F). While CFA-treated males displayed a downward trend in mRNA expression, this change was not significant.

**Allosteric modulation of the δ subunit by DS2 decreases morphine antinociception in vivo.** In order to determine if the $GABA_A$ δ subunit is important for antinociception mediated by the vlPAG, we microinjected DS2 (3 μg), a positive allosteric modulator of the δ subunit into the vlPAG. Microinjection of DS2 alone did not alter nociceptive thresholds on the hot plate test in male rats (DS2 = 14 ± 1s, n = 5) compared to vehicle (100 % DMSO = 14 ± 1 s, n = 7, t-test $t(10)= 0.383$, $p > 0.05$)(Figure 2.4). However, the dose-response curve for morphine-induced antinociception was significantly shifted to the right with prior administration of DS2 ($F_{(1,61)} = 6.57$, $p < 0.05$). The ED50 for morphine in vehicle treated rats was 4.8 μg (95% Confidence Interval (CI) = 3.0 – 6.7 μg) and for

DS2 pretreatment the ED50 was 10.8 μg (CI = 6.2 – 15.5 μg). These data indicate that potentiation of the current elicited by GABA at $GABA_A$ δ subunits decreases morphine antinociception induced by microinjections into the vlPAG. Interestingly, baseline hot plate latencies were significantly lower in females (9 ± 1 s, n = 6) than in males (13 ± 1, n = 11; t-test, $t(15) = 2.753$, $p < 0.05$). This difference in baseline latencies on the hot plate makes it difficult to directly compare male and females rats. However, consistent with previous studies using female rats (Bobeck et al., 2009), we found that morphine potency in the vlPAG was dramatically reduced in female rats (Figure 2.4). Only high doses of morphine increase hot plate latencies when microinjected into the vlPAG of female rats. These doses may actually induce antinociception via local anesthetic actions in the vlPAG. Thus, it is not possible to determine the effect of DS2 on morphine antinociception in female rats.

## 2.5 Discussion

In this study, the tonic $GABA_A$ current in vlPAG neurons was characterized in male and female rats during chronic inflammatory pain. The tonic current measured in a subpopulation of vlPAG neurons was mediated through $GABA_A$ receptors containing the δ subunit. Chronic inflammatory pain induced by CFA increased the extrasynaptic $GABA_A$ current, $GABA_A$ δ protein levels and mRNA expression in female, but not male rats. Finally, microinjections of the δ subunit allosteric modulator DS2 directly into the vlPAG attenuates morphine antinociception indicating that activation of the $GABA_A$ δ subunit decreases descending antinociception. Together, these data support a role of the δ-subunit mediated extrasynaptic $GABA_A$ current in the development and maintenance of chronic pain in females.

The tonic $GABA_A$ current is detected in around 60% of all vlPAG neurons tested regardless of sex. These data may suggest that not all vlPAG neurons express $GABA_A$ receptors containing the δ subunit. However, we determined that low concentrations of the δ-selective agonist THIP induced small changes in the holding current in all vlPAG neurons tested indicating that most vlPAG neurons express these subunits but GABA does not activate the receptors under basal conditions in the slice preparation. This may be due to the localization of $GABA_A$ δ subunits in extrasynaptic locations. Extrasynaptic receptors are typically activated by spillover of neurotransmitter to the extrasynaptic sites or via non-synaptic release of GABA (Brickley and Mody, 2012). These mechanisms may be reduced in slice preparations or at the lower than physiological temperatures used for these studies. We observed that low concentrations of gabazine (GBZ), thought to be selective for synaptic $GABA_A$ signaling, blocked spontaneous mIPSCs but did not affect the holding current confirming the contention that $GABA_A$ δ receptors in the vlPAG are extrasynaptic. We also found that THIP increased the tonic current in vlPAG neurons from both male and female rats (Lau et al., 2014), but that only tonic currents in female rats were increased in CFA-pretreated rats. This change is likely mediated by an upregulation of the $GABA_A$ δ subunit, as indicated by mRNA and protein expression supporting previous data (Lovick et al., 2005; Griffiths and Lovick, 2005). A possible reason for the increase in tonic current in females compared to males is that the CFA treatment produces a greater inflammatory response in females than in males. While some studies have found CFA induces a greater change in paw thickness in females than males (Cook and Nickerson, 2005), this effect appears dependent on location of injection site and time after injection (Cook and Moore, 2006), and we observed no differences in the amount of change in paw thickness between males and females.

Morphine-induced analgesia is thought to arise from disinhibition of vlPAG output neurons by blocking presynaptic GABA release (reviewed in Lau and Vaughan (2014)). We found that microinjections of the positive allosteric agonist DS2 into the vlPAG of male rats significantly reduced the potency of microinjected morphine as measured by the hot plate assay. These data suggest that modulation of postsynaptic $GABA_A$ receptors can reduce the presynaptic effects of opioids on GABA release. Our data support previous findings that microinjection of THIP into the vlPAG also attenuates morphine analgesia (Depaulis et al., 1987). The selectivity of DS2 for the $GABA_A$ $\delta$ subunit (Drasbek and Jensen, 2006; Wafford et al., 1996) indicates this effect is mediated through activation of the extrasynaptic $GABA_A$ receptors.

In our study, we found that CFA treatment increased $\delta$ subunit mRNA and protein. We believe this effect is due to the chronic inflammatory pain and not the influence of ovarian hormones, because of the prepubertal status of most female rats used. These data suggest an organization effect of ovarian hormones on vlPAG neurons, as we do not see a similar change in males. However, without manipulating gonadal hormone status at birth, it is difficult to determine the exact role of ovarian hormones. In cycling females, $GABA_A$ $\delta$ subunit expression in the vlPAG is highest in late diestrus (Griffiths and Lovick, 2005). However, CFA treatment disrupts the estrous cycle and produces a prolonged diestrus (Wang et al., 2006). Further studies are needed to examine if the inflammatory pain increases the extrasynaptic $GABA_A$ current in cycling females. The functional consequences of an increase in extrasynaptic $GABA_A$ current function and expression are perhaps best illustrated by actions of DS2. DS2 had no effect on baseline paw withdrawal latency in males, but thermal assays are not particularly sensitive to hyperalgesia. Using a behavioral assay more sensitive to hyperalgesia, such as pressure thresholds, may reveal a hyperalgesic effect of

DS2. However, the GABAergic inhibition of vlPAG output neurons may be sufficient under basal conditions that increasing inhibition has no further effect on pain behaviors (eg. a ceiling effect). In any case, the ability of the extrasynaptic $GABA_A$ current to attenuate morphine analgesia is of particular relevance to female physiology and the etiology of chronic pain in females. Human females report more chronic pain conditions (Berkley, 1997) and less relief from opioid analgesics (Cepeda and Carr, 2003) than men, and these differences are likely supraspinal in origin (Bartley et al., 2014). The vlPAG has been postulated as a main site of action of this effect, both because of its significant role in opioid analgesia, sexually dimorphic behaviors, and mediation of opioid and sex steroid interactions (Krzanowska and Bodnar, 1999). Indeed, morphine microinjections into the vlPAG produce less antinociception in female rats than males, an effect that appears to be dependent on developmental actions of estrogen rather than acute effects of circulating estrogen (Krzanowska et al., 2002).

Overall, these data suggest that chronic pain impairs the ability of vlPAG neurons to inhibit pain, which would perpetuate the chronic pain state. Disinhibition of the vlPAG-RVM pathway - such as is achieved during morphine administration - activates antinociception from the RVM, and increased $GABA_A$ currents prevent the ability of opioids to activate the descending antinociception circuit. Therefore, CFA induces changes in the vlPAG that would be consistent with a loss of descending inhibition in females (De Felice et al., 2011; Hahm et al., 2005).

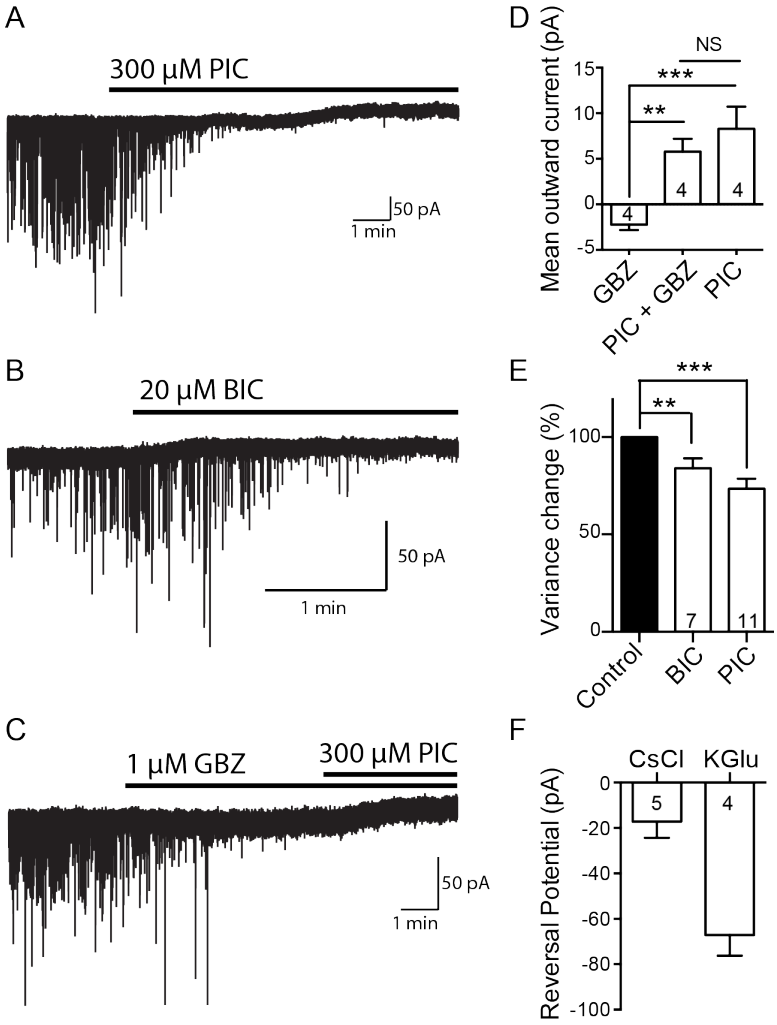


Figure 2.1: vlPAG neurons have an extrasynaptic $GABA_A$ current

Figure 2.1 Legend: A. Representative trace from a female vlPAG neuron following 20 μM DNQX application demonstrating that 300 μM PIC blocks sIPSCs and causes an outward shift in holding current. B. Representative trace from a vlPAG neuron demonstrating that 20 uM BIC blocks sIPSCs and causes an outward shift in holding current. C. GBZ (1 μM), a selective synaptic $GABA_A$ antagonist at low concentrations, blocks sIPSCs but does not affect the holding current. PIC (300 μM) shifts the holding current in the presence of GBZ (one-way ANOVA, Tukey's post-hoc analysis). D. Bar graph quantifying change in mean holding current with PIC (300 μM; 8.30 ± 2.42 pA), GBZ (1 μM; 5.78 ± 1.41 pA), and PIC + GBZ (-2.24 ± 0.59 pA), illustrating no significant change in current with GBZ application. PIC application significantly increased the holding current, regardless of the presence of GBZ (one-way ANOVA, $p < 0.01$, Tukey's post-hoc). E. Bar graph quantifying the effects of BIC and PIC on variance. BIC reduced the variance 73.5 ± 0.5% (n = 11). PIC reduced the variance 84.0 ± 0.5% (n = 7) **, $p < 0.01$; *** $p < 0.005$, one-way ANOVA. F. The reversal potential of the BIC-sensitive current is close to the predicted values for different $[Cl^-_{in}]$ and $[Cl^-_{out}]$ ratios.

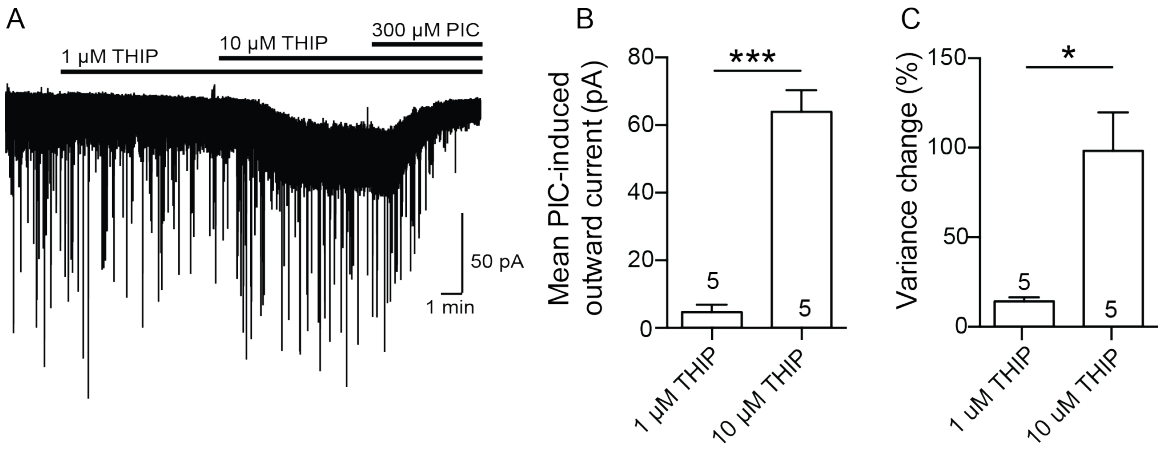


Figure 2.2: Agonists of the $GABA_A$ δ subunit enhance an inward current in vlPAG neurons in a concentration-dependent manner

A. Representative trace of the effects of the δ subunit agonist THIP (1 and 10 μM) on the holding current and variance of a vlPAG neuron. B. Quantification of the change in holding current induced by THIP. 10 μM significantly increased the current enhanced the current evoked by 1 μM THIP ($p < 0.001$, paired t-test). 10 μM THIP also significantly increased the variance over 1 μM THIP ($p < 0.01$, paired t-test).

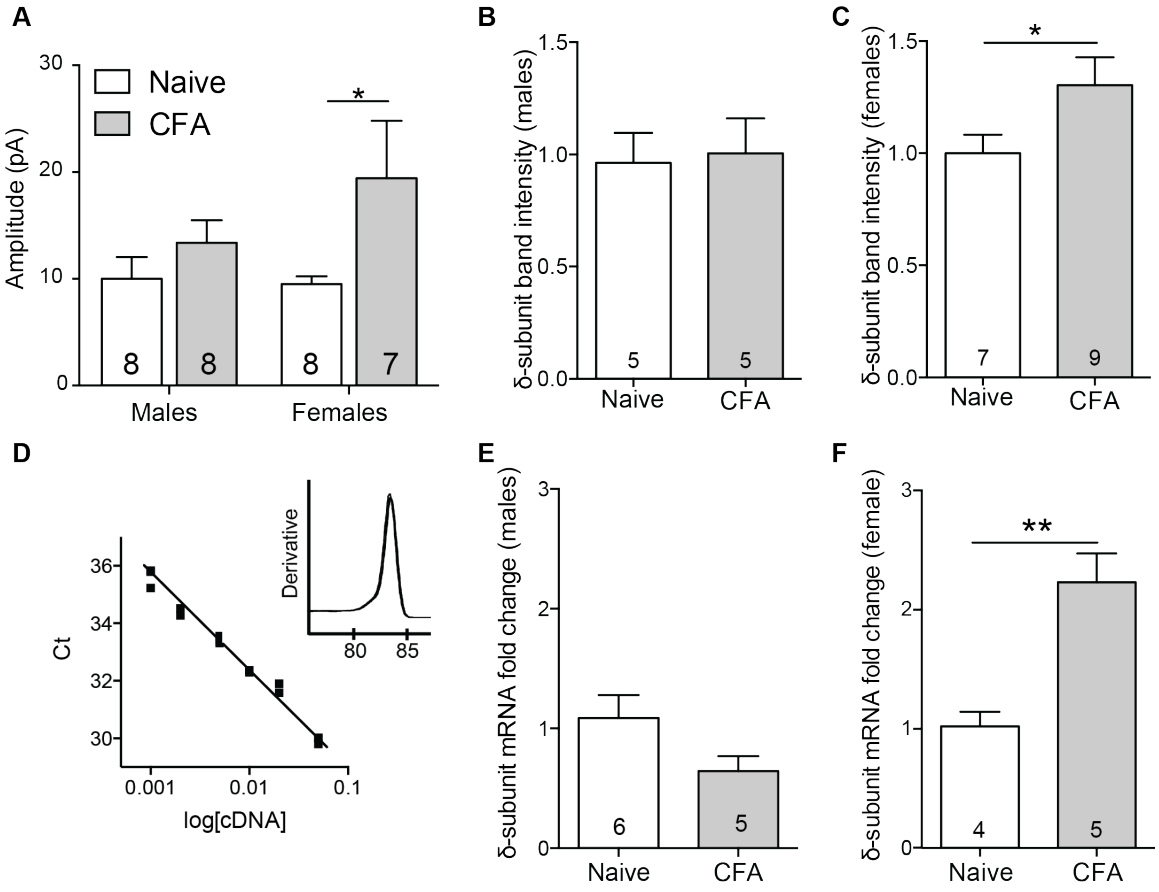


Figure 2.3: Chronic inflammatory pain increases $GABA_A$ δ function, protein, and mRNA expression in females, but not males.

A. Chronic inflammatory pain significantly increases the extrasynaptic GABAA current in vlPAG neurons in females. There was a significant effect of Treatment. The tonic current revealed with PIC (300 μM) was larger in CFA-treated females than males (2-way ANOVA, Bonferroni's, *$p < 0.05$) B. Chronic inflammatory pain has no effect on $GABA_A$ δ subunit protein expression in males. C. Chronic inflammatory pain significantly increases GABAA ? subunit protein expression in females (one-way t-test, $p < 0.05$). D. Standard curve regression line and slope of the GABAA ? subunit primers prepared using PAG cDNA (1:20 - 1:6400). The primer efficiency of 100% for the $GABA_A$ δ subunit as well as the β-actin control (95%, not shown) allowed analysis using the ΔΔCt method for quantification. Inset: Representative melting curve of $GABA_A$ δ, clearly illustrating one product without evidence of interference. E. Chronic inflammatory pain does not significantly affect $GABA_A$ δ subunit mRNA expression in males. F. Chronic inflammatory pain significantly increases $GABA_A$ δ subunit mRNA expression in females, as analyzed using the ΔΔCt method. (t-test,** $p < 0.01$).

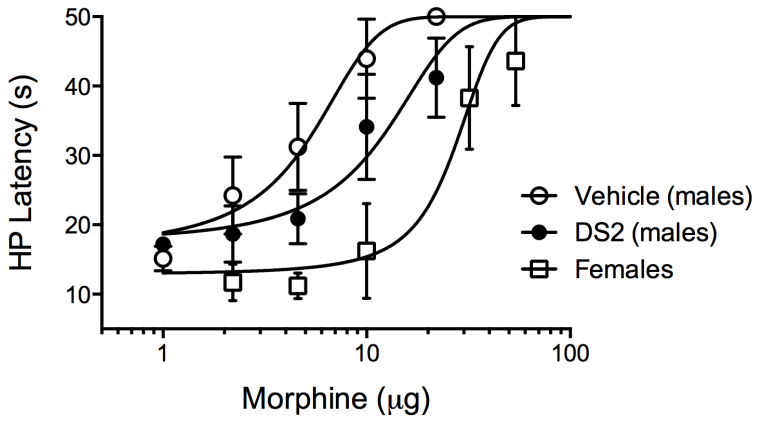


Figure 2.4: Allosteric modulation of the δ subunit by DS2 decreases morphine antinociception in vivo.

A. Dose response of morphine in animals pretreated with DMSO (n=6, vehicle, 0.5 mL) or DS2 (n=7, 3 mg in 0.5 mL) measured by hot plate latency. DS2-treated animals experience a significant rightward shift of the dose response curve, indicating a decrease in morphine potency (comparison of fits, $p < 0.05$). Females rats (n=6) are shifted even further to the right, and only very high morphine doses increased HP latency.

# Chapter 3

**Gene expression changes in the ventrolateral periaqueductal gray induced by two models of persistent inflammation in male and female rats.**

## 3.1 Abstract

During chronic pain, central nervous system plasticity contributes to the development of enhanced nociception. Some of these effects occur supraspinally in the descending modulatory pathway, which includes the ventrolateral periaqueductal gray (vlPAG). We sought to describe the plasticity induced by inflammatory pain in the vlPAG of amino acid receptors, transporters, and opioid receptors in prepubertal male and female rats. Gene expression of the $GABA_A$ receptor subunits $\alpha$ 1-6, $\beta$ 1-3, $\gamma$ 1-3, $\delta$, $\varepsilon$, $\vartheta$, $\pi$, and $\rho$ 1-3, GABA transporters 1-3, glutamate receptors GluR1-2, NR1, 2A-D, glutamate transport EAAT3, and mu, delta, and kappa opioid receptor were analyzed using Nanostring technology, a new method of gene expression that does not require amplification. Expression in the male vlPAG was investigated in naive, complete Fruend's adjuvant (CFA)- treated, and osteoarthritic (OA) rats. Females were evaluated between naive and CFA states. Naive males and females were also compared. CFA and OA treatment significantly downregulated DOPr in male rats,

and overall expression changed showed similar pattern between the two types of chronic inflammatory pain, indicating CFA represents long-term vlPAG plasticity changes. In females, GAT 1-3, NR1, NR2B-D, DOPr, and $GABA_A$ $\alpha 3$ subunit were upregulated by CFA treatment. Between naive males and females, DOPr and GAT3 were significantly higher in males, whereas $GABA_A$ $\varepsilon$ and $\vartheta$ were significantly higher in females. These findings identify targets that may underly the development and maintenance of chronic pain in the vlPAG. It also establishes that sexually dimorphic regulation of chronic pain occurs in the vlPAG.

## 3.2 Introduction

The ventrolateral periaqueductal gray (vlPAG) is an important site of control of the descending pain modulatory pathway (Heinricher and Ingram, 2008), where it primarily acts to inhibit pain. Opioid actions in the vlPAG are analgesic, as are $GABA_A$ antagonists and excitatory amino acids (Morgan et al., 1991; Jacquet and Lajtha, 1976; Bobeck et al., 2014). Conversely, the vlPAG can produce hyperalgesia following microinjection of bradykinin or capsaicin (Burdin et al., 1992; McGaraughty et al., 2003), which is believed to occur through a decrease in descending inhibition from the vlPAG. These *in vivo* studies indicate that the balance of excitatory and inhibitory signaling in the vlPAG is important during descending modulation.

The mechanisms that lead to the development of chronic pain are unknown. While changes to the rostral ventromedial medulla (RVM) and spinal cord have received significant attention during chronic pain, few studies have examined modulation within the vlPAG

(Sandkühler and Gebhart, 1984; Odeh and Antal, 2001; Tortorici and Morgan, 2002; Morgan et al., 2008). Upregulation of NMDA receptors (McGaraughty et al., 2003; Hu et al., 2009) and increased expression of specific serotonin receptors (Renno, 1998; Zhang et al., 2000, 2001) has been observed during chronic inflammatory pain indicating that the vlPAG undergoes expression changes during pain states.. These studies examined changes in male rats, using the Complete Freund's Adjuvant (CFA) model of inflammatory pain.

The CFA model of inflammatory pain is not completely analogous to human inflammatory pain, as it involves a prolonged immune response to an antigen. Recent models have attempted to more accurately model chronic pain conditions seen in humans. The osteoarthritis (OA) model most closely associated with human OA involves a single injection of monosodium iodoacetate (MIA) in the knee intra-articularly. This model produces acute and chronic pain states, joint destruction, mechanical hyperalgesia and allodynia, and CNS plasticity (Marker and Pomonis, 2012; Rahman et al., 2009; Ferreira-Gomes et al., 2012; Liu et al.; Thakur et al., 2012). This model may be better for chronic pain research, but it is not known how supraspinal plasticity may compare to CFA models.

Females have received little attention in inflammatory pain research, despite the overwhelming majority of pain patients being female (Berkley, 1997). Previous studies have illustrated a difference in the vlPAG anatomy and function in naïve and chronic pain states between males and females (Loyd and Murphy, 2006). These studies describe important differences in vlPAG Fos activation between males and females during chronic pain, suggesting that the balance of excitatory and inhibitory signaling is regulated differently between the sexes. However, specific genetic changes are unknown.

In order to examine the effect of chronic inflammatory pain in males and females, and between a CFA and OA model, we used a custom Nanostring codeset to look for changes

in mRNA expression. Nanostring is a proprietary method of gene expression analysis in which color-coded probes are designed against specific mRNA targets. This approach does not involve amplification, so bias is lower and the output is reflective of actual mRNA amount (Vaes et al., 2014). Genes of interest were those associated with excitatory and inhibitory signaling in the vlPAG: $GABA_A$ receptors, glutamate receptors, related transporters and opioid receptors (**Table 3.1**). mRNA levels were then evaluated for detectability, fold change, and significance between groups.

## 3.3 Materials & Methods

### Animals

Male (30-60 PND) and female (25-30 PND) Sprague Dawley rats were used for all experiments. 60 day old males were due to the length of OA treatment (28 days after injection); the remainder of males were used between 25-30 days. Animals were housed by treatment group in 12:12 light:dark cycle. Food and water were available ad libitum. All procedures were approved by the OHSU Animal Care and Use Committee.

### Complete Freund's Adjuvant (CFA) treatment

Animals were lightly anesthetized with inhalant isofluorane. 100 uL CFA was injected into the plantar surface of the hindpaw. At the time of sacrifice, 6 days after injection, paws were measured to confirm inflammation.

### Osteoarthritis (OA)

Sodium iodoacetate (MIA, Sigma, St. Louis MO) was dissolved in saline at a concentration of 4 mg/mL. 28-day old rats were anesthetized with inhalant isofluorane and the knee

was prepared for injection. 2 mg MIA was injected into the intraarticular space of the knee in a volume of 25 uL. Rats were allowed to recover for 4 weeks, to optimize development of OA (Pomonis et al., 2005; Marker and Pomonis, 2012).

**vlPAG dissections**

Rats were anesthetized with inhalant isofluorane and decapitated. The brains were rapidly removed and immersed in ice cold sterile artificial cerebrospinal fluid (aCSF) containing (in MM): 126 NaCl, 21.4 NaHC3, 11.1 Dextrose, 2.5 KCl, 2.4 CaCl2, 1.2 MgCl2, and 1.2 NaH2PO4. The midbrain was cut in to 5-6 100 mm segments using a block. Midbrain slices were placed on an ice-cold, RNAse free cutting surface. The vlPAG was quickly and carefully dissected using a dissecting microscope and placed in a 1:1 solution of RNAlater:water (Invitrogen, Carlsbad CA). Samples were placed at 4ºC until RNA isolation (within one week).

**RNA isolation**

Tissue was homogenized and RNA isolated according to instructions of the RNAqueous-Micro Total RNA Isolation Kit (Ambion, Carlsbad CA). RNA was measured on a Nanodrop (Thermoscientific, Waltham MA) for quantification and quality control. In general, 260/280 ratios were >2 and the 260/230 ratio >1.75, indicating little DNA or phenol contamination, respectively.

**Nanostring analysis**

Samples were prepared at 20 ng/uL and shipped to Nanostring (Seattle, WA) for hybridization. Briefly, samples were mixed with buffer and custom made CodeSet (Table 3.1) and allowed to hybridize overnight. The samples were then purified to remove excess

probes, and pipetted into an nCounter cartridge and placed in the nCounter device. The nCounter then quantified the light barcodes of each gene for sample mRNA. Six positive controls (128, 32, 8, 2, 0.5, and 0.125 fMol mRNA) as well as 8 negative (non-homologous sequences) controls were examined. One technical replicate per sample and 4-6 experimental replicates per group were performed.

**Data analysis**

Data were received as raw counts and analyzed using Nanostring's nSolver software. Because normalization depends on the positive controls and house keeping genes of the sample data, samples were analyzed all together. Samples were first normalized to the geometric mean of the positive controls to reduce plate variability. A ROUT outlier test (Q = 1%) was then performed on the "plate normalized" data (Motulsky and Brown, 2006). Samples that were identified as outliers in more than half of the test genes were removed from future analysis. Housekeeping gene counts ($\beta$-actin, Pgk1, Rpl19, and B2M) were analyzed next. Housekeeping genes were significantly different (t-test) between treated and untreated samples so values from each four housekeeping genes were subjected to analysis by geNorm, NormFinder and BestKeeper algorithms (Vandesompele et al., 2002; Andersen et al., 2004; Pfaffl et al., 2004). Data were renormalized to the plate without outlying samples or housekeeping genes (if any), the geometric mean of the background was removed, and the samples were normalized to housekeeping genes. Genes were removed if their expression fell below 5 counts after background subtraction. Detectability was listed based on the positive control ranges: Lowest (< 0.5 fM), low (0.5 – 2 fM) medium (2-8 fM), high (8-32 fM), highest (32-128 fM). Fold change was calculated using the ratios of count averages. When ratios were <1, the ratios were inversed to preserve distribution.

### Statistics

Statistics were performed using Prism (GraphPad, La Jolla CA). A one-way ANOVA was used, followed with a Holm-Sidak test of the following pairs: Male naïve vs male CFA, male naïve vs male OA, male naïve vs female naïve, female naïve vs female CFA. Genes of interest are reported by significance compared to their control, and/or a fold change above threshold (1.3). The term "significant" is only used in reference to significant statistical increases, not supra-threshold ratio values.

## 3.4 Results

### Data analysis

The three most stable housekeeping genes were PGK1, Rpl19, and B2M. $GABA_A\rho 2$, $\pi$, and $\alpha 6$ sununits were removed because expression was below threshold (< 5 counts after background subtraction). A recent study using RNAseq - a technique similar to Nanostring in its low bias and precise counts - demonstrated that biologically relevant genes undergo fold changes less than 2 (St Laurent et al., 2013). Based on these findings and considering the heterogeneity of the vlPAG, genes with either a significant change between groups or a fold change greater than 1.3 are discussed. All five groups were analyzed together using a one-way ANOVA.

### Males: CFA vs Naïve

In males, the effect of CFA on gene expression (n = 6) was compared against untreated males (n = 5) (Table 3.2). DOPr was decreased 1.47-fold in CFA-treated animals, and the values were significantly lower than naïve animals. The $GABA_A$ $\alpha 2$ was also significantly decreased by CFA treatment, but only experienced a 1.23-fold change in expression

(below threshold). Similarly, GAT3 was significantly reduced by CFA treatment, but had sub-threshold fold-change (1.26-fold). $GABA_A$ δ, ρ3, and ρ1 had a >1.3-fold decrease following CFA treatment, but were not significantly different between CFA and naïve groups.

**Males: OA vs. Naïve**

The effect of OA on gene expression was compared between OA-treated males (n = 4) and naïve males (n = 5) (Table 3.3). DOPr was significantly decreased by OA treatment 1.59-fold. The $GABA_A$ ϑ subunit was significantly increased by OA 1.72-fold. GAT1 was significantly decreased by OA treatment, but the degree of change was sub-threshold. $GABA_A$ δ subunit was 1.64-fold lower in OA animals, but the change was not significant. The $GABA_A$ ε subunit was 1.45-fold greater in OA animals, but also not significantly different from naïve.

**Females: CFA vs Naïve**

Naïve (n = 4) and CFA-treated (n = 5) females were compared (Table 3.4). Unlike males, females tended to show an increase in gene expression with CFA treatment. DOPr was significantly increased by CFA treatment, and expression was 1.5-fold greater. The $GABA_A$ α3 subunit 1.42-fold by CFA treatment, and was significantly increased over naïve. GAT1, GAT2, and GAT3 were significantly greater in CFA-treated animals, and upregulated 1.39, 1.8, and 1.31-fold, respectively. The AMPA receptor GluR1was increased 1.35-fold by CFA and was significantly greater than naïve animals. The NMDA receptors NR1, NR2B, NR2C, and NR2D were significantly increased by CFA treatment 1.35, 1.32, 1.77, and 1.83-fold, respectively. EAAT3 was significantly increased over naïve, but the fold change was <1.3.

**Naïve: Males vs. Females**

Expression differences between the sexes were also compared between naïve males (n = 5) and naive females (n = 5) (Table 3.5, Figure 3.5). DOPr was significantly lower in females than in males, and was reduced 1.92-fold. GAT3 was also significantly lower in females, at 1.36-fold less. The ε subunit of the $GABA_A$ receptor was significantly greater in females, with a 2.38-fold increase in expression. Similarly, the $GABA_A$ϑ subunit was significantly higher in females, with a fold-change of 1.95-fold. $GABA_A$δ, ρ1, NR2C, and GAT2 were more than 1.3-fold greater in females, but were not significantly different between the groups.

## 3.5 Discussion

**$GABA_A$subunits**

The α2 subunit of the $GABA_A$ receptor was significantly downregulated in CFA males, but the fold change was not substantial (Figure 3.1). This gene is linked to antinociception in the spinal cord (but not supraspinally; (Paul et al., 2014; Witschi et al., 2011)), but is of little interest due to its low degree of change. The α3 subunit was significantly increased 1.42-fold in CFA females. The α3 subunit is associated with preventing the development of hyperalgesia in the spinal cord (Zeilhofer et al., 2009). GABA currents mediated through $GABA_A$ receptors containing the α3 subunit have a longer decay, slower rise time and lower GABA affinity than α1-mediated receptors (Gingrich et al., 1995). Future electrophysiology studies in females should determine if the kinetics of inhibitory postsysnaptic currents show consistent changes following CFA treatment.

Little is known about the $\vartheta$ and $\varepsilon$ subunits. We found that both subunits showed a significant, above-threshold fold change in females compared to males. The $\varepsilon$ subunit of the $GABA_A$ receptor is homologous to the $\gamma$ subunit, can substitute for either the $\gamma$ or $\beta$ subunit of the synaptic $GABA_A$receptor (Jones and Henderson, 2007; Bollan et al., 2008). The presence of $\varepsilon$ in native tissue decreases the rise time of miniature inhibitory post-synaptic currents, and can be identified by insensitivity to flunitrazepam but sensitivity to diazepam (Belujon et al., 2009). The $\vartheta$ subunit is homologous to the $\alpha$ subunit, and is sensitive to etomidate (Bonnert et al., 1999; Ranna et al., 2006). Future work will have to examine the role of $\vartheta$ and $\varepsilon$ more closely. It is worth observing that $\vartheta$ and $\varepsilon$ are highly expressed in the locus coeruleus (Belujon et al., 2009), but it is unlikely that contamination is the source of expression in this experiment based on our dissection technique.

Several studies have shown the presence of the $\delta$ subunit protein in the vlPAG (Lovick et al., 2005; Griffiths and Lovick, 2005). However, in this study the $\delta$ subunit had low detectability in the vlPAG, and thus a greater degree of variability. The low detectability may be due to the probe design or overall low mRNA expression. However, the fact that the $\delta$ subunit is lower in females is interesting in light of our previous work, which found sex differences in the regulation of the $\delta$ subunit during chronic pain. The Nanostring results did not reflect the qRT-PCR results, which is likely due to the poor detectability of the $\delta$ subunit in the Nanostring array. A similar pattern of downregulation was observed in CFA males in the Nanostring and qRT-PCR (Figure 2.3), but neither of these changes were significant.

For the first time, the $\rho$1 and 3 subunits of the $GABA_A$ receptor (previously $GABA_C$) have been reported in the vlPAG. Unlike the other $GABA_A$ receptors, rho subunits assemble in homo- or heteropentamers with other $\rho$ subunits (Olsen and Sieghart, 2008).

Rho-containing receptors mediate currents that have a low conductance, low rate of desensitization, and low mean opening time (Chebib, 2004). The ρ1 knockout mice have decreased mechanical pain thresholds, but it's difficult to know where this effect is localized (Zheng et al., 2003). However, Lau et al. (2014) found that the ρ antagonist 1,2,5,6-tetrahydropyridin-4-yl)methylphosphinic acid hydrate (TPMPA) had no effect on the tonic current in the vlPAG, and their low detectability may be indicative of weak expression or contamination by neighboring regions.

**Glutamate receptors**

The glutamate receptors generally showed more change by CFA females than in males (Figure 3.2). The expression levels were the same between the sexes, except for GluR2, which was significantly greater in females but less than 1.3-fold higher. The significant increase of AMPA receptor GluR1 was above threshold in CFA females. In addition, the NMDA receptors NR1, NR2B, NR2C, and NR2D were significantly increased above threshold in CFA females. CFA increases glutamate mEPSC amplitude in vlPAG in males, with a coincident increase in NR2B and GluR1 from whole PAG homogenate (Hu et al., 2009). Our data did not reflect this in males, but that could be due to limiting the study to the ventrolateral portion of the PAG.

**Opioid receptors**

Changes in MOPr and DOPr were of particular interest, as both are expressed in RVM-projecting vlPAG neurons (Wang and Wessendorf, 2002). DOPr was the only gene that changed in all conditions measured, although females showed opposite regulation from males (Figure 3.3). These data are consistent with other studies that demonstrate that DOPr

is a site of regulation in dorsal root neurons during CFA-induced chronic pain (Cahill et al., 2003; Pradhan et al., 2013).

### GABA transporters

The GABA transporters GAT1, GAT2, and GAT3 were very different between males and females, and between CFA/OA and naïve groups (Figure 3.4). The GAT1 was significantly lower in OA males animals, but the fold change of this regulation was subthreshold. In CFA males, GAT3 was significantly lower, but this change was also subthreshold. Interestingly, all of the GAT transporters were significantly increased in CFA females more than 1.3-fold. Blockade of GAT1 and 3 can increase extrasynaptic $GABA_A$ signaling (Farrant and Nusser, 2005). GAT1 is localized presynaptically, while GAT3 is found on astrocytes (Kersanté et al., 2013). The role of GAT2 in the brain is less clear because it is has been shown to be localized to ependymal and arachnoid cells (Ikegaki et al., 1994). This inverse regulation of GABA transport may be driven by the increase in GABA release in CFA females (Chapter 2). The changes in GAT subtypes in males and females during chronic inflammation are promising as mediators of GABA signaling changes during chronic pain, and warrant further investigation.

### Pattern expressions

Overall, OA males showed similar changes as CFA males. The notable differences are in $GABA_A\alpha2$ and $\beta1$, KOPr, and MOPr; however, these changes were not above threshold. Besides the mode of inflammation, these models vary in time course. The similarity between male OA and CFA rats indicates that long-term plasticity changes seen in the 4-week OA model may have already developed in the 6-day CFA model. These data indicate that

the CFA model is an accurate representation of long term chronic pain plasticity changes, at least the vlPAG.

The differences between male and female vlPAG expression was striking (Figure 3.5). Not only were a number of genes differentially expressed between the sexes, but also CFA females had a very different pattern of gene regulation during CFA. The most promising targets are the $GABA_A$ epsilon and theta subunits, which are higher in females but a site of regulation during chronic pain in males.

The advantage of the Nanostring approach is that it does not require amplification and thus introduces less bias, and results (counts) accurately quantify the amount of mRNA in the cells (Kulkarni, 2011; Vaes et al., 2014). Furthermore, it enables us to run a number of genes at once while maintaining a narrow scope. We have used selective vlPAG microdissections to limit our findings to the area relevant to descending modulation of pain. We have described data both in terms of significant changes between groups and fold change, based on findings from St. Laurent et al. (2013). These data give us targets for future studies of the differences in vlPAG signaling between males and females, as well as changes after CFA and OA treatment. We will follow up on these targets using electrophysiology, behavior and/or protein expression analysis, to confirm physiological relevance of the changes detected.

| Identifier | Gene | Accession No. | Probe Target (bp) | Detectability |
|---|---|---|---|---|
| $GABA_A\alpha1$ | *Gabra1* | NM_183326.2 | 2747-2846 | Higher |
| $GABA_A\alpha2$ | *Gabra2* | NM_001135779.1 | 61-160 | High |
| $GABA_A\alpha3$ | *Gabra3* | NM_017069.3 | 191-290 | Low |
| $GABA_A\alpha4$ | *Gabra4* | NM_080587.3 | 716-815 | Medium |
| $GABA_A\alpha5$ | *Gabra5* | NM_017295.1 | 1357-1456 | Medium |
| $GABA_A\alpha6$ | *Gabra6* | NM_021841.1 | 19-118 | ND |
| $GABA_A\beta1$ | *Gabrb1* | NM_012956.1 | 751-850 | High |
| $GABA_A\beta2$ | *Gabrb2* | NM_012957.2 | 673-772 | Higher |
| $GABA_A\beta3$ | *Gabrb3* | NM_017065.1 | 1161-1260 | High |
| $GABA_A\gamma1$ | *Gabrg1* | NM_080586.1 | 1249-1348 | High |
| $GABA_A\gamma2$ | *Gabrg2* | NM_183327.1 | 731-830 | High |
| $GABA_A\gamma3$ | *Gabrg3* | NM_024370.3 | 1047-1146 | High |
| $GABA_A\delta$ | *Gabrd* | NM_017289.1 | 411-510 | Low |
| $GABA_A\varepsilon$ | *Gabre* | NM_023091.1 | 2551-2650 | Medium |
| $GABA_A\pi$ | *Gabrp* | NM_031029.1 | 181-280 | ND |
| $GABA_A\rho1$ | *Gabrr1* | NM_017291.1 | 3371-3470 | Lowest |
| $GABA_A\rho2$ | *Gabrr2* | NM_017292.1 | 1546-1645 | ND |
| $GABA_A\rho3$ | *Gabrr3* | NM_138897.1 | 441-540 | Lower |
| $GABA_A\vartheta$ | *Gabrq* | NM_031733.1 | 159-258 | Medium |
| GluR1 | *Gria1* | NM_031608.1 | 856-955 | High |
| GluR2 | *Gria2* | NM_017261.2 | 1533-1632 | High |
| NR1 | *Grin1* | NM_001270602.1 | 1963-2062 | High |
| NR2A | *Grin2a* | NM_012573.3 | 3495-3594 | Medium |
| NR2B | *Grin2b* | NM_012574.1 | 3169-3268 | Medium |
| NR2C | *Grin2c* | NM_012575.3 | 4237-4336 | Medium |
| NR2D | *Grin2d* | NM_022797.1 | 3297-3396 | Low |
| DOPr | *Oprd1* | NM_012617.1 | 731-830 | Low |
| KOPr | *Oprk1* | NM_017167.2 | 571-670 | Medium |
| MOPr | *Oprm1* | NM_001038597.2 | 1119-1218 | Medium |
| GAT1 | *Slc6a1* | NM_024371.2 | 2901-3000 | High |
| GAT2 | *Slc6a11* | NM_024372.1 | 1391-1490 | Low |
| GAT3 | *Slc6a13* | NM_133623.1 | 1509-1608 | Higher |
| EAAT3 | *Slc1a1* | NM_013032.3 | 1576-1675 | High |
| $\beta$-actin | *Actb* | NM_031144.3 | 73-172 | High |
| B2M | *B2m* | NM_012512.1 | 286-385 | Highest |
| PGK1 | *Pgk1* | NM_053291.3 | 1566-1665 | High |
| Rpl19 | *Rpl19* | NM_031103.1 | 593-692 | High |

Table 3.1: Gene list and expression levels in the vlPAG

Table 3.1 legend: Genes are listed by colloquial identifier, gene, and accession number. The probe target is given in bp. Detectability in the vlPAG is listed as follows: Lowest (< 0.125 fM), Lower (0.125-0.5 fM), Low (0.5-2 fM), Medium (2-8 fM), High (8-32 fM), Higher (32-128 fM), Highest (> 128 fM), or not detected (ND).

| Gene | Fold Change | Signficant? |
|---|---|---|
| $GABA_A\delta$ | -1.86 | |
| $GABA_A\rho3$ | -1.5 | |
| DOPr | -1.47 | Yes |
| $GABA_A\rho1$ | -1.39 | |
| GAT3 | -1.26 | Yes |
| GAT2 | -1.18 | |
| NR2D | -1.17 | |
| MOPr | -1.15 | |
| NR1 | -1.14 | |
| $GABA_A\gamma1$ | -1.14 | |
| EAAT3 | -1.13 | |
| $GABA_A\alpha2$ | -1.13 | Yes |
| $GABA_A\alpha3$ | -1.13 | |
| GAT1 | -1.12 | |
| NR2C | -1.11 | |
| GluR1 | -1.09 | |
| NR2B | -1.08 | |
| $GABA_A\gamma2$ | -1.07 | |
| $GABA_A\beta3$ | -1.07 | |
| NR2A | -1.06 | |
| $GABA_A\beta1$ | -1.06 | |
| $GABA_A\alpha5$ | -1.05 | |
| $GABA_A\gamma3$ | -1.04 | |
| $GABA_A\beta2$ | -1.03 | |
| KOPr | -1.03 | |
| $GABA_A\alpha1$ | 1.01 | |
| $GABA_A\alpha4$ | 1.05 | |
| GluR2 | 1.09 | |
| $GABA_A\vartheta$ | 1.36 | |
| $GABA_A\varepsilon$ | 1.41 | |

Table 3.2: Expression changes in CFA males

Genes are listed in order of magnitude of the ratio of CFA (n = 6) vs naive (n = 5) animals (fold change). Values greater than 1 are upregulated in CFA animals. A fold change was considered relevant if it was greater than 1.3. Significance between CFA and naive within a particular gene were caluclated by a one-way ANOVA, followed by the Holm-Šidák post-hoc test. Significant values were $p < 0.05$.

| Gene | Fold Change | Signficant? |
|---|---|---|
| $GABA_A\delta$ | -1.64 | |
| DOPr | -1.59 | Yes |
| NR2C | -1.24 | |
| GAT2 | -1.21 | |
| $GABA_A\rho1$ | -1.21 | |
| NR2D | -1.2 | |
| $GABA_A\rho3$ | -1.19 | |
| GAT1 | -1.18 | |
| EAAT3 | -1.16 | Yes |
| NR1 | -1.14 | |
| GAT3 | -1.08 | |
| $GABA_A\beta2$ | -1.06 | |
| NR2A | -1.06 | |
| $GABA_A\alpha1$ | -1.05 | |
| $GABA_A\gamma2$ | -1.05 | |
| $GABA_A\alpha5$ | -1.04 | |
| $GABA_A\alpha3$ | -1.03 | |
| $GABA_A\alpha2$ | -1.02 | |
| GluR1 | -1.01 | |
| NR2B | -1.01 | |
| $GABA_A\beta3$ | 1.01 | |
| $GABA_A\gamma1$ | 1.02 | |
| MOPr | 1.04 | |
| $GABA_A\gamma3$ | 1.06 | |
| $GABA_A\alpha4$ | 1.08 | |
| $GABA_A\beta1$ | 1.15 | Yes |
| KOPr | 1.16 | |
| GluR2 | 1.17 | |
| $GABA_A\varepsilon$ | 1.45 | |
| $GABA_A\vartheta$ | 1.72 | Yes |

Table 3.3: Expression changes in OA males

Genes are listed in order of magnitude of the ratio of OA (n = 4) vs naive (n = 5) animals (fold change). Values greater than 1 are greater in OA animals. A fold change was considered relevant if it was greater than 1.3. Significance between OA and naive within a particular gene were caluclated by a one-way ANOVA, followed by the Holm-Šidák post-hoc test. Significant values were $p < 0.05$.

| Gene | Fold Change | Significant? |
|---|---|---|
| $GABA_A\vartheta$ | -1.16 | |
| $GABA_A\gamma 2$ | -1.10 | |
| $GABA_A\beta 2$ | -1.10 | |
| $GABA_A\alpha 1$ | -1.09 | |
| Kopr | -1.09 | |
| $GABA_A\gamma 1$ | -1.08 | |
| $GABA_A\beta 1$ | -1.06 | |
| $GABA_A\beta 3$ | -1.05 | |
| GluR2 | 1.00 | |
| $GABA_A\alpha 5$ | 1.02 | |
| $GABA_A\rho 1$ | 1.05 | |
| $GABA_A\rho 3$ | 1.05 | |
| $GABA_A\delta$ | 1.05 | |
| $GABA_A\alpha 4$ | 1.10 | |
| Mopr | 1.10 | |
| $GABA_A\alpha 2$ | 1.10 | |
| $GABA_A\varepsilon$ | 1.13 | |
| NR2A | 1.14 | |
| $GABA_A\gamma 3$ | 1.15 | |
| EAAT3 | 1.20 | |
| GAT3 | 1.31 | Yes |
| NR2B | 1.32 | Yes |
| GluR1 | 1.35 | Yes |
| NR1 | 1.35 | Yes |
| GAT1 | 1.39 | Yes |
| $GABA_A\alpha 3$ | 1.42 | Yes |
| DOPr | 1.50 | Yes |
| NR2C | 1.77 | Yes |
| GAT2 | 1.81 | Yes |
| NR2D | 1.83 | Yes |

Table 3.4: Expression changes in CFA females

Genes are listed in order of magnitude of the ratio of CFA (n = 5) vs naive (n = 4) animals (fold change). Values greater than 1 are higher in CFA animals. A fold change was considered relevant if it was greater than 1.3. Significance between CFA and naive within a particular gene were caluclated by a one-way ANOVA, followed by the Holm-Šidák post-hoc test. Significant values were $p < 0.05$.

| Gene | Fold change | Significant? |
|---|---|---|
| DOPr | -1.92 | Yes |
| $GABA_A\rho 1$ | -1.79 | |
| GAT2 | -1.52 | |
| NR2C | -1.41 | |
| $GABA_A\delta$ | -1.39 | |
| GAT3 | -1.36 | Yes |
| NR2D | -1.25 | |
| GAT1 | -1.22 | Yes |
| $GABA_A\alpha 3$ | -1.19 | |
| NR2A | -1.17 | |
| NR1 | -1.15 | |
| GluR1 | -1.13 | |
| NR2B | -1.12 | |
| MOPr | -1.12 | |
| $GABA_A\alpha 2$ | -1.08 | |
| EAAT3 | -1.08 | |
| $GABA_A\beta 2$ | -1.01 | |
| $GABA_A\alpha 1$ | -1.01 | |
| $GABA_A\beta 3$ | 1.03 | |
| $GABA_A\alpha 5$ | 1.03 | |
| $GABA_A\beta 1$ | 1.03 | |
| $GABA_A\gamma 1$ | 1.04 | |
| $GABA_A\gamma 3$ | 1.05 | |
| $GABA_A\alpha 4$ | 1.05 | |
| $GABA_A\gamma 2$ | 1.06 | |
| KOPr | 1.07 | |
| GluR2 | 1.22 | Yes |
| $GABA_A\rho 3$ | 1.36 | |
| $GABA_A\vartheta$ | 1.95 | Yes |
| $GABA_A\varepsilon$ | 2.38 | Yes |

Table 3.5: Expression changes between males and females

Genes are listed in order of magnitude of the ratio of naive males (n = 5) vs naive females (n = 5) (fold change). Values greater than 1 are higher in females animals. A fold change was considered relevant if it was greater than 1.3. Significance between CFA and naive within a particular gene were caluclated by a one-way ANOVA, followed by the Holm-Šidák post-hoc test. Significant values were $p < 0.05$.

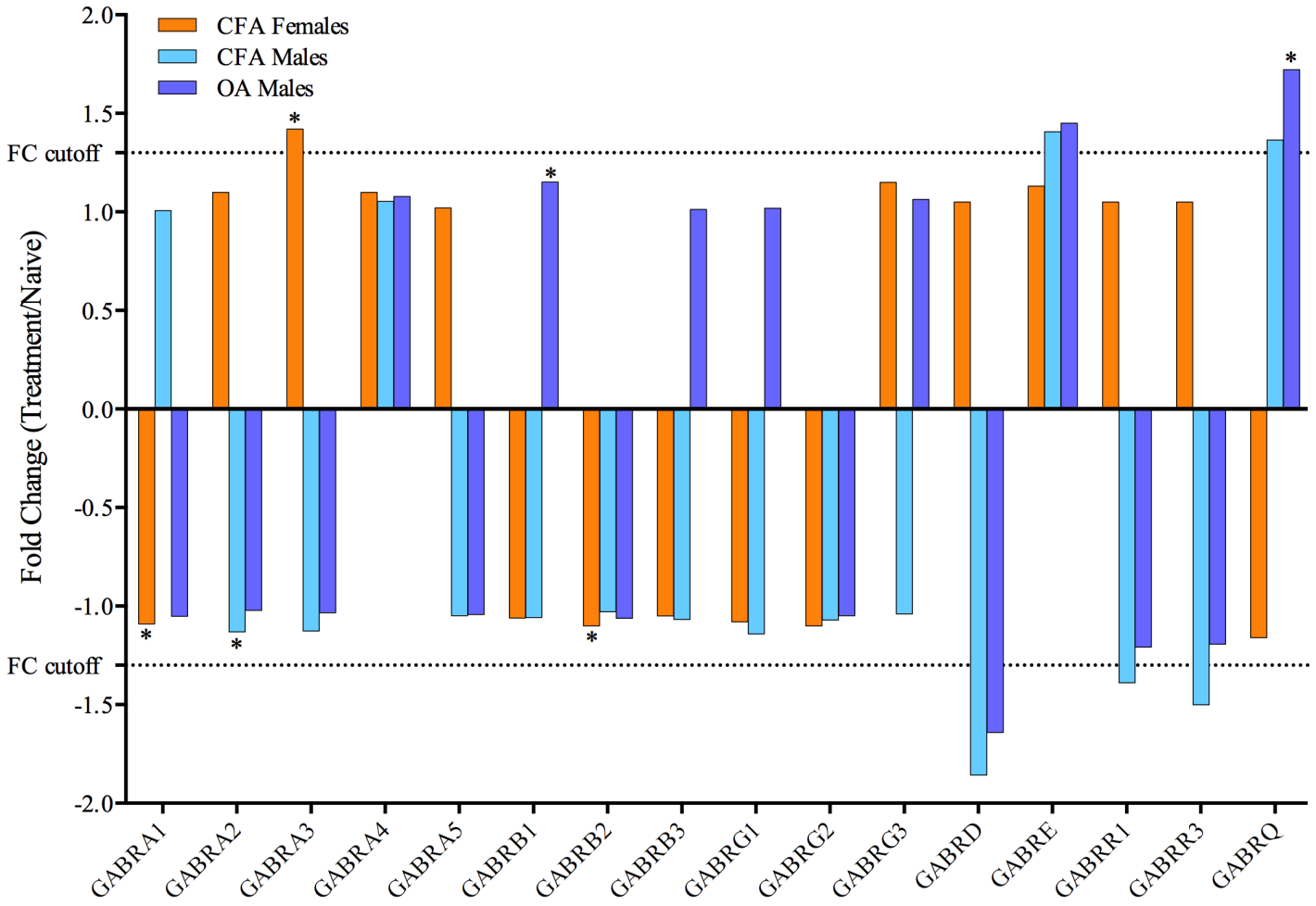


Figure 3.1: Fold change in $GABA_A$ receptor subunit expression of CFA females, CFA males, and OA males. All ratios were made from the appropriate control: CFA females vs. naive females, OA and CFA males vs. naive males. Asterisks indicate significance between CFA or OA and naive within a particular gene, and were caluclated by a one-way ANOVA followed by the Holm-Šidák post-hoc test. Significant values were $p < 0.05$.

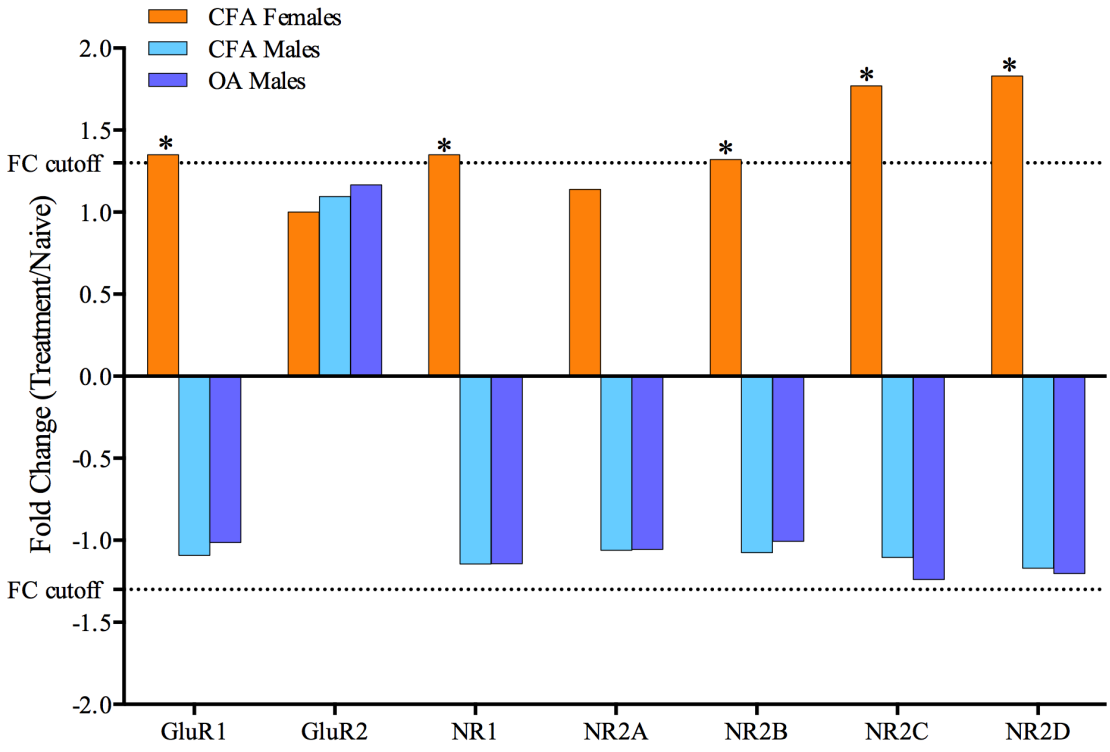


Figure 3.2: Fold change in AMPA and NMDA receptor expression among CFA females, CFA males, and OA males.

Asterisks indicate significance between CFA or OA and naive within a particular gene, and were caluclated by a one-way ANOVA followed by the Holm-Šidák post-hoc test. Significant values were $p < 0.05$.

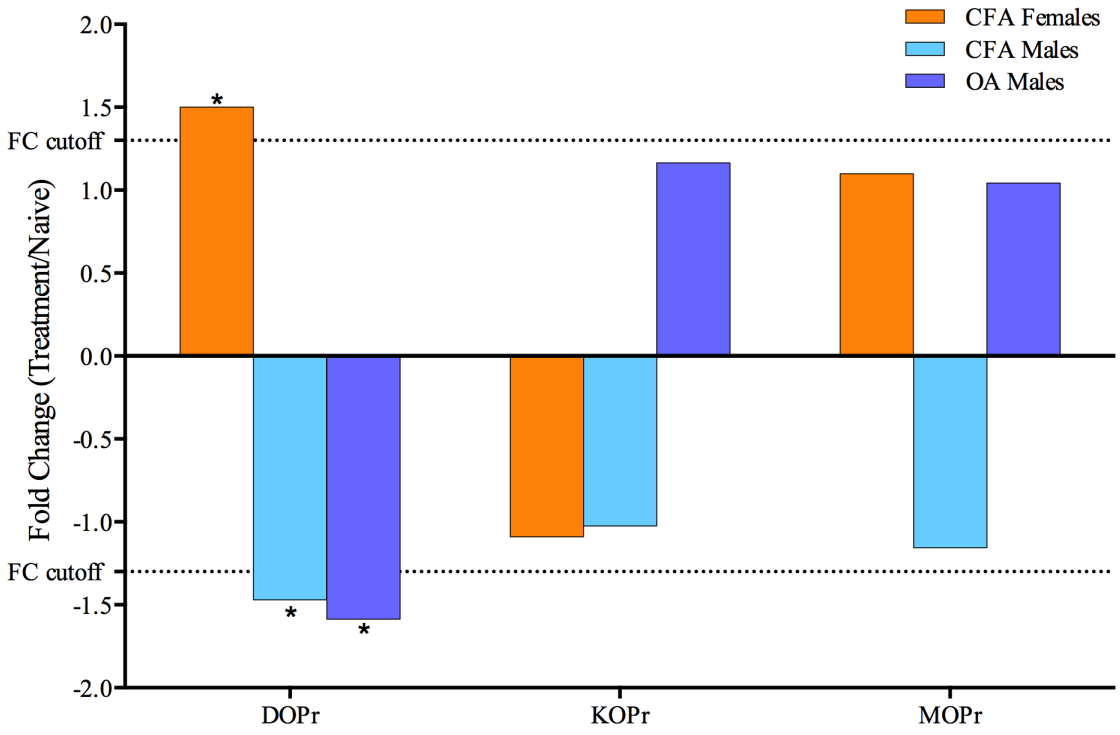


Figure 3.3: Fold change in opioid receptor expression among CFA females, CFA males, and OA males

Asterisks indicate significance between CFA or OA and naive within a particular gene, and were caluclated by a one-way ANOVA followed by the Holm-Šidák post-hoc test. Significant values were $p < 0.05$.

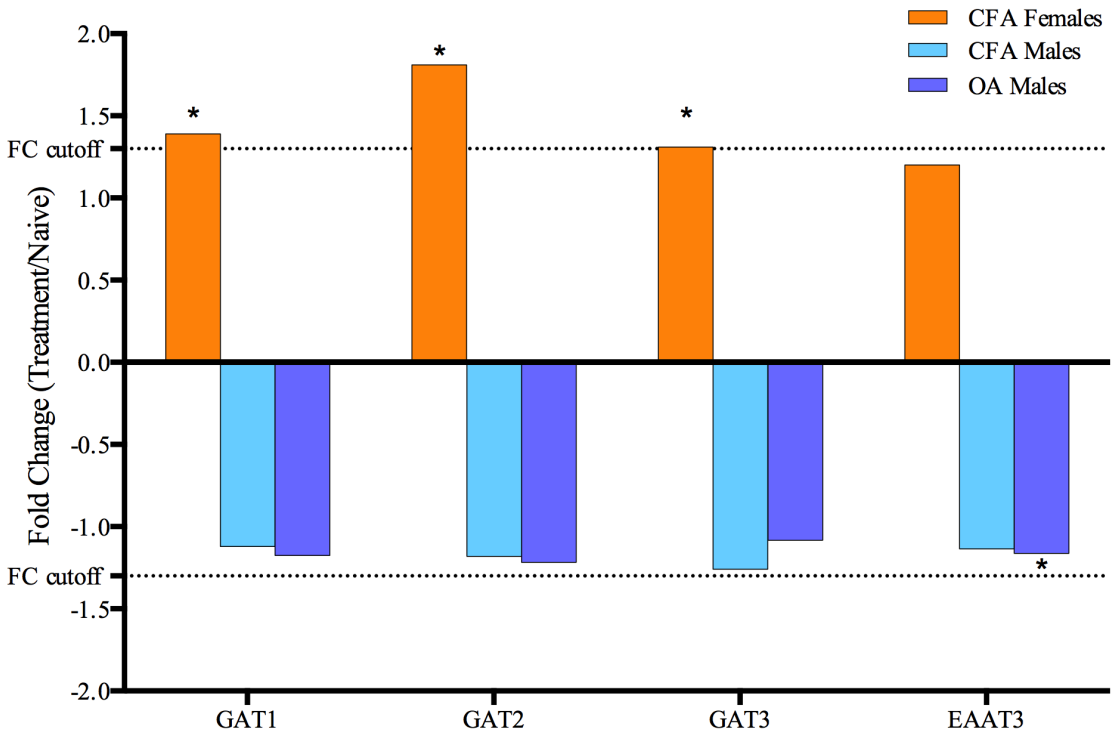


Figure 3.4: Fold change in amino acid transporter expression among CFA females, CFA males, and OA males

Asterisks indicate significance between CFA or OA and naive within a particular gene, and were caluclated by a one-way ANOVA followed by the Holm-Šidák post-hoc test. Significant values were $p < 0.05$.

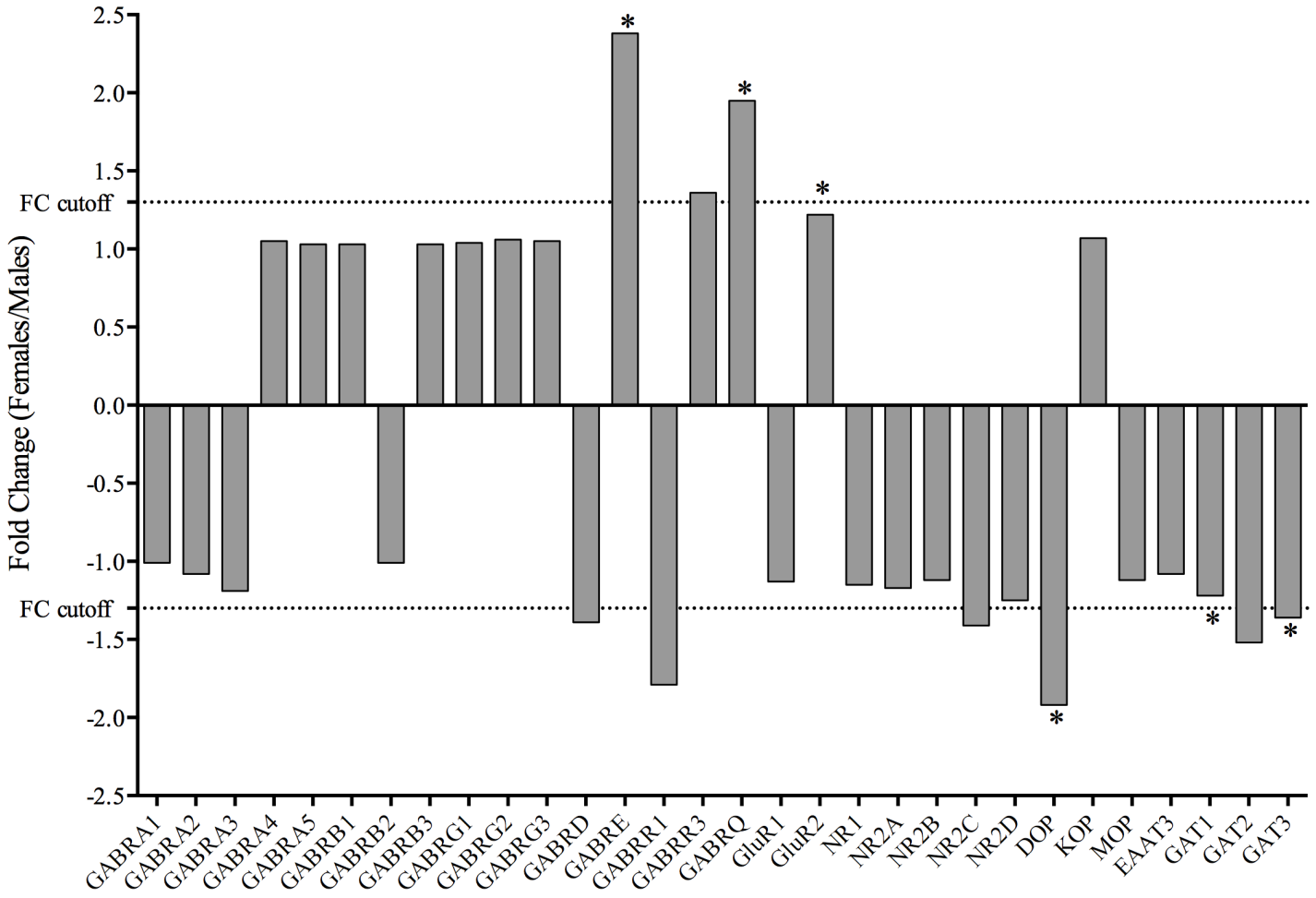


Figure 3.5: Fold change between males and females for all genes

Graphical representation of the fold changes between naive males and naive females (Table 4.5). Ratio is males vs females, so positive values are greater in females. Asterisks indicate significance between males and females within a particular gene, caluclated by a one-way ANOVA followed by the Holm-Šidák post-hoc test. Significant values were $p < 0.05$.

# Chapter 4

**Fibromyalgia patients exhibit photoaversion compared to healthy controls: A pilot study.**

## 4.1 Abstract

Abnormal widespread pain in fibromyalgia (FM) is thought to involve pathological amplification of pain signals in a phenomenon known as central sensitization. FM patients exhibit widespread hyperalgesia and allodynia, but no evidence of tissue damage or inflammation. These observations indicate that abnormal sensory processing, potentially caused by central sensitization, may underlie FM. However, there are no diagnostic tests for central sensitization in FM or other chronic pain states.

Observations by Martenson et. al (unpublished) suggest that light can enhance pain-facilitating neurons in animals models of central sensitization. Because central sensitization is believed to underly chronic pain in humans, we tested the hypothesis that photosensitivity is greater in patients with FM compared to healthy controls. Photosensitivity was measured in healthy controls (n = 24) and subjects with FM (n = 24). Pressure sensitivity was also measured. FM subjects exhibited lower thresholds for light-evoked discomfort and pain

compared to healthy controls, and light thresholds were positively correlated with pressure thresholds. Thus, photosensitivity is a potentially novel clinical test for evaluating central sensitization in patients with FM and other chronic pain conditions.

## 4.2 Introduction

Chronic pain is one of the most costly and disabling chronic health care conditions in the world. In the United States, chronic pain is estimated to affect around 100 million adults - more than heart disease, cancer, and diabetes combined (Institute of Medicine, 2011). Clinically significant chronic pain can be disproportionate to any identifiable injury or inflammation, persist long after any triggering insult has healed, or arise without injury (Mackey and Maeda, 2004; Staud, 2013). Sensitization, peripheral and/or central, can contribute to the development and maintenance of chronic pain in animal models (Woolf, 2011; Latremoliere and Woolf, 2009; Cagnie et al., 2014). In idiopathic chronic pain conditions, such as fibromyalgia, irritable bowel syndrome, or migraines, central sensitization is believed to be the source of the pathological pain. However, the ability to connect our findings of central sensitization in animal models to the human condition of chronic pain is hindered by the invasiveness of studying neuronal activity in these subjects.

Fibromyalgia (FM) is a chronic pain condition of unknown etiology that affects 2% of the United States population, predominately women (Wolfe et al., 1995). It is characterized by deep, continuous musculoskeletal pain (Merskey and Bogduk, 1994). FM is diagnosed by a "tender point" exam, in which pressure is applied to sites identified as producing pain in FM patients (Merskey and Bogduk, 1994). This exam is effectively a test of hyperalgesia, and it is contingent on activation of peripheral of nociceptors. While it is widely believed

that FM is caused by central sensitization (Heinricher et al., 2009; Porreca et al., 2002), there is no diagnostic tool available to distinguish peripheral and central sensitization.

Pain-facilitating neurons in the rostral ventromedial medulla (RVM) have been shown to be activated by light in rat models of central sensitization (Martenson et al., unpublished observations). There are anecdotal reports that patients with FM exhibit extreme sensitivity to light (Yunus 2008), but this sensitivity has never been quantified. We hypothesize that light may also activate these pain-facilitating neurons in FM patients. To this end, we investigated photosensitivity in patients with FM compared to healthy controls.

## 4.3 Materials & Methods

### Study Participants

The cross-sectional study was reviewed and approved by the Oregon Health & Science University institutional review board, and written consent was obtained from all study participants. There were 48 participants: 24 FM and 24 pain-free healthy control (HC) subjects. All subjects were female and predominately Caucasian (Table 1). FM subjects were aged 21 to 70 years with a verified FM diagnosis (with 1990 ACR-criteria)(Wolfe et al., 1990) recruited from a local FM network in the Pacific Northwest (Fibromyalgia Information Foundation). HCs were age-matched females (within 5 years) recruited from OHSU's research message board. FM subjects had average overall pain scores of 6 or greater over the past month. Exclusion criteria included male sex, current use of certain prescription medications (patients must have had more than three days of abstinence from tricyclic antidepressants, trazadone, nortriptyline, SNRIs, pregabalin, gabapentin, and/or narcotics to be included), significant eye pathology (glaucoma, blindness, macular degeneration),

drugs known to alter pupillary dilation, and diseases typically associated with light sensitivity (uveitis, iritis, dry eyes requiring prescription medication, glaucoma, panic attacks, and post-concussive syndrome).

**Questionnaires**

All subjects gave consent after explanation of the study and verification of medication list. Basic demographic information and associated symptoms were assessed using standardized questionnaires validated for use in the FM population, the Revised Fibromyalgia Impact Questionnaire (FIQR) and its non-FM variant the Revised Symptom Impact Questionnaire (SIQR) for FM and HC, respectively (Friend and Bennett, 2011; Bennett et al., 2009).

**Procedure**

Subjects were dark-adapted for 30 minutes in a dark room on a massage table with adjustable pillows and blankets. Pressure sensitivity was then determined using pressure algometry (dolorimetry) at the mid-volar forearm of the subject's dominant arm in 3 trials. Subjects were then positioned with their heads on an adjustable chinrest in front of an Espion E2 photostimulator (Diagnosys LLC, Cambridge UK). Light was delivered for 2 seconds on followed by 2 seconds off, and flashes measured from 0.25 - 3981 candelas/m2 (luminance; cd/m2). The first stimulus measured 0.25 cd/m2, and each subsequent stimulus was twice as bright as the previous one. The researcher specified: "As I increase the brightness of the light, please let me know when it starts to bother you." The mean intensity at which subjects indicated discomfort was determined on each of five trials, separated by two-minute darkness intervals. Following five "discomfort" trials, light intensity was

increased until the subject indicated pain (intolerance; single trial). Thresholds for discomfort and intolerance to brightness were recorded. The lights were then turned on slowly, and dolorimetry at the mid-volar forearm was performed again.

### Data analysis

Data analysis was performed in Graphpad (La Jolla, CA) or R. Demographics (age, ethnicity), baseline clinical characteristics (current pain, associated symptoms), and overall impact of disease (FIQR, SIQR) were assessed and compared using independent sample t-tests or chi-squared tests. Dolorimetry was analyzed by a 2-way ANOVA. Luminance measures were converted to logarithmic values and analyzed with an unpaired t-test for discomfort and pain thresholds.

## 4.4 Results

### Clinical characteristics

In total, 802 female subjects were emailed, 131 responded and were assessed for eligibility (16.33%), 50 were offered an interview, and 48 subjects were enrolled (24 per group). Basic demographic information of both study groups is provided in Table 4.1. Mean age for FM patients was 50 years compared to 47 years in control group (not significant). Both groups were 92% Caucasian. For the disease functional domain, FM patients had significantly higher mean FIQR scores compared to control SIQR scores (53.1 and 2.9; $p < 0.001$, t-test).

### Dolorimetry

The median pressure thresholds for FM and HC subjects prior to testing were 1.3 ±

0.1 and 2.3 ± 0.3 kg respectively. Pressure thresholds for FM and HC subjects after the light testing were 1.3 ± 0.7 and 3.4 ± 0.4 kg, respectively (Figure 4.1). 2-way ANOVA revealed a significant effect of group on pressure threshold, with no effect of time or group by time interactions. Pressure thresholds were significantly greater in HCs in both trials ( $p < 0.0001$, Tukey's post-hoc test). Within group, there was no difference between trials (Tukey's post-hoc test).

**Photosensitivity analysis**

The five discomfort trials were averaged and one value was reported for each subject. Mean light discomfort thresholds were 9.38 ± 3.64 and 1150 ± 234.8 cd/m2 for FM and HC subjects respectively ($p < 0.001$, t-test, Figure 4.2). Mean light intolerance threshold was 140.7 ± 83.80 and 1862 ± 381.7 cd/m2 for FM and HC subjects respectively ($p < 0.001$, t-test, Figure 4.3).

**Correlation analysis**

Light discomfort and pressure threshold were significantly correlated ($r = 0.60$, $p < 0.0001$, Spearman correlation), as were light threshold and pressure threshold ($r = 0.67$, $p < 0.0001$, Spearman correlation).

## 4.5 Discussion

In this study, we observed that fibromyalgia subjects experienced significantly more photoaversion than healthy controls measured on light-provoked discomfort or pain. We also found that light discomfort and pain were significantly correlated with pressure threshold, a validated measure of hyperalgesia in FM patients (Kosek et al., 1995; Jespersen et al., 2007;

Gracely et al., 2003). These findings indicate that the processes underlying photoaversion are sensitized during FM.

Light does not activate nociceptors, and the mechanism through which it becomes painful is unknown. The eye is innervated by small-diameter sensory fibers that sense mechanical, temperature, and noxious stimuli (Zander and Weddell, 1951). One study has found that extremely bright light (10-20,000 lux, daylight) intensity can activate nociceptive neurons in the trigeminal ganglion, presumable through these ocular afferents (Okamoto et al., 2010). However, as the FM subjects showed light discomfort and pain at substantially lower intensities (~10 - 150 cd/m2), we believe the photoaversion does not arise through activation of the trigeminal ganglion.

Light sensitive cells, such as rods, cones, and intrinsically-photosensitive retinal ganglion cells, relay light detection to the occipital cortex, olivary pretectal nucleus, thalamus, and suprachiasmatic nucleus (Noseda et al., 2010; Berson et al., 2002; Do and Yau, 2010; Wilhelm, 2008). Because light detection is a critical component of photophobia (Digre and Brennan, 2012), we believe that light pain may be produced through one or more of these central relays. Unpublished observations from M. Martenson demonstrate light shone in the eye of a rat can activate pain-facilitating neurons in the RVM. Furthermore, this effect is enhanced during models of central sensitization. These observations support our findings in FM patients, identifying light as a promising marker of impaired descending pain modulation.

In order to validate abnormal photosensitivity as a marker of central sensitization, future studies will measure this parameter in other chronic pain populations. Differential light sensitivity between chronic pain syndromes with and without suspected central sensitization would demonstrate that this effect is central in nature. Alternatively, functional

MRI could be used to detect activation of the brainstem areas involved in descending modulation, such as the RVM. Future animal studies will attempt to elucidate the signaling mechanisms of photophobia and the cellular mechanisms behind the enhanced excitability of the pain-facilitating neurons.

| **Patient Characteristic** | **FM subjects (n = 24)** | **Control subjects (n = 24)** |
|---|---|---|
| Age (mean (SD) in years) | 50 (14) | 47 (14) |
| Ethnicity (% Caucasian) | 92% | 92% |
| FIQR/SIQR* (mean (SD)) | 53.1 (18) | 2.3 (3) |

** FIQR = Fibromyalgia Impact Questionnaire-Revised; SIQR = Symptom Impact Questionnaire-Revised*

Table 4.1: Fibromyalgia and healthy control subject characteristics

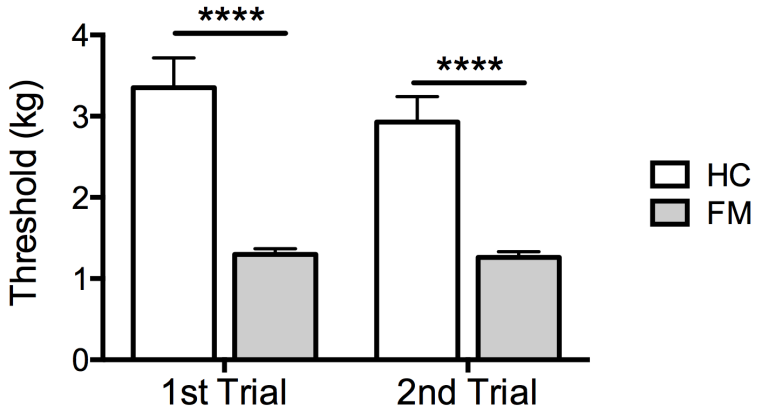


Figure 4.1: Pressure thresholds of healthy control and fibromyalgia subjects before and after light test

Pressure thresholds of healthy controls and fibromyalgia subjects before (1st) and after (2nd) photosensitivity protocol. FM subjects had significantly lower threshold scores than HCs (**** $p<0.0001$, Tukey's post-hoc). No difference existed within groups between the two trials.

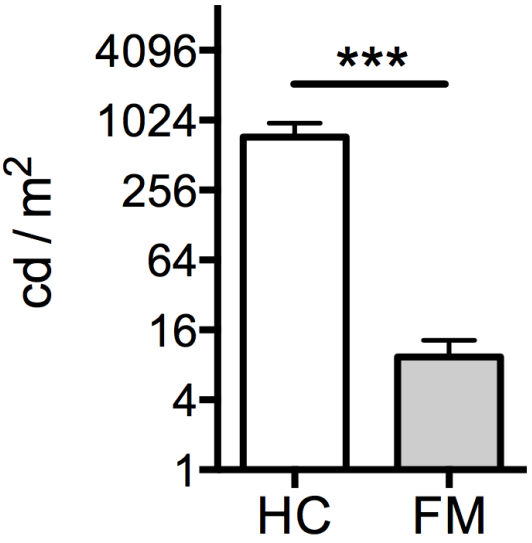


Figure 4.2: Light discomfort of healthy control and fibromyalgia subjects

Mean luminance (cd/m2) of light discomfort threshold in fibromyalgia patients and healthy controls. FM subjects had significantly lower light discomfort thresholds than HCs (*** $p < 0.001$, unpaired t-test). Error bars are in SEM.

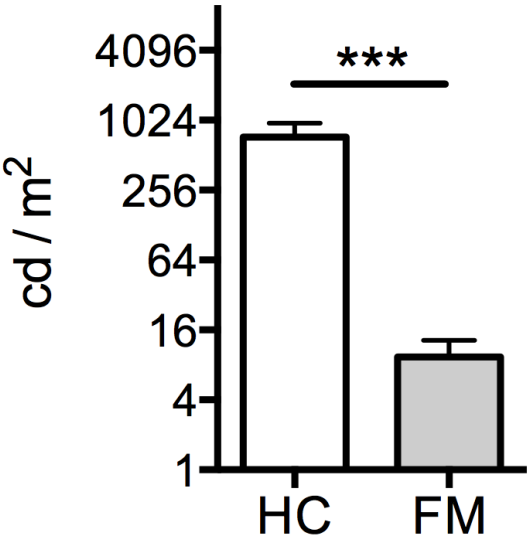


Figure 4.3: Light threshold of healthy control and fibromyalgia subjects

Mean luminance (cd/m2) of light pain threshold in fibromyalgia patients and healthy controls. FM subjects had significantly lower light discomfort thresholds than HCs (*** $p < 0.001$, unpaired t-test). Error bars are in SEM.

# Chapter 5

# Discussion

Females have lower pain thresholds than males, and MOPr agonists in the vlPAG are dramatically less potent and efficacious (Mogil and Chanda, 2005; Bobeck et al., 2009; Krzanowska and Bodnar, 1999; Loyd et al., 2007). It is clear that the periaqueductal gray may be the source of sex-dependent effects of pain. The present results demonstrate differential expression of GABA, glutamate, and opioid receptors in the vlPAG of males and females. Furthermore, chronic inflammatory pain initiates different plasticity mechanisms between the sexes. These findings indicate a distinct role for the vlPAG in mediating sex differences in pain.

Most chronic pain patients are middle-aged women, and a disproportionate number of chronic pain conditions affect more women than men (Greenspan et al., 2007). Chronic pain causes pathological changes in the neural substrates that underly descending modulation of pain (Kuner, 2010; Puretić and Demarin, 2012; Ossipov et al., 2014; Kwon et al., 2013). These changes sometimes manifest as central sensitization, in which there is a heightened response to pain. However, central sensitization is a laboratory phenomenon,

and has not been demonstrated in humans. Herein, data demonstrate that light is a novel marker of central sensitization in fibromyalgia patients.

## 5.1 Sex differences

**Genomic analysis**

The vlPAG has a different genomic "thumbprint" in males and females. Recent studies in humans have identified variable gene expression between males and females throughout most of the brain, and involving 2.5% of genes (Trabzuni et al., 2013). We discovered that almost one third of the genes on our array had an estrogen response element in either humans or rats (Bourdeau et al., 2004). Unsurprisingly, the genes that increased more than 1.3-fold and were significantly greater in females than males - DOPr and GAT3 - have estrogen response elements, although estrogen hasn't been demonstrated to upregulate expression of these specific genes (Herbison and Fénelon, 1995). To confirm that these differences are truly sex-specific and not an experimental artifact, the expression analysis should be repeated in postnatally gonadectomized animals. By removing the organization effect of ovarian steroid hormones, we would expect to see no difference between male and female vlPAG gene expression.

By identifying expression changes between the sexes, we can develop strategies to understand the mechanisms behind lower nociceptive thresholds and reduce morphine analgesia in females relative to males. For example, the increase in GAT3 expression in males indicates that females may have less GAT function than males, and that GABA may persist in the synaptic cleft longer. Furthermore, GAT3 is decreased in CFA-treated males, where as GAT 1, 2, and 3 are increased in CFA females. Interestingly, GAT1 expression also

increases in the vlPAG during opioid withdrawal (Bagley et al., 2011). These data suggest GAT function and subsequent effects on GABA signaling may be very important during both chronic pain and opioid withdrawal, functions mediated by the vlPAG. While preliminary studies revealed no effect of GAT inhibition on the holding current (Tonsfeldt et al., unpublished observations), future studies should examine GAT function in evoked IPSCs to determine how modulation could affect vlPAG neuron regulation.

Another interesting finding was upregulation of glutamate receptors in females during chronic pain. This effect was not seen in males. Previous findings have shown that MOPr agonists can block presynaptic glutamate release on vlPAG neurons (Chieng and Christie, 1994b). *In vivo* studies show that microinjection of excitatory amino acids into the vlPAG produces antinociception (Jacquet and Lajtha, 1976). These studies were performed in males. Given the robust change in glutamate receptor expression in females, it would be interesting to investigate if glutamate signaling plays a greater role in females, with or without chronic pain. Future studies could evaluate the behavioral effect of vlPAG glutamate antagonism in females, as well as the ability of morphine to block glutamate release *in vitro.*

**Functional analysis**

vlPAG neurons are believed to produce descending inhibition through an increase in activity to the RVM. Therefore, the extrasynaptic $GABA_A$ current in the vlPAG may contribute to chronic pain through a decrease in descending inhibition. It is a critical regulator of neuronal excitability in many systems, including the hippocampus and cerebellum (Luscher et al., 2011). The presence of an extrasynaptic $GABA_A$ current in the vlPAG (Chapter 3, (Lau, 2011)) indicates that this current may be involved in regulated vlPAG output neuron excitability. Chronic pain, induced by CFA treatment, increases the expression

and function of the extrasynaptic current in females. The extrasynaptic current produces inhibition through shunting or Cl- influx. The antianalgesic actions of THIP (Depaulis et al., 1987) and DS2 (Figure 2.4) support an inhibitory role of the extrasynaptic $GABA_A$ current in the vlPAG. Therefore, an increase in the extrasynaptic current in RVM-projecting vlPAG neurons would make activation of these neurons - which produces antinociception - harder to achieve (Figure 5.1). This hypothesis is supported by *in vivo* data of the effect of microinjections of the extrasynaptic $GABA_A$ agonist THIP in the vlPAG: THIP administration attenuates the ability of the vlPAG to produce opioid analgesia (Depaulis et al., 1987).

The vlPAG has been implicated in a number of sex specific behaviors, including lordosis (Arendash and Gorski, 1983) and maternal behaviors (Lonstein and Stern, 1998) that relay through the RVM (Cottingham et al., 1987). Therefore, the increase in the number of vlPAG-RVM projections in females isn't particularly surprising (Loyd and Murphy, 2006). However, the differential regulation of the extrasynaptic $GABA_A$ current in males and females during chronic pain suggests different cellular mechanisms may contribute to chronic pain between males and females. The extrasynaptic $GABA_A$ current was not different between naive pre-pubertal males and females (Figure 2.3). However, as estrogen can increase $GABA_A$ delta expression (including in the vlPAG), the extrasynaptic $GABA_A$ current should be compared between adult male and females.

It has been repeatedly demonstrated that vlPAG administration of morphine has lower analgesic efficacy and potency in adult females than males (Bobeck et al., 2009; Wang et al., 2006; Krzanowska and Bodnar, 1999). Enhancement of the extrasynaptic $GABA_A$ current in males attenuates morphine potency (Depaulis et al., 1987). The differential regulation of the extrasynaptic current in juvenile females may persist into adulthood, where

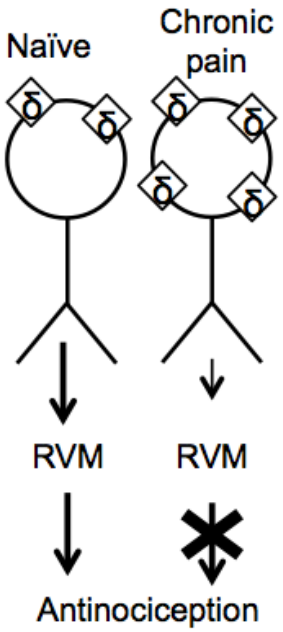


Figure 5.1: Diagram of extrasynaptic $GABA_A$subunit plasticity during chronic inflammatory pain
Diagram shows expression of the extrasynaptic $GABA_A$ receptors ($\delta$ subunit) in RVM-projecting PAG neuron during naïve (left) and chronic inflammation (right) states. Increased expression of the $\delta$ subunit and tonic $GABA_A$ signaling increases inhibition of vlPAG neurons, which may decrease the ability of the vlPAG to activate the RVM and diminish antinociception.

the expression of the delta subunit will also be subject to estrogen regulation. A reduced ability to activate vlPAG neurons through an increase in the extrasynaptic $GABA_A$ current - whether from chronic pain or estrogen - could contribute to the decrease in morphine analgesia in females. The ability of enhanced extrasynaptic $GABA_A$ current to attenuate morphine antinociception should be investigated in adult, intact females. These studies should also investigate if MOPr agonists can block presynaptic $GABA_A$ release with the same potency in males and females.

These findings are especially interesting in light of data that bicuculline injection into the vlPAG is significantly less effective at producing analgesia in adult females than in males (Bobeck et al., 2009). These results could be due to an increase in GABA signaling in females compared to males (including the extrasynaptic current). The inability of GABA blockade, through opioids or bicuculline, to produce the same degree of analgesia in females as males points to distinct mechanisms that make the vlPAG less effective at producing analgesia in females.

## 5.2 Translational potential

If the extrasynaptic $GABA_A$ current attenuates antinociception by decreasing vlPAG neuronal excitability, it may be possible to inhibit the $GABA_A$ delta subunit to control pain. Selective inhibition of the extrasynaptic $GABA_A$ current in the vlPAG would be analgesic, which is supported by the analgesic actions of bicuculline microinjection (Bobeck et al., 2009). So far, no compounds selectively inhibit the extrasynaptic $GABA_A$ receptor. Broad

$GABA_A$ antagonists, such as pentylenetetrazol (metrazol), are anxiogenic and epileptogenic, and would therefore be a poor choice for treating chronic pain (Jung et al., 2002; Papp et al., 1987).

The $GABA_A$ δ is also expressed in the spinal cord, although at low levels (Ma et al., 1993). Intrathecal and systemic administration of the $GABA_A$ agonist THIP can produce antinociception (Bonin et al., 2011; Kendall et al., 1982; Murray et al., 1983), suggesting opposite effects between the periphery and the vlPAG. If enhancement of the extrasynaptic $GABA_A$ current in the periphery is analgesic, it would preclude the use of a systemic extrasynaptic $GABA_A$ antagonist as an analgesic. Of course, these studies were all performed in males, and whether estrogen modulation of the δ subunit expression could generate a sex-specific effect is unknown.

## 5.3 Diagnostic utility of light

Patients with chronic pain have altered nociception. The term "central sensitization," which describes the amplification of nociceptive signals, arose from phenomena observed in laboratory studies. The term is used to define facilitory mechanisms attributed to the development and maintenance of chronic pain in humans, but central sensitization has never been demonstrated in chronic pain patients. The disparity is due to the invasive nature of the methods used to demonstrate central sensitization, including electrophysiology and gene expression analysis of central tissues. The presence of central sensitization is inferred by increased responsiveness in behavioral tests, such as the tender point exam described in Chapter 2; however, these tests rely on relays through the peripheral nervous system.

In contrast, light-evoked pain is not believed to depend on activation of the spinal cord, or at least not at low thresholds (Okamoto et al., 2010). Instead, preliminary findings in rodent models of central sensitization suggest light acts through a purely central pathway to activate pain-facilitating RVM neurons and produce photophobia (Martenson et al., unpublished observations). Thus, the increase in nociceptive response to light in patients with chronic pain is a promising marker of central sensitization in this population. If light-evoked pain is a truly supraspinal process, it could be used to further separate central sensitivity into that originating at the spine versus the brain. To investigate the transduction of light, future animal studies should attempt to determine which of the potential pathways outlined in Chapter 4 could activate RVM neurons.

These findings increase the translational potential of laboratory findings of central sensitization to patients with actual chronic pain. By expanding central sensitization from a laboratory to a clinical setting, these findings enhance our understanding of the mechanisms that maintain chronic pain in human populations. While the etiology of FM is unknown, these findings suggest that these patients have similar increases in descending facilitation as seen in rodents. By confirming that FM arises from abnormal plasticity of central and not peripheral circuits, these pathways can be targeted by pharmaceuticals to enhance FM treatment.

Following further validation of the photosensitivity assay, it could also be used to indicate central nervous system involvement in other chronic pain conditions. We would expect to see a similar finding in conditions in which central sensitization is strongly implicated - for example, inflammatory bowel syndrome or migraine. However, photosensitivity could also be useful to detect the degree of central sensitization in conditions with more complex etiologies, such as osteoarthritis or neuropathic pain. Not all patients with conditions like

osteoarthritis develop chronic pain, and in many musculoskeletal pain conditions, the degree of pain experienced is unrelated to the amount of tissue damage. Early identification of patients with a central component of pain will help direct treatment in this population.

## 5.4 Conclusion

The etiology of chronic pain caused by central sensitization is complex. The results confirm findings in rodents that light activates pain-facilitating neurons, implying an increase in descending facilitation. On the other hand, the increase in the extrasynaptic $GABA_A$ current with chronic pain implies a decrease in descending inhibition. These results support one mechanism of chronic pain to be decreased descending inhibition from the vlPAG. Further characterization of the vlPAG - RVM connection will help illuminate the importance of these changes during chronic pain.

Furthermore, the present results challenge the almost exclusive use of males in chronic pain research. The nature of the distinct expression profiles and functional differences between male and female rats suggests similar mechanisms may underly the sex differences in pain. Further analysis in adult animals will help establish the vlPAG as a sexually dimorphic region of pain control.

# References


Adkins CE, Pillai GV, Kerby J, Bonnert TP, Haldon C, McKernan RM, Gonzalez JE, Oades K, Whiting PJ, Simpson PB (2001) alpha4beta3delta GABA(A) receptors characterized by fluorescence resonance energy transfer-derived measurements of membrane potential. *The Journal of Biological Chemistry* 276:38934–9.

Andersen CL, Jensen JL, Orntoft TF (2004) Normalization of real-time quantitative reverse transcription-PCR data: a model-based variance estimation approach to identify genes suited for normalization, applied to bladder and colon cancer data sets. *Cancer Research* 64:5245–50.

Arancibia-Cárcamo IL, Kittler JT (2009) Regulation of GABA(A) receptor membrane trafficking and synaptic localization. *Pharmacology & Therapeutics* 123:17–31.

Arendash GW, Gorski RA (1983) Suppression of lordotic responsiveness in the female rat during mesencephalic electrical stimulation. *Pharmacology, Biochemistry, and Behavior* 19:351–7.

Arnold AP (2009) The organizational-activational hypothesis as the foundation for a unified theory of sexual differentiation of all mammalian tissues. *Hormones and Behavior* 55:570–8.

Bagley EE, Hacker J, Chefer VI, Mallet C, McNally GP, Chieng BCH, Perroud J, Shippenberg TS, Christie MJ (2011) Drug-induced GABA transporter currents enhance GABA release to induce opioid withdrawal behaviors. *Nature Neuroscience* 14:1548–54.

Bandler R, Shipley MT (1994) Columnar organization in the midbrain periaqueductal gray: modules for emotional expression? *Trends in Neurosciences* 17:379–389.

Barbaro NM (1988) Studies of PAG/PVG stimulation for pain relief in humans. *Progress in Brain Research* 77:165–73.

Barnard EA, Seeburg PH (1988) Structural basis of the GABA-activated chloride channel: molecular biology and molecular electrophysiology. *Advances in biochemical psychopharmacology* 45:1–18.

Bartley EJ, Palit S, Kuhn BL, Kerr KL, Terry EL, Delventura JL, Rhudy JL (2014) Nociceptive processing in women with premenstrual dysphoric disorder (PMDD): The role of menstrual phase and sex hormones. *The Clinical Journal of Pain* .

Basbaum AI, Fields HL (1984) Endogenous pain control systems: brainstem spinal pathways and endorphin circuitry. *Annual Review of Neuroscience* 7:309–38.

Basbaum AI, Jessell TM (2013) Pain In Kandel E, Schwartz J, Jessell T, Siegelbaum S, Hudspeth A, editors, *Principles of Neural Science*, chapter 24, pp. 530–553. New York, fifth edition.

Behbehani MM, Jiang MR, Chandler SD, Ennis M (1990) The effect of GABA and its antagonists on midbrain periaqueductal gray neurons in the rat. *Pain* 40:195–204.

Beitz A (1982) The organization of afferent projections to the midbrain periaqueductal gray of the rat. *Neuroscience* 7:133–159.

Belujon P, Baufreton J, Grandoso L, Boué-Grabot E, Batten TFC, Ugedo L, Garret M, Taupignon AI (2009) Inhibitory transmission in locus coeruleus neurons expressing GABAA receptor epsilon subunit has a number of unique properties. *Journal of Neurophysiology* 102:2312–25.

Bennett RM, Friend R, Jones KD, Ward R, Han BK, Ross RL (2009) The Revised Fibromyalgia Impact Questionnaire (FIQR): validation and psychometric properties. *Arthritis Research & Therapy* 11:R120.

Berkley KJ (1997) Sex differences in pain. *The Behavioral and Brain Sciences* 20:371–80.

Berson DM, Dunn FA, Takao M (2002) Phototransduction by retinal ganglion cells that set the circadian clock. *Science* 295:1070–3.

Bobeck EN, Chen Q, Morgan MM, Ingram SL (2014) Contribution of Adenylyl Cyclase Modulation of Pre- and Postsynaptic GABA Neurotransmission to Morphine Antinociception and Tolerance. *Neuropsychopharmacology* 39:2142–52.

Bobeck EN, McNeal AL, Morgan MM (2009) Drug dependent sex-differences in periaqueducatal gray mediated antinociception in the rat. *Pain* 147:210–6.

Bodnar RJ, Romero MT, Kramer E (1988) Organismic variables and pain inhibition: Roles of gender and aging. *Brain Research Bulletin* 21:947–953.

Bollan KA, Baur R, Hales TG, Sigel E, Connolly CN (2008) The promiscuous role of the epsilon subunit in GABAA receptor biogenesis. *Molecular and Cellular Neurosciences* 37:610–21.

Bonin RP, Labrakakis C, Eng DG, Whissell PD, De Koninck Y, Orser BA (2011) Pharmacological enhancement of $\delta$-subunit-containing GABA(A) receptors that generate a tonic inhibitory conductance in spinal neurons attenuates acute nociception in mice. *Pain* 152:1317–26.

Bonnert TP, McKernan RM, Farrar S, le Bourdellès B, Heavens RP, Smith DW, Hewson L, Rigby MR, Sirinathsinghji DJ, Brown N, Wafford KA, Whiting PJ (1999) theta, a novel gamma-aminobutyric acid type A receptor subunit. *Proceedings of the National Academy of Sciences of the United States of America* 96:9891–6.

Bourdeau V, Deschênes J, Métivier R, Nagai Y, Nguyen D, Bretschneider N, Gannon F, White JH, Mader S (2004) Genome-wide identification of high-affinity estrogen response elements in human and mouse. *Molecular Endocrinology* 18:1411–27.

Brack KE, Lovick TA (2007) Neuronal excitability in the periaqueductal grey matter during the estrous cycle in female Wistar rats. *Neuroscience* 144:325–35.

Bradshaw H, Miller J, Ling Q, Malsnee K, Ruda M (2000) Sex differences and phases of the estrous cycle alter the response of spinal cord dynorphin neurons to peripheral inflammation and hyperalgesia. *Pain* 85:93–99.

Breivik H, Collett B, Ventafridda V, Cohen R, Gallacher D (2006) Survey of chronic pain in Europe: prevalence, impact on daily life, and treatment. *European Journal of Pain* 10:287–333.

Brickley SG, Mody I (2012) Extrasynaptic GABA(A) receptors: their function in the CNS and implications for disease. *Neuron* 73:23–34.

Bright DP, Smart TG (2013) Methods for recording and measuring tonic GABAA receptor-mediated inhibition. *Frontiers in Neural Circuits* 7:193.

Brown N, Kerby J, Bonnert TP, Whiting PJ, Wafford KA (2002) Pharmacological characterization of a novel cell line expressing human alpha(4)beta(3)delta GABA(A) receptors. *British Journal of Pharmacology* 136:965–74.

Burdin TA, Graeff FG, Pelá IR (1992) Opioid mediation of the antiaversive and hyperalgesic actions of bradykinin injected into the dorsal periaqueductal gray of the rat. *Physiology & Behavior* 52:405–10.

Burnham LJ, Dickenson AH (2013) The antinociceptive effect of milnacipran in the monosodium iodoacetate model of osteoarthritis pain and its relation to changes in descending inhibition. *The Journal of Pharmacology and Experimental Therapeutics* 344:696–707.

Burstein R, Potrebic S (1993) Retrograde labeling of neurons in the spinal cord that project directly to the amygdala or the orbital cortex in the rat. *The Journal of Comparative Neurology* 335:469–85.

Cagnie B, Coppieters I, Denecker S, Six J, Danneels L, Meeus M (2014) Central sensitization in fibromyalgia? A systematic review on structural and functional brain MRI. *Seminars in Arthritis and Rheumatism* 44:68–75.

Cahill CM, Morinville A, Hoffert C, O'Donnell D, Beaudet A (2003) Up-regulation and trafficking of delta opioid receptor in a model of chronic inflammation: implications for pain control. *Pain* 101:199–208.

Calza A, Sogliano C, Santoru F, Marra C, Angioni MM, Mostallino MC, Biggio G, Concas A (2010) Neonatal exposure to estradiol in rats influences neuroactive steroid concentrations, GABAA receptor expression, and behavioral sensitivity to anxiolytic drugs. *Journal of Neurochemistry* 113:1285–95.

Cepeda MS, Carr DB (2003) Women experience more pain and require more morphine than men to achieve a similar degree of analgesia. *Anesthesia and Analgesia* 97:1464–8.

Chappell AS, Ossanna MJ, Liu-Seifert H, Iyengar S, Skljarevski V, Li LC, Bennett RM, Collins H (2009) Duloxetine, a centrally acting analgesic, in the treatment of patients with osteoarthritis knee pain: a 13-week, randomized, placebo-controlled trial. *Pain* 146:253–60.

Chebib M (2004) GABAC receptor ion channels. *Clinical and Experimental Pharmacology & Physiology* 31:800–4.

Chia YY, Chow LH, Hung CC, Liu K, Ger LP, Wang PN (2002) Gender and pain upon movement are associated with the requirements for postoperative patient-controlled iv analgesia: a prospective survey of 2,298 Chinese patients. *Canadian Journal of Anaesthesia* 49:249–55.

Chieng B, Christie MJ (1994a) Hyperpolarization by opioids acting on mu-receptors of a sub-population of rat periaqueductal gray neurones in vitro. *British Journal of Pharmacology* 113:121–8.

Chieng B, Christie MJ (1994b) Inhibition by opioids acting on mu-receptors of GABAergic and glutamatergic postsynaptic potentials in single rat periaqueductal gray neurones in vitro. *British Journal of Pharmacology* 113:303–9.

Cicero TJ, Nock B, Meyer ER (1997) Sex-related differences in morphine's antinociceptive activity: relationship to serum and brain morphine concentrations. *The Journal of Pharmacology and Experimental Therapeutics* 282:939–44.

Combe R, Bramwell S, Field MJ (2004) The monosodium iodoacetate model of osteoarthritis: a model of chronic nociceptive pain in rats? *Neuroscience Letters* 370:236–40.

Cook CD, Moore KI (2006) Effects of sex, hindpaw injection site and stimulus modality on nociceptive sensitivity in arthritic rats. *Physiology & Behavior* 87:552–62.

Cook CD, Nickerson MD (2005) Nociceptive sensitivity and opioid antinociception and antihyperalgesia in Freund's adjuvant-induced arthritic male and female rats. *The Journal of Pharmacology and Experimental Therapeutics* 313:449–59.

Cope DW, Hughes SW, Crunelli V (2005) GABAA receptor-mediated tonic inhibition in thalamic neurons. *The Journal of Neuroscience* 25:11553–63.

Cottingham SL, Femano PA, Pfaff DW (1987) Electrical stimulation of the midbrain central gray facilitates reticulospinal activation of axial muscle EMG. *Experimental Neurology* 97:704–724.

De Felice M, Sanoja R, Wang R, Vera-Portocarrero L, Oyarzo J, King T, Ossipov MH, Vanderah TW, Lai J, Dussor GO, Fields HL, Price TJ, Porreca F (2011) Engagement of descending inhibition from the rostral ventromedial medulla protects against chronic neuropathic pain. *Pain* 152:2701–9.

Depaulis A, Morgan MM, Liebeskind JC (1987) GABAergic modulation of the analgesic effects of morphine microinjected in the ventral periaqueductal gray matter of the rat. *Brain Research* 436:223–8.

Depaulis A, Keay K, Bandler R (1992) Longitudinal neuronal organization of defensive reactions in the midbrain periaqueductal gray region of the rat. *Experimental Brain Research* 90.

Digre KB, Brennan KC (2012) Shedding light on photophobia. *Journal of Neuro-Ophthalmology* 32:68–81.

Do MTH, Yau KW (2010) Intrinsically photosensitive retinal ganglion cells. *Physiological Reviews* 90:1547–81.

Donahue RR, LaGraize SC, Fuchs PN (2001) Electrolytic lesion of the anterior cingulate cortex decreases inflammatory, but not neuropathic nociceptive behavior in rats. *Brain research* 897:131–8.

Drasbek KR, Jensen K (2006) THIP, a hypnotic and antinociceptive drug, enhances an extrasynaptic GABAA receptor-mediated conductance in mouse neocortex. *Cerebral Cortex* 16:1134–41.

Ebert B, Wafford KA, Whiting PJ, Krogsgaard-Larsen P, Kemp JA (1994) Molecular pharmacology of gamma-aminobutyric acid type A receptor agonists and partial agonists in oocytes injected with different alpha, beta, and gamma receptor subunit combinations. *Molecular Pharmacology* 46:957–63.

Eidson LN, Murphy AZ (2013) Persistent peripheral inflammation attenuates morphine-induced periaqueductal gray glial cell activation and analgesic tolerance in the male rat. *The Journal of Pain* 14:393–404.

Ellmann S, Sticht H, Thiel F, Beckmann MW, Strick R, Strissel PL (2009) Estrogen and progesterone receptors: from molecular structures to clinical targets. *Cellular and Molecular Life Sciences* 66:2405–26.

Essrich C, Lorez M, Benson JA, Fritschy JM, Lüscher B (1998) Postsynaptic clustering of major GABAA receptor subtypes requires the gamma 2 subunit and gephyrin. *Nature Neuroscience* 1:563–71.

Fang FG, Haws CM, Drasner K, Williamson A, Fields HL (1989) Opioid peptides (DAGO-enkephalin, dynorphin A(1-13), BAM 22P) microinjected into the rat brainstem: comparison of their antinociceptive effect and their effect on neuronal firing in the rostral ventromedial medulla. *Brain Research* 501:116–28.

Farrant M, Nusser Z (2005) Variations on an inhibitory theme: phasic and tonic activation of GABA(A) receptors. *Nature Reviews. Neuroscience* 6:215–29.

Ferreira-Gomes J, Adães S, Sousa RM, Mendonça M, Castro-Lopes JM (2012) Dose-dependent expression of neuronal injury markers during experimental osteoarthritis induced by monoiodoacetate in the rat. *Molecular Pain* 8:50.

Fields H (2004) State-dependent opioid control of pain. *Nature Reviews. Neuroscience* 5:565–75.

Fillingim RB, King CD, Ribeiro-Dasilva MC, Rahim-Williams B, Riley JL (2009) Sex, gender, and pain: a review of recent clinical and experimental findings. *The Journal of Pain* 10:447–85.

Fillingim RB, Ness TJ, Glover TL, Campbell CM, Hastie BA, Price DD, Staud R (2005) Morphine responses and experimental pain: sex differences in side effects and cardiovascular responses but not analgesia. *The Journal of Pain* 6:116–24.

Finnegan TF, Chen SR, Pan HL (2005) Effect of the {mu} opioid on excitatory and inhibitory synaptic inputs to periaqueductal gray-projecting neurons in the amygdala. *The Journal of Pharmacology and Experimental Therapeutics* 312:441–8.

Friend R, Bennett RM (2011) Distinguishing fibromyalgia from rheumatoid arthritis and systemic lupus in clinical questionnaires: an analysis of the revised Fibromyalgia Impact Questionnaire (FIQR) and its variant, the Symptom Impact Questionnaire (SIQR), along with pain locations. *Arthritis Research & Therapy* 13:R58.

Gao YJ, Ji RR (2010) Light touch induces ERK activation in superficial dorsal horn neurons after inflammation: involvement of spinal astrocytes and JNK signaling in touch-evoked central sensitization and mechanical allodynia. *Journal of Neurochemistry* 115:505–14.

Gaskin DJ, Richard P (2012) The economic costs of pain in the United States. *The Journal of Pain* 13:715–24.

Gauriau C, Bernard JF (2004) Posterior triangular thalamic neurons convey nociceptive messages to the secondary somatosensory and insular cortices in the rat. *The Journal of Neuroscience* 24:752–61.

Gingrich KJ, Roberts WA, Kass RS (1995) Dependence of the GABAA receptor gating kinetics on the alpha-subunit isoform: implications for structure-function relations and synaptic transmission. *The Journal of Physiology* 489 ( Pt 2:529–43.

Glykys J, Mody I (2006) Hippocampal network hyperactivity after selective reduction of tonic inhibition in GABA A receptor alpha5 subunit-deficient mice. *Journal of Neurophysiology* 95:2796–807.

Goldberg DS, McGee SJ (2011) Pain as a global public health priority. *BMC Public Health* 11:770.

Gould HJ (2000) Complete Freund's adjuvant-induced hyperalgesia: a human perception. *Pain* 85:301–3.

Gracely RH, Grant MAB, Giesecke T (2003) Evoked pain measures in fibromyalgia. *Best Practice & Research. Clinical Rheumatology* 17:593–609.

Greenspan JD, Craft RM, LeResche L, Arendt-Nielsen L, Berkley KJ, Fillingim RB, Gold MS, Holdcroft A, Lautenbacher S, Mayer EA, Mogil JS, Murphy AZ, Traub RJ (2007) Studying sex and gender differences in pain and analgesia: a consensus report. *Pain* 132 Suppl:S26–45.

Griffiths JL, Lovick TA (2005) GABAergic neurones in the rat periaqueductal grey matter express alpha4, beta1 and delta GABAA receptor subunits: plasticity of expression during the estrous cycle. *Neuroscience* 136:457–66.

Guan Y, Terayama R, Dubner R, Ren K (2002) Plasticity in excitatory amino acid receptor-mediated descending pain modulation after inflammation. *The Journal of Pharmacology and Experimental Therapeutics* 300:513–20.

Guingamp C, Gegout-Pottie P, Philippe L, Terlain B, Netter P, Gillet P (1997) Mono-iodoacetate-induced experimental osteoarthritis: a dose-response study of loss of mobility, morphology, and biochemistry. *Arthritis and Rheumatism* 40:1670–9.

Guo W, Robbins MT, Wei F, Zou S, Dubner R, Ren K (2006) Supraspinal brain-derived neurotrophic factor signaling: a novel mechanism for descending pain facilitation. *The Journal of Neuroscience* 26:126–37.

Gwilym SE, Keltner JR, Warnaby CE, Carr AJ, Chizh B, Chessell I, Tracey I (2009) Psychophysical and functional imaging evidence supporting the presence of central sensitization in a cohort of osteoarthritis patients. *Arthritis and Rheumatism* 61:1226–34.

Hahm ET, Kim Y, Lee JJ, Cho YW (2011) GABAergic synaptic response and its opioidergic modulation in periaqueductal gray neurons of rats with neuropathic pain. *BMC Neuroscience* 12:41.

Hahm ET, Lee JJ, Min BI, Cho YW (2005) Developmental change of GABAergic postsynaptic current in rat periaqueductal gray. *Neuroscience Letters* 380:187–92.

Heinricher MM, Tavares I, Leith JL, Lumb BM (2009) Descending control of nociception: Specificity, recruitment and plasticity. *Brain Research Reviews* 60:214–25.

Heinricher MM, Fields HL (2003) The Delta Opioid Receptor and Brain Pain-Modulating Circuits In Chang K, Porreca F, Woods J, editors, *The Delta Receptor*, pp. 467–480. Marcel Dekker.

Heinricher MM, Neubert MJ (2004) Neural basis for the hyperalgesic action of cholecystokinin in the rostral ventromedial medulla. *Journal of Neurophysiology* 92:1982–9.

Heinricher M, Ingram S (2008) The Brainstem and Nociceptive Modulation In *The Senses: a Comprehensive Reference*, pp. 593–626.

Herbison AE, Fénelon VS (1995) Estrogen regulation of GABAA receptor subunit mRNA expression in preoptic area and bed nucleus of the stria terminalis of female rat brain. *The Journal of Neuroscience* 15:2328–37.

Herd MB, Brown AR, Lambert JJ, Belelli D (2013) Extrasynaptic GABAA Receptors Couple Presynaptic Activity to Postsynaptic Inhibition in the Somatosensory Thalamus. *Journal of Neuroscience* 33:14850–14868.

Hu J, Wang Z, Guo YY, Zhang XN, Xu ZH, Liu SB, Guo HJ, Yang Q, Zhang FX, Sun XL, Zhao MG (2009) A role of periaqueductal grey NR2B-containing NMDA receptor in mediating persistent inflammatory pain. *Molecular Pain* 5:71.

Hylden JL, Nahin RL, Traub RJ, Dubner R (1989) Expansion of receptive fields of spinal lamina I projection neurons in rats with unilateral adjuvant-induced inflammation: the contribution of dorsal horn mechanisms. *Pain* 37:229–243.

Iannetti GD, Zambreanu L, Wise RG, Buchanan TJ, Huggins JP, Smart TS, Vennart W, Tracey I (2005) Pharmacological modulation of pain-related brain activity during normal and central sensitization states in humans. *Proceedings of the National Academy of Sciences of the United States of America* 102:18195–200.

Ikegaki N, Saito N, Hashima M, Tanaka C (1994) Production of specific antibodies against GABA transporter subtypes (GAT1, GAT2, GAT3) and their application to immunocytochemistry. *Molecular Brain Research* 26:47–54.

Institute of Medicine (2011) *Relieving Pain in America: A Blueprint for Transforming Prevention, Care, Education, and Research* The National Academies Press, Washington DC.

Jacquet YF, Lajtha A (1976) The periaqueductal gray: site of morphine analgesia and tolerance as shown by 2-way cross tolerance between systemic and intracerebral injections. *Brain Research* 103:501–13.

Jensen ML, Wafford KA, Brown AR, Belelli D, Lambert JJ, Mirza NR (2013) A study of subunit selectivity, mechanism and site of action of the delta selective compound 2 (DS2) at human recombinant and rodent native GABA(A) receptors. *British Journal of Pharmacology* 168:1118–32.

Jespersen A, Dreyer L, Kendall S, Graven-Nielsen T, Arendt-Nielsen L, Bliddal H, Danneskiold-Samsoe B (2007) Computerized cuff pressure algometry: A new method to assess deep-tissue hypersensitivity in fibromyalgia. *Pain* 131:57–62.

Jones BL, Henderson LP (2007) Trafficking and potential assembly patterns of epsilon-containing GABAA receptors. *Journal of Neurochemistry* 103:1258–71.

Jung ME, Lal H, Gatch MB (2002) The discriminative stimulus effects of pentylenetetrazol as a model of anxiety: recent developments. *Neuroscience & Biobehavioral Reviews* 26:429–439.

Keay KA, Crowfoot LJ, Floyd NS, Henderson LA, Christie MJ, Bandler R (1997) Cardiovascular effects of microinjections of opioid agonists into the 'Depressor Region' of the ventrolateral periaqueductal gray region. *Brain Research* 762:61–71.

Kelly S, Dobson KL, Harris J (2013) Spinal nociceptive reflexes are sensitized in the monosodium iodoacetate model of osteoarthritis pain in the rat. *Osteoarthritis and Cartilage* 21:1327–35.

Kendall DA, Browner M, Enna SJ (1982) Comparison of the antinociceptive effect of gamma-aminobutyric acid (GABA) agonists: evidence for a cholinergic involvement. *The Journal of Pharmacology and Experimental Therapeutics* 220:482–7.

Kersanté F, Rowley SCS, Pavlov I, Gutièrrez-Mecinas M, Semyanov A, Reul JMHM, Walker MC, Linthorst ACE (2013) A functional role for both -aminobutyric acid (GABA) transporter-1 and GABA transporter-3 in the modulation of extracellular GABA and GABAergic tonic conductances in the rat hippocampus. *The Journal of Physiology* 591:2429–41.

Kieffer BL (1999) Opioids: first lessons from knockout mice. *Trends in Pharmacological Sciences* 20:19–26.

Kirouac GJ, Li S, Mabrouk G (2004) GABAergic projection from the ventral tegmental area and substantia nigra to the periaqueductal gray region and the dorsal raphe nucleus. *The Journal of Comparative Neurology* 469:170–84.

Konkle ATM, McCarthy MM (2011) Developmental time course of estradiol, testosterone, and dihydrotestosterone levels in discrete regions of male and female rat brain. *Endocrinology* 152:223–35.

Koressaar T, Remm M (2007) Enhancements and modifications of primer design program Primer3. *Bioinformatics (Oxford, England)* 23:1289–91.

Kosek E, Ekholm J, Hansson P (1995) Increased pressure pain sensibility in fibromyalgia patients is located deep to the skin but not restricted to muscle tissue. *Pain* 63:335–9.

Kosek E, Ordeberg G (2000a) Abnormalities of somatosensory perception in patients with painful osteoarthritis normalize following successful treatment. *European Journal of Pain* 4:229–38.

Kosek E, Ordeberg G (2000b) Lack of pressure pain modulation by heterotopic noxious conditioning stimulation in patients with painful osteoarthritis before, but not following, surgical pain relief. *Pain* 88:69–78.

Krieger JE, Graeff FG (1985) Defensive behavior and hypertension induced by glutamate in the midbrain central gray of the rat. *Brazilian Journal of Medical and Biological Research* 18:61–67.

Krishek BJ, Moss SJ, Smart TG (1998) Interaction of H+ and Zn2+ on recombinant and native rat neuronal GABAA receptors. *The Journal of Physiology* 507 ( Pt 3:639–52.

Krogsgaard-Larsen P, Frø lund B, Liljefors T (2002) Specific GABA(A) agonists and partial agonists. *Chemical Record* 2:419–30.

Krzanowska EK, Bodnar RJ (1999) Morphine antinociception elicited from the ventrolateral periaqueductal gray is sensitive to sex and gonadectomy differences in rats. *Brain Research* 821:224–30.

Krzanowska EK, Ogawa S, Pfaff DW, Bodnar RJ (2002) Reversal of sex differences in morphine analgesia elicited from the ventrolateral periaqueductal gray in rats by neonatal hormone manipulations. *Brain Research* 929:1–9.

Kulkarni MM (2011) Digital multiplexed gene expression analysis using the NanoString nCounter system. *Current Protocols in Molecular Biology* Chapter 25:Unit25B.10.

Kuner R (2010) Central mechanisms of pathological pain. *Nature Medicine* 16:1258–66.

Kwon M, Altin M, Duenas H, Alev L (2013) The Role of Descending Inhibitory Pathways on Chronic Pain Modulation and Clinical Implications. *Pain Practice* .

LaGraize SC, Labuda CJ, Rutledge MA, Jackson RL, Fuchs PN (2004) Differential effect of anterior cingulate cortex lesion on mechanical hypersensitivity and escape/avoidance behavior in an animal model of neuropathic pain. *Experimental Neurology* 188:139–48.

Latremoliere A, Woolf CJ (2009) Central sensitization: a generator of pain hypersensitivity by central neural plasticity. *The Journal of Pain* 10:895–926.

Lau BK (2011) Cellular mechanisms underlying opioid and cannabinoid analgesia in the periaqueductal grey Ph.D. diss., University of Sydney, Australia.

Lau BK, Karim S, Goodchild AK, Vaughan CW, Drew GM (2014) Menthol enhances phasic and tonic GABAA receptor-mediated currents in midbrain periaqueductal grey neurons. *British Journal of Pharmacology* 171:2803–13.

Lau BK, Vaughan CW (2014) Descending modulation of pain: the GABA disinhibition hypothesis of analgesia. *Current Opinion in Neurobiology* 29C:159–164.

Lee Y, Pai M, Brederson JD, Wilcox D, Hsieh G, Jarvis MF, Bitner RS (2011) Monosodium iodoacetate-induced joint pain is associated with increased phosphorylation of mitogen activated protein kinases in the rat spinal cord. *Molecular Pain* 7:39.

Leith JL, Wilson AW, Donaldson LF, Lumb BM (2007) Cyclooxygenase-1-derived prostaglandins in the periaqueductal gray differentially control C- versus A-fiber-evoked spinal nociception. *The Journal of Neuroscience* 27:11296–305.

Lewis EM, Barnett JF, Freshwater L, Hoberman AM, Christian MS (2002) Sexual maturation data for Crl Sprague-Dawley rats: criteria and confounding factors. *Drug and Chemical Toxicology* 25:437–58.

Liu P, Okun A, Ren J, Guo Rc, Ossipov MH, Xie J, King T, Porreca F Ongoing pain in the MIA model of osteoarthritis. *Neuroscience Letters* 493:72–5.

Lonstein JS, Blaustein JD (2004) Immunocytochemical investigation of nuclear progestin receptor expression within dopaminergic neurones of the female rat brain. *Journal of Neuroendocrinology* 16:534–43.

Lonstein JS, Stern JM (1998) Site and behavioral specificity of periaqueductal gray lesions on postpartum sexual, maternal, and aggressive behaviors in rats. *Brain Research* 804:21–35.

Lovick TA (1985) Ventrolateral medullary lesions block the antinociceptive and cardiovascular responses elicited by stimulating the dorsal periaqueductal grey matter in rats. *Pain* 21:241–52.

Lovick TA, Griffiths JL, Dunn SMJ, Martin IL (2005) Changes in GABA(A) receptor subunit expression in the midbrain during the oestrous cycle in Wistar rats. *Neuroscience* 131:397–405.

Loyd DR, Morgan MM, Murphy AZ (2007) Morphine preferentially activates the periaqueductal gray-rostral ventromedial medullary pathway in the male rat: a potential mechanism for sex differences in antinociception. *Neuroscience* 147:456–68.

Loyd DR, Morgan MM, Murphy AZ (2008) Sexually dimorphic activation of the periaqueductal gray-rostral ventromedial medullary circuit during the development of tolerance to morphine in the rat. *The European Journal of Neuroscience* 27:1517–24.

Loyd DR, Murphy AZ (2006) Sex differences in the anatomical and functional organization of the periaqueductal gray-rostral ventromedial medullary pathway in the rat: a potential circuit mediating the sexually dimorphic actions of morphine. *The Journal of Comparative Neurology* 496:723–38.

Loyd DR, Wang X, Murphy AZ (2008) Sex differences in micro-opioid receptor expression in the rat midbrain periaqueductal gray are essential for eliciting sex differences in morphine analgesia. *The Journal of Neuroscience* 28:14007–17.

Luscher B, Fuchs T, Kilpatrick CL (2011) GABAA receptor trafficking-mediated plasticity of inhibitory synapses. *Neuron* 70:385–409.

Ma W, Saunders PA, Somogyi R, Poulter MO, Barker JL (1993) Ontogeny of GABAA receptor subunit mRNAs in rat spinal cord and dorsal root ganglia. *The Journal of Comparative Neurology* 338:337–59.

Mackey SC, Maeda F (2004) Functional imaging and the neural systems of chronic pain. *Neurosurgery Clinics of North America* 15:269–88.

Mantyh PW (1982) The midbrain periaqueductal gray in the rat, cat, and monkey: a Nissl, Weil, and Golgi analysis. *The Journal of Comparative Neurology* 204:349–63.

Marino M, Galluzzo P, Ascenzi P (2006) Estrogen signaling multiple pathways to impact gene transcription. *Current Genomics* 7:497–508.

Marker CL, Pomonis JD (2012) The monosodium iodoacetate model of osteoarthritis pain in the rat. *Methods in Molecular Biology* 851:239–48.

Martin AR, Branch CL (1958) Spontaneous activity of Betz cells in cats with midbrain lesions. *Journal of Neurophysiology* 21:368–70.

McGaraughty S, Chu KL, Bitner RS, Martino B, El Kouhen R, Han P, Nikkel AL, Burgard EC, Faltynek CR, Jarvis MF (2003) Capsaicin infused into the PAG affects rat tail flick responses to noxious heat and alters neuronal firing in the RVM. *Journal of Neurophysiology* 90:2702–10.

McGee TP, Houston CM, Brickley SG (2013) Copper block of extrasynaptic GABAA receptors in the mature cerebellum and striatum. *The Journal of Neuroscience* 33:13431–5.

McLemore S, Crown ED, Meagher MW, Grau JW (1999) Shock-induced hyperalgesia: II. Role of the dorsolateral periaqueductal gray. *Behavioral Neuroscience* 113:539–49.

McMullan S, Lumb BM (2006) Midbrain control of spinal nociception discriminates between responses evoked by myelinated and unmyelinated heat nociceptors in the rat. *Pain* 124:59–68.

Merskey H, Bogduk N (1994) Part III: Pain Terms, A Current LIst with Definitions and Notes on Usage In Merskey H, Bogduk N, editors, *Classification of Chronic Pain*, pp. 209–214. Seattle, WA, second edition.

Miki K, Zhou Q, Guo Y, Guan R, Terayama R, Dubner R, Ren K (2002) Changes in Gene Expression and Neuronal Phenotype in Brain Stem Pain Modulatory Circuitry After Inflammation. *Journal of Neurophysiology* 87:750–760.

Mogil JS (2009) Animal models of pain: progress and challenges. *Nature Reviews. Neuroscience* 10:283–94.

Mogil JS, Chanda ML (2005) The case for the inclusion of female subjects in basic science studies of pain. *Pain* 117:1–5.

Mogil J, Chesler E, Wilson S, Juraska J, Sternberg W (2000) Sex differences in thermal nociception and morphine antinociception in rodents depend on genotype. *Neuroscience & Biobehavioral Reviews* 24:375–389.

Montano MM (1995) Free estradiol in serum and brain uptake of estradiol during fetal and neonatal sexual differentiation in female rats. *Biology of Reproduction* 53:1198–1207.

Moreau JL, Fields HL (1986) Evidence for GABA involvement in midbrain control of medullary neurons that modulate nociceptive transmission. *Brain Research* 397:37–46.

Morgan MM (1991) Differences in antinociception evoked from dorsal and ventral regions of the caudal periaqueductal gray matter In *The Midbrain Periaqueductal Gray Matter*, pp. 139–150.

Morgan MM, Gold MS, Liebeskind JC, Stein C (1991) Periaqueductal gray stimulation produces a spinally mediated, opioid antinociception for the inflamed hindpaw of the rat. *Brain research* 545:17–23.

Morgan MM, Whittier KL, Hegarty DM, Aicher SA (2008) Periaqueductal gray neurons project to spinally projecting GABAergic neurons in the rostral ventromedial medulla. *Pain* 140:376–86.

Mortensen M, Kristiansen U, Ebert B, Frø lund B, Krogsgaard-Larsen P, Smart TG (2004) Activation of single heteromeric GABA(A) receptor ion channels by full and partial agonists. *The Journal of Physiology* 557:389–413.

Motulsky HJ, Brown RE (2006) Detecting outliers when fitting data with nonlinear regression - a new method based on robust nonlinear regression and the false discovery rate. *BMC Bioinformatics* 7:123.

Murray TF, McGill W, Cheney DL (1983) A comparison of the analgesic activities of 4,5,6,7-tetrahydroisoxazolo[5,4-c]pyridin-3-ol (THIP) and 6-chloro-2[1-piperazinyl]pyrazine (MK 212). *European Journal of Pharmacology* 90:179–84.

Nagakura Y, Okada M, Kohara A, Kiso T, Toya T, Iwai A, Wanibuchi F, Yamaguchi T (2003) Allodynia and hyperalgesia in adjuvant-induced arthritic rats: time course of progression and efficacy of analgesics. *The Journal of Pharmacology and Experimental Therapeutics* 306:490–7.

Nashold BS, Wilson WP, Slaughter DG (1969) Sensations evoked by stimulation in the midbrain of man. *Journal of Neurosurgery* 30:14–24.

Noseda R, Constandil L, Bourgeais L, Chalus M, Villanueva L (2010) Changes of meningeal excitability mediated by corticotrigeminal networks: a link for the endogenous modulation of migraine pain. *The Journal of Neuroscience* 30:14420–9.

Odeh F, Antal M (2001) The projections of the midbrain periaqueductal grey to the pons and medulla oblongata in rats. *The European Journal of Neuroscience* 14:1275–86.

Ogawa S, Kow LM, Pfaff DW (1994) In vitro electrophysiological characterization of midbrain periaqueductal gray neurons in female rats: responses to GABA- and Met-enkephalin-related agents. *Brain Research* 666:239–49.

Okamoto K, Tashiro A, Chang Z, Bereiter DA (2010) Bright light activates a trigeminal nociceptive pathway. *Pain* 149:235–42.

Olsen RW, Sieghart W (2008) International Union of Pharmacology . LXX . Subtypes of Gamma-Aminobutyric Acid A Receptors : Classification on the Basis of Subunit Composition , Pharmacology , and Function . Update 60:243–260.

Osborne PB, Vaughan CW, Wilson HI, Christie MJ (1996) Opioid inhibition of rat periaqueductal grey neurones with identified projections to rostral ventromedial medulla in vitro. *The Journal of Physiology* 490 ( Pt 2:383–9.

Ossipov MH, Kovelowski CJ, Nichols ML, Hruby VJ, Porreca F (1995) Characterization of supraspinal antinociceptive actions of opioid delta agonists in the rat. *Pain* 62:287–93.

Ossipov MH, Morimura K, Porreca F (2014) Descending pain modulation and chronification of pain. *Current Opinion in Supportive and Palliative Care* 8:143–51.

Papp A, Fehér O, Erdélyi L (1987) The ionic mechanism of the pentylenetetrazol convulsions. *Acta Biologica Hungarica* 38:349–61.

Park JB, Skalska S, Son S, Stern JE (2007) Dual GABAA receptor-mediated inhibition in rat presympathetic paraventricular nucleus neurons. *The Journal of Physiology* 582:539–51.

Parker C (1976) Hormonal Events Surrounding the Natural Onset of Puberty in Female Rats. *Biology of Reproduction* 14:347–353.

Pastoriza LN, Morrow TJ, Casey KL (1996) Medial frontal cortex lesions selectively attenuate the hot plate response: possible nocifensive apraxia in the rat. *Pain* 64:11–7.

Paul J, Yévenes GE, Benke D, Di Lio A, Ralvenius WT, Witschi R, Scheurer L, Cook JM, Rudolph U, Fritschy JM, Zeilhofer HU (2014) Antihyperalgesia by $\alpha$2-GABAA receptors occurs via a genuine spinal action and does not involve supraspinal sites. *Neuropsychopharmacology* 39:477–87.

Pavlov I, Savtchenko LP, Song I, Koo J, Pimashkin A, Rusakov DA (2014) Tonic GABA A conductance bidirectionally controls interneuron fi ring pattern and synchronization in the CA3 hippocampal network pp. 2–7.

Paxinos G, Watson C (2005) *The Rat Brain in Stereotaxic Coordinates* Elsevier Academic Press.

Pfaffl MW, Tichopad A, Prgomet C, Neuvians TP (2004) Determination of stable housekeeping genes, differentially regulated target genes and sample integrity: BestKeeper, Excel based tool using pairwise correlations. *Biotechnology Letters* 26:509–515.

Phillips K, Clauw DJ (2011) Central pain mechanisms in chronic pain states–maybe it is all in their head. *Best Practice & Research. Clinical Rheumatology* 25:141–54.

Phoenix C, Goy R, Gerall A, Young W (1959) Organizing action of prenatally administered testosterone propionate on the tissues mediating mating behavior in the female guinea pig. *Endocrinology* 65:369–82.

Pomonis JD, Boulet JM, Gottshall SL, Phillips S, Sellers R, Bunton T, Walker K (2005) Development and pharmacological characterization of a rat model of osteoarthritis pain. *Pain* 114:339–46.

Porreca F, Burgess SE, Gardell LR, Vanderah TW, Malan TP, Ossipov MH, Lappi Da, Lai J (2001) Inhibition of neuropathic pain by selective ablation of brainstem medullary cells expressing the mu-opioid receptor. *The Journal of Neuroscience* 21:5281–8.

Porreca F, Ossipov MH, Gebhart GF (2002) Chronic pain and medullary descending facilitation. *Trends in Neurosciences* 25:319–25.

Pradhan A, Smith M, McGuire B, Evans C, Walwyn W (2013) Chronic inflammatory injury results in increased coupling of delta opioid receptors to voltage-gated Ca2+ channels. *Molecular Pain* 9:8.

Puretić MB, Demarin V (2012) Neuroplasticity mechanisms in the pathophysiology of chronic pain. *Acta Clinica Croatica* 51:425–9.

Quadros PS, Schlueter LJ, Wagner CK (2008) Distribution of progesterone receptor immunoreactivity in the midbrain and hindbrain of postnatal rats. *Developmental Neurobiology* 68:1378–90.

Rahman W, Bauer CS, Bannister K, Vonsy JL, Dolphin AC, Dickenson AH (2009) Descending serotonergic facilitation and the antinociceptive effects of pregabalin in a rat model of osteoarthritic pain. *Molecular Pain* 5:45.

Rahn EJ, Iannitti T, Donahue RR, Taylor BK (2014) Sex differences in a mouse model of multiple sclerosis: neuropathic pain behavior in females but not males and protection from neurological deficits during proestrus. *Biology of Sex Differences* 5:4.

Ranna M, Sinkkonen ST, Möykkynen T, Uusi-Oukari M, Korpi ER (2006) Impact of epsilon and theta subunits on pharmacological properties of alpha3beta1 GABAA receptors expressed in Xenopus oocytes. *BMC Pharmacology* 6:1.

Ren K, Dubner R (1993) NMDA receptor antagonists attenuate mechanical hyperalgesia in rats with unilateral inflammation of the hindpaw. *Neuroscience Letters* 163:22–6.

Ren K, Dubner R (1999) Inflammatory Models of Pain and Hyperalgesia. *Intitute of Laboratory Animal Research Journal* 40:111–118.

Ren K, Dubner R (2002) Descending modulation in persistent pain: an update. *Pain* 100:1–6.

Renno WM (1998) Prolonged noxious stimulation increases periaqueductal gray NMDA MRNA expression: A hybridization study using two different rat models for nociception. *Irish Journal of Medical Science* 167:181–192.

Reynolds DV (1969) Surgery in the rat during electrical analgesia induced by focal brain stimulation. *Science* 164:444–5.

Riley III JL, E. Robinson M, Wise EA, Price D (1999) A meta-analytic review of pain perception across the menstrual cycle. *Pain* 81:225–235.

Rivest RW (1991) Sexual maturation in female rats: Hereditary, developmental and environmental aspects. *Experientia* 47:1026–1038.

Robb GW, Amann RP, Killian GJ (1978) Daily sperm production and epididymal sperm reserves of pubertal and adult rats. *Journal of Reproduction and Fertility* 54:103–7.

Roepke TA, Ronnekleiv OK, Kelly MJ (2011) Physiological consequences of membrane-initiated estrogen signaling in the brain. *Frontiers in Bioscience* 16:1560–73.

Rudolph U, Möhler H (2006) GABA-based therapeutic approaches: GABAA receptor subtype functions. *Current Opinion in Pharmacology* 6:18–23.

Ruiz-Lopez R (1995) The Epidemiology of Chronic Pain. *Pain Digest* 5:67–68.

Sandkühler J, Gebhart GF (1984) Relative contributions of the nucleus raphe magnus and adjacent medullary reticular formation to the inhibition by stimulation in the periaqueductal gray of a spinal nociceptive reflex in the pentobarbital-anesthetized rat. *Brain research* 305:77–87.

Sandkühler J, Zimmermann M (1988) Neuronal effects of controlled superfusion of the spinal cord with monoaminergic receptor antagonists in the cat. *Progress in Brain Research* 77:321–7.

Sandkühler J (2009) Models and mechanisms of hyperalgesia and allodynia. *Physiological Reviews* 89:707–58.

Sarton E, Olofsen E, Romberg R, den Hartigh J, Kest B, Nieuwenhuijs D, Burm A, Teppema L, Dahan A (2000) Sex differences in morphine analgesia: an experimental study in healthy volunteers. *Anesthesiology* 93:1245–54; discussion 6A.

Scholz J, Woolf CJ (2002) Can we conquer pain? *Nature Neuroscience* 5:1067–7.

Sedelnikova A, Erkkila BE, Harris H, Zakharkin SO, Weiss DS (2006) Stoichiometry of a pore mutation that abolishes picrotoxin-mediated antagonism of the GABAA receptor. *The Journal of Physiology* 577:569–77.

Semenenko FM, Lumb BM (1992) Projections of anterior hypothalamic neurones to the dorsal and ventral periaqueductal grey in the rat. *Brain Research* 582:237–45.

Semyanov A, Walker MC, Kullmann DM (2003) GABA uptake regulates cortical excitability via cell type-specific tonic inhibition. *Nature Neuroscience* 6:484–90.

Serwanski DR, Miralles CP, Christie SB, Mehta AK, Li X, De Blas AL (2006) Synaptic and nonsynaptic localization of GABAA receptors containing the alpha5 subunit in the rat brain. *The Journal of Comparative Neurology* 499:458–70.

Seutin V, Johnson SW (1999) Recent advances in the pharmacology of quaternary salts of bicuculline. *Trends in Pharmacological Sciences* 20:268–70.

Shen H, Gong QH, Yuan M, Smith SS (2005) Short-term steroid treatment increases delta GABAA receptor subunit expression in rat CA1 hippocampus: pharmacological and behavioral effects. *Neuropharmacology* 49:573–86.

Sieghart W (2006) Structure, pharmacology, and function of GABAA receptor subtypes. *Advances in Pharmacology* 54:231–63.

Smart TG, Constanti A (1982) A novel effect of zinc on the lobster muscle GABA receptor. *Proceedings of the Royal Society of London. Series B, Containing papers of a Biological character. Royal Society (Great Britain)* 215:327–41.

Smith DJ, Perrotti JM, Crisp T, Cabral ME, Long JT, Scalzitti JM (1988) The mu opiate receptor is responsible for descending pain inhibition originating in the periaqueductal gray region of the rat brain. *European journal of pharmacology* 156:47–54.

Song P, Mabrouk OS, Hershey ND, Kennedy RT (2012) In vivo neurochemical monitoring using benzoyl chloride derivatization and liquid chromatography-mass spectrometry. *Analytical chemistry* 84:412–9.

St Laurent G, Shtokalo D, Tackett MR, Yang Z, Vyatkin Y, Milos PM, Seilheimer B, McCaffrey TA, Kapranov P (2013) On the importance of small changes in RNA expression. *Methods (San Diego, Calif.)* 63:18–24.

Staud R (2013) The important role of CNS facilitation and inhibition for chronic pain. *International Journal of Clinical Rheumatology* 8:639–646.

Stell BM, Mody I (2002) Receptors with different affinities mediate phasic and tonic GABA(A) conductances in hippocampal neurons. *The Journal of Neuroscience* 22:RC223.

Szabadics J, Varga C, Molnár G, Oláh S, Barzó P, Tamás G (2006) Excitatory effect of GABAergic axo-axonic cells in cortical microcircuits. *Science* 311:233–5.

Thakur M, Rahman W, Hobbs C, Dickenson AH, Bennett DLH (2012) Characterisation of a peripheral neuropathic component of the rat monoiodoacetate model of osteoarthritis. *PloS one* 7:e33730.

Tortorici V, Morgan MM (2002) Comparison of morphine and kainic acid microinjections into identical PAG sites on the activity of RVM neurons. *Journal of Neurophysiology* 88:1707–15.

Trabzuni D, Ramasamy A, Imran S, Walker R, Smith C, Weale ME, Hardy J, Ryten M (2013) Widespread sex differences in gene expression and splicing in the adult human brain. *Nature Communications* 4:2771.

Tsang A, Von Korff M, Lee S, Alonso J, Karam E, Angermeyer MC, Borges GLG, Bromet EJ, Demytteneare K, de Girolamo G, de Graaf R, Gureje O, Lepine JP, Haro JM, Levinson D, Oakley Browne MA, Posada-Villa J, Seedat S, Watanabe M (2008) Common chronic pain conditions in developed and developing countries: gender and age differences and comorbidity with depression-anxiety disorders. *The Journal of Pain* 9:883–91.

Unruh AM (1996) Gender variations in clinical pain experience. *Pain* 65:123–67.

Vaes E, Khan M, Mombaerts P (2014) Statistical analysis of differential gene expression relative to a fold change threshold on NanoString data of mouse odorant receptor genes. *BMC Bioinformatics* 15:39.

van Hecke O, Torrance N, Smith BH (2013) Chronic pain epidemiology and its clinical relevance. *British Journal of Anaesthesia* 111:13–8.

Vandesompele J, De Preter K, Pattyn F, Poppe B, Van Roy N, De Paepe A, Speleman F (2002) Accurate normalization of real-time quantitative RT-PCR data by geometric averaging of multiple internal control genes. *Genome Biology* 3:1–11.

Vaughan CW, Christie MJ (1997) Presynaptic inhibitory action of opioids on synaptic transmission in the rat periaqueductal grey in vitro. *The Journal of Physiology* 498 ( Pt 2:463–72.

Vaughan CW, Ingram SL, Connor Ma, Christie MJ (1997) How opioids inhibit GABA-mediated neurotransmission. *Nature* 390:611–4.

Vaughan CW, Bagley EE, Drew GM, Schuller A, Pintar JE, Hack SP, Christie MJ (2003) Cellular actions of opioids on periaqueductal grey neurons from C57B16/J mice and mutant mice lacking MOR-1. *British Journal of Pharmacology* 139:362–7.

Vera-Portocarrero LP, Zhang ET, Ossipov MH, Xie JY, King T, Lai J, Porreca F (2006) Descending facilitation from the rostral ventromedial medulla maintains nerve injury-induced central sensitization. *Neuroscience* 140:1311–20.

Wafford KA, Thompson SA, Thomas D, Sikela J, Wilcox AS, Whiting PJ (1996) Functional characterization of human gamma-aminobutyric acidA receptors containing the alpha 4 subunit. *Molecular Pharmacology* 50:670–8.

Wang H, Wessendorf MW (2002) Mu- and delta-opioid receptor mRNAs are expressed in periaqueductal gray neurons projecting to the rostral ventromedial medulla. *Neuroscience* 109:619–34.

Wang X, Traub RJ, Murphy AZ (2006) Persistent pain model reveals sex difference in morphine potency. *American journal of physiology. Regulatory, integrative and comparative physiology* 291:R300–6.

Waters AJ, Lumb BM (1997) Inhibitory effects evoked from both the lateral and ventrolateral periaqueductal grey are selective for the nociceptive responses of rat dorsal horn neurones. *Brain Research* 752:239–49.

Wei F, Dubner R, Ren K (1999) Nucleus reticularis gigantocellularis and nucleus raphe magnus in the brain stem exert opposite effects on behavioral hyperalgesia and spinal Fos protein expression after peripheral inflammation. *Pain* 80:127–41.

Wilhelm H (2008) The pupil. *Current Opinion in Neurology* 21:36–42.

Witschi R, Punnakkal P, Paul J, Walczak JS, Cervero F, Fritschy JM, Kuner R, Keist R, Rudolph U, Zeilhofer HU (2011) Presynaptic alpha2-GABAA receptors in primary afferent depolarization and spinal pain control. *The Journal of Neuroscience* 31:8134–42.

Wolfe F, Ross K, Anderson J, Russell IJ, Hebert L (1995) The prevalence and characteristics of fibromyalgia in the general population. *Arthritis and Rheumatism* 38:19–28.

Wolfe F, Smythe HA, Yunus MB, Bennett RM, Bombardier C, Goldenberg DL, Tugwell P, Campbell SM, Abeles M, Clark P (1990) The American College of Rheumatology 1990 Criteria for the Classification of Fibromyalgia. Report of the Multicenter Criteria Committee. *Arthritis and Rheumatism* 33:160–72.

Woolf CJ (2011) Central sensitization: implications for the diagnosis and treatment of pain. *Pain* 152:S2–15.

Xu Q, Hamada T, Kiyama R, Sakuma Y, Wada-Kiyama Y (2008) Site-specific regulation of gene expression by estrogen in the hypothalamus of adult female rats. *Neuroscience Letters* 436:35–9.

Yamada J, Furukawa T, Ueno S, Yamamoto S, Fukuda A (2007) Molecular basis for the GABAA receptor-mediated tonic inhibition in rat somatosensory cortex. *Cerebral Cortex* 17:1782–7.

Yardley CP, Hilton SM (1986) The hypothalamic and brainstem areas from which the cardiovascular and behavioural components of the defence reaction are elicited in the rat. *Journal of the Autonomic Nervous System* 15:227–244.

Ye Z, McGee TP, Houston CM, Brickley SG (2013) The contribution of $\delta$ subunit-containing GABAA receptors to phasic and tonic conductance changes in cerebellum, thalamus and neocortex. *Frontiers in Neural Circuits* 7:203.

Yunus MB (2008) Central sensitivity syndromes: a new paradigm and group nosology for fibromyalgia and overlapping conditions, and the related issue of disease versus illness. *Seminars in Arthritis and Rheumatism* 37:339–52.

Zambotti F, Zonta N, Parenti M, Tommasi R, Vicentini L, Conci F, Mantegazza P (1982) Periaqueductal gray matter involvement in the muscimol-induced decrease of morphine antinociception. *Naunyn-Schmiedeberg's Archives of Pharmacology* 318:368–9.

Zanato VF, Martins MP, Anselmo-Franci JA, Petenusci SO, Lamano-Carvalho TL (1994) Sexual development of male Wistar rats. *Brazilian Journal of Medical and Biological Research* 27:1273–80.

Zander E, Weddell G (1951) Observations on the innervation of the cornea. *Journal of Anatomy* 85:68–99.

Zeilhofer HU, Möhler H, Di Lio A (2009) GABAergic analgesia: new insights from mutant mice and subtype-selective agonists. *Trends in Pharmacological Sciences* 30:397–402.

Zemunik T, Peruzovic M, Capkun V, Zekan L, Tomic S, Milkovic K (2003) Reproductive ability of pubertal male and female rats. *Brazilian Journal of Medical and Biological Research* 36:871–7.

Zhang L, Hammond DL (2009) Substance P enhances excitatory synaptic transmission on spinally projecting neurons in the rostral ventromedial medulla after inflammatory injury. *Journal of Neurophysiology* 102:1139–51.

Zhang YQ, Gao X, Huang YL, Wu GC (2000) Expression of 5-HT1A receptor mRNA in rat dorsal raphe nucleus and ventrolateral periaqueductal gray neurons after peripheral inflammation. *Neuroreport* 11:3361–5.

Zhang YQ, Gao X, Ji GC, Wu GC (2001) Expression of 5-HT2A receptor mRNA in rat spinal dorsal horn and some nuclei of brainstem after peripheral inflammation. *Brain research* 900:146–51.

Zheng W, Xie W, Zhang J, Strong JA, Wang L, Yu L, Xu M, Lu L (2003) Function of gamma-aminobutyric acid receptor/channel rho 1 subunits in spinal cord. *The Journal of biological chemistry* 278:48321–9.

# Appendix A

**Molecular properties of Kiss1 neurons in the arcuate nucleus of the mouse**

Michelle L. Gottsch[1,2], Simina M. Popa[5], Janessa K. Lawhorn[1], Jian Qiu[7], **Karen J. Tonsfeldt[7]**, Martha A. Bosch[7], Martin J. Kelly[7], Oline K. Rønnekleiv[7], Elisenda Sanz[4], G. Stanley McKnight[4], Donald K. Clifton[1], Richard D. Palmiter[3,6], Robert A. Steiner[1,2]

[1]Departments of Obstetrics and Gynecology, 1,2Physiology and Biophysics, 3Biochemistry, [4]Pharmacology, [5]Molecular and Cellular Biology PhD Program, and [6]Howard Hughes Medical Institute, University of Washington, Seattle, Washington 98195; and [7]Department of Physiology and Pharmacology, Oregon Health and Sciences University, Portland, Oregon 97239

Appendix A was modified from a manuscript published in Endocrinology Novmeber 2011, 152(11):4298-4309.

# Foreward

In 2003, the hypothalamic peptide kisspeptin was identified as a critical regulator of puberty and neuroendocrine control of reproduction (1, 2). In the subsequent years, kisspeptin was found to exert powerful stimulatory effects on gonadotropin-releasing hormone (GnRH) neurons, confirming its role as a key regulator of reproductive function (3). Kisspeptin neurons are found in the arcuate nucleus of males and females, and in the anterior ventral periventricular nucleus (AVPV) of females (3, 4). Because of the heterogeneity of the hypothalamus, neurophysiology of neuroendocrine circuits have benefitted dramatically from the use of GFP-tagged peptides to identify cell types. Following the discovery of kisspeptin and recognition of its importance, the development of a Kiss1-GFP mouse became desirable.

In collaboration with Robert Steiner and Richard Palmiter at the University of Washington, I aided in the confirmation of the developed mouse line and the initial characterization of arcuate kisspeptin neurons in mice (Figures 6, 7, and 8). I used single cell reverse-transcription PCR (scRT-PCR) and quantitative reverse transcription PCR (qRT-PCR) to analyze gene expression in singly-harvest individual GFP-tagged neurons. I examined genes involved in the generation of burst firing, based on initial electrophysiology experiments performed by Jian Qiu in the Kelly lab.

Burst firing is associated with the expression of $I_h$ and $I_T$. The underpinnings of $I_h$ are HCN channels (1-4). The $I_T$ is produced by CaV3.1-3 channels. I examined the percentage of cells that expressed HCN1, 2, 3, and 4 transcripts to determine the approximate percentage of arcuate kisspeptin neurons that may express $I_h$. I also examined pools of 5 kisspeptin neurons to quantify HCN1-4 transcript in the cells. These experiments revealed HCN2 mRNA was the most abundant in arcuate kisspeptin neurons, and that over half

of arcuate kisspeptin neurons expressed HCN2 or HCN3. I also evaluated the amount of CaV3.1 in arcuate kisspeptin neurons, where I found that approximately half of these neurons expressed CaV3.1. CaV3.2 was not expressed well enough for analysis, and CaV3.3 was not found. These findings confirmed the presence of $I_h$ and $I_T$ in the electrophysiological results, and contributed to the initial characterization of Kiss1 neurons in the arcuate nucleus.

## A.1 Abstract

Neurons that produce kisspeptin play a critical role in reproduction. However, understanding the molecular physiology of kisspeptin neurons has been limited by the lack of an in vivomarker for those cells. Here, we report the development of a Kiss1-CreGFP knockin mouse, wherein the endogenous Kiss1 promoter directs the expression of a Cre recombinase-enhanced green fluorescent protein (GFP) fusion protein. The pattern of GFP expression in the brain of the knockin recapitulates what has been described earlier for Kiss1 in the male and female mouse, with prominent expression in the arcuate nucleus (ARC) (in both sexes) and the anteroventral periventricular nucleus (in females). Single-cell RT-PCR showed that the Kiss1 transcript is expressed in 100% of GFP-labeled cells, and the CreGFP transcript was regulated by estradiol in the same manner as the Kiss1 gene (i.e. inhibited in the ARC and induced in the anteroventral periventricular nucleus). We used this mouse to evaluate the biophysical properties of kisspeptin (Kiss1) neurons in the ARC of the female mouse. GFP-expressing Kiss1 neurons were identified in hypothalamic slice preparations of the ARC and patch clamped. Whole-cell (and loose attached) recordings revealed that Kiss1 neurons exhibit spontaneous activity and expressed both h- (pacemaker) and T-type calcium currents, and hyperpolarization-activated cyclic nucleotide-regulated 1–4 and CaV3.1 channel subtypes (measured by single cell RT-PCR), respectively. N-methyl-D-aspartate induced bursting activity, characterized by depolarizing/hyperpolarizing oscillations. Therefore, Kiss1 neurons in the ARC share molecular and electrophysiological properties of other CNS pacemaker neurons.

## A.2 Introduction

Kisspeptin (encoded by the *Kiss1* gene) and its receptor (Kiss1r) are essential for gating the onset of puberty and regulating reproductive function in mammals (1-2). In the rodent, *Kiss1*mRNA is expressed in the hypothalamic arcuate nucleus (ARC) and anteroventral periventricular nucleus (AVPV) (3-4), where kisspeptin (Kiss1) neurons are thought to serve as conduits for mediating the negative and positive feedback effects of gonadal steroids on GnRH and LH secretion (5–10). Evidence drawn from multiple species suggests that Kiss1 neurons in the ARC may also act as a proximate pacemaker for GnRH neurons. First, GnRH neurons appear to be targets of Kiss1 neurons (4, 11). Virtually all GnRH neurons express *Kiss1r* (12, 13), and kisspeptin potently stimulates the release of GnRH (3) by depolarizing and inducing the sustained firing of action potentials in GnRH neurons (14–17). Second, multiple unit activity recordings in the region of the goat ARC containing Kiss1 neurons show rhythmic volleys of electrical activity that are temporally correlated with discrete pulses of LH secretion (18). Furthermore, measurement of kisspeptin and GnRH by push-pull cannulae placed near the median eminence of the monkey show that both peptides are secreted in a pulsatile and synchronized fashion (19). Third, kisspeptin antagonists inhibit pulsatile GnRH/LH secretion (20). These observations provide tantalizing, albeit indirect, evidence that Kiss1 neurons in the ARC have the properties of central pacemakers, which are capable of driving pulsatile GnRH secretion.

To study the molecular and biophysical properties of living Kiss1 neurons, we have developed a *Kiss1-CreGFP* knockin mouse, wherein it is possible to identify Kiss1 neurons in vivo, investigate their behavior, and study their molecular fingerprint. This new mouse bears a fusion cassette of enhanced green fluorescent protein (GFP) and Cre recombinase (*Cre*) driven by the endogenous *Kiss1* promoter, which directs the expression of *CreGFP*

specifically in Kiss1 neurons. Because expression of the fusion protein is controlled by the endogenous Kiss1 promoter, GFP is regulated in precisely the same manner as the normal *Kiss1* gene and is expressed only when the endogenous *Kiss1* gene is turned on. Cell-specific expression of *GFP* allows visualization of *Kiss1*-expressing neurons for purposes of characterizing their molecular properties in slice recordings and conducting single cell RT-PCR to identify the coexpression of important regulatory genes (e.g. ionic channels). The cell-specific expression of *Cre* also affords the opportunity to create mice with targeted expression of unique reporters or with targeted genetic modifications specifically in cells that express the *Kiss1* gene at some point in their lifetime. Here, we report the initial biophysical and molecular characterization of Kiss1 neurons in the ARC of female mice and demonstrate that Kiss1 neurons have unique properties shared by central pacemaker cells.

## A.3 Materials & Methods

### Animals

Female Kiss1-CreGFP mice (F2 generation) were housed at either the University of Washington (UW) or the Oregon Health and Sciences University (OHSU), and surgeries were conducted at each location, according to the National Institutes of Health Guide for the Care and Use of Laboratory Animals. The UW and OHSU Animal Care and Use Committees approved all of the animal use procedures. At the UW, mice were housed in a light (14-h light, 10-h dark cycle, lights on at 0400)-controlled and temperature (21–23 C)-controlled environment. They were fed standard chow diet and had free access to water. At OHSU, mice were maintained under constant temperature (21–23 C) and 12-h light,

12-h dark cycle schedule (lights on between 0600 and 1800 h), with standard chow and water provided ad libitum.

**Generation of the Kiss1-CreGFP mouse (UW)**

The Kiss1-CreGFP mice were produced by gene targeting technology (21, 22). Briefly, a 13.2-kb Afe1-Sal1 fragment, including approximately 5.0-kb DNA 5´ of the Kiss1 translation start site and approximately 8 kb on the 3´ side, was subcloned from a C57Bl/6 BAC clone (Invitrogen, Carlsbad, CA) into Bluescript. The targeting construct contained a CreGFP fusion protein cassette, followed by an frt-flanked SvNeo gene (for positive selection) inserted just upstream of the normal translation start site for Kiss1. The construct also contained Pgk-DTAand HSV-TK genes for negative selection (Fig. 1). G4 ES cells were electroporated, and 10 positive clones (of 65 analyzed) were identified by digesting DNA with BspH1 and performing Southern blottings using a 350-bp probe located just outside the 5´ boundary of the targeting construct. Positive clones were injected into C57Bl/6 blastocysts, and high percentage chimeras were bred to achieve germline transfer. The frt-Neo gene was removed by breeding the heterozygous mice with FLPer mice (23).

**Ovariectomies (OVX) and estradiol (E2) replacement (UW)**

OVX was performed on adult female mice through bilateral lumbar incisions while maintaining the animals under isoflurane inhalation anesthesia (Abbott Laboratory, Abbott Park, IL) delivered by vaporizer (VetEquip, Pleasanton, CA). Vasculature to the ovary and body wall were sutured, and wound clips were used to close the incision. Immediately after OVX, oil-filled capsules (sham) or E2 plus oil-filled capsules were implanted sc via a small midscapular incision at the base of the neck; wound clips were used to close the incision. For E2 implants, SILASTIC tubing (inner diameter, 1.47 mm; outer diameter, 1.95 mm;

Dow Corning Corp., Midland, MI) was cut to 1.5 cm; one end was sealed with silicone cement (0.25 cm) and allowed to cure overnight. Crystalline E2 (Sigma, St. Louis, MO) at a dose of 1 mg/ml was dissolved in safflower oil based on previous studies (5, 8). After capsules were filled with E2 in oil, the end of the capsule was sealed with silicone cement (0.25 cm) and allowed to cure overnight. The day before the surgery, implants were washed in two changes of 100% ethanol for 10 min and then placed in sterile physiological saline overnight. All animals were given ketoprofen analgesia before surgery and for 48 h after surgery.

**Castration of adult males (UW)**

Testes were removed from adult males through a midline ventral incision while maintaining the animals under isoflurane inhalation anesthesia (Abbott Laboratory) delivered by vaporizer (VetEquip). Vasculature to the testes was sutured to prevent internal bleeding, the body wall was sutured, and wound clips were used to close the incision. Gonadectomized males were given a sham implant and compared with gonad-intact males. All animals were given ketoprofen analgesia before surgery and for 48 h after surgery.

**Validation of GFP expression and regulation in Kiss1-CreGFP mice (UW)**

To establish that the pattern of GFP expression in the brain of Kiss1-CreGFP mice recapitulates that reported earlier for the distribution of Kiss1 mRNA and determine whether gonadal steroids control the expression of GFP, we analyzed the pattern of GFP expression in male and female Kiss1-CreGFP mice. Males were either left intact or gonadectomized, and females were OVX and treated with either sham or E2 (as described above). On d 7 after gonadectomized, mice were anesthetized with ketamine/xylazine cocktail and perfused with 4% paraformaldehyde (PFA) + 0.1 m PBS. Brains were extracted and placed

into 4% PFA + 0.1 m PBS overnight in a dark environment. Once the brains sank, they were transferred into a 1:1 solution of 4% PFA + 0.1 m PBS: 30% sucrose + 0.1% sodium azide (NaN3) in 0.1 mPBS, and upon sinking, the brains were transferred to 30% sucrose + 0.1% NaN3 in 0.1 mPBS. Sections were cut on a cryostat at 30 μm and mounted on slides. Twelve series were collected into 0.1 m PBS/0.1% NaN3 and stored at 4 C. Sections were processed by immunohistochemistry for GFP. Briefly, 30-μm free-floating sections were blocked in PBS with 10% normal goat serum (NGS) and 0.2% Triton X-100 for 1 h at room temperature followed by an overnight incubation with primary antibody solution containing rabbit anti-GFP (1:1000; Invitrogen) in PBS with 1% NGS and 0.2% Triton X-100. After three washes in PBS with 0.2% Triton X-100, a secondary antibody solution containing antirabbit antibody conjugated to Alexa Fluor 488 (1:500; Invitrogen) was added to the sections and incubated for 2 h at room temperature. After the incubation, sections were washed three times for 5 min in PBS with 0.2% Triton X-100, mounted onto slides, and analyzed with confocal microscopy.

**Generation of Kiss1-CreGFP x lacZ mice (UW)**

To determine the pattern of Cre expression in the Kiss1-CreGFP mice and develop a line of mice that express the β-galactosidase (β-Gal) reporter in cells that either produce the Kiss1transcript in adulthood or once expressed Kiss1 during development but no longer do as adults, we crossed the Kiss1-CreGFP mice to the Cre reporter strain B6.129S4Gt(ROSA)26Sortm1Sor/J (stock no. 003474; The Jackson Laboratory, Bar Harbor, ME). In these mice, the expression of the reporter gene (lacZ) is prevented by a loxP-flanked STOP sequence. Crossing the Kiss1-CreGFP mouse to this reporter mouse results in the deletion of the floxed STOP sequence and allows the expression of lacZ in the cell types wherein Cre is expressed. Once recombination has occurred, lacZ is continuously

expressed in that cell. While generating the Kiss1-CreGFP:lacZRep mice, we noticed that some animals (three out of 15) showed early Cre expression, which produced a nonspecific widespread β-Gal staining detected by immunofluorescence. To identify this early recombination event, a standard PCR of tail DNA using primers across the loxP sites (forward, 5′-AAAGTCGCTCTGAGTTGTTAT-3′; reverse, 5′-ATTAAGTTGGGTAACGCC-3′) was performed. The presence of recombination results in a PCR product of 500–600 bp, and animals showing this recombination product in the tail DNA were excluded from the study.

**Double-labeling for GFP and β-Gal (UW)**

To map and compare the distribution of β-Gal and GFP in Kiss1-CreGFP x lacZ female mice, we double-labeled GFP and β-Gal in these mice and analyzed their distribution in various areas of the brain, focusing on the ARC, where our biophysical studies were conducted. Cells that were single- and double-labeled with GFP and β-Gal were counted, and their anatomical distributions were qualitatively assessed. For double-labeling of GFP and β-Gal, adult OVX females (n = 3) were transcardiacally perfused 7 d after OVX with PBS containing 4% PFA. Brains were removed, postfixed overnight, and cryo-protected with 30% sucrose in PBS. For cryo-sectioning, brains were frozen for 5 min on dry ice and sectioned in a freezing microtome. For immunofluorescence, 30-μm free-floating sections were blocked in PBS with 10% NGS and 0.2% Triton X-100 for 1 h at room temperature followed by an overnight incubation with primary antibody solution containing chicken anti-β-Gal antibody (1:5000; Abcam, Cambridge, MA) and rabbit anti-GFP antibody (1:1000; Invitrogen) in PBS with 1% NGS and 0.2% Triton X-100. After three washes in PBS with 0.2% Triton X-100, a secondary antibody solution containing antichicken antibody conjugated to Alexa Fluor 568 and antirabbit antibody conjugated to Alexa Fluor

488 (both 1:500; Invitrogen) was added to the sections and incubated for 1 h at room temperature. After the incubation, sections were washed three times for 5 min in PBS with 0.2% Triton X-100 and mounted onto slides before imaging with an epi-fluorescent microscope (Eclipse E600; Nikon, Melville, NY). To determine the percentage of colocalization of β-Gal and GFP, the total number of β-Gal-positive cells in the ARC was counted, and the percentage double-labeling for GFP (i.e. β-Gal + GFP) was calculated in one of every six sections (180 μm apart, eight sections per mouse) for the three different animals.

**Electrophysiological characterization of GFP-expressing Kiss1 neurons in female mice (OHSU)**

Animals were OVX under isofluorane anesthesia 7 d before experimentation and were given a dose of 4 mg/kg carprofen (Rimadyl, Pfizer Animal Health, NY) immediately after surgery for analgesia. On the 7th d after OVX, animals were killed by decapitation. The brain was quickly removed, and a block containing the basal hypothalamus (BH) was immediately dissected. The BH block was submerged in cold (4 C) oxygenated (95% O2, 5% CO2) high sucrose artificial cerebrospinal fluid (aCSF): 208 mm sucrose, 2 mm KCl, 26 mm NaHCO3, 10 mmglucose, 1.25 mm NaH2PO4, 2 mm MgSO4, 1 mm CaCl2, and 10 mm HEPES (pH 7.4). Coronal slices (∼250 μm) were cut on a vibratome, during which time (10 min) the slices were bathed in high sucrose aCSF at 4 C. The slices were then transferred to an auxiliary chamber where they were kept at room temperature (25 C) in aCSF consisting of 124 mm NaCl, 5 mmKCl, 2.6 mm NaH2PO4, 2 mm MgSO4, 2 mm CaCl2, 26 mm NaHCO3, 10 mm HEPES, and 10 mm glucose (pH 7.4) until recording (recovery for 2 h). A single slice from the ARC was transferred to the recording chamber one at a time and was kept viable by continually perfusing with warm (35 C) oxygenated aCSF at 1.5 ml/min.

**Visualized whole-cell patch recording (OHSU)**

Whole-cell patch recordings were made in ARC-GFP-tagged Kiss1 neurons using an Olympus BX51 fixed-stage scope out-fitted with IR-DIC video imaging (Olympus, Center Valley, PA), as described (24). Patch pipettes (1.5 mm outer diameter borosilicate glass; A-M Systems, Seattle, WA) were pulled on a Flaming/Brown puller (Model P-97; Sutter Instrument Co., Novato, CA) and filled with the following solution: 128 mm potassium gluconate, 10 mm NaCl, 1 mm MgCl2, 11 mm EGTA, 10 mm HEPES, 2 mm ATP, and 0.25 mm GTP; adjusted to pH 7.3 with KOH; 295 mOsm. Pipette resistances ranged from 3–5 mΩ. In whole-cell configuration, access resistance was less than 20 mΩ; the access resistance was 80% compensated. The input resistance was calculated by measuring the slope of the current-voltage relationship curve between −70 and −50 mV. Standard whole-cell patch recording procedures and pharmacological testing were followed, as described (16, 25, 26). Electrophysiological signals were amplified with an Axopatch 200B amplifier and digitized with a Digidata 1440A (Molecular Devices, Foster City, CA), and the data were analyzed with p-Clamp software (version 10.0; Molecular Devices). Steady-state current/voltage (I/V) plots were constructed, with step command potentials from −140 to −50 mV at an increment of 10 mV (with holding potential at −60 mV) and duration of 1 sec. The liquid junction potential was corrected for all analyses. For the loose-patch cell recordings, the patch pipettes were filled with aCSF, and a loose seal (20- to 60-mΩ seal resistance) was formed on the Kiss1 neurons to measure spontaneous action currents in voltage clamp mode with the voltage clamped to 0 mV relative to the bath potential (27). Consecutive current traces were filtered at 2 kHz and acquired at a sampling rate of 50 kHz.

**Molecular characterization of GFP-expressing Kiss1 neurons by single-cell RT-PCR (scRT-PCR) (OHSU)**

Tissue preparation On the day of experimentation, a 1-wk-OVX mouse was given a dose of ketamine (15 mg ip). The animal was then rapidly decapitated, its brain removed from the skull, and a diencephalic block was dissected. The resultant block was mounted on a cutting platform that was then secured in a vibratome well filled with ice-cold, oxygenated (95% O2, 5% CO2) high sucrose aCSF. Four coronal slices (240 μm) were cut through the hypothalamus. The slices were transferred to a multiwell auxiliary chamber containing oxygenated aCSF: 124 mm NaCl, 5 mm KCl, 1.44 mm NaH2PO4, 5 mm HEPES, 10 mm dextrose, 26 mm NaHCO3, and 2 mmCaCl2 and kept there until recovery (1–2 h).

**Neuronal harvesting in the ARC and RT**

The method used for neuronal harvesting was according to established procedures (28) with some modifications as follows. Briefly, the ARC was dissected and exposed to protease and gentle trituration to disperse the neurons. The dispersed cells were visualized using a Leitz inverted microscope, patched, and then harvested with gentle suction using the XenoWorks microinjector system (Sutter Instrument Co.). Cells were harvested as single cells or as pools of five individual cells. The contents of the pipette were expelled into a test tube containing a solution with 1× Invitrogen Superscript III buffer, 15 or 18 U of RNasin (Promega, Madison, WI) and 10 mm of dithiothreitol in 5 or 8 μl total volume for single cells and pools, respectively. Each harvested cell (or pool of cells) was reverse transcribed as described previously (28), with modifications in which both random primers (100 ng/cell; Promega) and anchored oligo(dT)20 primer (400 ng/cell; Invitrogen), and Superscript III reverse-transcriptase (100 U/cell, Invitrogen) was used. In addition, harvested aCSF in the vicinity of the dispersed cells also underwent RT and was used as a control. Cells and tissue RNA used as negative controls were processed as described above but

without RT (−RT). Each cell or pool of cells was analyzed by using either PCR or real-time PCR.

**Single-cell RT-PCR**

The PCR was performed using 2–3 μl of cDNA template from each RT reaction in a 30-μl PCR mix. Forty to 50 cycles of amplification were performed using a Bio-Rad C1000 Thermal Cycler (Bio-Rad, Hercules, CA) according to established protocols (28, 29). PCR products were visualized with ethidium bromide on a 2% agarose gel.

**Quantitative PCR (qPCR)**

qPCR was performed on an Applied Biosystems 7500 Fast real-time PCR system (Applied Biosystems, Foster City, CA) with the SybrGreen master-mix method according to established protocols (28). A standard curve was prepared for each primer pair [hyperpolarization-activated cyclic nucleotide-regulated (HCN)1, HCN2, HCN3, HCN4, and β-actin] with mediobasal hypothalamus (MBH) cDNA serial dilutions, and Kiss1 neuronal pools were analyzed. In all cases, real-time PCR assays were tested to determine and compare the efficiencies of the target and control gene amplifications. Serially diluted cDNA from mouse BH, assayed in triplicate, were used to construct standard curves (see figure 7), and the amplification efficiency for each primer pair was calculated as follows: $E = 10(-1/m) - 1$, where m is slope (30, 31). Amplification efficiencies were 100% for all primer sets, including β-actin. The Applied Biosystems sequence detection software system (version 1.3) was used to generate the standard curves. The comparative ΔΔ cycle threshold (CT) method was used to calculate the individual values for each sample as described previously (28). Briefly, cDNA samples (4 μl for HCN transcripts and 2 μl for β-actin) from Kiss1 pools were run in duplicates, and the mean ΔCT of the HCN1 values

for Kiss1 pools was used as a calibrator when comparing the mRNA quantities of HCN1, HCN2, and HCN3 (HCN4 was not detectable in 4-μl samples of the Kiss1 pools). The relative linear quantity of the target gene was calculated using the formula $2-\Delta\Delta CT$ (30). Therefore, the data were expressed as an n-fold change in gene expression normalized to a reference gene (β-actin) and relative to the HCN1 values. The data are reported as relative mRNA expression. For statistical analysis, a one-way ANOVA with Dunnett's post hoc test was performed with GraphPad Prism version 4.0 (GraphPad Software, San Diego, CA).

**Primer design and development**

Primer pairs for scRT-PCR and qPCR were developed by using the mRNA sequence of the respective genes from the National Center for Biotechnology Information (see Table 1). Primers were designed using the Clone Manager software (Sci Ed Software, Cary, NC) based on the mRNA sequences. The primers were designed to cross introns to preclude any genomic DNA amplification, and the PCR product from single cells was sequenced to confirm the correct product.

## A.4 Results

**Validation of the *Kiss1-CreGFP* knockin mouse**

Cells expressing GFP were clearly observed in the ARC and the AVPV/periventricular nucleus, areas previously shown to comprise Kiss1- and kisspeptin-expressing cells in the brain of the female (Fig. 2) (3, 7), as well as the male mouse (Supplemental Fig. 1) (6). Furthermore, analysis by RT-PCR of 160 cells from six animals revealed that all GFP-expressing cells were positive for *Kiss1*, whereas none of the 13 nonfluorescent cells from those same animals had detectable levels of *Kiss1* mRNA (13 cells from six animals). We

also tested whether any of the GFP-expressing neurons expressed *Pomc* mRNA (n = 43 cells from two different animals) and found that none of the GFP-labeled cells expressed detectable levels of *Pomc* mRNA. To confirm that expression of *GFP* in the *Kiss1-CreGFP* mice is under the control of the endogenous *Kiss1* promoter (as expected), we compared the relative expression of GFP in the presence and absence of E2 and found that E2 regulate-sCreGFP in precisely the same manner as Kiss1, inducing its expression in the AVPV and inhibiting its expression in the ARC (Fig. 2). Thus, based on their anatomical distribution, confirmation of Kiss1 expression in the GFP-labeled cells by scRT-PCR, and evidence of regulation by the endogenous promoter, we deduce that GFP-expressing cells visualized in *Kiss1-CreGFP* knockin mice represent Kiss1 neurons.

*Kiss1-CreGFP* mice crossed with *lacZ* reporter mice produced F1 mice in which β-Gal is expressed in cells that either currently (in adulthood) or earlier in development expressed the *CreGFP* fusion protein driven by the endogenous Kiss1 promoter. Thus, β-Gal marks every cell that ever expressed the *Kiss1* gene at any time in its history. First, we found that the anatomical distribution of GFP-expressing cells in the cross was indistinguishable from that observed in the *Kiss1-CreGFP* mouse (e.g. prominent expression in the ARC and AVPV). Second, the number of cells showing GFP staining alone was insignificant (Fig. 3, A–C). Third, the distribution of cells stained for β-Gal only in the MBH extended well beyond the distribution of cells that were double-labeled for both markers, (Fig. 3, A–C) and outside of the boundary previously reported for *Kiss1* mRNA in the ARC (5, 6), extending into the dorsomedial and ventrolateral parts of the ventromedial hypothalamic nucleus. Analysis revealed that approximately 75% (74 ± 5%) of the cells comprised within the arcuate were colabeled, whereas the remaining cells were immunopositive for β-Gal only. This implies that a significant number of β-Gal-labeled cells once expressed *Kiss1*

during development but no longer do so as adults, whereas cells that express both β-Gal and *GFP* represent the population that currently express *Kiss1* and would thus constitute "Kiss1 neurons."

**Biophysical properties of GFP-labeled Kiss1 neurons in the ARC**

Using whole-cell patch recording in oil-treated OVX females, we found that Kiss1 neurons in the ARC exhibited a resting membrane potential of −63.8 ± 2.3 mV (n = 20). Kiss1 neurons in the ARC exhibited tonic, irregular, and silent firing patterns (Fig. 4, A–D). Under loose-patch, recording conditions in which the cell's internal milieu is undisturbed, Kiss1 neurons in the ARC exhibited virtually the same tonic, irregular, and silent firing patterns (Fig. 5, A–D). Moreover, the majority (>80%) of Kiss1 neurons in the ARC expressed both pacemaker (h-current) and T-type $Ca^{2+}$ currents, as revealed by measuring the response to hyperpolarizing steps from −65 to −140 mV, where Vhold= −60 mV (n = 49) (Fig. 4E). Because the expression of h-current and T-type calcium currents is critical for generating burst firing in hypothalamic and thalamic neurons (32–34), we determined whether or not Kiss1 cells in the ARC exhibit burst-firing behavior. To evaluate this possibility, we applied the glutamate receptor agonist N-methyl-D-aspartate (NMDA) (40 μm) to Kiss1 neurons in the ARC and found that these cells exhibited clear burst firing in both whole-cell patch (Fig. 4, F–H) and loose-patch (Fig. 5, E and F) cell recordings, similar to that described for Kiss1 neurons in the guinea pig (24). Moreover, in the presence of tetrodotoxin (applied to block fast Na+spikes), NMDA-dependent membrane oscillations (up and down states) were clearly evident (Fig. 4H). Therefore, Kiss1 neurons in the ARC exhibit NMDA-driven and presumably glutamate-driven burst firing. Moreover, it appears that Kiss1 neurons in the ARC of the female mouse express two endogenous pacemaker conductances (T-type calcium and h-currents), which can be activated through

glutamatergic inputs to generate burst firing. In addition, the application of γ-aminobutyric acid (GABA) (100 μm) to the bath silenced the firing of Kiss1 neurons in the ARC (Figs. 4I and 5, G and H).

**scRT-PCR for channel subunits**

The whole-cell analysis revealed that the pacemaker (hyperpolarization-activated, non-selective cation) current ($I_h$) was prominent in Kiss1 neurons in the ARC. Because hyperpolarization-activated cyclic nucleotide-gated (HCN) channels underlie the h-current, we used scRT-PCR to determine which of the HCN channel subtypes might be expressed in these Kiss1 cells. We found HCN1, HCN2, and HCN3 transcript in 40, 54, and 53%, of Kiss1 cells, respectively, whereas HCN4 was only found in 23% of Kiss1 neurons (an average of 25 cells/animal from four animals) (Fig. 6, A and B). For a more quantitative analysis, we measured HCN channel subtypes in pools of Kiss1 neurons in the ARC by using real-time PCR (an average of three pools per animal from three animals) (Fig. 7A). This analysis revealed that HCN2 and HCN3 were more highly expressed than HCN1, corroborating the scRT-PCR findings. The amount of the HCN1 channel subtype mRNA was about 50% of that found for the HCN2 and HCN3 channel subunit mRNA (Fig. 7B), and HCN4 mRNA was undetectable at the cDNA level used.

Because the T-type calcium channels also play a prominent role in burst firing activity [McCormick and Huguenard (34), Erickson et al. (32), and Kelly and co-workers (33)], we sought evidence for their expression in Kiss1 neurons in the ARC. Again, by scRT-PCR, we found that T-type subunits were expressed in Kiss1 neurons in the ARC, with CaV3.1 mRNA being coexpressed in 44% of Kiss1 neurons (an average of 20 cells/animal from six animals) (Fig. 8). The CaV3.2 subunit was also detectable, but CaV3.3 was nondetectable in Kiss1 neurons (data not shown).

## A.5 Discussion

We describe the initial characterization of a mouse that expresses a Cre-GFP fusion protein, knocked into the endogenous *Kiss1* locus. This mouse expresses *GFP* and *Cre* in neurons that are actively transcribing the *Kiss1* gene. We verified that *GFP*-expressing neurons in these mice are in fact Kiss1 neurons by confirming that such cells express *Kiss1* mRNA by scRT-PCR of *GFP*-expressing cells and documenting that *GFP*-expressing cells show a distribution profile comparable with the expression of *Kiss1* mRNA as mapped by *in situ* hybridization (3, 5, 6). Because the construct was knocked into the endogenous *Kiss1* locus, we anticipated that *GFP* would be regulated by factors known to regulate the expression of *Kiss1* mRNA, including sex steroids. We affirmed this supposition by demonstrating that E2 regulates the expression of GFP in the same manner as *Kiss1* in both males and females (i.e. inhibits GFP expression in the ARC and induces its expression in the AVPV) (5, 6).

The *Kiss1-CreGFP* mice described here differ in several respects from two other previously reported models (35, 36). We used a targeted knockin strategy to direct the expression of both GFP and Cre under the endogenous Kiss1 promoter, whereas Cravo et al. (35) used a BAC transgenic to produce their model, and Mayer et al. (36) inserted an IRES-*Cre* downstream of the *Kiss1* coding region to produce their mice. Second, our mice express a *GFP-Cre* fusion cassette under the transcriptional control of the endogenous *Kiss1* promoter. Thus, in the *Kiss1-CreGFP* knockin mouse, GFP is expressed by *Kiss1* neurons (and can be visualized *in vivo*), without having to be crossed with a reporter mouse. This is important, because we have observed that when the *Kiss1-CreGFP* mouse is crossed with the *lac Z*/β-Gal mouse, we see a greater number and wider distribution of β-Gal-positive cells in the *Kiss1-CreGFP* x reporter cross than can be seen by either GFP-labeling in the *Kiss1-CreGFP* mouse or single label in situ hybridization for Kiss1 mRNA

in wild-type mice (Fig. 3) (5, 6). The distribution of β-Gal in the *Kiss1-Cre* transgenic x *lacZ* cross described by Cravo et al.(35) shows a similar extended expression pattern. Therefore, when any *Kiss1-Cre* model is bred to a reporter mouse, one cannot be certain that the cells labeled with the reporter in the adult are, in fact, contemporaneously expressing the *Kiss1* gene, without independent corroboration of the identity of those cells (e.g. scRT-PCR). This phenomenon may reflect the complex lineage of *Kiss1* neurons during embryonic development, wherein some *Kiss1*-expressing progenitor cells differentiate into a non-*Kiss1* lineage, as has been reported for Pomc neurons (37). It may also be the case that *Kiss1* is turned on transiently (at low levels) in many cells in the brain (and elsewhere) during embryonic development, only to be silenced in adulthood. This fact has no bearing on our recordings (or scRT-PCR) results, because our mice have *GFP* knocked into the endogenous *Kiss1* locus (under the *Kiss1* promoter). However, care must be exercised when interpreting results from either electrophysiological measurements or targeted gene disruption studies based on mice produced by crossing any *Kiss1-Cre* mouse with a mouse bearing either a reporter or a conditional allele to create cell-specific knockouts (e.g. estrogen receptor α) (36, 38). This is because *Kiss1* promoter-dependent Cre recombination during development is likely to be more extensive and more variable than predicted simply based on the pattern of Kiss1 expression in the adult.

Although GnRH neurons themselves exhibit spontaneous tonic and burst firing activity (39), growing evidence suggests that Kiss1 neurons in the ARC provide the rhythmic drive to GnRH neurons that leads to pulsatile GnRH and LH secretion (18–20, 40–43). Indeed, we argued that if *Kiss1* neurons in the ARC were the source of the rhythmic drive to pulsatile GnRH secretion, they would exhibit biophysical properties shared by other pacemaker-type cells in the hypothalamus, thalamus, and subthalamic nucleus (24, 32–34,

44). Using whole-cell patch recording techniques, we targeted GFP-expressing cells in the ARC of *Kiss1-CreGFP* mice and studied their electrophysiological properties. First, we demonstrated the expression of a hyperpolarization-induced cation current (h-current) and a transient (T-type) Ca2+ current, both of which are critical conductances exhibited by pacemaker neurons (34,45). Second, we found that Kiss1 neurons in the ARC express the requisite transcripts, HCN and CaV3.1 channels, that underlie these pacemaker currents. Third, we observed that Kiss1 neurons exhibit NMDA-induced burst firing activity, characterized by membrane oscillations. Finally, we learned that GABA profoundly inhibits Kiss1 neurons and could thus serve as one arc in a feedback circuit that governs rhythmic burst firing of Kiss1 neurons (34, 44). These observations in the female mouse extend and corroborate earlier findings in "native" Kiss1 neurons in the ARC of the guinea pig, which also express h- and T-currents and exhibit burst firing in response to NMDA and may thus represent shared features among these neurons across species (29).

Although Kiss1 neurons in the ARC sit at a relatively negative resting membrane potential (−63.8 mV in OVX mice), this potential is depolarized relative to the range necessary to recruit a critical fraction of T-type calcium channels (16). In addition, the vast majority of the h-current is activated at even more negative potentials (46). Thus, inhibitory synaptic inputs (e.g. GABA via GABA-B receptors and dynorphin via $\kappa$ opioid receptors) may be necessary for reaching these hyperpolarized states to recruit more T-type calcium channels and activate a critical fraction of the h-current. GABAergic neurons are abundant in the ARC (47), and dynorphin is colocalized in Kiss1 neurons (42) Thus, it is conceivable that either (or both) GABA and dynorphin produced by Kiss1 neurons themselves could act autosynaptically to hyperpolarized Kiss1 neurons between bouts of activity, as has been previously suggested (18, 42). Therefore, we conclude that Kiss1 neurons in the ARC of

the mouse contain the requisite molecular components and elicit electrophysiological behaviors that would allow them to act in a pacemaker network and serve as a proximate source of the stimulatory input to GnRH neurons.

| Name | Product Length (bp) | Primer sequence | bp no. | Accession no. |
|---|---|---|---|---|
| Kiss1 | 132 | TGCTGCTTCTCCTCTGT<br>ACCGCGATTCCTTTTCC | 64–80<br>195–179 | NM_178260 |
| HCN1 | 136 | TTGCTGGCGTTATCACCAAG<br>AGGGAGTAAAGAC-<br>GACAGTAGG | 1527-1546<br>1662-1641 | NM_010408 |
| HCN2 | 97 | ATGCTGCAAGACTTCCCCAGCG<br>TGGCCTTGAAGAGCGCGAAC | 1423-1444<br>1561-1572 | NM_008226 |
| HCN3 | 118 | TGCGGTGCTTGAGGAGTTCC<br>ACTCGGCTCAGAGCGTTTC | 1664–1682<br>1781–1763 | NM_008227 |
| HCN4 | 123 | CACTAAGGGCAACAAAGAGACC<br>AGTGAGTAGAGGCG-<br>GCAATAAG | 1929–1948<br>2051–2030 | NM_001081192 |
| CaV3.1 | 144 | TACTTCATCGCCCTCATGAC<br>GTTGACAGGCAGCTGAATAC | 2935–2954<br>3059–3078 | NM_009783 |
| CaV3.2 | 284 | CTCTGGGCTTCCTTTAGTAG<br>ATCTCCCAGACGCTTATG | 2640–2659<br>2906–2923 | NM_021415 |
| CaV3.3 | 128 | TGGGCATTTTTGGCAAGAA<br>CAGTGCGGATGGCTGACA | 965–973<br>1093–1110 | NM_001044308 |
| POMC | 242 | CCTCCTGCTTCAGACCTCCAT<br>CAGCACTGCTGCTGTTCCT | 45–65<br>286–304 | NM_008895 |
| β-actin | 110 | AAGGCCAACCGTGAAAAGAT<br>GTGGTACGACCAGAGGCATAC | 416–435<br>505–525 | NM_007393 |

Table A.1: Primers used for generating probes for scRT-PCR in GFP-expressing neurons in the ARC of Kiss1-CreGFP female mice

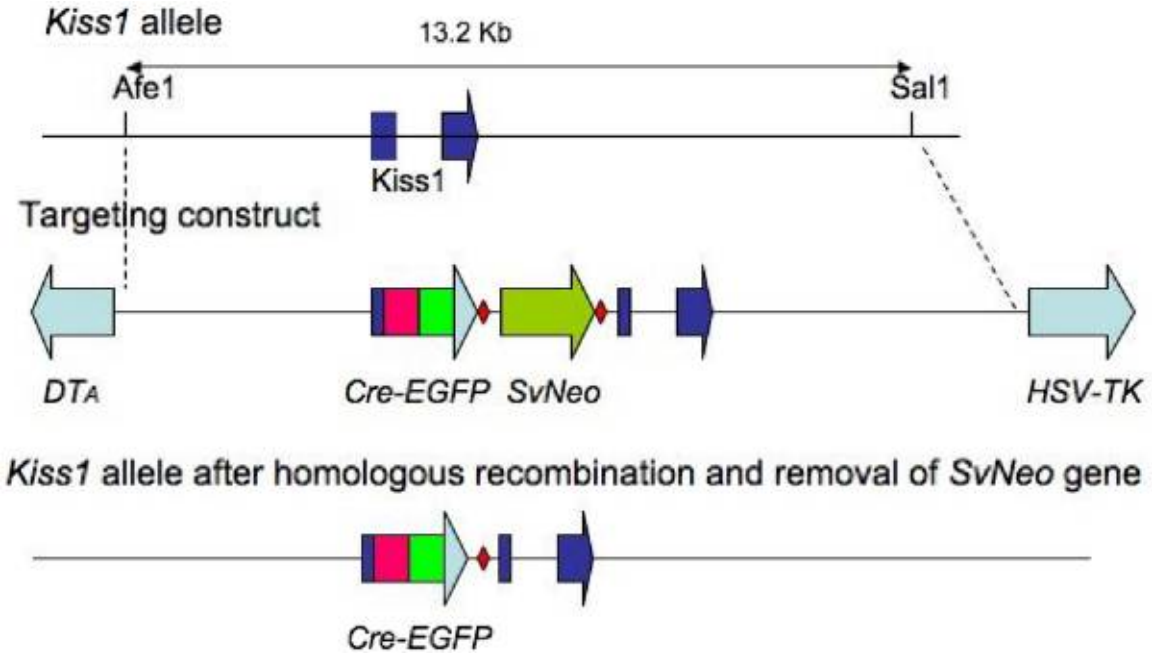


Figure A.1: Kiss1-CreGFP targeting construct

A 13.2-kb Afe1-Sal1 fragment, including approximately 5.0-kb DNA 5´of the Kiss1translation start site and approximately 8 kb on the 3´ side (depicted as broken dark blue arrow with a line through it in the top panel), was subcloned from a C57Bl/6 BAC clone into Bluescript. The targeting construct (depicted in the middle panel) contained a CreGFP fusion protein cassette (red and green arrow inserted in the middle of the first segment of the dark blue broken arrow from the top panel), followed by an frt-flanked SvNeo gene [for positive selection, illustrated by red diamonds (frt sites) surrounding a green arrow(SvNeo)] inserted just upstream of the normal start site for Kiss1. The construct also contained Pgk-DTA and HSV-TK (light blue arrows) genes for negative selection. The frt-Neo gene was removed by breeding the heterozygous mice with FLPer mice. The final construct is depicted in the bottom panel, illustrating a new Kiss1 allele that contains a Cre-eGFP cassette inserted before the native Kiss1 start site.

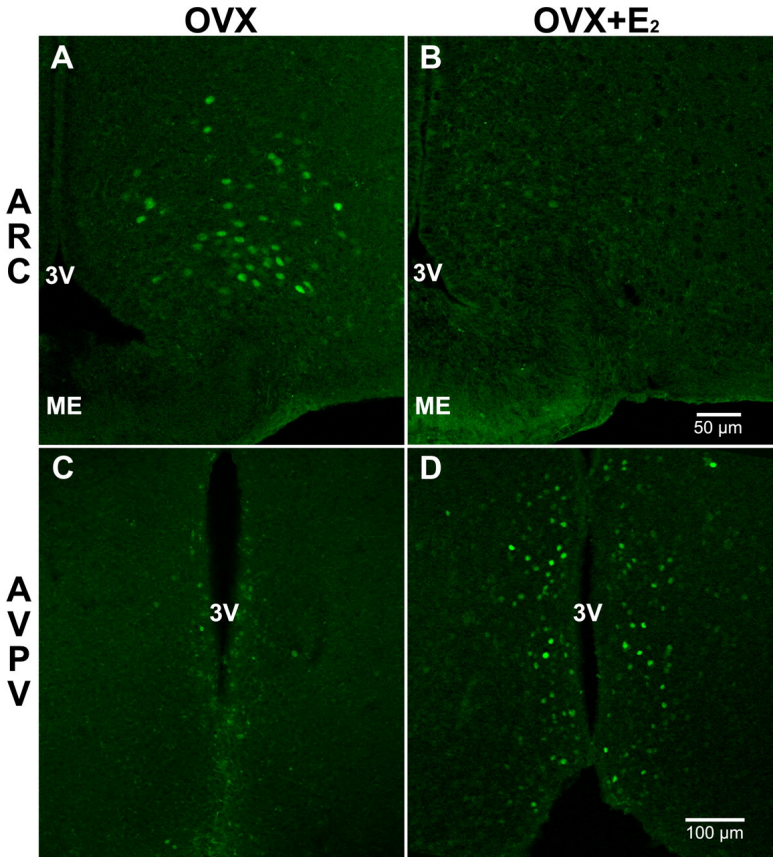


Figure A.2: Photomicrographs of GFP-expressing cells in the ARC and the AVPV of OVX Kiss1-CreGFP knockin mice with and without E2treatment.

The distributions of GFP expression in the ARC (A and B) and the AVPV (C and D) are similar to the known distributions ofKiss1 mRNA in those same regions. Furthermore, E2 treatment reduces GFP expression in the ARC (B) compared with controls (A) but increases GFP expression in the AVPV (D) compared with controls (C), just as E2 has been shown to inhibit Kiss1 mRNA expression in the ARC and induce its expression in the AVPV (5). A and B show endogenous GFP fluorescence. In C and D, fluorescent immunohistochemistry was used to improve the visualization of GFP. ME, Median eminence; 3V, third ventricle.

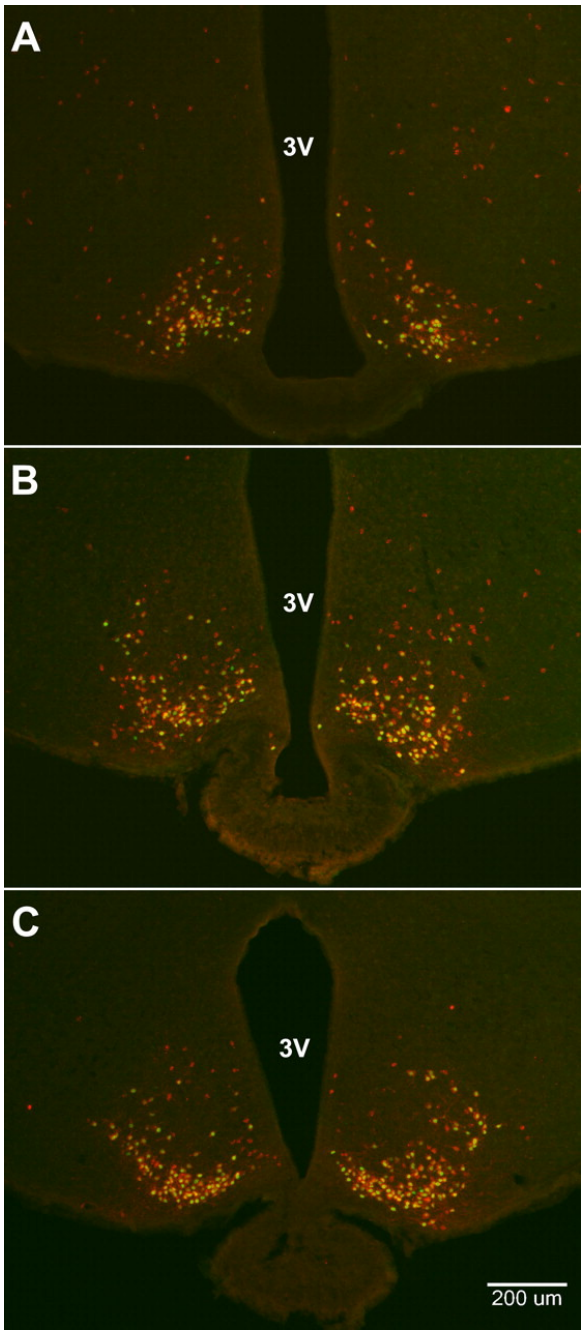


Figure A.3: Photomicrographs of GFP (green)- and β-Gal (red)-stained neurons in the ARC of OVX female Kiss1-CreGFP:LacZRep mice.

Neurons labeled for both GFP and β-Gal appear yellow. Panels show sections from the rostral (A), middle (B), and caudal (C) arcuate. 3V, Third ventricle.

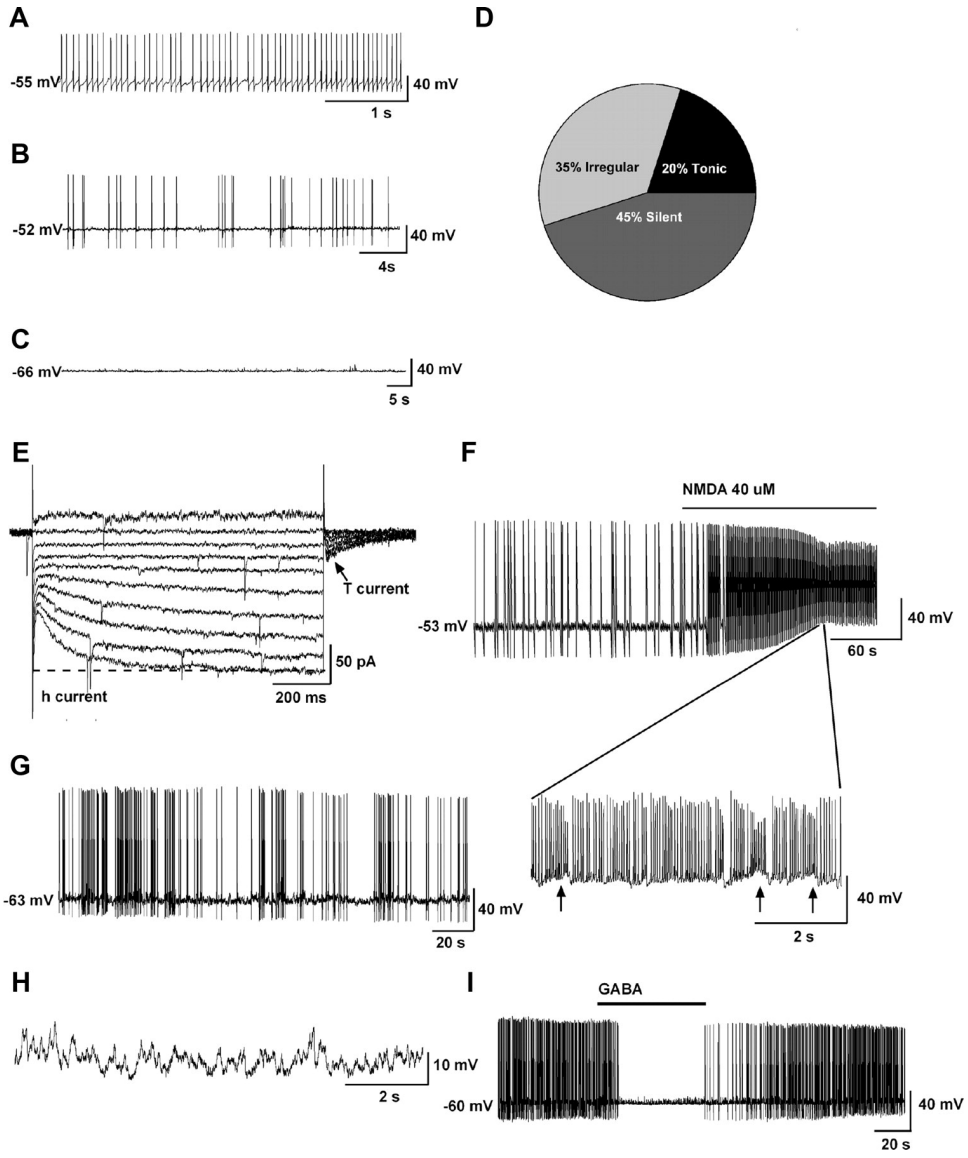


Figure A.4: Electrophysiological characteristics of arcuate Kiss1 neurons in oil-treated OVX Kiss1-CreGFP mice using whole-cell patch recording.

Figure A.4 legend: Kiss1 neurons in the ARC (of the female) rest at −63.8 ± 2.3 mV (n = 20). A–C, Representative traces of action potentials recorded from arcuate Kiss1 neurons showing tonic (A), irregular (B), and silent (C) firing patterns. D, Summary pie chart of the firing pattern distribution in ARC Kiss1 neurons (n = 20). E–H, Endogenous conductances and NMDA-induced burst firing of an ARC Kiss1 neuron. E, Ensemble of currents in response to depolarizing/hyperpolarizing steps from −50 to −140 mV illustrating the expression of a hyperpolarization-activated cation current (h-current) and a T-type Ca2+ current (arrow) in a representative Kiss1 neuron. Vhold = −60 mV. F, Current clamp recording in an ARC Kiss1 neuron showing the response to NMDA (40 μm). The spiking in F was expanded to illustrate the pronounced effects of NMDA on burst firing activity of Kiss1 neurons with an ensemble of spikes riding on top of low-threshold spikes (arrows). G, In a current clamped state close to the resting membrane potential, one can see the bursting activity in the presence of NMDA. H, In the presence of tetrodotoxin to block the fast Na+ spikes, one can clearly see the membrane oscillations (up and down states) induced by NMDA. Eighty percent of ARC Kiss1 neurons expressed the endogenous conductances (h-current, T-current) that are critical for generating burst firing activity. Although ARC Kiss1 neurons did not exhibit spontaneous burst firing activity, glutamate (NMDA) was able to induce burst firing activity in all of the cells. I, GABA (100 μm) inhibited firing in another arcuate kisspeptin neuron. Drugs were rapidly perfused into the bath as a 100-μl bolus.

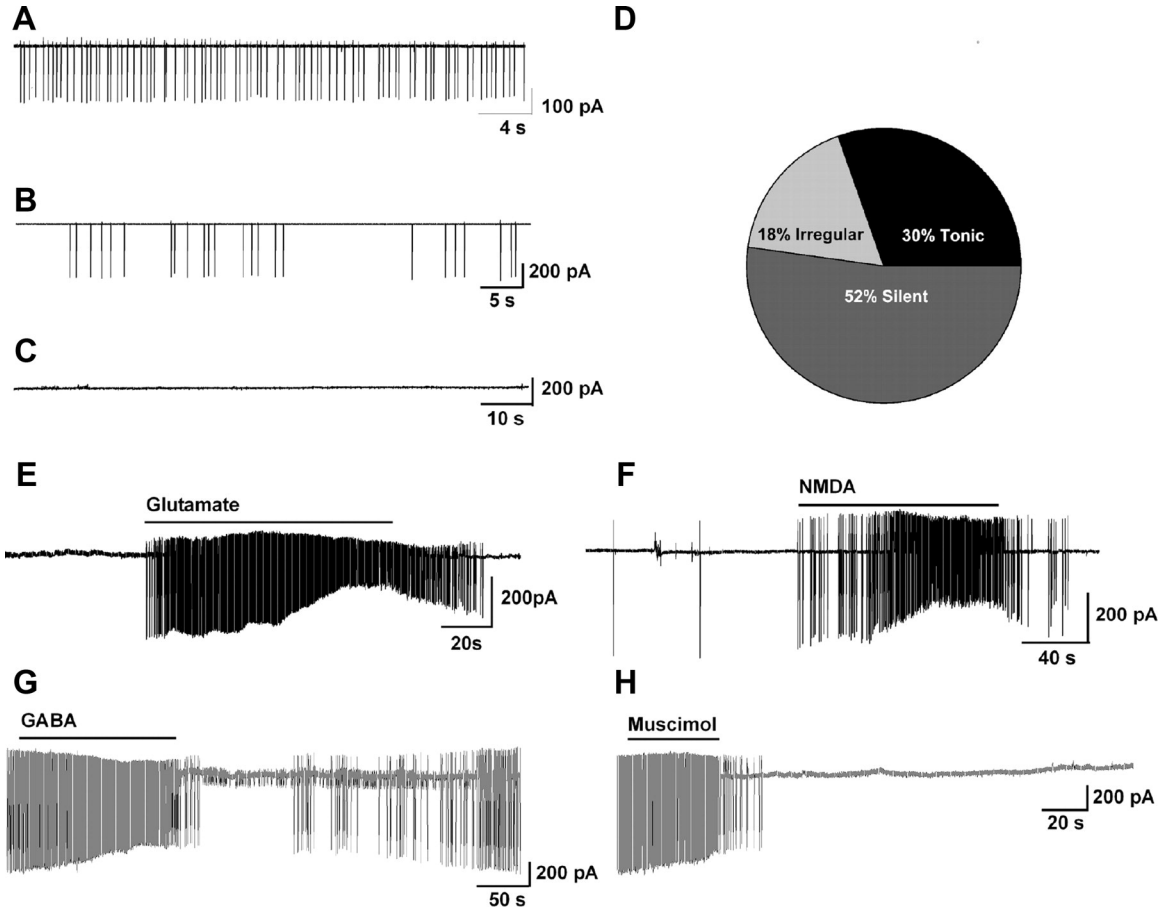


Figure A.5: Cellular characterization of arcuate Kiss1 neurons in oil-treated, OVX Kiss1-CreGFP mice in loose-patch cell recordings.

A–C, Representative traces of action potentials recorded from Kiss1 neurons showing tonic (A), irregular (B), and silent (C) firing patterns. D, Summary pie chart of the firing pattern distribution in arcuate Kiss1 neurons (n = 23). E and F, Glutamate-induced (100 μm, n = 4) (E) and NMDA-induced (40 μm, n = 4) (F) burst firing in arcuate kisspeptin neurons. G and H, GABA-inhibited (100 μm, n = 5) (G) and muscimol-inhibited (10 μm, n = 4) (H) firing in arcuate Kis1 neurons. Drugs were rapidly perfused into the bath as a 100-μl bolus.

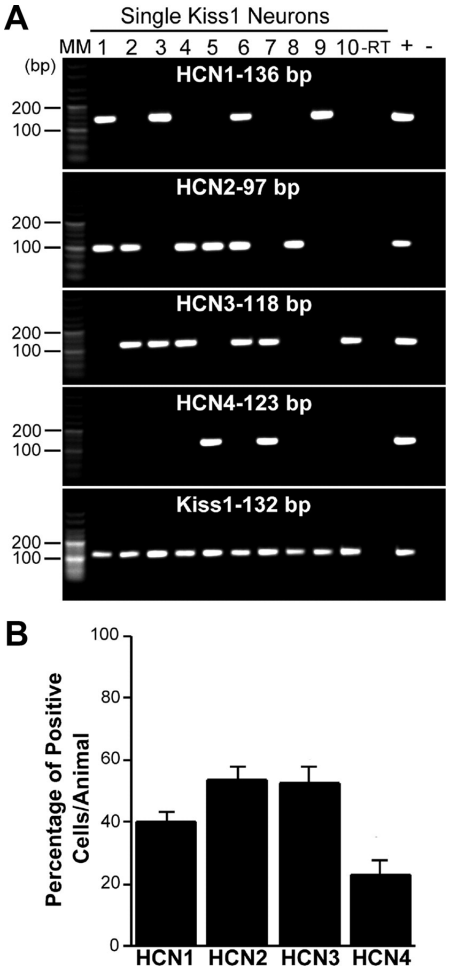


Figure A.6: Expression of HCN channels in single Kiss1 neurons from the ARC of OVX Kiss1-CreGFP mice.

A, Representative gels illustrating the mRNA expression of HCN channel subtypes 1–4. The expected sizes for the PCR products are as follows: for HCN1, 136 bp; for HCN2, 97 bp; for HCN3, 118 bp; for HCN4; 123 bp; and for Kiss1, 132 bp. As a negative control, a cell reacted −RT did not express any of the transcripts. MBH tissue RNA was also included as a positive control (+, With RT) and negative control (−, Without RT). MM, Molecular markers. B, Summary bar graphs of the percentage expression of HCN1, HCN2, HCN3, and HCN4. An average of 25 cells/animal from six animals was analyzed by scRT-PCR, and the mean number of neurons expressing HCN channel subtypes from each animal was determined. Bar graphs represent the mean ± sem of the percentage of Kiss1 neurons expressing each HCN subtype per animal.

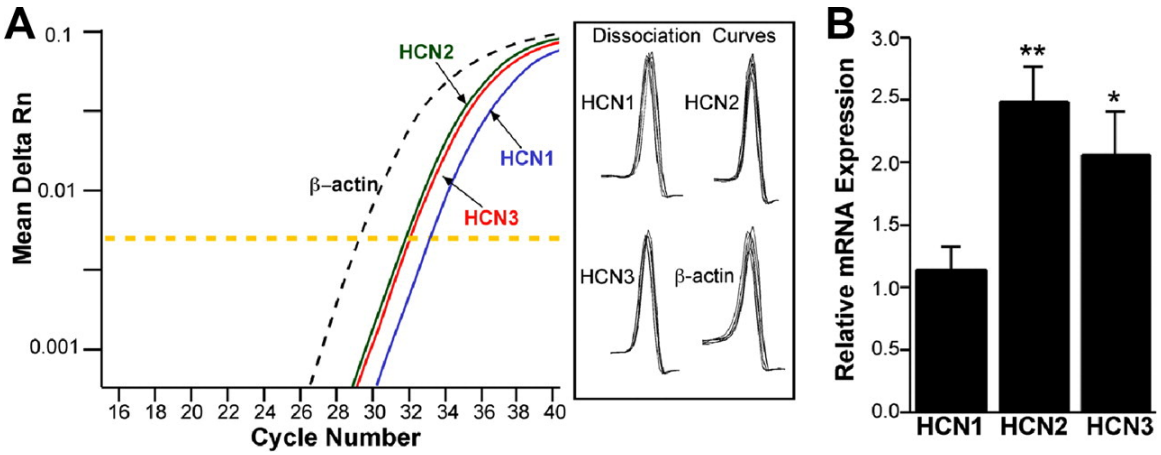


Figure A.7: Relative HCN subtype expression in Kiss1 neurons in the ARC of Kiss1-CreGFP mice.

A, Real-time PCR amplification and dissociation curves for HCN1–3 and β-actin. The HCN1 (blue line), HCN2 (green line), and HCN3 (red line) depict the mean CT values for each of the three channel subtypes. The expression values were normalized to β-actin (black dotted line). The yellow dotted line is the midpoint of the exponential phase of amplification at which the CT was determined. B, qPCR measurements of HCN1, HCN2, and HCN3 mRNA in Kiss1 neuronal pools (three to six pools per animal) from OVX mice (n = 3 animals). HCN2 and HCN3 had higher expression relative to HCN1. The expression values were calculated via the $\Delta\Delta$CT method and normalized to the mean $\Delta$CT of HCN1 expression levels. Bar graphs represent the mean ± sem. *, $P < 0.05$, HCN3 vs. HCN1 (ANOVA); **, $P < 0.01$, HCN2 vs. HCN1 (ANOVA).

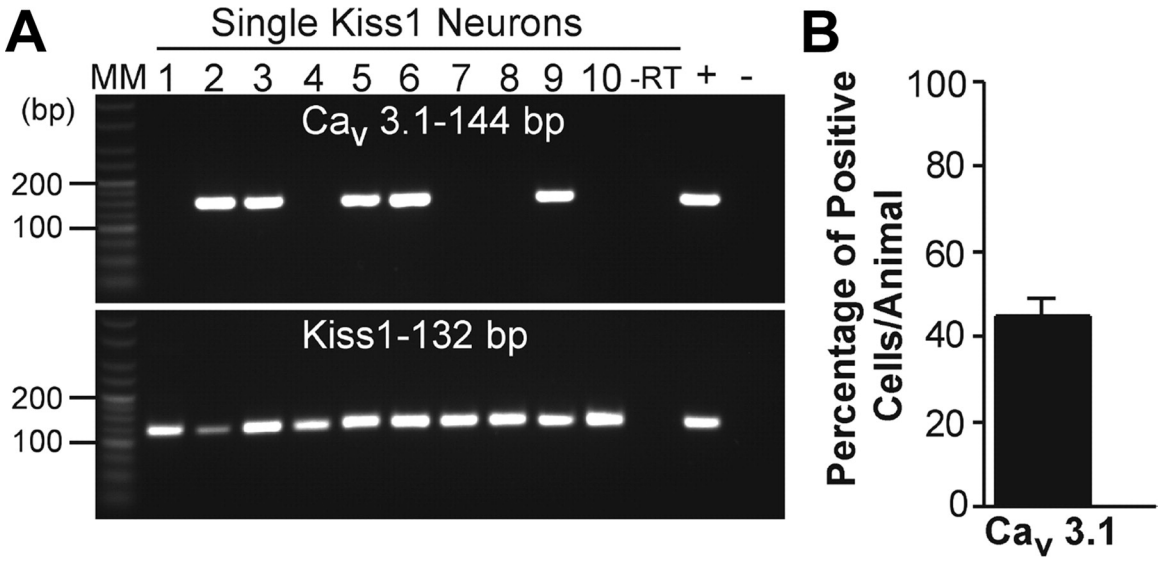


Figure A.8: Expression the T-type Ca2+ channel CaV3.1 subtype in single Kiss1 neurons of female Kiss1-CreGFP OVX female mice.

A, A representative gel illustrating the expression of CaV 3.1 andKiss1 mRNA in Kiss1 neurons of the ARC. As a negative control, a cell reacted –RT did not express any of the transcripts. BH tissue was also included as a positive control (+, With RT) and negative control (–, Without RT). MM, Molecular markers. B, Summary bar graph of percentage expression of CaV3.1 in Kiss1 ARC neurons. An average of 20 cells/animal were harvested from six mice and were analyzed for CaV3.1 expression by scRT-PCR. Bar graphs represent the mean ± sem of the percentage of Kiss1 neurons expressing CaV3.1 per animal.

## A.6 References


1. de Roux N, Genin E, Carel JC, Matsuda F, Chaussain JL, Milgrom E 2003Hypogonadotropic hypogonadism due to loss of function of the KiSS1-derived peptide receptor GPR54. Proc Natl Acad Sci USA 100:10972–10976.

2. Seminara SB, Messager S, Chatzidaki EE, Thresher RR, Acierno JS, Shagoury JK,Bo-Abbas Y, Kuohung W, Schwinof KM, Hendrick AG, Zahn D, Dixon J, Kaiser UB,Slaugenhaupt SA, Gusella JF, O'Rahilly S, Carlton MB, Crowley WF, Aparicio SA,Colledge WH 2003 The GPR54 gene as a regulator of puberty. N Engl J Med 349:1614–1627.

3. Gottsch ML, Cunningham MJ, Smith JT, Popa SM, Acohido BV, Crowley WF, Seminara S, Clifton DK, Steiner RA 2004 A role for kisspeptins in the regulation of gonadotropin secretion in the mouse. Endocrinology 145:4073–4077.

4. Mikkelsen JD, Simonneaux V 2009 The neuroanatomy of the kisspeptin system in the mammalian brain. Peptides 30:26–33.

5. Smith JT, Cunningham MJ, Rissman EF, Clifton DK, Steiner RA 2005 Regulation of Kiss1 gene expression in the brain of the female mouse. Endocrinology 146:3686–3692.

6. Smith JT, Dungan HM, Stoll EA, Gottsch ML, Braun RE, Eacker SM, Clifton DK,Steiner RA 2005 Differential regulation of KiSS-1 mRNA expression by sex steroids in the brain of the male mouse. Endocrinology 146:2976–2984.

7. Clarkson J, Herbison AE 2009 Oestrogen, kisspeptin, GPR54 and the pre-ovulatory luteinising hormone surge. J Neuroendocrinol 21:305–311.

8. Dungan HM, Gottsch ML, Zeng H, Gragerov A, Bergmann JE, Vassilatis DK, Clifton DK, Steiner RA 2007 The role of kisspeptin-GPR54 signaling in the tonic regulation and surge release of gonadotropin-releasing hormone/luteinizing hormone. J Neurosci27:12088–12095.

9. Glidewell-Kenney C, Weiss J, Hurley LA, Levine JE, Jameson JL 2008 Estrogen receptor $\alpha$ signaling pathways differentially regulate gonadotropin subunit gene expression and serum follicle-stimulating hormone in the female mouse. Endocrinology 149:4168–4176.

10. Oakley AE, Clifton DK, Steiner RA 2009 Kisspeptin signaling in the brain. Endocr Rev30:713–743.

11. Clarkson J, d'Anglemont de Tassigny X, Moreno AS, Colledge WH, Herbison AE 2008 Kisspeptin-GPR54 signaling is essential for preovulatory gonadotropin-releasing hormone neuron activation and the luteinizing hormone surge. J Neurosci 28:8691–8697.

12. Irwig MS, Fraley GS, Smith JT, Acohido BV, Popa SM, Cunningham MJ, Gottsch ML, Clifton DK, Steiner RA 2004 Kisspeptin activation of gonadotropin releasing hormone neurons and regulation of KiSS-1 mRNA in the male rat. Neuroendocrinology 80:264–272.

13. Parhar IS 2005 GnRH and GPCR: laser-captured single cell gene profiling. Fish Physiol Biochem 31:153–156.

14. Han SK, Gottsch ML, Lee KJ, Popa SM, Smith JT, Jakawich SK, Clifton DK,Steiner RA, Herbison AE 2005 Activation of gonadotropin-releasing hormone neurons by kisspeptin as a neuroendocrine switch for the onset of puberty. J Neurosci 25:11349–11356.

15. Pielecka-Fortuna J, Chu Z, Moenter SM 2008 Kisspeptin acts directly and indirectly to increase gonadotropin-releasing hormone neuron activity and its effects are modulated by estradiol. Endocrinology 149:1979–1986.

16. Zhang C, Roepke TA, Kelly MJ, Rønnekleiv OK 2008 Kisspeptin depolarizes gonadotropin-releasing hormone neurons through activation of TRPC-like cationic channels. J Neurosci 28:4423–4434.

17. Liu X, Lee K, Herbison AE 2008 Kisspeptin excites gonadotropin-releasing hormone neurons through a phospholipase C/calcium-dependent pathway regulating multiple ion channels. Endocrinology 149:4605–4614.

18. Wakabayashi Y, Nakada T, Murata K, Ohkura S, Mogi K, Navarro VM, Clifton DK,Mori Y, Tsukamura H, Maeda K, Steiner RA, Okamura H 2010 Neurokinin B and dynorphin A in kisspeptin neurons of the arcuate nucleus participate in generation of periodic oscillation of neural activity driving pulsatile gonadotropin-releasing hormone secretion in the goat. J Neurosci 30:3124–3132.

19. Keen KL, Wegner FH, Bloom SR, Ghatei MA, Terasawa E 2008 An increase in kisspeptin-54 release occurs with the pubertal increase in luteinizing hormone-releasing hormone-1 release in the stalk-median eminence of female rhesus monkeys in vivo.Endocrinology 149:4151–4157.

20. Roseweir AK, Kauffman AS, Smith JT, Guerriero KA, Morgan K, Pielecka-Fortuna J,Pineda R, Gottsch ML, Tena-Sempere M, Moenter SM, Terasawa E, Clarke IJ,

Steiner RA, Millar RP 2009 Discovery of potent kisspeptin antagonists delineate physiological mechanisms of gonadotropin regulation. J Neurosci 29:3920–3929.

21. Thomas KR, Capecchi MR 1987 Site-directed mutagenesis by gene targeting in mouse embryo-derived stem cells. Cell 51:503–512.

22. Thomas KR, Deng C, Capecchi MR 1992 High-fidelity gene targeting in embryonic stem cells by using sequence replacement vectors. Mol Cell Biol 12:2919–2923.

23. Farley FW, Soriano P, Steffen LS, Dymecki SM 2000 Widespread recombinase expression using FLPeR (flipper) mice. Genesis 28:106–110.

24. Qiu J, Fang Y, Rønnekleiv OK, Kelly MJ 2010 Leptin excites proopiomelanocortin neurons via activation of TRPC channels. J Neurosci 30:1560–1565.

25. Ibrahim N, Bosch MA, Smart JL, Qiu J, Rubinstein M, Rønnekleiv OK, Low MJ,Kelly MJ 2003 Hypothalamic proopiomelanocortin neurons are glucose responsive and express K(ATP) channels. Endocrinology 144:1331–1340.

26. Zhang C, Bosch MA, Levine JE, Rønnekleiv OK, Kelly MJ 2007 Gonadotropin-releasing hormone neurons express K(ATP) channels that are regulated by estrogen and responsive to glucose and metabolic inhibition. J Neurosci 27:10153–10164.

27. Nunemaker CS, DeFazio RA, Moenter SM 2003 A targeted extracellular approach for recording long-term firing patterns of excitable cells: a practical guide. Biol Proced Online5:53–62.

28. Zhang C, Bosch MA, Rick EA, Kelly MJ, Rønnekleiv OK 2009 17Beta-estradiol regulation of T-type calcium channels in gonadotropin-releasing hormone neurons. J Neurosci29:10552–10562.

29. Qiu J, Fang Y, Bosch MA, Rønnekleiv OK, Kelly MJ 2011 Guinea pig kisspeptin neurons are depolarized by leptin via activation of TRPC channels. Endocrinology152:1503–1514.

30. Livak KJ, Schmittgen TD 2001 Analysis of relative gene expression data using real-time quantitative PCR and the 2(−$\Delta\Delta$C(T)) method. Methods 25:402–408.

31. Pfaffl MW 2001 A new mathematical model for relative quantification in real-time RT-PCR. Nucleic Acids Res 29:e45.

32. Erickson KR, Ronnekleiv OK, Kelly MJ 1993 Role of a T-type calcium current in supporting a depolarizing potential, damped oscillations, and phasic firing in vasopressinergic guinea pig supraoptic neurons. Neuroendocrinology 57:789–800.

33. Erickson KR, Ronnekleiv OK, Kelly MJ 1993 Electrophysiology of guinea-pig supraoptic neurones: role of a hyperpolarization-activated cation current in phasic firing. J Physiol460:407–425.

34. McCormick DA, Huguenard JR 1992 A model of the electrophysiological properties of thalamocortical relay neurons. J Neurophysiol 68:1384–1400.

35. Cravo RM, Margatho LO, Osborne-Lawrence S, Donato J, Atkin S, Bookout AL,Rovinsky S, Frazão R, Lee CE, Gautron L, Zigman JM, Elias CF 2011 Characterization of Kiss1 neurons using transgenic mouse models. Neuroscience 173:37–56.

36. Mayer C, Acosta-Martinez M, Dubois SL, Wolfe A, Radovick S, Boehm U, Levine JE2010 Timing and completion of puberty in female mice depend on estrogen receptor $\alpha$-signaling in kisspeptin neurons. Proc Natl Acad Sci USA 107:22693–22698.

37. Padilla SL, Carmody JS, Zeltser LM 2010 Pomc-expressing progenitors give rise to antagonistic neuronal populations in hypothalamic feeding circuits. Nat Med 16:403–405.

38. Donato J, Cravo RM, Frazão R, Gautron L, Scott MM, Lachey J, Castro IA,Margatho LO, Lee S, Lee C, Richardson JA, Friedman J, Chua S, Coppari R, Zigman JM, Elmquist JK, Elias CF 2011 Leptin's effect on puberty in mice is relayed by the ventral premammillary nucleus and does not require signaling in Kiss1 neurons. J Clin Invest121:355–368.

39. Ronnekleiv OK, Bosch MA, Xhang C 18 May 2011 17$\beta$-Estradiol regulation of GnRH neuronal excitability. J Neuroendocrinol 10.1111/j.1365-2826.2011.02160.x

40. Li XF, Kinsey-Jones JS, Cheng Y., Knox AM, Lin Y, Petrou NA, Roseweir A,Lightman SL, Milligan SR, Millar RP, O'Byrne KT 2009 Kisspeptin signalling in the hypothalamic arcuate nucleus regulates GnRH pulse generator frequency in the rat. PLoS One 4:e8334.

41. Navarro VM, Castellano JM, McConkey SM, Pineda R, Ruiz-Pino F, Pinilla L, Clifton DK, Tena-Sempere M, Steiner RA 2011 Interactions between kisspeptin and neurokinin B in the control of GnRH secretion in the female rat. Am J Physiol Endocrinol Metab300:E202–E210.

42. Navarro VM, Gottsch ML, Chavkin C, Okamura H, Clifton DK, Steiner RA 2009 Regulation of gonadotropin-releasing hormone secretion by kisspeptin/dynorphin/neurokinin B neurons in the arcuate nucleus of the mouse. J Neurosci 29:11859–11866.

43. Ramaswamy S, Seminara SB, Ali B, Ciofi P, Amin NA, Plant TM 2010 Neurokinin B stimulates GnRH release in the male monkey (Macaca mulatta) and is colocalized with kisspeptin in the arcuate nucleus. Endocrinology 151:4494–4503.

44. Bevan MD, Wilson CJ 1999 Mechanisms underlying spontaneous oscillation and rhythmic firing in rat subthalamic neurons. J Neurosci 19:7617–7628.

45. Santoro B, Tibbs GR 1999 The HCN gene family: molecular basis of the hyperpolarization-activated pacemaker channels. Ann NY Acad Sci 868:741–764.

46. Chu Z, Takagi H, Moenter SM 2010 Hyperpolarization-activated currents in gonadotropin-releasing hormone (GnRH) neurons contribute to intrinsic excitability and are regulated by gonadal steroid feedback. J Neurosci 30:13373–13383.

47. 47. Wagner EJ, Bosch MA, Kelly MJ, Rønnekleiv OK 1999 A powerful GABA(B) receptor-mediated inhibition of GABAergic neurons in arcuate nucleus. Neuroreport 10:2681–2687.

# Appendix B

**Molecular mechanisms that drive estradiol-dependent burst firing of Kiss1 neurons in the rostral periventricular preoptic area**

Chunguang Zhang[1], Karen J Tonsfeldt[1], Martha A Bosch[1], Kazuto Kobayashi[3], Robert A. Steiner[4,5], Martin J. Kelly[1,2], and Oline K. Rønnekleiv[1,2]

[1]Department of Physiology and Pharmacology, Oregon Health and Science University, Portland Oregon; [2]Division of Neuroscience, Oregon National Primate Research Center, Oregon Health and Science University, Beaverton, Oregon; [3]Department of Molecular Genetics, Fukushima Medical University, Fukushima, Japan; [4]Department of Obstetrics and Gynecology, University of Washington, Seattle, Washington; and [5]Department of Physiology and Biophysics, University of Washington, Seattle, Washington

Appendix B was modified from a manuscript published in American Journal of Physiology -Endocrinology and Metabolism, Dec 1 2013, 305:E1384-E1397.

# Foreward

The goal of this study was to use the previously-validated Kiss-CreGFP mouse to determine basic characteristics of Kiss1 neurons in the rostral periventricular area of the third ventricle (RP3V, previously called anteroventral periventricular nucleus (AVPV)). The RP3V population is more robust in females, due in part the upregulation of Kiss1 by estrogen. These neurons are beleived to be critical for the generation of the preovulatory gonadotropin-releasing hormone surge. We used a model that reliably reproduced the preovulatory surge in ovariectomized Kiss1-CreGFP mice to explore the biophysical properties of the RP3V Kiss1 neurons, specifically investigating burst firing (Ih and IT) and opioid receptor function and expression in these neurons.

These findings confirmed our group's previous findings in the arcuate nucleus that the vast majority of Kiss1 neurons express Ih and IT. Interestingly, only RP3V Kiss1 neurons exhibited spontaneous burst firing, likely due to estrogen regulation of CaV3.1. HCN regulation is also different between the arcuate, where HCN2 and HCN3 are most abundantly expressed, and the RP3V, where HCN1 is the highest expresser. Mu, kappa, and delta opioid receptor transcripts were found in the RP3V neurons, which were also inhibited by KOPr and MOPr agonists.

I contributed most of the single-cell PCR results to this paper (with the exception of the results from recorded neurons): Figures 2A, 5B and E, 6F, and 9E. I also designed primers against the mu, kappa, and delta opioid receptor. I wrote and assembled the original submission of this manuscript, which was ultimately resubmitted and published as this version.

## B.1 Abstract

Kisspeptin (Kiss1) neurons in the rostral periventricular area of the third ventricle (RP3V) provide excitatory drive to gonadotropin-releasing hormone (GnRH) neurons to control fertility. Using whole cell patch clamp recording and single-cell (sc)RT-PCR techniques targeting Kiss1-CreGFP or tyrosine hydroxylase (TH)-EGFP neurons, we characterized the biophysical properties of these neurons and identified the critical intrinsic properties required for burst firing in 17β-estradiol (E2)-treated, ovariectomized female mice. One-fourth of the RP3V Kiss1 neurons exhibited spontaneous burst firing. RP3V Kiss1 neurons expressed a hyperpolarization-activated h-current (Ih) and a T-type calcium current (IT), which supported hyperpolarization-induced rebound burst firing. Under voltage clamp conditions, all Kiss1 neurons expressed a kinetically fast Ih that was augmented 3.4-fold by high (LH surge-producing)-E2 treatment. scPCR analysis of Kiss1 neurons revealed abundant expression of the HCN1 channel transcripts. Kiss1 neurons also expressed a Ni2+- and TTA-P2-sensitive IT that was augmented sixfold with high-E2 treatment. CaV3.1 mRNA was also highly expressed in these cells. Current clamp analysis revealed that rebound burst firing was induced in RP3V Kiss1 neurons in high-E2-treated animals, and the majority of Kiss1 neurons had a hyperpolarization threshold of −84.7 mV, which corresponded to the V½ for IT de-inactivation. Finally, Kiss1 neurons in the RP3V were hyperpolarized by μ- and κ-opioid and GABAB receptor agonists, suggesting that these pathways also contribute to rebound burst firing. Therefore, Kiss1 neurons in the RP3V express the critical channels and receptors that permit E2-dependent rebound burst firing and provide the biophysical substrate that drives the preovulatory surge of GnRH.

## B.2 Introduction

Kisspeptin (Kiss1) neurons in the rostral periventricular area of the third ventricle (RP3V) project to GnRH neurons in the preoptic area (POA) (7) and have been identified as excitatory afferents to the gonadotropin-releasing hormone (GnRH) neurons (26). Kisspeptin is one of the most potent agonists and induces sustained firing in GnRH neurons (18, 39, 56). Although cell-attached recordings of firing rates of Kiss1 neurons in the RP3V have been reported (9, 11), there have been few studies characterizing the biophysical properties and molecular signature of these cells. A recent report documented the expression of an h-current (Ih) in RP3V neurons (40), but the underlying kinetic properties and channels intrinsic to these unique cells have not been characterized.

Single-action potential-generated calcium influx is sufficient to spark the release of classical neurotransmitters; however, burst firing or tetanic stimulation is required for the release of neuropeptides (1, 32, 46). Burst firing in many CNS neurons is generated primarily by the T-type calcium channel current (IT) (e.g., thalamic relay neurons), and the rhythmicity of the burst firing is dependent on the Ih (30, 53). Ih is mediated by the hyperpolarization-activated cyclic nucleotide-gated (HCN) channel family, which includes channel subtypes 1–4. Ih depolarizes neurons from hyperpolarized states, raising the membrane potential into the range of IT activation (12, 13, 23, 30, 55). IT is mediated by the low-threshold voltage-gated calcium channels CaV3.1–3.3 (37). Upon activation, IT initiates a transient Ca2+-driven depolarization above the threshold of action potential initiation (i.e., a low threshold spike) (27, 49). This depolarization then drives the neuron to fire an ensemble (burst) of Na+-driven action potentials. Since burst firing facilitates neuropeptide release and a “preovulatory” release of kisspeptin would, in theory, depend on burst firing,

we used in vitro recordings and single-cell (sc)RT-PCR of Kiss1 neurons in slice preparation to determine whether Kiss1 neurons in the RP3V exhibit burst firing and display the channels and currents necessary for this special property.

Critical for reaching a hyperpolarized membrane potential for de-inactivating CaV3 channels and activating HCN channels for initiating burst firing are a class of inwardly rectifying K+ channels that are activated by G protein-coupled receptors known as GIRK channels. Opioid receptors are coupled to GIRK channels, and activation of GIRK channels can facilitate rebound burst firing (4, 50). The vast majority of hypothalamic neurons express opioid receptors, and μ- and δ-opioid receptors are coupled to GIRK channels (21, 25, 28, 51, 57). Thus, we argue that rebound burst firing of Kiss1 neurons in the RP3V is facilitated by opioidergic afferents that operate through one or more of the classical opioid receptors expressed by these Kiss1 neurons. We know that the RP3V also expresses a sexually dimorphic, estrogen-sensitive population of endogenous opioid peptides, enkephalin and dynorphin, that activate primarily μ- and δ-opioid, and κ-opioid receptors, respectively (15, 47, 48). Therefore, we also tested the hypothesis that Kiss1 neurons in the RP3V are the direct targets for regulation by opioidergic afferents. We used whole cell voltage clamp recordings from Kiss1 neurons in slice preparation to assess the effects of opioid agonists on the excitability of Kiss1 neurons in the RP3V. In addition, we used scPCR to verify that the cognate opioid receptor transcripts are expressed in these Kiss1 neurons.

## B.3 Materials & Methods

### Animals

All procedures performed with animals were in accord with the NIH Guidelines for the Care and Use of Laboratory Animals and were approved by our local committee on animal

care and use. Kiss1-CreGFP (C57BL6/J and S129 background) mice were produced by Dr. Robert Steiner and colleagues at the University of Washington (17), and tyrosine hydroxylase (TH)-EGFP mice (C57BL6/J) were produced by Dr. Kobayashi and colleagues at the Fukushima Medical University in Japan (33, 45). In each case, offspring that carried the transgene were identified by PCR on the genomic DNA extracted from tail biopsies. Transgenic animals were maintained as heterozygous by breeding with WT C57BL6/J mice. Animals were housed under constant temperature and light in a 12:12-h light-dark cycle with lights on at 0600 [zeitgeber time (ZT)0] and lights off at 1800 (ZT12). Food and water was provided ad libitum. Female animals between 6 and 30 wk of age were used for all experiments. Bilateral ovariectomies (OVX) were performed under inhalant isofluorane anesthesia. Carprofen (Rimadyl; Pfizer, NY) was given immediately after surgery at a dose of 4 mg/kg as an analgesic. Following OVX, animals were treated with 17$\beta$-estradiol benzoate (E2), demonstrated to induce an LH surge in CBB6 (EGFP-GnRH) mice (3). Five days (D5) after OVX, animals were treated with a subcutaneous injection of 0.25 $\mu$g E2 in sesame oil at ZT4 (lights on/off at ZT0/ZT12). On the following day (D6), animals were given a subcutaneous injection of 1.5 –2.0 $\mu$g of E2 in sesame oil. On the day of the induced surge (D7), E2-treated animals were euthanized at ZT4 (n = 8). E2-treated animals were also euthanized at ZT12 (n = 8). LH levels were 0.35 ± 0.10 ng/ml in the ZT4 E2-treated females (Fig. 1). In the ZT12 E2-treated animals, LH levels were 4.69 ± 1.5 ng/ml (Fig. 1). The low LH levels in the E2-treated animals at ZT4 vs. ZT12 are consistent with the presence of E2-mediated negative and positive feedback.

Animals used for cell harvesting and for the majority of the electrophysiology experiments were treated with the surge-inducing dose of E2 as described above. The E2 injections (high E2) resulted in a uterine weight of 109.7 ± 4.1 mg; n = 28 (the mean uterine

weight of proestrus animals in our colony is 135.4 ± 7.7 mg; n = 15). An additional group of animals used for electrophysiology was treated as above but received less E2 as a model for the diestrous stage of the estrus cycle. These animals received injections of 0.08 μg of E2 in sesame oil on D5 and D6 following OVX and were used for experiments on D7. The low-E2 injections (low-E2) resulted in a uterine weight of 56.1 ± 7.4 mg; n = 5 (the mean uterine weight of diestrus animals in our colony is 57.0 ± 2.9 mg; n = 24).

In the Kiss1-CreGFP mice, the fluorescent intensity of the POA neurons was dependent on the circulating E2 levels (as measured by the uterine weights). Therefore, low levels of E2 resulted in only faint Kiss1-GFP neurons. Since we were interested in comparing IT and Ih under low (diestrus type) and high (proestrus type) E2 states, and Kiss1 and Th mRNAs are coexpressed in RP3V neurons (8), these experiments were done with both Kiss1-CreGFP and TH-EGFP mice. The fluorescent intensity of TH-EGFP neurons is not dependent on circulating levels of E2.

For whole cell recording of IT and Ih in Kiss1 neurons during low (uterine weight <80 mg) and high (uterine weights >80 mg) E2 states, GFP-expressing cells in the RP3V area were patched, and the electrical activity was recorded for 30–40 min. After whole cell recording, the cell content was harvested for RT-PCR identification of Kiss1 and Th mRNA expressions (see below).

**Radioimmunoassay for LH**

Radioimmunoassay (RIA) for mouse LH was performed by the Endocrine Technology and Support Lab at the Oregon National Primate Research Center (Oregon Health and Science University, Beaverton, OR) by using a traditional double-antibody RIA procedure described in Pau et al. (3) and Bosch et al. (36). The detection limit of the assay was 0.2

ng/ml. A mouse serum pool (ET mouse #4) was used in triplicate in each assay as a quality control. The interassay variation (CV) was 14.7% and the intra-assay CV was 3.8%.

**Slice preparation**

On the day of experimentation, the animal was euthanized by decapitation. Trunk blood was collected, and the brain was removed from the skull. The brain stem was removed, and the resulting block was mounted on a cutting vibratome and submerged in ice-cold oxygenated (95% O2-5% CO2) high-sucrose artificial cerebral spinal fluid (aCSF) (in mM: 208 sucrose, 2 KCl, 1 MgCl, 1.25 NaH2PO4, 10 HEPES, 26 NaHCO3, 10 dextrose, 2 MgSO4, and 1 CaCl2). Two to three 220-μm slices were cut through the RP3V. Slices were transferred to an auxiliary chamber containing oxygenated aCSF at room temperature (in mM: 124 NaCl, 5 KCl, 1.44 NaH2PO4, 5 HEPES, 10 dextrose, 26 NaHCO3, 2 MgCl2, and 2 CaCl2) and allowed to recover for at least 1 h. The uteri were removed, trimmed of fat, blotted dry, and weighed. Weights were recorded as an indicator of E2 levels.

**Cell harvesting and reverse transcription PCR**

Slices were individually visualized under a Leica inverted microscope to confirm GFP fluorescence. Two to three slices containing the RP3V were microdissected under a dissecting microscope. The tissue was digested with protease (from Streptomyces griseus, Sigma) at 37°C for 15 min and then washed three times with low-Ca2+ aCSF (1 mM Ca2+) and two times in aCSF. Using flame-polished glass Pasteur pipettes of decreasing sizes, slices were titurated and plated onto a 60-mm cell culture dish with a glass bottom. The cells were allowed to settle for 12 min until being moved to the harvesting microscope. Oxygenated aCSF at room temperature was constantly perfused into the dish at a rate of 2 ml/min. The cells were allowed to rest after perfusion began for at least 15 min. Fully

intact, healthy cells that showed uniform fluorescence and were anchored to the glass plate were harvested. Harvesting was done by using a visualized patch-clamping with a standard glass pipette (1.5 mm OD/0.83 mm ID; World Precision Instruments, Sarasota, FL) that had been pulled to a 10-μm tip. Using the XenoWorks microinjector system (Sutter Instruments, Navato, CA), we applied gentle suction to pull the cell off of the plate. Collected cells were ejected from the pipette into a siliconized 0.5-ml tube containing a solution of 1× Invitrogen Superscript III Buffer, 15 U RNasin (Promega, Madison WI), 10 mM dithiothreitol (DTT), and diethylpyrocarbonate (DEPC)-treated water in a total of 5 μl (single cells) or 8 μl (pools of cells). Cells were harvested individually or as pools of 5 individual cells. Collection tubes were kept in a chilled metal block to avoid freeze/thaw cycling, but each completed pool of cells was frozen as soon as possible on dry ice and stored at −80°C until further processing. Cells were dissociated and harvested as we previously reported (3, 55).

Harvested cells were reverse transcribed according to the manufacturer's instructions (SuperScript III; Invitrogen, Carlsbad CA) and as described previously (3). The final products were stored at −20°C. Cells and controls underwent reverse transcription within 48 h of harvesting. The positive and negative controls included hypothalamic RNA samples that were subjected to reverse transcription with reverse transcriptase added (+RT) or without reverse transcriptase (−RT), respectively. After conversion to cDNA, individual cells and pools were confirmed to exhibit Kiss1 expression by amplifying Kiss1 mRNA using primers on a 1- to 2-μl template for 35 cycles (Table 1). PCR analysis of individual cells was used to determine the expression of Kiss1 mRNA and Th mRNA in GFP-Kiss1 neurons. PCR analysis of cell pools allowed determining a certain level of Kiss1 expression that was deemed consistent in all harvested pools used for further analysis. Pools that

showed a faint or no Kiss1 expression were excluded from analysis. Control +RT and −RT tissue mRNAs were also run for Kiss1 expression to confirm there had been no contamination during the RT process. Each pool of cells was then evaluated using quantitative real-time PCR (qPCR).

**Primer design**

PCR primers were designed from the most recent National Center for Biotechnology Information on DNA and mRNA sequences using Clone Manager (Sci Ed Software, Cary, NC). Primers were designed to produce products between 75 and 200 base pairs (bp) and to be as efficient as possible. To distinguish cDNA from genomic DNA products, all primers crossed an intron/exon boundary. Only primers that demonstrated a single-peak melting curve and had efficiency between 95 and 100% were used (Table 1).

**qPCR**

Quantitative analysis by PCR was performed using the Power Sybr Green Mastermix method as described previously (55) on an Applied Biosystems 7500 Fast real-time PCR system (Life Technologies, Carlsbad, CA). Primer efficiencies and data were analyzed as described previously (3, 55). All efficiencies are listed in Table 1. cDNA samples from Kiss1 neurons collected from the RP3V were run in duplicates, using 3.5–4 μl of cDNA per duplicate. Melting curves were analyzed for each reaction, and all genes were normalized to β-actin as a reference. One gene from each family (i.e., HCN1, CaV3.1, μ-opioid receptor) was then used as a "calibrator" to compare levels of mRNA among genes. Data were analyzed following the comparative ΔΔCT method described previously (38, 55) and are reported as relative amounts of mRNA expression to the calibrator. Data are expressed

as means ± SE, and differences in gene expression among families of genes were analyzed by a one-way ANOVA (e.g., HCN, CaV3, opioid receptors).

**Electrophysiological recording and cell harvesting**

Whole cell patch clamp recordings were conducted for GFP-tagged Kiss1 or TH neurons with the use of an Olympus BX51 (Olympus, Center Valley, PA) or a Zeiss Axioskop FS upright microscope (Carl Zeiss Microscopy, Thornwood, NY) equipped with fluorescence and infrared differential interference contrast (IR-DIC) imaging devices (17, 42, 54, 56). Patch pipettes (1.5-mm OD borosilicate glass; A-M Systems, Seattle, WA) were pulled on a Flaming/Brown puller (model P-97; Sutter Instrument, Novato, CA) and usually filled with the following internal solution (in mM): 128 potassium gluconate, 10 NaCl, 1 MgCl2, 11 EGTA, 10 HEPES, 4 ATP, and 0.25 GTP; adjusted to pH 7.3 with KOH; 290 mOsm. Pipettes filled with the above internal solution had a resistance of 2–3 MΩ. For loose-patch cell recordings, the patch pipettes were filled with aCSF, and a loose seal (20–60 MΩ seal resistance) was formed on the Kiss1 neurons to measure spontaneous action currents as previously described (17). For the whole cell configuration, access resistance was less than 25 MΩ and was 80% compensated when the recorded current was larger than 100 pA. Steady-state current/voltage (I/V) plots were constructed with step command potentials from −120 to −40 mV at an increment of 5 or 10 mV (with holding potential at −60 mV) and a duration of 0.5 or 1 s. Membrane input resistances of cells were calculated by measuring the slope of the I/V relationship curve between −70 and −50 mV. Postinhibitory rebound that caused low-threshold burst firing was examined at resting membrane potentials after a series of hyperpolarization of 1s duration from −70 mV to −120 mV. The liquid junction potential of −10 mV was corrected for in all analyses. Consecutive current traces were filtered at 2–10 kHz and acquired at a sampling rate of 0.5–5k Hz. Standard whole cell patch clamp

recording procedures and pharmacological testing were conducted as described previously (17, 42, 54, 56). Electrophysiological signals were amplified with an Axopatch 200B amplifier and digitized with a Digidata 1440A (Molecular Devices, Foster City, CA) or with an Axopatch 1D amplifier and digitized with a Digidata 1322 (Axon Instruments, Foster City, CA). Data were analyzed with Clampfit software (v. 9.0 or 10.0, Molecular Devices).

After recording, the cell was harvested by applying negative pressure until visualizing the cell content being gently aspirated into the tip of the recording pipette. The cell content was expelled into a 500-μl harvesting tube containing 5 μl of RT solution and stored at −80°C until further processing. All recorded cells that were harvested were reverse transcribed as described above. cDNA was analyzed for Kiss1 and Th mRNAs by using a 4-μl template in a 30-μl PCR reaction as described above. Cells that were negative to both Th and Kiss1 mRNA were further subjected to the detection of β-actin mRNA used as a positive control.

**Drugs and chemicals**

TTA-P2 ({3,5-dichloro-N-[1-(2,2-dimethyl-tetrahydro-pyran-4-ylmethyl)-4-fluoropiperidin-4-ylmethyl]-benzamide}, a gift from Merck) was made up as a 10 mM stock solution in DMSO. ZD-7288 was purchased from Tocris Bioscience (Minneapolis, MN) and was made up as a stock of 100 mM in DMSO. TTX was purchased from Alomone Laboratories (Jerusalem, Israel) and was made up as 1 mM in stock in Milli-Q water.

**Data analysis**

The firing pattern of individual neurons was determined with similar criteria as previously reported for RP3V Kiss neurons (11). Silent neurons had low spontaneous spiking activity (mean firing rate <0.5 Hz); tonic neurons fired regularly with a mean firing rate

>4 Hz and a coefficient of variation (defined as SD/mean) of the interspike interval (ISI) <0.25. Burst firing was defined as a cluster of spikes occurring with an ISI of $\leq$250 ms and terminating with an ISI of $\geq$500 ms. Bursting neurons had more than 50% of their spikes occurring in bursts with intraburst frequency higher than 4 Hz. All other neurons were classified as irregular (CV greater than 0.25). Rebound burst firing was defined as the hyperpolarization-induced high-frequency (>10 Hz) firing with two or more spikes in a cluster. To be consistent, the maximal rebound burst firing frequency was determined from the first two spikes. Data were analyzed with Mini Analysis and Clampfit 9.2 software. Graphs were plotted using GraphPad Prism 4, Sigma Plot 8.0, and Macromedia Freehand 10 software. Comparisons between different treatments were performed using an unpaired Student's t-test or a one-way or two-way ANOVA with Bonferroni post hoc tests. Differences were considered significant if the probability of error was <5%. All data are presented as means ± SE.

## B.4 Results

**Kiss1-GFP neurons in the RP3V area express Kiss1 mRNA.**

Kiss1-CreGFP mice were used to target fluorescent Kiss1 neurons in the RP3V. Kiss1-GFP neurons in the RP3V area were dispersed, harvested individually, and subjected to RT-PCR to confirm Kiss1 mRNA expression. The analysis of 139 cells from five OVX E2-treated (surge model) females revealed that 94% expressed Kiss1 mRNA (Fig. 2A). Kiss1-positive cells were also tested for coexpression with Th mRNA, and 88% expressed Th mRNA in addition to Kiss1 mRNA. Adjacent nonfluorescent cells (n = 10) were negative for Kiss1 or Th mRNA. As reported previously (17), OVX oil-treated control animals had

little or no GFP-labeled cells in the RP3V area. Therefore, only E2-treated (low and high dose) animals were used for cell harvesting and electrophysiological recordings.

**Identification of Kiss1 and Kiss1/TH dual phenotype in the slice.**

To identify the Kiss1 and Th transcript from recorded Kiss1-GFP and TH-EGFP neurons, cells were harvested after recording for RT-PCR analysis. A total of 63 neurons from 10 Kiss1-GFP mice and 9 TH-EGFP mice were recorded and analyzed. In the high-E2 group (uterine weights >80 mg), we found that 100% (27/27) of fluorescently identified Kiss1-GFP neurons were positive for Kiss1 mRNA. 75% (20/27) of these Kiss1 mRNA-positive neurons (Kiss1-CreGFP mice) coexpressed Th mRNA (Fig. 2B). In addition, 60% (12/20) of the fluorescently identified TH-EGFP neurons were positive for Kiss1 mRNA. There was no difference among Kiss1 neurons that were recorded in the Kiss-GFP mice vs. the TH-EGFP mice in terms of resting membrane potential, cell membrane capacitance, input resistance, spike threshold, and IT and Ih amplitudes (Table 2). These parameters were also similar in Th-positive and Th-negative Kiss1 neurons. Therefore, the data from the Kiss-CreGFP and TH-EGFP mice were combined for further analysis.

**Spontaneous firing properties of RP3V Kiss1-CreGFP neurons.**

In the next series of experiments, we examined the spontaneous firing characteristics of identified RP3V Kiss1 Cre-GFP neurons from high-E2-treated animals in coronal slices by using whole cell electrophysiological recordings. We also did cell-attached recording for comparison (17). The expression of GFP was used to identify individual Kiss1 neurons. One to two cells were recorded in each coronal slice. Whole cell current clamp recordings revealed that the mean resting membrane potential of Kiss1 neurons in the RP3V was −54.7

± 0.6 mV (n = 29) from high-E2 animals. The vast majority (78%) of Kiss1 neurons exhibited spontaneous firing at resting membrane potential that could be classified into three types of firing pattern: burst, tonic, and irregular (Fig. 3, A–C). Among the 77 neurons recorded (whole cell) from high-E2-treated animals, ∼52% displayed tonic/irregular firing; 26% exhibited burst firing; and 22% were silent during the recording (Fig. 3E). These firing patterns were consistent with those obtained from loose patch recordings, which showed 46% tonic/irregular firing, 29% burst firing, and 25% silent (n = 63; Fig. 3E). There was no correlation in firing pattern or frequency between cells recorded in the same slice. For example, we found tonic and irregular firing cells, silent and bursting cells, or tonic and bursting cells in the same slice. Moreover, bath-applied glutamate (100 μM) or NMDA (40 μM) depolarized (11.5 ± 4.3 mV in glutamate, 10.8 ± 3.2 mV in NMDA, n = 7) and increased the firing rate of all RP3V Kiss1 neurons examined (Fig. 3, E and F). Consistent with a previous report (9), the percentage of cells exhibiting spontaneous burst firing was low (26–29%), which indicates that synaptic input and activation of endogenous conductances for burst firing were missing. Indeed, when cells were hyperpolarized to −100 mV by constant current injection of −15 pA, rebound burst firing was induced (Fig. 3G). This implies that RP3V Kiss1 neurons may express the intrinsic conductances for postinhibitory rebound burst firing, and synaptic input may be critical for producing a hyperpolarizing stimulus.

**Basic membrane properties and hyperpolarization recruited conductances in RP3V Kiss1 neurons.**

To examine whether RP3V neurons express intrinsic membrane conductances for burst firing, the basic membrane properties and the conductances recruited through hyperpolarization were examined in voltage clamp recordings from high-E2-treated animals. Since

RP3V Kiss1 neurons express KATP channels that will affect the resting membrane potential as the cells are dialyzed with a low (2 mM) ATP internal solution (present findings) (14), the biophysical measurements of the Ih and IT were done under 4 mM ATP (internal) concentrations to minimize the effects of Kir6.2 (KATP) channel activity. In voltage clamp, a series of depolarization and hyperpolarization steps were delivered to examine the input resistance and the hyperpolarization-dependent Ih and IT that contribute to postinhibitory rebound burst in many neurons in the CNS (30, 53). Under voltage clamp conditions, both hyperpolarization-activated Ih and IT were evident in RP3V Kiss1 neurons (Fig. 4A). In the high-E2-treated animal, all fluorescently identified RP3V Kiss1 neurons displayed Ih greater than 5 pA at −120 mV (39.4 ± 4.9 pA, n = 36; Fig. 4C and Table 3). Eighty-three percent (30/36) of these neurons expressed IT with a mean amplitude of 42.94 ± 4.6 pA at −60 mV (Fig. 4C and Table 3); 11% (4/36) of them expressed A-type potassium currents (IA) (19.2 ± 4.8 pA, n = 4). Similarly for Kiss1 and TH dual-phenotype (Kiss+/TH+) neurons, all of them expressed an Ih, and 84% of them expressed IT (Table 3). Moreover, all of the Kiss1 neurons expressed a persistent sodium current (INaP) with a mean amplitude of 35.3 ± 5.2 pA (Fig. 4, B and C). The persistent INaP generated a significant inward current that contributed to the rebound burst firing (see DISCUSSION). The slope conductance between −70 and −50 mV was significantly increased from 0.74 ± 0.17 pS to 1.5 ± 0.2 pS by TTX (500 nM), indicative that TTX-sensitive, voltage-gated Na channels are responsible for this robust inward current (43).

**RP3V Kiss1/TH neurons express a rapid Ih that is primarily composed of HCN1.**

Whole cell voltage clamp recordings revealed that all of the Kiss1 neurons in the RP3V from high-E2-treated animals expressed Ih (Fig. 5, A–D, and Table 3). Ih was recognized by its characteristic slowly developing inward current following hyperpolarizing voltage

steps with the steady-state current reached early during the more hyperpolarized voltage step (Fig. 5A). Single-cell RT-PCR from recorded cells showed that the majority of these cells expressed HCN1 mRNA and CaV3.1 mRNA (Fig. 5B and see below). Ih was completely blocked in Kiss1 neurons by the selective blocker ZD-7288 (50 μM; Fig. 5A). Ih could be evoked in Kiss1 neurons at voltages up to −75 mV (Fig. 5, C and D). qPCR of Kiss1 neurons harvested from the RP3V demonstrated that these neurons express HCN1, -2, and -3 (Fig. 5E); HCN4 was undetectable (data not shown). The expression of HCN2 and HCN3 mRNAs was ∼30% of the HCN1 level. The Ih in Kiss1 neurons displayed fast activation kinetics with a $\tau$ = 84 ± 10 ms at −120 mV (Fig. 5A), consistent with the relatively high expression level of HCN1 mRNA (Fig. 5, B and E).

**RP3V Kiss1/TH neurons express IT that is primarily composed of CaV3.1.**

Whole cell voltage clamp recordings revealed that 80% of RP3V Kiss1 neurons from the high-E2-treated animals displayed an IT larger than 5 pA (fully recovered at −120 mV and activated at −60 mV; Figs. 4 and 6, A and B). All of these neurons also expressed Ih. The V1/2 for the recovery, as determined by fitting the data to a Boltzmann equation, was −86.4 ± 0.2 mV (Fig. 5E), which was similar to the V1/2 in GnRH neurons (55). Furthermore, the IT in these Kiss1 neurons was rapidly inactivated (at −60 mV, $\tau$-fast = 19.4 ± 3.3 ms, $\tau$-slow = 86.3 ± 29.5 ms, n = 8). IT in these Kiss1 neurons was blocked by 50 μM Ni2+ (Fig. 6A) and also by the selective IT blocker TTA-P2 (10). As shown in Fig. 6B, perfusing TTA-P2 (5 μM) blocked the IT within 3 min of bath application by 90.9 ± 5.3% (Fig. 6, C and D). Measurements by qPCR analysis of RP3V Kiss1 neuronal pools revealed that these neurons express primarily CaV3.1 mRNA and to a lesser extent CaV3.2 and CaV3.3 transcripts (Fig. 6F). CaV3.2 and CaV3.3 were significantly less abundant than CaV3.1 transcripts ($P < 0.01$ and $P < 0.05$, respectively). These data indicate that Kiss1 neurons

in the RP3V preferentially express CaV3.1 channels, which is the T-type Ca2+ channel with the fastest kinetics. Despite lower expression, CaV3.2 and CaV3.3 were detectable in the pooled neurons, indicating that they may also contribute to IT in Kiss1 neurons in this region.

**Hyperpolarization-induced rebound burst firing in RP3V Kiss1 neurons is dependent on expression of IT.**

Since T-channels in RP3V Kiss1 neurons were recruited by hyperpolarization, we examined the ability of these neurons to generate rebound burst firing through current injection-induced hyperpolarization. As an example, the Kiss1 neuron in Fig. 7A had a resting membrane potential of −62 mV and fired irregularly at a mean frequency of 0.8 Hz. This cell had a T-current amplitude of 52 pA. The hyperpolarization threshold, defined as the minimum hyperpolarization (or current injection) required to induce rebound burst firing, was −76 mV (or −20 pA), and its corresponding burst firing rate determined by the first interspike interval was 36 Hz. Greater hyperpolarization to −80, −85, and −89 mV or current injection of −30, −40, and −50 pA induced higher firing frequencies of 104, 156, and 172 Hz, respectively (Fig. 7B). The burst firing frequency increased nonlinearly, with the largest changes near the hyperpolarization threshold (Fig. 7B). At resting membrane potential, we found that 82% of neurons had a hyperpolarization threshold of −84.7 ± 1.2 mV (n = 18), which, as predicted, is close to the V1/2 for de-inactivation of the T-channel. Next we examined the contribution of IT and Ih to the rebound burst firing. Rebound burst firing was clearly blocked by the selective Cav3 channel blocker TTA-P2 (Fig. 7, C and D), whereas rebound burst firing was not blocked by the HCN channel blocker ZD-7288 (Fig. 7E). However, blocking HCN channels did increase the delay for the initiation of first spike

(Fig. 7E). Therefore the T-channel and h-channel play different roles in the generation of rebound burst firing.

**Expressions of IT and Ih are dependent on circulating levels of E2.**

Our previous studies showed that the expression of T-type calcium channels and HCN channels in GnRH neurons are regulated by estrogens (2, 3, 55). Therefore, we examined the effects of low-E2 vs. high-E2 treatment on the expression of IT and Ih in RP3V Kiss1 neurons. To identify the Kiss1 neurons from low-E2-treated OVX females, both TH-EGFP and Kiss-GFP mice were used. For recordings from TH-EGFP mice, cells were targeted by EGFP fluorescence; for recordings from Kiss-GFP mice, cells were blindly targeted. All recorded neurons were harvested for RT-PCR identification of Kiss1 transcripts. A total of 18 neurons were recorded from the low-E2 group, and 10 of them were identified as Kiss1 mRNA positive. We found that, in the low-E2-group, few Kiss1+/TH+ neurons (3 of 10) expressed an IT (Table 3). The mean amplitude of the IT for all Kiss1-positive cells was 4.8 ± 2.4 pA (n = 10). The majority of Kiss1 neurons in the low-E2 group expressed an Ih (7 of 10) with a mean amplitude of 10.8 ± 2.7 pA (n = 10). In the high-E2 group, the vast majority of Kiss1-positive neurons (83%; total n = 36) expressed an IT (Table 3) with a mean amplitude of 34.8 ± 4.3 pA (n = 36) and an Ih of mean amplitude of 39.1 ± 4.4. pA (n = 36). We found that there was no difference between the low-E2 Kiss1 neurons and the high-E2 Kiss1 neurons in the resting membrane potential (−54.1.5 ± 1.5 mV, n = 9 in low-E2 vs. −54.7 ± 0.9 mV, n = 36 in high-E2) or the cell membrane capacitance (18.6 ± 1.5 pF, n = 10 in low-E2 vs. 18.4 ± 1.0 pF, n = 36 in high-E2). The IT density in the high-E2 group was sixfold higher than in the low-E2 group (1.85 pA ± 0.24 pA/pF vs. 0.31 ± 0.6 pA/pF, $P < 0.01$), and the Ih density in the high-E2 group was 3.4-fold higher than in the low-E2 group (1.94 pA ± 0.15 pA/pF vs. 0.58 ± 0.13 pA/pF, $P < 0.01$; Fig. 8). In

contrast, only two of nine Kiss1−/TH+ neurons in the high-E2 group expressed an IT with an overall mean amplitude of 5.8 ± 5.8 pA (n = 9), whereas 89% (n = 8) of them expressed an Ih (Table 3) with mean amplitude of 20.8 ± 6.8 pA. Therefore, the IT is highly expressed in RP3V Kiss1 neurons and is exquisitely sensitive to E2, whereas the expression of the Ih is less sensitive to E2.

**Opioid peptides and GABAB agonist hyperpolarize RP3V Kiss1 neurons.**

Clearly, the rebound burst firing is dependent on the hyperpolarization threshold. To search for possible metabotropic inhibitory inputs onto RP3V Kiss1 neurons, we examined responses of Kiss1 neurons to the μ- and κ-opioid receptor agonists by measuring the agonist-activated outward K+ currents at −60 mV using whole cell voltage clamp recordings (Fig. 9). In Kiss1 neurons in the RP3V (high-E2 group), the μ-opioid receptor agonist DAMGO (1 μM) induced a small outward current (Fig. 9A). The outward current reversed at EK+ and exhibited inward rectification (data not shown). Of the cells tested, 75% (9 of 12) responded to DAMGO with a mean evoked current of 6.7 ± 0.6 pA (Fig. 9D; n = 9). On the other hand, the κ-opioid receptor agonist U-69593 (1 μM) induced an outward current of 11.8 ± 2.2 pA (Fig. 9, B–D; n = 9) that exhibited inward rectification (Fig. 9C), indicative of the opening of GIRK channels. The effects were blocked by the nonselective opioid receptor antagonist naloxone (Fig. 9B). We also examined the κ-opioid receptor agonist U-69593 (1 μM) and GABAB receptor agonist baclofen (20 μM)-induced hyperpolarization. As shown in Fig. 9, F–H, U-69593 induced a hyperpolarization of 6.8 ± 1.0 mV (n = 5), and baclofen induced a similar hyperpolarization (5.8 ± 1.4 mV, n = 5). Therefore, RP3V Kiss1 neurons, like the vast majority of hypothalamic neurons (21, 23, 29), respond to opioid and

GABAB agonists. Consistent with these electrophysiological observations, the qPCR analysis from pooled Kiss1 neurons confirmed that expression of the κ-opioid receptor mRNA was significantly greater than either the μ- or δ-receptor mRNA (Fig. 9E).

## B.5 Discussion

Here, we profile the endogenous electrophysiological properties of Kiss1 neurons in the RP3V of the female mouse. We show that the T-type calcium current is crucial for rebound burst firing and that this phenomenon is estrogen dependent. A significant fraction of these neurons exhibit spontaneous burst firing, and the vast majority of these cells express the pacemaker currents Ih and IT. The Ih displayed rapid kinetics, consistent with the abundant expression of HCN1 channels, which was amplified by E2. The predominance of the T-type Ca2+ channel CaV3.1 corroborated the presence of a rapidly inactivating IT in these cells, which was increased manyfold by E2 treatment. The presence of a robust T-current is essential for the high-frequency rebound bursting that is manifested following a hyperpolarizing stimulus. Furthermore, both κ- and μ-opioid receptor agonists hyperpolarized Kiss1 neurons, which suggests that opioid synaptic input provides a portion of the stimulus required for reaching the hyperpolarization threshold necessary for recruitment of CaV3.1 channels. The Kiss1 neurons were also hyperpolarized by the GABAB agonist baclofen, which would further contribute to reaching the hyperpolarization threshold. Notably, the majority of the Kiss1 neurons in the RP3V expressed Th mRNA, which is consonant with the observation that these Kiss1 neurons in the RP3V exhibit rebound burst firing reminiscent of dopamine neurons in the arcuate nucleus (29).

Kiss1 neurons in the RP3V are similar to those in the arcuate nucleus (ARC) but differ in important ways. Kiss1 neurons in the ARC (so-called KNDy neurons) coexpress

neurokinin B (NKB) and dynorphin (16, 34). In contrast, Kiss1 neurons in the RP3V express neither NKB nor dynorphin but express one or more classical transmitters including dopamine (8, 20, 34; present findings). We have previously shown that Kiss1 neurons in the ARC of mice and guinea pigs are either silent (∼50%) or show tonic/irregular firing (∼50%) (17, 42), and a report in a cross-bred kisspeptin-IRES-Cre × ROSA26-CAGS-τGFP mouse described similar findings (9). Although Kiss1 neurons in the ARC and RP3V exhibit ionotropic glutamate-dependent burst firing (17; present findings), one-quarter of the Kiss1 neurons in the RP3V exhibit spontaneous burst firing. This suggests that, although Kiss1 neurons in the ARC and RP3V express a common neuropeptide and share the capacity to exhibit burst firing in response to glutamate, Kiss1 neurons in these two regions exhibit different biophysical properties and/or synaptic inputs.

The "pacemaker" current (Ih) is required for rhythmic firing, and virtually all Kiss1 neurons in both the ARC and RP3V express this current (present findings; 17, 40, 42). Ih is a noninactivating, nonselective cation current. This current is activated at hyperpolarized membrane potentials, and it depolarizes the cell into the range required for activation of the low-threshold IT, which is responsible for generating a burst of action potentials. The activation kinetics of Ih are determined by the properties of the underlying channels, and the HCN1 channel exhibits the fastest kinetics (30, 44). The relative abundance of these subunits within a neuronal population can modulate the frequency and pattern of burst firing in these cells. The rapid depolarization mediated by HCN1 channels decreases interburst interval. Therefore, the kinetic properties of HCN1 endow RP3V Kiss1 neurons with the ability to generate rhythmic burst firing. Also contributing to the rhythmicity of burst firing in Kiss1 neurons is the persistent Na+ current, which is active in the range subthreshold to action potential generation (43). A similar persistent Na+ current is recognized to be

important for generating a pacemaker potential in GnRH neurons in the telost (35). We found that Ih was regulated by E2 such that the whole cell current increased 3.4-fold with an E2 treatment that produced an LH surge in our mice, corroborating a recent report in cross-bred kisspeptin-IRES-Cre × ROSA26-CAGS-τGFP mice studied throughout the estrous cycle (40). Most likely, this is attributable to an E2-dependent increase in HCN channel expression, as is the case for E2 regulation of such channels in GnRH neurons (3).

Although Ih is responsible for the rhythmicity of burst firing, IT is the most critical for generating the depolarizing stimulus (low threshold spike) that supports an ensemble of action potentials (19, 12, 13). IT is a low-threshold activated Ca2+ current, whose primary physiological function is to generate burst firing (5, 37). Since the T-type Ca2+ (CaV3) channels are activated by low voltage, they open in a voltage range that induces a strong inward Ca2+ current. The primary difference between the various T-type Ca2+ channels is their rate of inactivation, with CaV3.1 exhibiting the fastest and CaV3.3 the slowest kinetics (24). In Kiss1 neurons in the RP3V, we found a rapidly inactivating, Ni2+- and TTA-P2-sensitive T-type current, consistent with the expression of CaV3.1 mRNA (10). The combination of the rapid kinetics of Ih and IT in Kiss1 neurons in the RP3V would support a higher frequency of burst firing. Previous studies have suggested that Kiss1 neurons in the RP3V must fire at a minimum of 5 Hz (spikes/s) to produce a sustained release of kisspeptin onto GnRH neurons (26), and our data indicate that Kiss1 neurons are capable of firing at much higher frequencies (Fig. 7B). Although a rapidly inactivating IT produced by CaV3.1 channels will produce a shorter duration of Ca2+ depolarization, CaV3.1 also de-inactivates more rapidly than other CaV3 channels, which would allow more CaV3.1 channels to be recruited during the hyperpolarization for the next burst. Remarkably, IT was increased sixfold with an E2 treatment that produced an LH surge in these mice. This would indicate

that there is an increase in CaV3 channel density as we have previously demonstrated for the expression of these channels in GnRH neurons (22, 55). This means that, once the cells reach the hyperpolarization threshold for recruiting CaV3 channels, there is greater rebound burst of action potentials. Moreover, we deduce that high-frequency burst firing of Kiss1 neurons in the RP3V has the capacity to drive a sustained output from downstream synaptic targets and may explain the prolonged firing of GnRH neurons associated with the preovulatory surge (6).

Notably, we determined that Kiss1 neurons in the RP3V exhibit a hyperpolarization threshold that is close to the V1/2 for de-inactivation of the T-channel, which is the most critical for dictating the rebound burst firing frequency. GIRK channels are critical for driving the membrane potential into the hyperpolarized state necessary to de-inactivate the CaV3 channels underlying the T-current. The majority of hypothalamic neurons express GABAB and opioid receptors, which are coupled to GIRK channels, and Kiss1 neurons in the RP3V are no exception (present findings; 21, 25, 28, 51, 57). In fact, these cells express $\kappa$-, $\mu$-, and $\delta$-opioid receptor transcripts, and the vast majority of these cells respond to $\kappa$- and $\mu$-agonists. The $\mu$-opioid receptor agonist DAMGO induced an outward current in RP3V Kiss1 neurons, similar to other hypothalamic neurons (present findings; 21, 25, 28, 51). The $\kappa$-opioid receptor agonist U-69593 generated an even greater GIRK current, which correlated with the relative abundance of the $\kappa$- vs. $\mu$-receptor transcripts in these neurons. GABAB and opioid receptors coupled to GIRK channels in these cells would help provide the hyperpolarization stimulus required to de-inactivate CaV3.1 channels. Also, opioidergic afferents may make direct contact with Kiss1 neurons in the RP3V. Met-enkephalin is coexpressed in 28–38% of Kiss1 neurons in the RP3V area of mice (41). Since met-enkephalin is a potent endogenous agonist for the $\mu$-opioid receptor (52), and

Kiss1 neurons respond to the enkephalin analog DAMGO, met-enkephalin may serve an autoregulatory role in hyperpolarizing Kiss1 neurons. Prodynorphin neurons are also abundant in the RP3V and much more prevalent in females than males (47). Moreover, Kiss1 neurons in the RP3V express the κ-opioid receptor (which mediates the effects of dynorphin), and these cells are robustly hyperpolarized by the κ-opioid receptor agonist U-69593. Thus, we infer that κ- and/or μ-receptor-dependent signaling combined with GABAB signaling to Kiss1 neurons in the RP3V provides some of the critical input required for deinactivating CaV3 channels in Kiss1 neurons. Interestingly, A12 dopamine neurons in the ARC also express Ih and IT. They are hyperpolarized by μ-opioid and GABAB agonists and show similar rebound burst characteristics (29). Since the majority of Kiss1 neurons in the RP3V coexpress Th transcript, their electrophysiological and molecular signatures suggest that these neurons belong to an important class of hypothalamic parvocellular "pacemaker" neurons (29, 31).

In summary, we have characterized the endogenous conductances and channels critical for producing burst firing in the Kiss1 neurons in the RP3V. The majority of these neurons colocalized Th mRNA. Kiss1/TH neurons in the RP3V express a rapidly activating Ih, mediated primarily through HCN1 channels, and a T-type calcium current, mediated primarily through CaV3.1 channels. We have defined a hyperpolarization threshold that is critical for recruiting CaV3.1 channels for generating a high-frequency rebound burst firing. Importantly, the expression of both IT and Ih was augmented by an E2 treatment paradigm that generates an LH surge in the ovariectomized female. We have also discovered a robust hyperpolarizing response to GABAB as well as κ-, and to a lesser extent, μ-opioid receptor agonists, indicative of GABAergic synaptic input and input from opioidergic neurons,

most plausibly dynorphin or met-enkephalin. Thus, the biophysical and molecular fingerprints of Kiss1 neurons in the RP3V are consistent with their putative role in generating the sustained, high-frequency burst firing required for driving the preovulatory GnRH surge.

| Gene | Product Length (bp) | Sense Primer | Antisense Primer | Accession no. | Slope | Efficiency (%) | $r^2$ |
|---|---|---|---|---|---|---|---|
| HCN1 | 136 | 1527-1546 | 1662-1641 | NM_010408 | -3.25 | 100 | 0.96 |
| HCN2 | 97 | 1423-1444 | 1561-1572 | NM_008226 | -3.27 | 100 | 0.97 |
| HCN3 | 118 | 1664–1682 | 1781–1763 | NM_008227 | -3.18 | 100 | 0.98 |
| HCN4 | 123 | 1929–1950 | 2051–2030 | NM_001081192 | -3.17 | 100 | 0.95 |
| CaV3.1 | 144 | 2935–295 | 3059–3078 | NM_009783 | -3.37 | 98 | 0.95 |
| CaV3.2 | 284 | 2640–265 | 2906–2923 | NM_021415 | -3.18 | 100 | 0.95 |
| CaV3.3 | 128 | 965–973 | 1093–1110 | NM_001044308 | -3.42 | 96 | 0.99 |
| DOPr | 123 | 326–347 | 427–448 | NM_013622.3 | -3.22 | 100 | 0.98 |
| KOPr | 92 | 82–101 | 154–173 | NM_001039652.1 | -3.22 | 100 | 0.93 |
| MOPr | 102 | 489–509 | 572–590 | NM_178260 | -3.22 | 99 | 0.96 |
| Kiss1 | 120 | 64–80 | 195–179 | NM_178260 | -3.41 | 97 | 0.99 |
| TH | 131 | 1266–1285 | 1377–1396 | NM_007393298 | -3.1 | 100 | 0.99 |
| β-actin | 110 | 416–435 | 505–525 | NM_007393 | -3.46 | 95 | 0.99 |

Table B.1: Primer sequences for PCR

The sense (forward) primer is listed first, with the antisense (reverse) primer below. HCN, hyperpolarization-activated cyclic nucleotide-gated channel; CaV, voltage-gated calcium channel; OR, opioid recptor; Kiss1, kisspeptin; TH, tyrosine hydroxylase.

| **Mice (cell no.)** | **$C_m$ (pF)** | **$R_{in}$(GΩ)** | **$I_T$ (pA)** | **$I_h$(pA)** | **AP threshold (mV)** | **RMP (mV)** |
|---|---|---|---|---|---|---|
| TH (n = 12) | 19.1 ± 2.6 | 2.7 ± 0.5 | 41.7 ± 10.1 | 46.0 ± 12.8 | -44.9 ± 0.7 | -54.6 ± 1.1 |
| Kiss (n = 14) | 18.5 ± 1.1 | 2.3 ± 0.6 | 44.0 ± 4.9 | 38.4 ± 4.9 | -45.1 ± 0.9 | -54.7 ± 0.6 |

Table B.2: Electrotonic properties of RP3V Kiss1+/TH+ neurons in high-E2-treated TH-EGFP and Kiss-Cre GFP mice.

Values are means ± SE. IT, T-type calcium channel current; Ih, hyperpolarization-activated h-current; AP, action potential, RMP, resting membrane potential.

| Cell type | Low $E_2$ | | High $E_2$ | | |
|---|---|---|---|---|---|
| | $Kiss1^+/TH^+$ | $Kiss1^-/TH^+$ | $Kiss1^+/TH^+$ | $Kiss1^+/TH^-$ | $Kiss1^-/TH^+$ |
| With $I_T$ | 3 (33%) | 1 (20%) | 26 (84%) | 4 (80%) | 2 (22%) |
| With $I_h$ | 7 (78%) | 5 (100%) | 31 (100%) | 5 (100%) | 8 (89%) |
| Cell nos. | 10 | 5 | 31 | 5 | 9 |

Table B.3: Effects of high vs. low dose of E2 on expressions of IT and Ih in RP3V Kiss1 neurons

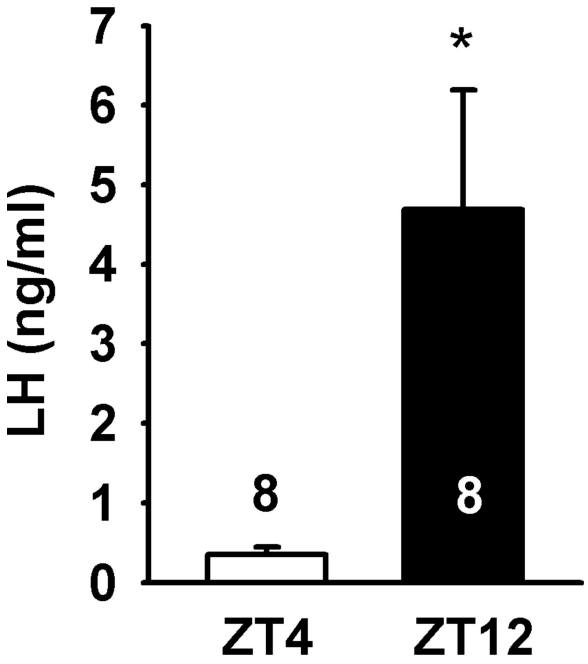


Figure B.1: LH levels in two-dose 17β-estradiol (E2) treatment regimen of ovariectomized (OVX) Kiss1-CreGFP mice.

LH levels in two-dose 17β-estradiol (E2) treatment regimen of ovariectomized (OVX) Kiss1-CreGFP mice.

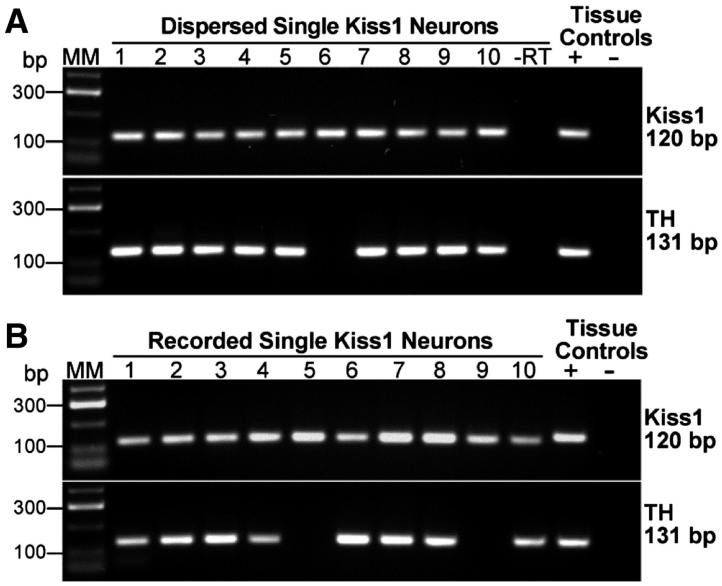


Figure B.2: Single-cell RT-PCR identification of Kiss1 mRNA and Th mRNA

A: expression of kisspeptin (Kiss1) and tyrosine hydroxylase (Th) mRNA in Kiss1-CreGFP neurons in the periventricular POA. Representative gels illustrating coexpression of Kiss1 mRNA and Th mRNA in dispersed and harvested Kiss1-GFP neurons from high-E2 (surge-level)-treated animals. Expected sizes for the PCR products are 120 bp for Kiss1 and 131 bp for Th. As a negative control, cells reacted without reverse transcriptase (−RT) did not express any of the transcripts (a total of 6 cells were reacted −RT). POA tissue RNA was also included as a positive control (+RT) and negative control (−RT). MM, molecular markers. Kiss1 mRNA was expressed in 94% of Kiss1-GFP harvested neurons (n = 139); 88% of Kiss1-positive cells coexpressed Th mRNA. B: expression of Kiss1 and Th mRNA in Kiss1-CreGFP neurons harvested in the POA slice. Representative gels illustrating co-expression of Kiss1 and Th mRNA in Kiss1-GFP neurons harvested in the slice following whole cell recording for 30–40 min. Expected sizes for PCR products are 120 bp for Kiss1 and 131 bp for Th. POA tissue RNA was included as a positive control (+RT) and negative control (−RT). Kiss1 mRNA was expressed in 100% of Kiss1-GFP neurons (n = 27) that were located in the periventricular POA of high-E2-treated mice. Th mRNA was expressed in 75% of these neurons.

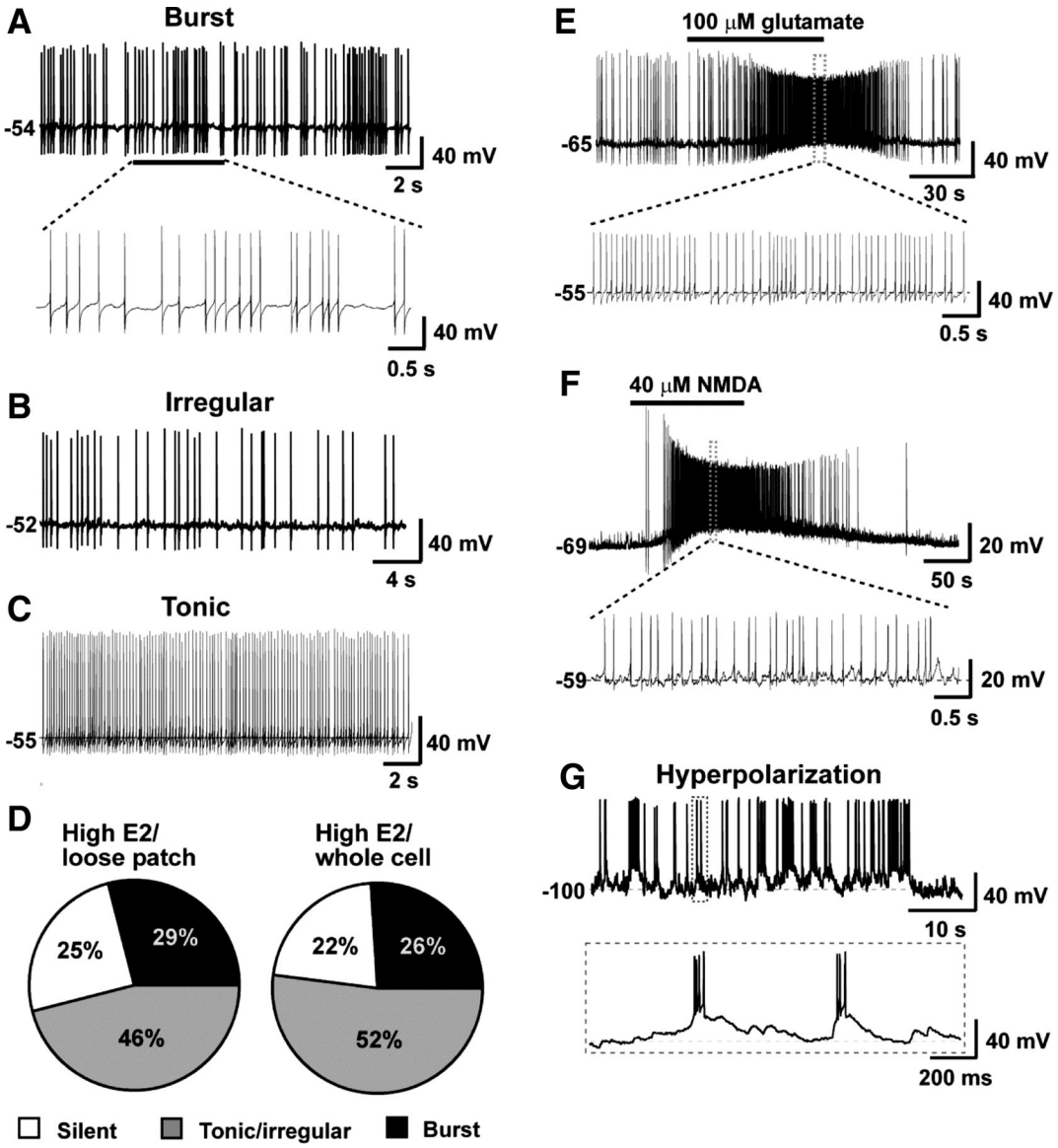


Figure B.3: Properties of spontaneous firing of Kiss1 neurons in the rostral periventricular area of the 3rd ventricle (RP3V) from E2-treated OVX mice.

A–C: representative whole cell, current clamp recordings of spontaneous burst firing (A), irregular firing (B), and tonic firing (C) in RP3V Kiss1 neurons. D: summary of percentage of cells showing different firing pattern in whole cell and loose patch recordings. E and F: representative recordings showing glutamate- or NMDA-induced firing in Kiss1 neurons. G: hyperpolarization-induced spontaneous rebound burst firing recorded from a RP3V Kiss1 neuron. The cell was hyperpolarized by constant current injection of −15 pA.

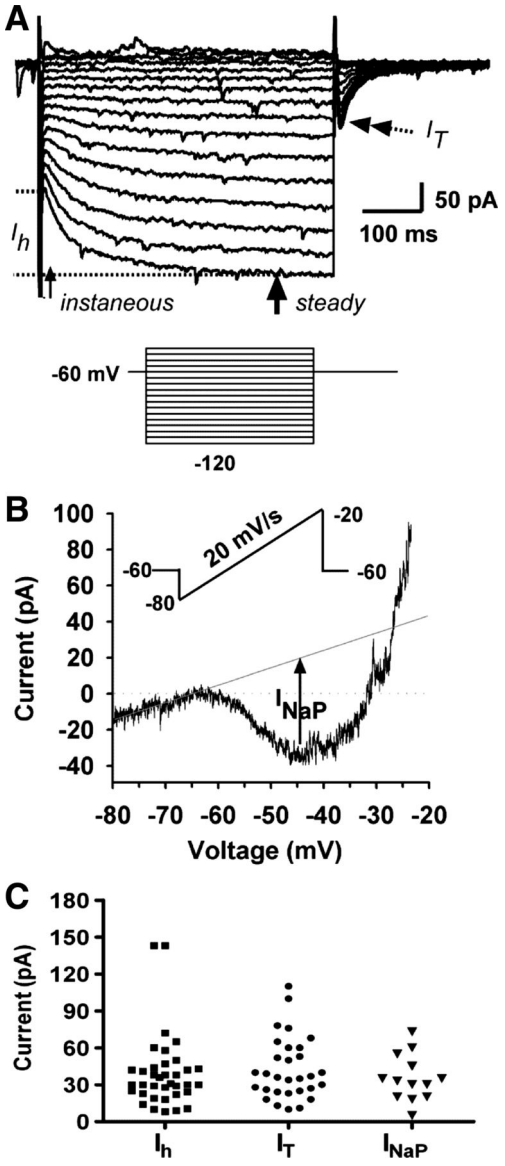


Figure B.4: Kiss1 neurons in the RP3V expressed intrinsic conductances for postinhibitory rebound burst firing.

Figure B.4 legend: A: Representative recording showing a series of hyperpolarizing/depolarizing pulses induced current (inset: voltage protocol: holding potential = −60 mV; steps from −45 to −120 mV, duration 500 ms). Single-head arrows indicate where instantaneous and steady-state hyperpolarization-activated h current (Ih) were measured. Steady-state current (Isteady state) was taken as an average from the arrow to the end of the pulse. Double-head arrow indicates peak T-type calcium current (IT), which was activated when the voltage was stepped back to −60 mV. B: Representative recording showing persistent sodium current (INaP) in RP3V Kiss1 neurons. INaP was activated by a slow ramp of voltage (20 mV/s) from −80 to −20 mV (see inset protocol). Measurement of INaP was indicated as the difference between the inward peak at −50 mV and the extrapolated leak current from −80 mV (dashed line). C: Scatter plot of amplitude distribution of the IT, Ih, and INaP that were larger than 5 pA in RP3V Kiss1 neurons. (IT: 42.9 ± 4.6 pA, n = 30; Ih: 39.4 ± 4.9 pA, n = 36; INaP: 35.3 ± 5.2 pA, n = 13, respectively). Ih and INaP were expressed in 100% of Kiss1 neurons; IT was expressed in 83% of cells.

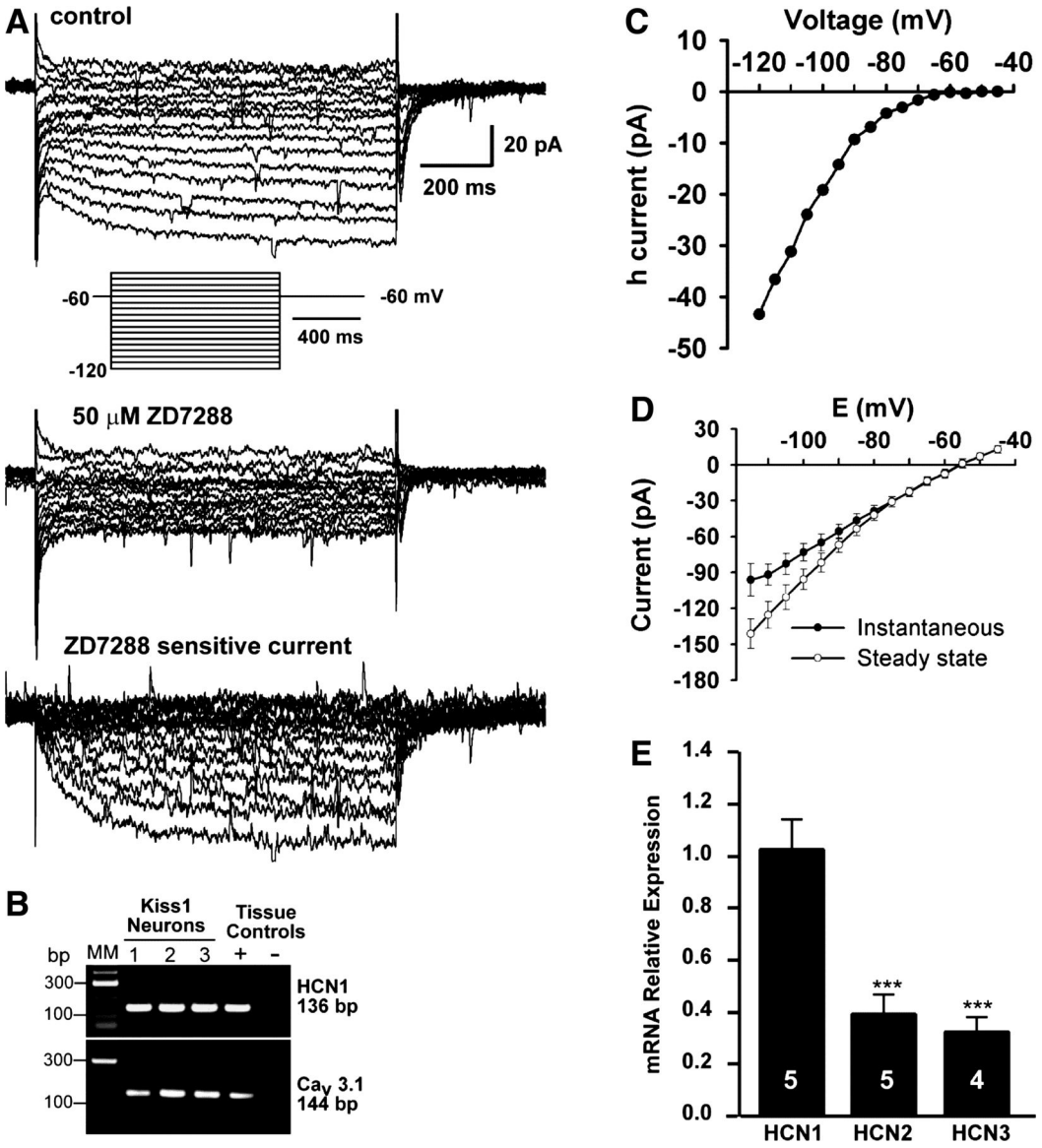


Figure B.5: RP3V Kiss1 neurons express ZD-7288-sensitive Ih and mRNA for HCN channels.

Figure B.5: A: representative voltage-clamp recording of Ih with a hyperpolarizing voltage step protocol. Top: characteristic Ih are visible as slowly activated inward currents at hyperpolarized membrane potentials. Inset: voltage clamp protocol: Vhold = −60 mV; range from −40 to −120 mV, step size 5 mV, step duration 1 s. Middle: Ih is blocked by 50 μM ZD-7288, evidenced by lack of slowly developed inward current. Bottom: ZD-7288-sensitive current, which represents the isolated Ih. B: film image of representative Kiss1 neurons that expressed HCN1 and Cav3.1 transcripts following whole cell recording for 30–40 min. C: I/V relationship of Ih from A, showing voltage-dependent activation and inward rectification at increasingly hyperpolarized voltages. D: mean I/V relationship of 16 Kiss1 neurons showing instantaneous (filled circles) and steady-state (open circles) whole cell currents. Vhold = −60 mV. Protocol is indicated in Fig. 4A. The difference between instantaneous and steady-state I/V was due to activation of Ih. E: relative levels of mRNA for HCN1, -2, and -3 in pools of Kiss1 neurons within the RP3V (n = 4–5 animals, 3 pools/animal). Levels of HCN2 and HCN3 mRNA were significantly lower than HCN1 mRNA. Relative expression was calculated by $\Delta\Delta$CT method and normalized to the mean $\Delta$CT of HCN1. ***P < 0.001 for HCN2 vs. HCN1 and HCN3 vs. HCN1 (ANOVA).

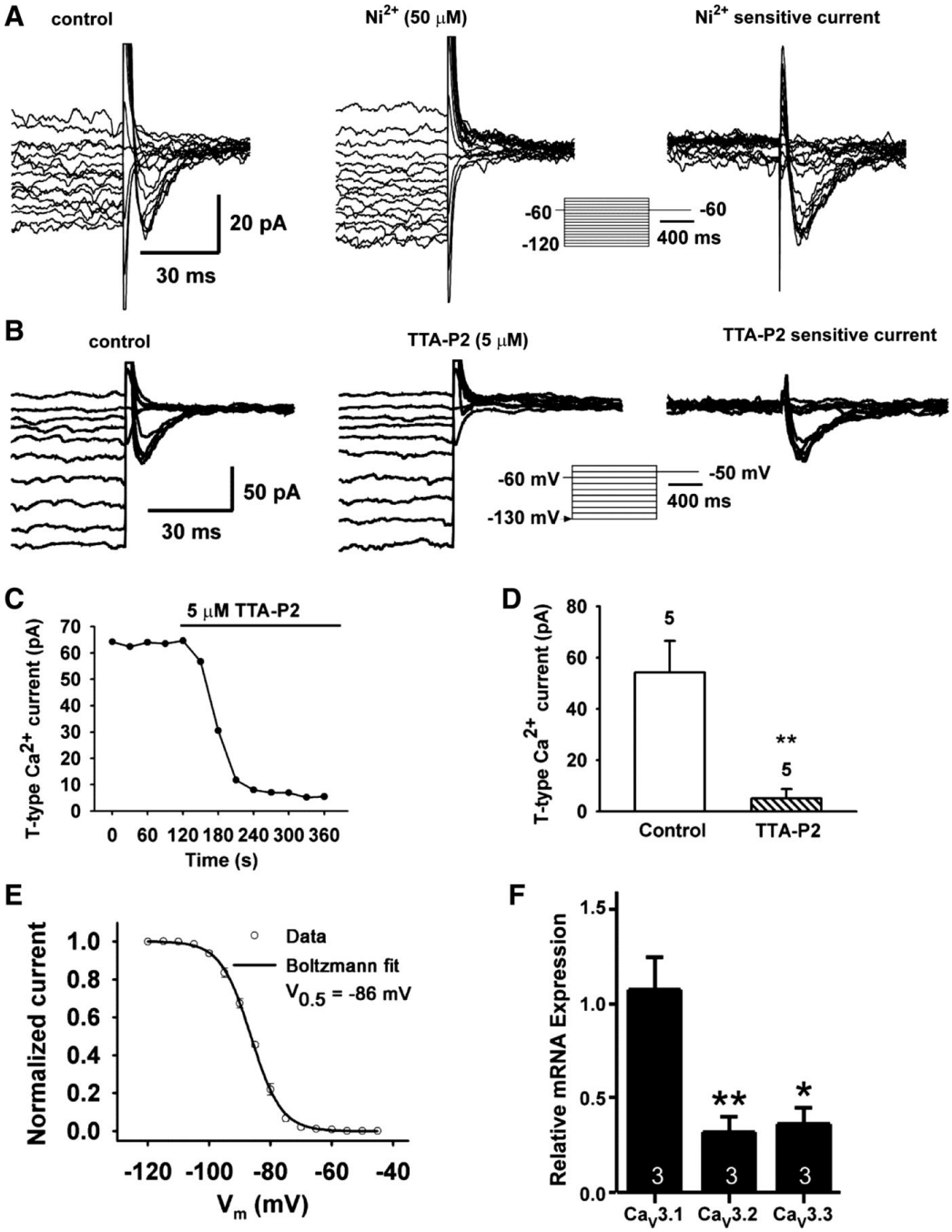


Figure B.6: RP3V Kiss1 neurons express nickel- and TTA-P2-sensitive IT and mRNA for CaV3 channels.

Figure B.6 legend: A: representative traces showing I-V relationship of IT before (left, control) and after exposure to 50 μM Ni2+ for 10 min (middle, Ni2+), and the subtracted Ni2+-sensitive IT (right) recorded from a RP3V Kiss1 neuron. Traces were truncated to highlight inward IT. The insert panel shows the voltage-clamp protocol used to measure IT. The pulse protocol consisted of 5-mV steps, from −40 to −120 mV, before returning to −60 mV. Pulses were of 1-s duration to ensure complete de-inactivation of the T-channel. B: representative traces showing I-V relationship of IT before (left, control) and after exposure to 5 μM TTA-P2 for 10 min (middle) and the subtracted, TTA-P2-sensitive IT (right) recorded from a RP3V Kiss1 neuron. Traces were truncated to highlight the inward IT following de-inactivation steps. Bottom: voltage-clamp protocol used to measure IT in Kiss1 neurons. C: analysis of time course of TTA-P2 blockade of IT in a Kiss1 neuron. D: summary of effects of TTA-P2 on maximum peak amplitude of IT at −50 mV. **P < 0.01 vs. control, with Student's unpaired t-test; n = 5 cells. Mean inhibition of IT by 5 μM TTA-P2 was 90.9 ± 5.3%. E: Boltzmann equation fit of the voltage-dependent de-inactivation of the T-channel. Half-maximum de-inactivation voltage is indicated: V1/2 = −86.4 ± 0.2 mV (n = 5, r2 = 0.999). F: levels of mRNA for Cav3.1, −3.2, and −3.3 derived from qPCR (n = 3 animals; 3 pools/animal). Relative expression was calculated by ΔΔCT method and normalized to mean ΔCT of CaV3.1. *P < 0.05 for CaV3.3 vs. CaV3.1; **P < 0.01, CaV3.2 vs. CaV3.1 (ANOVA).

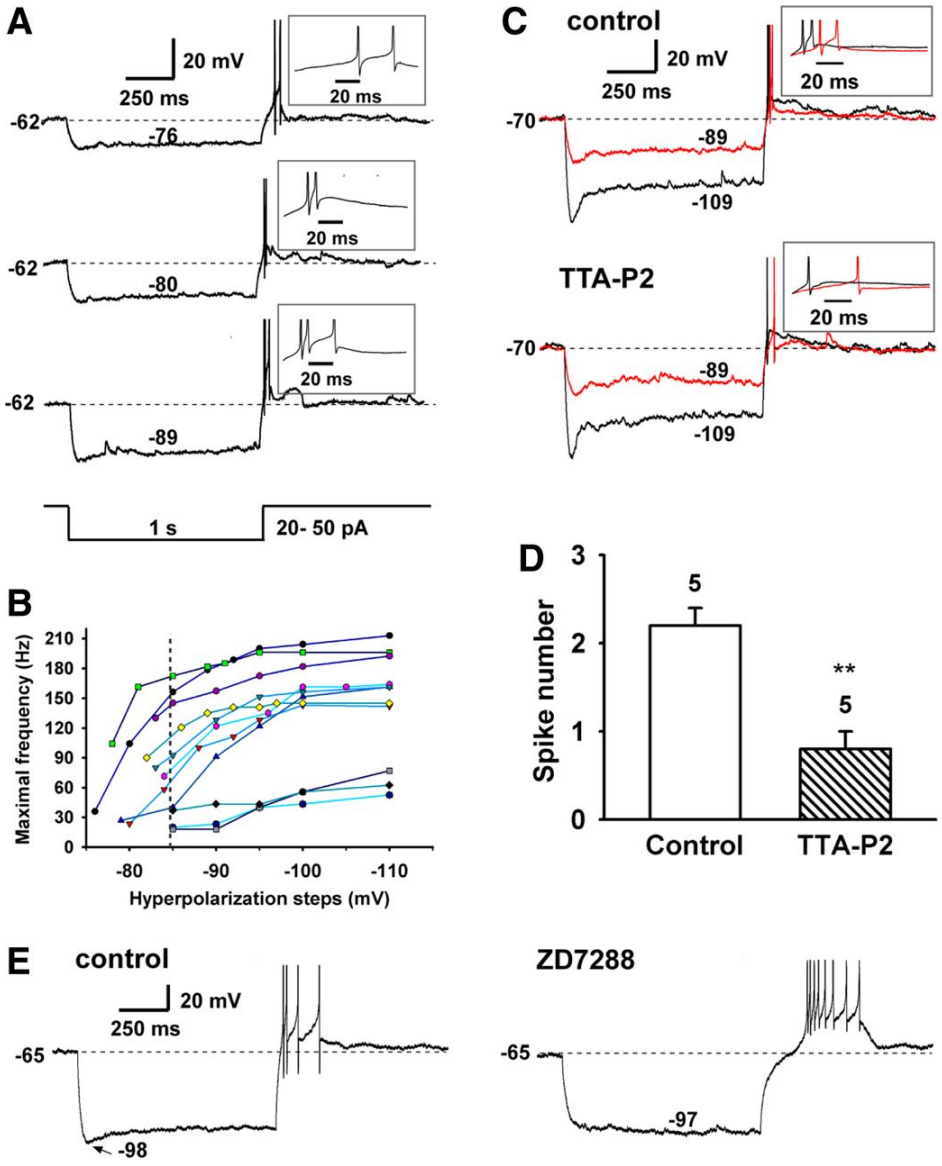


Figure B.7: Hyperpolarization-induced rebound burst firing in RP3V Kiss1 neurons.

Figure B.7 legend: A: hyperpolarization-induced rebound burst firing from a Kiss1+/TH+ cell that expressed IT of 52 pA (activated at −60 mV) and had input resistances of 0.53 and 2.0 GΩ between −80 and −60 mV and between −70 and −50 mV, respectively. B: analysis of the effect of hyperpolarizing steps on maximal burst frequency in 11 cells. Dashed line, mean hyperpolarization threshold for burst firing of 82% of neurons. C: example recording showing that T-channel blocker TTA-P2 (5 μM) blocked the rebound burst firing. This cell had IT of 67 pA and Ih of 46 pA. Current injections of −30 and −90 pA yielded hyperpolarizations of −89 and −109 mV, respectively. D: summary of effects of TTA-P2 on spike number of rebound burst firing. **P < 0.01, paired Student's t-test. E: example recording showing that h-channel blocker ZD-7288 (50 μM) did not block the rebound burst firing but increased the delay to the first spike. This cell had IT of 30 pA and Ih of 38 pA. Current injection of −60 pA hyperpolarized the cell membrane to −98 mV.

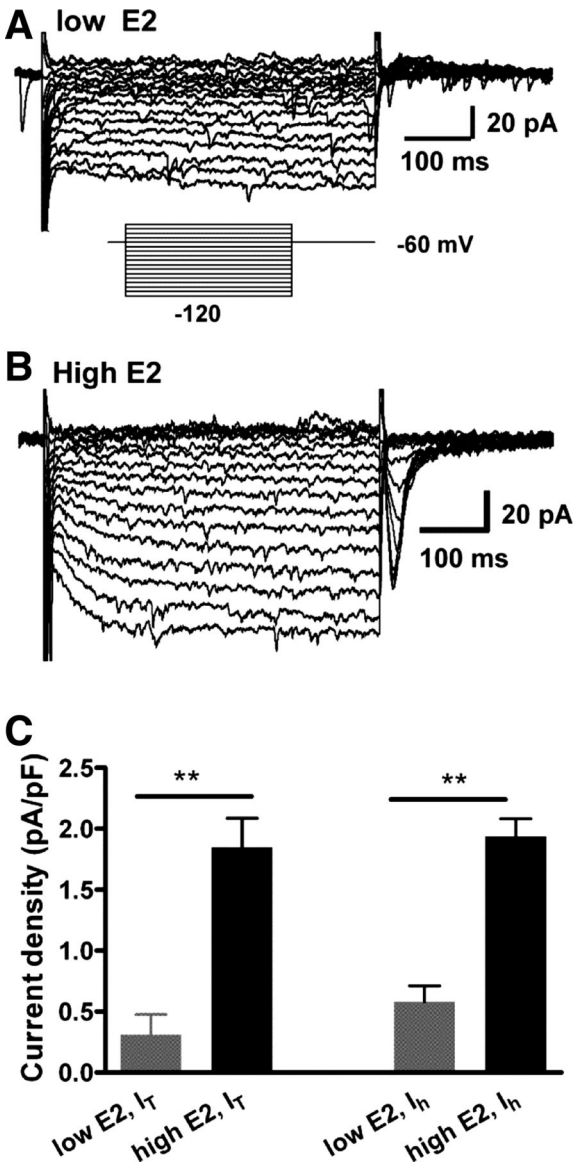


Figure B.8: Expression of IT and Ih is estrogen state dependent in RP3V Kiss1 neurons.

A and B: 2 representative recordings showing that IT and Ih greatly increased in high-E2-treated vs. low-E2-treated mice. C: summary of current density of IT and Ih in RP3V Kiss1 neurons from low-E2 and high-E2 animals. All cells were included for statistical analysis (n = 10 for low-E2 group, 5 animals; n = 36 for high-E2 group, 16 animals). **P < 0.01, unpaired Student's t-test.

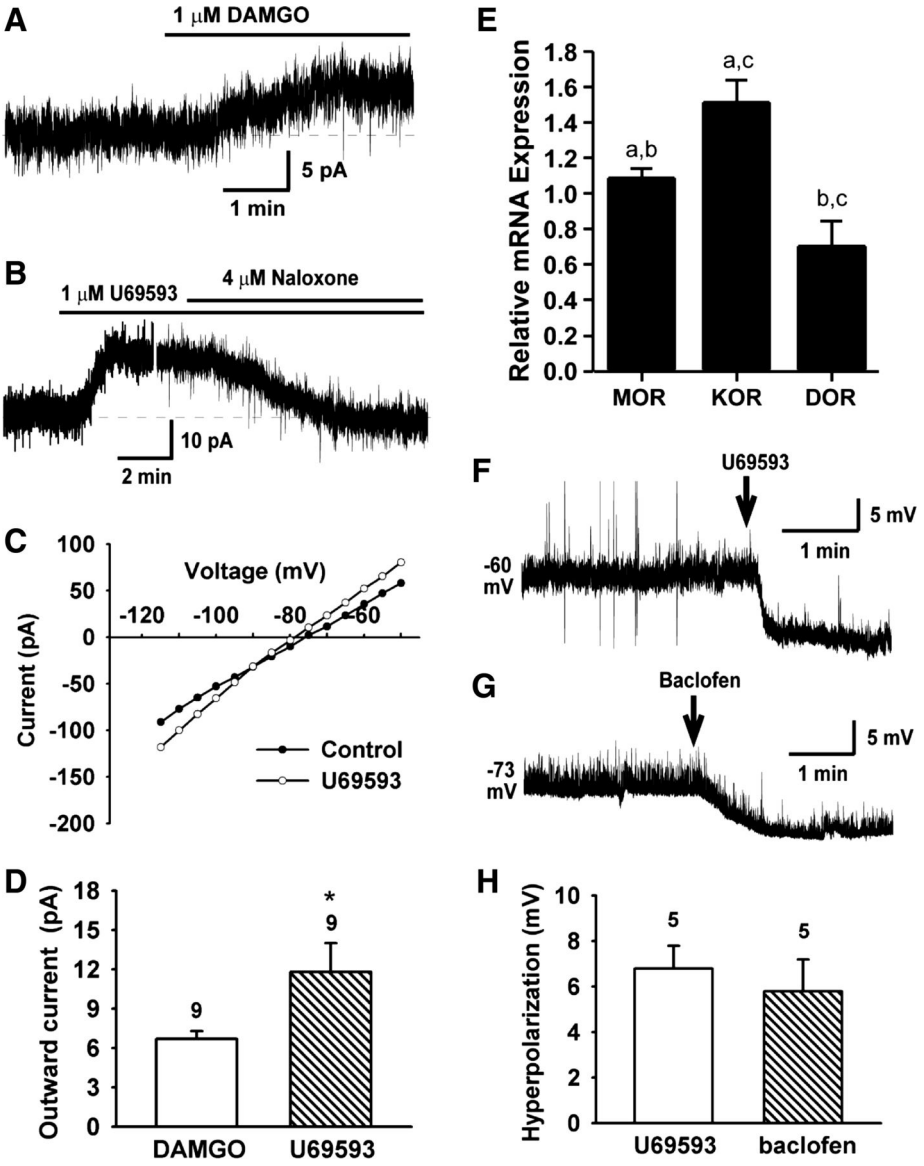


Figure B.9: Effects of MOPr, KOPr and GABAB receptor agonists on Kiss1 neurons in the RP3V.

Figure B.9 legend: A: in voltage-clamp and in the presence of TTX (0.5 μM), the selective μ-opioid receptor agonist DAMGO (1 μM) induced an outward current. Vhold = −60 mV. B and C: selective κ-opioid receptor agonist U-69593 (1 μM) induced an outward current (B), which reversed near −90 mV (C), indicating activation of a K+ current. Effects of U-69593 were antagonized by naloxone Vhold = −60mV. D: summary of outward K+ current amplitude induced by DAMGO and U-69593 at −60 mV (n = 9, *P < 0.05). E: relative expressions of DOPr, KOPr, and MOPr receptor mRNAs based on qPCR (n = 4–5 animals, 3 pools/animal). Relative expression was calculated by $\Delta\Delta$CT method and normalized to mean $\Delta$CT of μ-opioid receptors; a-a, b-b, P < 0.05; c-c, P < 0.001 (one-way ANOVA). F and G: selective KOPr agonist U-69593 (1 μM)-induced and GABAB receptor agonist baclofen (20 μM)-induced hyperpolarization of RP3V Kiss1 neurons. H: summary results of U-69593- and baclofen-induced hyperpolarization.

## B.6 References


1. Bicknell RJ. Optimizing release from peptide hormone secretory nerve terminals. J exp Biol 139: 51–65, 1988.

2. Bosch MA, Hou J, Fang Y, Kelly MJ, Rønnekleiv OK. 17β-Estradiol regulation of the mRNA expression of T-type calcium channel subunits: role of estrogen receptor α and estrogen receptor β. J Comp Neurol 512: 347–358, 2009.

3. Bosch MA, Tonsfeldt KJ, Ronnekleiv OK. mRNA expression of ion channels in GnRH neurons: subtype-specific regulation by 17β-estradiol. J Mol Cell Endocrinol 367: 85–97, 2013.CrossRef

4. Brunton J, Charpak S. μ-Opioid peptides inhibit thalamic neurons. J Neurosci 5: 1671–1678, 1998.

5. Catterall WA, Perez-Reyes E, Snutch TP, Striessnig J. International Union of Pharmacology. XLVIII. Nomenclature and structure-function relationship of voltage-gated calcium channels. Pharmacol Rev 57: 411–425, 2005.

6. Christian CA, Mobley JL, Moenter SM. Diurnal and estradiol-dependent changes in gonadotropin-releasing hormone neuron firing activity. Proc Natl Acad Sci USA 102: 15682–15687, 2005.

7. Clarkson J, Herbison AE. Postnatal development of kisspeptin neurons in mouse hypothalamus: sexual dimorphism and projections to gonadotropin-releasing hormone neurons. Endocrinology 147: 5817–5825, 2006.

8. Clarkson J, Herbison AE. Dual phenotype kisspeptin-dopamine neurones of the rostral periventricular area of the third ventricle project to GnRH hormones. J Neuroendocrinol 23: 293–301, 2011.

9. de Croft S, Piet R, Mayer C, Mai O, Boehm U, Herbison AE. Spontaneous kisspeptin neuron firing in the adult mouse reveals marked sex and brain region differences but no support for a direct role in negative feedback. Endocrinology 153: 1–10, 2012.

10. Dreyfus FM, Tscherter A, Errington AC, Renger JJ, Shin HS, Uebele VN, Crunelli V, Lambert RC, Leresche N. Selective T-type calcium channel block in thalamic neurons reveals channelredundancy and physiological impact of ITwindow. J Neurosci 30: 99–109, 2010.

11. Ducret E, Gaidamaka G, Herbison AE. Electrical and morphological characteristics of anteroventral periventricular nucleus kisspeptin and other neurons in the female mouse. Endocrinolgy 151: 2223–2232, 2010.

12. Erickson KR, Rønnekleiv OK, Kelly MJ. Electrophysiology of guinea-pig supraoptic neurones: role of a hyperpolarization-activated cation current in phasic firing. J Physiol (Lond) 460: 407–425, 1993.

13. Erickson KR, Rønnekleiv OK, Kelly MJ. Role of a T-type calcium current in supporting a depolarizing potential, damped oscillations, and phasic firing in vasopressinergic guinea pig supraoptic neurons. Neuroendocrinology 57: 789–800, 1993.

14. Frazão R, Cravo RM, Donato J Jr., Ratra DV, Clegg DJ, Elmquist JK, Zigman JM, Williams KW, Elias CF. Shift in kiss1 cell activity requires estrogen receptor $\alpha$. J Neurosci 33: 2807–2820, 2013.

15. Goldstein A, Naidu A. Multiple opioid receptors: ligand selectivity profiles and binding site signatures. Mol Pharm 36: 265–272, 1989.Abstract

16. Goodman RL, Lehman MN, Smith JT, Coolen LM, de Oliveira CVR, Jafarzadehshirazi MR, Pereira A, Iqbal J, Caraty A, Ciofi P, Clarke IJ. Kisspeptin neurons in the arcuate nucleus of the ewe express both dynorphin A and neurokinin B. Endocrinology 148: 5752–5760, 2007.

17. Gottsch ML, Popa SM, Lawhorn JK, Qiu J, Tonsfeldt KJ, Bosch MA, Kelly MJ, Ronnekleiv OK, Sanz E, McKnight GS, Clifton DK, Palmiter RD, Steiner RA. Molecular properties of Kiss1 neurons in the arcuate nucleus of the mouse. Endocrinology 152: 4298–4309, 2011.

18. Han SK, Gottsch ML, Lee KJ, Popa SM, Smith JT, Jakawich SK, Clifton DK, Steiner RA, Herbison AE. Activation of gonadotropin-releasing hormone neurons by kisspeptin as a neuroendocrine switch for the onset of puberty. J Neurosci 25: 11349–11356, 2005.

19. Huguenard JR, McCormick DA. Simulation of the currents involved in rhythmic oscillations in thalamic relay neurons. J Neurophysiol 68: 1373–1383, 1992.

20. Kauffman AS, Gottsch ML, Roa J, Byquist AC, Crown A, Clifton DK, Hoffman GE, Steiner RA, Tena-Sempere M. Sexual differentiation of kiss1 gene expression in the brain of the rat. Endocrinology 148: 1774–1783, 2007.

21. Kelly MJ, Loose MD, Rønnekleiv OK. Estrogen suppresses $\mu$-opioid and GABAB-mediated hyperpolarization of hypothalamic arcuate neurons. J Neurosci 12: 2745–2750, 1992.Abstract

22. Kelly MJ, Qiu J. Estrogen signaling in hypothalamic circuits controlling reproduction. Brain Res 1364: 44–52, 2010.

23. Kelly MJ, Rønnekleiv OK. Electrophysiological analysis of neuroendocrine neuronal activity in hypothalamic slices. In: Methods in Neurosciences: Pulsatility in Neuroendocrine Systems, edited by Levine JE. San Diego: Academic, 1994, p. 47–67.

24. Klockner U, Lee JH, Cribbs LL, Daud A, Hescheler J, Pereverzev A, Perez-Reyes E, Schneider T. Comparison of the Ca2+ currents induced by expression of three cloned $\alpha$1 subunits,$\alpha$1G,$\alpha$1H and $\alpha$11, of low-voltage-activated T-type Ca2+ channels. Eur J Neurosci 11: 4171–4178, 1999.

25. Lagrange AH, Rønnekleiv OK, Kelly MJ. Estradiol-17$\beta$ and $\mu$-opioid peptides rapidly hyperpolarize GnRH neurons: a cellular mechanism of negative feedback? Endocrinology 136: 2341–2344, 1995.Abstract

26. Liu X, Porteous R, d'Anglemont de Tassigny X, Colledge WH, Millar R, Petersen SL, Herbison AE. Frequency-dependent recruitment of fast amino acid and slow neuropeptide neurotransmitter release controls gonadotropin-releasing hormone neuron excitability. J Neurosci 31: 2421–2430, 2011.

27. Llinás RR. The intrinsic electrophysiological properties of mammalian neurons: insights into central nervous system function. Science 242: 1654–1664, 1988.

28. Loose MD, Kelly MJ. Opioids act at $\mu$-receptors to hyperpolarize arcuate neurons via an inwardly rectifying potassium conductance. Brain Res 513: 15–23, 1990.

29. Loose MD, Rønnekleiv OK, Kelly MJ. Membrane properties and response to opioids of identified dopamine neurons in the guinea pig hypothalamus. J Neurosci 10: 3627–3634, 1990.Abstract

30. Lüthi A, McCormick DA. H-current: properties of a neuronal and network pacemaker. Neuron 21: 9–12, 1998.

31. Lyons DJ, Horjales-Araujo E, Broberger C. Synchronized network oscillations in rat tuberoinfundibular dopamine neurons: switch to tonic discharge by thyrotropin-releasing hormone. Neuron 65: 217–229, 2010.

32. Masterson SP, Li J, Bickford ME. Frequencey-dependent release of substance P mediates heterosynaptic potentiation of glutamatergic synaptic responses in the rat visual thalamus. J Neurophysiol 104: 1758–1767, 2010.

33. Matsushita N, Okada H, Yasoshima Y, Takahashi K, Kiuchi K, Kobayashi K. Dynamics of tyrosine hydroxylase promoter activity during midbrain dopaminergic neuron development. J Neurochem 82: 295–304, 2002.

34. Navarro VM, Gottsch ML, Chavkin C, Okamura H, Clifton DK, Steiner RA. Regulation of gonadotropin-releasing hormone secretion by kisspeptin/dynorphin/neurokinin B neurons in the arcuate nucleus of the mouse. J Neurosci 29: 11859–11866, 2009.

35. Oka Y. Tetrodotoxin-resistant persistent Na+ current underlying pacemaker potentials of fish gonadotrophin-releasing hormone neurones. J Physiol (Lond) 482: 1–6, 1995.

36. Pau KYF, Orstead KM, Hess DL, Spies HG. Feedback effects of ovarian steroids on the hypothalamic-hypophyseal axis in the rabbit. Biol Repro 35: 1009–1023, 1986.Abstract

37. Perez-Reyes E. Molecular physiology of low-voltage-activated T-type calcium channels. Physiol Rev 83: 117–161, 2003.

38. Pfaffl MW. A new mathematical model for relative quantification in real-time RT-PCR. Nucleic Acid Res 29: 2002–2007, 2001.

39. Pielecka-Fortuna J, Chu Z, Moenter SM. Kisspeptin acts directly and indirectly to increase gonadotropin-releasing hormone neuron activity and its effects are modulated by estradiol. Endocrinology 149: 1979–1986, 2008.

40. Piet R, Boehm U, Herbison AE. Estrous cycle plasticity in the hyperpolarization-activated current Ih is mediated by circulating 17$\beta$-estradiol in preoptic area kisspeptin neurons. J Neurosci 33: 10828–10839, 2013.

41. Porteous R, Petersen SL, Yeo SH, Bhattarai JP, Ciofi P, d'Anglemont de Tassigny X, Colledge WH, Caraty A, Herbison AE. Kisspeptin neurons co-express met-enkephalin and galanin in the rostral periventricular region of the female mouse hypothalamus. J Comp Neurol 519: 3456–69, 2011.CrossRefMedline

42. Qiu J, Fang Y, Bosch MA, Rønnekleiv OK, Kelly MJ. Guinea pig kisspeptin neurons are depolarized by leptin via activation of TRPC channels. Endocrinology 152: 1503–1514, 2011.

43. Robinson RB, Siegelbaum SA. Hyperpolarization-activated cation currents: from molecules to physiological function. Annu Rev Physiol 65: 453–480, 2003.

44. Santoro B, Chen S, Lüthi A, Pavlidis P, Shumyatsky GP, Tibbs GR, Siegelbaum SA. Molecular and functional heterogeneity of hyperpolarization-activated pacemaker channels in the mouse CNS. J Neurosci 20: 5264–5275, 2000.

45. Sawamoto K, Nakao N, Kobayashi K, Matsushita N, Takahashi H, Kakishita K, Yamamoto A, Yoshizaki T, Terashima T, Murakami F, Itakura T, Okano H. Visualization, direct isolation, and transplantation of midbrain dopaminergic neurons. Proc Natl Acad Sci USA 98: 6423–6428, 2001.

46. Shakiryanova D, Tully A, Hewes RS, Deitcher DL, Levitan ES. Activity-dependent liberation of synaptic neuropeptide vesicles. Nat Neurosci 8: 173–178, 2005.

47. Simerly RB. Prodynorphin and proenkephalin gene expression in the anteroventral periventricular nucleus of the rat: sexual differentiation and hormonal regulation. Mol Cell Neurosci 2: 473–484, 1991.CrossRefMedline

48. Simerly RB, McCall LD, Watson SJ. Distribution of opioid peptides in the preoptic region: immunohistochemical evidence for a steroid-sensitive enkephalin sexual dimorphism. J Comp Neurol 276: 442–459, 1988.

49. Tsien RW, Hess P, McCleskey EW, Rosenberg RL. Calcium channels: mechanisms of selectivity, permeation, and block. Annu Rev Biophys Biophys Chem 16: 265–290, 1987.

50. Ulrich D, Huguenard JR. Gamma-aminobutyric acid type B receptor-dependent burst-firing in thalamic neurons: a dynamic clamp study. Proc Natl Acad Sci USA 93: 13245–13249, 1996.

51. Wagner EJ, Rønnekleiv OK, Bosch MA, Kelly MJ. Estrogen biphasically modifies hypothalamic GABAergic function concomitantly with negative and positive control of luteinizing hormone release. J Neurosci 21: 2085–2093, 2001.

52. Williams JT, Egan TM, North RA. Enkephalin opens potassium channels on mammalian central neurones. Nature 299: 74–77, 1982.

53. Zagotta WN, Siegelbaum SA. Structure and function of cyclic nucleotide-gated channels. Annu Rev Neurosci 19: 235–263, 1996.

54. Zhang C, Bosch MA, Levine JE, Rønnekleiv OK, Kelly MJ. Gonadotropin-releasing hormone neurons express KATP channels that are regulated by estrogen and responsive to glucose and metabolic inhibition. J Neurosci 27: 10153–10164, 2007.

55. Zhang C, Bosch MA, Rick EA, Kelly MJ, Rønnekleiv OK. 17$\beta$-Estradiol regulation of T-type calcium channels in gonadotropin-releasing hormone neurons. J Neurosci 29: 10552–10562, 2009.

56. Zhang C, Roepke TA, Kelly MJ, Rønnekleiv OK. Kisspeptin depolarizes gonadotropin-releasing hormone neurons through activation of TRPC-like cationic channels. J Neurosci 28: 4423–4434, 2008.

57. Zheng SX, Bosch MA, Rønnekleiv OK. Mu-opioid receptor mRNA expression in identified hypothalamic neurons. J Comp Neurol 487: 332–344, 2005.

# Appendix C

**mRNA expression of ion channels in GnRH neurons: Subtype-specific regulation by 17beta-estradiol**

Martha A Bosch[1], Karen J Tonsfeldt[1], and Oline K. Rønnekleiv[1,2]

[1]Department of Physiology and Pharmacology, Oregon Health and Science University, Portland Oregon; [2]Division of Neuroscience, Oregon National Primate Research Center, Oregon Health and Science University, Beaverton, Oregon

Appendix C was modified from a manuscript published in Molecular and Cellular Endocrinology, Mar 10, 2013, 367(1-2):85-97.

# Foreward

In human and rodents, ovulation is initiated by a preovulatory surge of gonadotropin-releasing hormone (GnRH), which stimulates a similar surge of luteinizing hormone (LH), which initiates ovulation. This event is preceeded by a period of positive estrogen feedback, such that estrogen levels rise dramatically and indirectly stimulate GnRH release. The preovulatory surge is of significant research interest because of the departure of the hypothalamic-pituitary-gonad (HPG) axis from its usual negative feedback loop. However, it's somewhat impractical to study, because it occurs only once every 4-5 days in rodents (on proestrus), and is temporally confined to the end of the light cycle.

My primary contribution to this paper was assisting in the development of a mouse model of the preovulatory surge. A hormonal surge can be elicited in ovariectomized mice given exogenous estrogen. However, the HPG axis is sensitive to the mode, timing, and dose of estrogen delivery. We tested a number of models that had been described to evoke the preovulatory GnRH surge, and ultimately validated a two day, low- and high-dose estrogen treatment paradigm to reliably elevate LH levels at the end of the induced proestrus. With this model, one can conveniently study the two extremes of the female cycle - low estrogen states (short term ovariectomy), and high estrogen states (induced proestrus). Using this model, we then went on to define estrogen- and circadian regulation of a number of genes associated with the preovulatory surge.

## C.1 Abstract

Burst firing of neurons optimizes neurotransmitter release. Gonadotropin-releasing hormone (GnRH) neurons exhibit burst firing activity and T-type calcium channels, which are vital for burst firing activity, are regulated by 17$\beta$-estradiol (E2) in GnRH neurons. To further elucidate ion channel expression and E2 regulation during positive and negative feedback on GnRH neurosecretion, we used single cell RT-PCR and real-time qPCR to quantify channel mRNA expression in GnRH neurons. GFP-GnRH neurons expressed numerous ion channels important for burst firing activity. E2-treatment sufficient to induce an LH surge increased mRNA expression of HCN1channels, which underlie the pacemaker current, the calcium-permeable CaV1.3, CaV2.2, CaV2.3 channels, and TRPC4 channels, which mediate the kisspeptin excitatory response. E2 also decreased mRNA expression of SK3 channels underlying the medium AHP current. Therefore, E2 exerts fundamental changes in ion channel expression in GnRH neurons, to prime them to respond to incoming stimuli with increased excitability at the time of the surge.

Highlights:

- Single-cell quantitative PCR of channel transcripts in GnRH neurons was validated and used.
- E2 increased or decreased the mRNA expression of ion channels in GnRH neurons.
- Altered channel mRNA expression leads to changes in the excitability of GnRH neurons.

## C.2 Introduction

As demonstrated in a number of species including the rat, sheep and rhesus monkey, the preovulatory luteinizing hormone (LH) surge is accompanied by a surge in gonadotropin-releasing hormone (GnRH) (Caraty et al., 1989, Chappell and Levine, 2000, Levine and Ramirez, 1982 and Pau et al., 1993), suggesting increased activity of GnRH neurons at the time of the GnRH surge. This increased activity is primarily due to increased estradiol levels, because treatment with 17$\beta$-estradiol (E2) in ovariectomized (OVX) females can mimic the positive feedback regulation of GnRH and LH secretion (Caraty et al., 1989 and Chappell and Levine, 2000). Cell-attached single-unit extracellular recording to evaluate GnRH neuronal firing activity during negative as compared to positive feedback has revealed that the GnRH neuronal firing rate is low during the morning negative feedback period and significantly higher during the evening positive feedback period (Christian et al., 2005). Collectively, these findings would indicate that there are fundamental changes in GnRH neuronal firing activity during the different stages of the ovulatory cycle and during E2-induced negative and positive feedback. The timing of the GnRH (LH) surge and thus the increased activity of GnRH neurons at the time of the surge is E2-dependent, but it is also entrained to a circadian input from the suprachiasmatic nucleus (SCN) at least in some rodent species (Chappell et al., 2009, Christian et al., 2005, Christian and Moenter, 2008 and Legan et al., 1975). The mechanism by which the SCN affects GnRH neuronal activity is not known, but circadian cues may involve vasopressin input to kisspeptin neurons and vasoactive intestinal peptide input to GnRH neurons (Christian and Moenter, 2008, Vida et al., 2010 and Ward et al., 2009).

In addition to GnRH neurons, kisspeptin neurons are essential for reproductive development and reproductive competence (Oakley et al., 2009). These hypothalamic neurons

express ERα, are affected by E2 feedback, and are strongly excitatory to GnRH neurons (Oakley et al., 2009). Kisspeptin excites GnRH neurons by actions on the G protein-coupled receptor 54 (GPR54), also called kisspeptin receptor (Zhang et al., 2008). Evidence from GT1–7 GnRH neuronal cells suggests that GPR54 exhibits an E2-dependent diurnal variation in mRNA expression (Tonsfeldt et al., 2011). These findings, however, have not been confirmed in native GnRH neurons.

Based on a model similar to that described and validated for thalamocortical relay neurons and hypothalamic neurosecretory neurons (Chemin et al., 2002, Erickson et al., 1993b, Kelly and Rønnekleiv, 1994 and Kim et al., 2001), we had predicted that T-type calcium channels together with the hyperpolarization-activated, cyclic nucleotide-gated channels (HCN) are essential for induction of burst firing in GnRH neurons, and that the calcium-dependent, small-conductance calcium-activated potassium channels (SK) -type channels, which underlie afterhyperpolarization (AHP) are crucial for allowing repetitive cycles of burst firing (Kelly and Rønnekleiv, 1994 and Kelly and Wagner, 2002). All of these channels are active in GnRH neurons and contribute significantly to their signaling pattern (Bosch et al., 2002, Chu et al., 2009, Chu et al., 2010, Kato et al., 2006, Lee et al., 2010, Liu and Herbison, 2008, Spergel, 2007, Zhang et al., 2007 and Zhang et al., 2009). Additional channels important for GnRH neuronal firing include canonical transient receptor potential (TRPC) channels, which are activated by kisspeptin, and high voltage activated (HVA) calcium channels, which are important for calcium homeostasis and peptide release (Sun et al., 2010 and Zhang et al., 2008).

While previous studies have demonstrated that E2 regulates the expression and/or function of a number of channels in GnRH neurons including T-type and L-type calcium channels (Sun et al., 2010 and Zhang et al., 2009), little is known about the channel subtype

expression and the E2 and diurnal regulation of the majority of ion channels in GnRH neurons. To begin to understand the E2-induced changes in GnRH neurons, we have explored the mRNA expression of HCN, TRPC, SK, and HVA calcium channels in the morning (negative feedback) and the expression in the evening (positive feedback) in oil- and E2-treated females. Indeed, we have found an E2-induced increased mRNA expression of HCN1, TRPC4, CaV1.3 (L), CaV2.2 (N) and CaV2.3 (R)-type calcium channels in GnRH neurons. In contrast, SK3 mRNA was decreased in GnRH neurons, whereas GPR54 mRNA was not altered at any time-points. These findings indicate that the rising E2-levels exert specific fundamental changes in ion channels expression in GnRH neurons, to prime these neurons for altered responsiveness to incoming stimuli leading to changes in excitability in an E2-dependent manner.

## C.3 Materials & Methods

### Animals

Adult female CBB6 mice (GnRH-GFP) (Suter et al., 2000) were maintained under constant temperature and lights. Two different lighting cycles were used, where lights were on between 0600 h (zeitgeber time (ZT) 0) and 1800 h (ZT 12) or where lights were on between 0200 h (ZT 0) and 1400 h (ZT 12) local time. The breeders and most of the research animals were kept permanently under reversed lighting schedule, and these animals were used for the majority of evening experiments with some exceptions as noted below. At time of weaning additional research animals were moved to an adjacent room with a regular lighting schedule (0600–1800 h) and were kept there until adulthood (at least 60 days of age). These animals were used for all of the morning experiments and selected evening experiments. We found no evidence for differences between the two lighting schedules.

Food and water were provided ad libitum. The females were exposed to male bedding to establish normal estrous cycle prior to bilateral ovariectomy (OVX) and increased response to E2 afterwards (Bronson and Whitten, 1968 and Dalal et al., 2001). The animals were OVXed under isofluorane inhalant anesthesia 5–7 days before experimentation, and were given a dose of 4 mg/kg carprofen (Rimadyl, Pfizer Animal Health, New York) immediately following surgery for analgesia. All animal procedures were according to NIH standards and were approved by the Institutional (Oregon Health and Science University) Animal Care and Use Committee.

**Induction of the LH surge**

For induction of positive feedback regulation of LH by ovarian steroids in mice, different models have been developed. One model, based on studies by Bronson and colleagues, used E2 implants at the time of OVX combined with a surge-inducing E2 injection 6 days later (Bronson and Vom Saal, 1979). Another similar model (Gee et al., 1984) used an E2 priming implant and an E2 surge implant of differing doses. Both of these models are critically dependent on the "appropriate" concentrations of E2, such that too little or too high levels of E2 will reduce or prevent the LH surge (Bronson and Vom Saal, 1979). We found that, with such sensitivity, we had too many inconsistencies inducing an LH surge in mice. Therefore, we have developed a two-step E2-injection procedure utilizing a priming E2 dose followed by a surge-inducing E2 dose. On day 5 following OVX, the animals were given a subcutaneous injection of a priming dose of 17β-estradiol benzoate (0.25 μg in 50 μl oil) or oil vehicle (50 μl) at ZT 4–5. On day 6, the animals were given a surge dose of 17β-estradiol benzoate (1.0–1.5 μg in 50 μl oil) or oil-vehicle (50 μl) at ZT 4–5. The animals were used for experimentation the following day. The LH surge was induced

under both lighting conditions with similar results. When intact animals were used, estrous stage was confirmed by vaginal smears.

**mRNA quantification in GnRH neuronal pools**

In initial experiments we tested the linearity of mRNA expression in single cells compared to pools of GnRH neurons. Since the mRNA expressions of GnRH and GPR54 are quite high in GnRH neurons and these RNAs can be quantified even in single cells, we compared the expression in single cells versus pools of 2, 4 and 8 cells in two intact animals killed during the second day of diestrus. The expression of $\beta$-actin was used as control as described below. In addition, we also tested the linearity of one of the high-expressing ion channels, SK3. Since this transcript could only be quantified in pools consisting of at least 5-cells, we compared the expression in pools of 5 and 10 GnRH neurons. For this experiment we used OVX animals, since the SK current (medium IAHP) is reduced acutely with E2 application in GnRH neurons (Chu et al., 2009) and E2-treatment in vivo leads to inhibition of the mIAHP in POA GABAergic neurons (Wagner et al., 2001).

**Distribution of mRNAs in single GnRH neurons and quantitative mRNA measurements in GnRH neuronal pools**

These studies were aimed at investigating the mRNA expression in GnRH neurons of a number of ion channels of which there exist several subunits. In order to determine which subtype is expressed in GnRH neurons, individual GnRH neurons were acutely dispersed, harvested and subjected to single cell RT-PCR using primers selective for each channel subtype (see Table 1). In addition, pools of 5 or 10 neurons were harvested and subjected to real-time qPCR in order to determine the quantitative expression of channel subtypes in GnRH neurons.

**Effects of oil- and E2-treatment on mRNA expression in GnRH neurons**

In initial experiments, we tested whether channel mRNA expression in GnRH neurons was different between morning and evening in ovariectomized (OVX) oil-treated animals. The analysis of 4 neuronal pools (5 cells each) from 3 animals revealed that there were no differences in mRNA expression between the two time-points (Table 2). Since oil-treatment did not change the mRNA expression irrespective of time of day, E2 treatment was compared to oil-treatment during the morning and in separate experiments also during the evening. Pools of 5 (or 10) GnRH neurons were harvested during the morning in one set of experiments (oil- and E2-treated animals) and during the evening in another set of experiments (oil- and E2-treated animals) and channel mRNA expression quantified using real-time qPCR.

**Tissue preparation**

On the day of experimentation, each animal was given an intraperitoneal dose of 15 mg ketamine for sedation purposes. The animal was then rapidly decapitated, trunk blood collected, the brain removed from the skull, and the brain stem removed. The resulting block was mounted on a cutting platform that was then secured in a vibratome well filled with ice-cold, oxygenated (95% O2, 5% CO2) high sucrose artificial cerebral spinal fluid (aCSF) (in mM: 208 sucrose, 2 KCl, 1 MgCl, 1.25 NaH2PO4, 10 HEPES, 26 NaHCO3, 10 dextrose, 2 MgSO4, and 1 CaCl2). Three to four coronal slices (240 μm) were cut through the diagonal band-preoptic area (DB-POA). The slices were transferred to a multiwell auxiliary chamber containing oxygenated aCSF (in mM: 124 NaCl, 5 KCl, 1.44 NaH2PO4, 5 HEPES, 10 Dextrose, 25.99 NaHCO3, 2 CaCl2) and kept there until recovery. In all cases, the uterine weights were recorded as a measure of serum E2 levels.

**GnRH neuronal harvesting and reverse transcription**

Each slice was visualized under a Leitz inverted microscope to confirm the exact area of fluorescence GnRH cells and then the medial DB-POA was microdissected under a dissecting microscope. The tissue was incubated in protease (1 mg/ml aCSF) (protease from streptomyces griseus, Sigma) for 15–17 min at 37 °C then washed four times in low Ca2+ aCSF (1 mM Ca2+) and two times in aCSF. Gentle trituration with flamed Pasteur pipettes of decreasing size were used to disperse the neurons onto a glass bottom dish (60 mm dish). We designed a glass-bottomed 60 mm dish using a 22 × 50 mm glass coverslip to increase the surface area of the plate, to allow greater segregation among cells. The cells settle on the glass bottom of the dish after approximately 12 min. For the 15 min prior to and during harvesting, a constant flow (2 ml/min) of oxygenated aCSF circulated into the plate while the effluent circulated out using a peristaltic pump. aCSF flow helped insure fresh, oxygenated media was reaching the cells, and assisted in clearing out unhealthy cells and debris from tituration. The cells harvested were those observed to be fully intact, with long processes extending from at least one axis of the cell. Some cells exhibited tiny hair-like projections from the membrane. The cell membrane was smooth, and the cell body shape was fusiform bipolar or unipolar. The dispersed cells were visualized, patched with a standard glass pipette (1.5 mm OD/0.84 mm ID, World Precision Instruments, Sarasota, FL) that had been pulled to a 10 μm tip and then harvested with gentle suction using the XenoWorks microinjector system (Sutter Instruments, Navato, CA). This microinjector system allows harvesting of cells with negligible uptake of perfusion fluid into the pipette. The contents of the pipette were expelled into a siliconized 0.5 ml tube containing a solution of 1X Invitrogen Superscript III Buffer, 15U of RNasin (Promega), 10 mM of dithiothreitol (DTT) and diethylpyrocarbonate (DEPC)-treated water in a total of 5 μl for single cells and

8 μl for pooled cells. Cells were harvested as single cells, or as pools of 5 or 10 individual cells. In each case, the tube containing the harvested cells was kept on a chilled (∼1 °C) metal block during the harvesting procedure (<10 min for pools of 5 cells and <20 min for pools of 10 cells) and then immediately frozen on dry ice. Each harvested cell and pool of cells were reverse transcribed by first adding dNTPs (0.5 mM, Promega) random primers (100 ng/per tube, Promega) and anchored oligo(dT)20 primer (400 ng/tube, Invitrogen) to each tube, incubated in a thermocycler at 65 °C for 5 min, and then cooled on ice for 5 min. Next, Superscript III reverse-transcriptase (100 U/per tube, Invitrogen), RNAsin (15 U), DTT (6 mM) and DEPC-treated water were added to a final 20 μl volume (25 μl for pooled cells). The reverse transcription (RT) reaction was as follows: 25 °C for 5 min, 50 °C for 60 min, 70 °C for 15 min and 4 °C for 5 min. Samples were stored at −20 °C. In addition, harvested aCSF in the vicinity of the dispersed cells also underwent RT and was used as a control. Cells and tissue RNA used as negative controls were processed as described above but without reverse transcriptase (−RT). Each cell, or pool of cells, was then evaluated using PCR or real-time PCR, respectively.

**Primer design and development**

Primer pairs for single cell PCR (scPCR) and quantitative real-time PCR (qPCR) were developed using the mRNA sequence of the respective genes from the National Center for Biotechnology Information (see Table 1). Primers were designed using the Clone Manager software (Sci Ed Software, Cary, NC), and each primer pair crossed intron/exon boundaries to distinguish cDNA amplification products from genomic DNA amplification. In order to measure ion channels and receptor mRNA expression in GnRH neurons using PCR, we designed the most efficient primers possible that were further optimized by adjusting the reaction temperature and magnesium concentrations. For real-time PCR analysis, the

amplification efficiency and melting curve were determined for each pair (Table 1). Only primers that exhibited 95–100% efficiency and a single product melting curve were used for the real-time PCR quantification. Most primers could be used for both single cell and real-time PCR analyses, whereas for others (CaV2.2, GPR54 and GnRH) we designed different primer pairs for the two different determinations (Table 1).

**Single cell PCR**

Single cell PCR (sc-PCR) was performed using 2–3 μl of cDNA template from each RT reaction in a 30 μl PCR mix. Forty to fifty cycles of amplification were performed using a Bio-Rad C1000 Thermal Cycler (Bio-Rad, Hercules, CA) according to established protocols (Qiu et al., 2011 and Zhang et al., 2009). PCR products were visualized with ethidium bromide on a 2% agarose gel. The PCR product in single cells for each primer pair was sequenced and confirmed to be identical to each respective mRNA sequence.

**Quantitative real-time PCR**

Quantitative real-time PCR (qPCR) was performed on an Applied Biosystems (ABI) 7500 Fast Real-time PCR System using the Power SybrGreen mastermix method according to established protocols (Zhang et al., 2009). In all cases, real-time PCR assays were tested to determine and compare the efficiencies of the target and control gene amplifications. Serially diluted cDNAs (1:50–1:12,800 for most primers; 1:1–1:12,800 for GnRH) from mouse POA, assayed in triplicate, were used to construct standard curves and the efficiency was calculated as follows: $E = 10(-1/m) - 1$, where m is slope (Livak and Schmittgen, 2001 and Pfaffl, 2001). Amplification efficiencies are listed in Table 1. The ABI sequence detection software system (version 1.3) was used to generate the standard curves. The comparative $\Delta\Delta$CT method was used to calculate the individual values for

each sample as described previously (Zhang et al., 2009). Briefly, cDNA samples from GnRH pools were run in duplicates and the mean $\Delta$CT of the oil-treated pool values was used as a calibrator when comparing the mRNA quantities to the E2-treated samples. The relative linear quantity of the target gene was calculated using the formula $2-\Delta\Delta$CT (Livak and Schmittgen, 2001). Therefore, the data were expressed as an n-fold change in gene expression normalized to a reference gene ($\beta$-actin) and relative to the oil-control values. The comparative $\Delta\Delta$CT method was also used in Experiment 2b to compare mRNA quantities between a single cell, and pools of cells. Here the mean $\Delta$CT of all the samples was used as calibrator and the relative quantity was calculated using the $2-\Delta\Delta$CT formula. When comparing mRNA expression levels between different genes, the mean $\Delta$CT of one of the gene values was used as a calibrator to which the other genes were compared. In all instances, the PCR efficiencies were similar between the different primer pairs (see Table 1). The data are reported as relative mRNA expression. Data were expressed as mean ± SEM and differences in gene expression were analyzed by two-tailed Student's t-test or one-way ANOVA followed by Newman–Keuls multiple comparison post hoc test.

**Radioimmunoassay for luteinizing hormone**

Mouse LH radioimmunoassay (RIA) was performed by the Endocrine Technology and Support Lab, Oregon National Primate Research Center (Oregon Health and Science University, Beaverton, OR) using a traditional double-antibody RIA procedure similar to that described previously (Pau et al., 1986). The mouse LH RIA kit was purchased from Dr. Parlow (NHPP, Harbor-UCLA Medical Center, Los Angeles) that includes rat LH (NIDDK-rLH-I-8, a.k.a. AFP-12066B; 100 mg) for iodination, mouse LH (AFP-5306A; 2.5 mg) for standards and rabbit anti-rat LH serum (NIDDK-anti-rLH-S-10) for use at a final dilution of 1:750,000. The detection limit of the assay was 0.2 ng/ml. A mouse serum

pool (ET-mouse # 4) was used in triplicate in each assay as quality control. The inter-assay variation was 14.7% and the intra-assay variation was 3.8%.

## C.4 Results

**E2-induced LH release**

OVX animals were injected with a low priming dose followed by a LH surge-inducing dose of E2. With this procedure, we consistently induced a LH surge in CBB6 GnRH mice (Fig. 1). The timing of the surge was similar to that reported previously in mice kept under 12 h light and 12 h dark conditions (Gee et al., 1984 and Wintermantel et al., 2006). All animals had low serum LH levels in the morning at ZT 4–5 (n = 6) following E2-treatment. The mean serum LH levels were slightly, but significantly elevated in animals euthanized at ZT11 ($p < 0.05$) (n = 8) and highly elevated in animals euthanized at ZT12 ($p < 0.001$; n = 14) or ZT 13 ($p < 0.01$; n = 10) (Fig. 1). LH levels were also measured in OVX oil-treated animals and as expected found to be elevated during the morning (ZT 4–5) and evening (ZT11–13) (Data not shown). The uterine weights (fluid expelled and fat trimmed) in OVX E2-treated mice were 104.5 ± 4.1 mg at ZT 4–5 (n = 6) and 112.7 ± 5.3 mg (n = 8) at ZT 11, 108.0 ± 3.1 mg (n = 14) at ZT 12, 111.6 ± 4.5 mg (n = 10) at ZT 13. As expected, OVX oil-treated mice had significantly lower uterine weights of 22.8 ± 1.2 mg (n = 10) and 22.1 ± 0.9 mg (n = 10) at ZT 4–5 and ZT 11–13, respectively.

**Linear regression analysis of mRNA expression in GnRH neurons**

In initial experiments, we analyzed the quantitative mRNA expression of highly expressed genes in individual neurons (n = 6 cells from 2 animals) and pools of 2 neurons (n = 6 pools from 2 animals), 4 neurons (n = 6 pools from 2 animals) and 8 GnRH neurons

(n = 5–6 pools from 2 animals). For analysis of GnRH, the cell content was diluted 1:10 to accommodate for the high expression of GnRH mRNA. Linear regression analysis revealed that increasing the number of cells resulted in a linear decrease in the CT values (r2 = 0.99 for both GnRH and GPR54; Fig. 2A and B), which resulted in a near linear increase in mRNA expression (Fig. 2C and D). We also measured the mRNA expression of small conductance calcium-activated potassium (SK3) channels in pools of 5 GnRH neurons (13 pools from 5 animals) and 10 GnRH neurons (10 pools from 5 animals). (SK3 could not be quantified by real-time PCR in single cells or in pools of 2–4 individual GnRH neurons). The analysis revealed a slope of −3.32 (Fig. 2B), and a doubling of SK3 mRNA levels in pools of 10 as compared to 5 neurons (Fig. 2B and E).

**mRNA expression in GnRH neurons**

These studies were designed to explore whether ion channels (hyperpolarization-activated cyclic nucleotide-gated (HCN), high voltage-activated (HVA) calcium, SK and canonical transient receptor potential (TRPC) channels) important for burst firing activity (Kelly and Rønnekleiv, 1994 and Lee et al., 2010) are expressed in mouse GnRH neurons, and which subtypes are the most prevalent. We also explored the expression of GPR54, which is required for activation of GnRH neurons by kisspeptin at the time of the LH surge (Clarkson et al., 2008). For these experiments we used intact female mice, killed at ZT 4–5 during the proestrus/estrus phase of their cycle with a mean uterine weight of 97.6 ± 8.2 mg (n = 6), confirming that E2 levels were high. For a more quantitative analysis of mRNA expression in GnRH neurons, we used real-time quantitative PCR (qPCR) in pools of GnRH neurons.

**HCN channel subtypes**

It has been reported previously in immature mouse GnRH neurons that HCN3 is the primary transcript, HCN4 was barely detectable, and HCN1 and HCN2 transcripts were not expressed (Constantin and Wray, 2008). Our analysis of 48–72 cells from four animals revealed that HCN1 and HCN2 transcripts were the most prevalent and were about equally expressed in adult mouse GnRH neurons, 61 ± 6% and 60 ± 7%, respectively (Fig 2A,B). Moreover, either HCN1 and/or HCN2 subtypes were expressed in at least 90% of the cells. HCN3 mRNA was detected in 34 ± 11% of GnRH neurons and HCN4 in 24 ± 6% (Fig. 3A, B).

For a more quantitative analysis of HCN channel expression in GnRH neurons, we used real-time quantitative PCR (qPCR) in pools of 5 or 10 cells. HCN1, HCN2 and HCN3 mRNAs were measured in 5-cell pools (3 pools from each of 4 animals), whereas HCN4 mRNA was not detected in 5-cell pools and borderline or below detectability in 10 cell pools (2 pools from each of 2 animals) by real-time PCR in GnRH neurons (Fig. 2C-E). The quantification revealed that HCN1 $\geqslant$ HCN2 > HCN3 $\gg$ HCN4 (Fig. 3E; one-way-ANOVA; a–a, $p < 0.005$, b–b, $p < 0.05$; $n = 4$).

**HVA calcium channel subtypes**

There are four L-type channel isoforms (CaV1.1, 1.2, 1.3, 1.4), but only CaV1.2 and CaV1.3 have been reported in rat GnRH neurons (Tanaka et al., 2010). We confirmed that CaV1.2 and CaV1.3, but not CaV1.4, were expressed in mouse GnRH neurons. Since CaV1.1 is expressed primarily in muscle (Catterall et al., 2003), we did not investigate this L-type subunit and instead focused our analysis on CaV1.2 and 1.3 L-type calcium channel isoforms. Based on the analysis of 48 cells from 4 animals, CaV1.2 was expressed in 22 ± 6%, and CaV1.3 was expressed in 60 ± 7% of GnRH neurons. P/Q-type channels, CaV2.1,

and N-type channels, CaV2.2, were expressed in 44 ± 9% and 52 ± 6% of GnRH neurons, respectively, while the R-type channel, CaV2.3, was detected in 65 ± 5% of GnRH neurons (Fig. 4A and B).

For quantification of HVA channel subtypes expression in GnRH neurons, the CaV1.3 (L), CaV2.1 (P/Q), and CaV2.3 (R) subtypes were quantified by qPCR in 5-cell pools (3 pools from each of 5 animals) and CaV1.2 and CaV2.2 in 10-cell pools (2 pools from each of 3–5 animals). The relative mRNA expression of CaV2.3 was significantly higher than the expression of the other HVA channel subtypes (Fig. 4C–E; $p < 0.001$). In addition, CaV1.3 mRNA expression was significantly higher than the expression of CaV1.2, 2.1 and 2.2 subtypes (Fig. 4C–E; $p < 0.01$). There were no significant differences between CaV1.2, 2.1 and 2.2 mRNA expressions.

**TRPC channel subtypes**

Using sc-PCR, we had determined previously that most TRPC channel subtypes are expressed in GnRH neurons (Zhang et al., 2008). However, based on the electrophysiological and pharmacological analysis, we had evidence that the TRPC1,4,5 channel subfamily was the primary effector of kisspeptin's actions (Zhang et al., 2008). Therefore, we focused our quantitative analysis on TRPC1, TRPC4 and TRPC5 channel subtypes in GnRH neurons. The qPCR analysis revealed that TRPC4 was the most highly expressed channel subtype in GnRH neurons compared to TRPC1 and TRPC5 mRNAs (Fig. 5: $p < 0.001$, $n = 3–5$). The mRNA expression of TRPC5 (10-cell pools) was quite low in GnRH neurons and was only detected in 3 of 5 animals.

**SK channel subtypes**

We had previously determined that SK3 is expressed in guinea pig GnRH neurons (Bosch

et al., 2002). In addition, Kato et al. (2006) reported that SK1, 2 and 3 are all expressed in rat GnRH neurons. However, based on analysis of 48 cells from 4 animals, we determined that SK3 is the major subtype in mouse GnRH neurons and that this SK subtype was found in 71 ± 7% of the cells (Fig. 6A, B). In contrast, SK 2 was found in only one cell in each animal (8%) and SK1 was not expressed in mouse GnRH single neurons.

### GnRH and kisspeptin receptor, GPR54

Based on in situ hybridization analysis in mice, approximately 90% of GnRH neurons express the GPR54 receptor (Han et al., 2005). Currently, we analyzed 48 GnRH neurons from 4 female mice using sc-PCR. This analysis revealed that GPR54 mRNA was expressed in 97% of GnRH neurons; only one cell in one of the animals did not express GPR54 mRNA (Fig. 7A and B). Based on qPCR analysis, GnRH mRNA was highly expressed in GnRH neurons as revealed by the very low CT value (see Fig. 2). GPR54 mRNA was also robustly expressed (see Fig. 2), but still more than 150-fold lower than GnRH mRNA expression (Fig. 7C).

## qPCR analysis of channel mRNA expression in GnRH neurons and modulation by E2 during negative and positive feedback

These experiments were done in OVX oil-treated control and E2-treated females analyzed during the morning (ZT 4–5 negative feedback) and/or during the evening (ZT 11–12 positive feedback. We used real-time PCR (qPCR) to quantify the relative expression of ion channel subtypes in GnRH neurons in E2-treated as compared to oil-treated animals using the primers outlined in Table 1. The quantifications were done in pools of 5 neurons except as noted in the text.

### HCN channel subtypes

HCN1, HCN2 and HCN3 mRNAs were quantified in cells obtained at ZT4–5, and HCN1 and HCN2 mRNAs were also quantified at ZT11–12 in oil control and E2-treated females. Based on this analysis, HCN1 mRNA expression was significantly increased in GnRH neurons from E2-treated as compared to oil-treated animals at both time points (Fig. 8; $p < 0.05$, n = 5–7). In contrast, there was no difference in HCN2 or HCN3 mRNA expression between oil- and E2-treated females (Fig. 8; n = 3–5). Due to the low mRNA expression of HCN4, we were not able to quantify differences between the two groups of animals, even in 10-cell pools.

### HVA calcium channel subtypes

Based on previous electrophysiology findings, HVA L-type and N-type calcium currents are regulated by E2 in GnRH neurons (Sun et al., 2010). We were, therefore, interested in exploring whether the mRNA expression of HVA channel subtypes was also regulated by E2 in GnRH neurons. CaV1.2 (L-type, 10-cell pools), CaV1.3 (another L-type), CaV2.1 (P/Q-type) and CaV2.3 (R-type) mRNAs were all quantified at ZT4–5 in oil- and E2-treated females, but only CaV1.3 and CaV2.3 mRNAs were increased with E2-treatment (Fig. 9A; $*p < 0.05$, n = 5). In contrast, CaV1.2 and CaV2.1 mRNA expression was not altered by E2-treatment and were not further analyzed. CaV1.3 and CaV2.3 mRNAs were also quantified at ZT11–12 and found to be increased in E2-treated as compared to oil-treated females during the evening (Fig. 9B; $*p < 0.05$, n = 5–6). CaV2.2 mRNA (N-type; 10-cell pools) was only evaluated during the evening and found to be significantly increased in GnRH neurons from E2-treated as compared to oil-treated animals (Fig. 9B; $**p < 0.01$, n = 5).

### TRPC channel subtypes

qPCR analysis of TRPC 1 and TRPC4 channel subtypes in GnRH neurons at ZT4–5 in oil- and E2-treated OVX female mice revealed that the E2 treatment increased TRPC4 mRNA levels (Fig. 10A; *$p < 0.05$, $n = 5$). In contrast, TRPC1 mRNA was not altered with E2 treatment and was not further analyzed (Fig. 10A). The mRNA expression of TRPC5 was quite low in GnRH neurons, even in 10-cell pools (see Fig. 4). Therefore, it was not possible to evaluate the effects of E2 on TRPC5 mRNA expression. Similar to the morning data, TRPC4 mRNA expression was increased with E2 treatment relative to oil-treatment at ZT 11–12 ($p < 0.05$; $n = 7$) (Fig. 10B).

### SK channel subtypes

Since SK1 was not expressed in mouse GnRH neurons and SK2 was expressed in <8% of the cells, we focused our analysis on the SK3 subtype. The E2-treatment decreased SK3 mRNA at ZT4–5 ($p < 0.05$; $n = 5$) and further decreased the expression of this channel subtype at ZT 11–12 ($p < 0.01$; $n = 5$) (Fig. 11).

## qPCR analysis of GnRH and GPR54 mRNA expression in GnRH neurons and modulation by E2 during negative and positive feedback

Prior to ovulation, it has been established that a surge of GnRH is released into the portal vasculature, which prompts a similar surge of LH (Caraty et al., 1989, Chappell and Levine, 2000, Levine and Ramirez, 1982 and Pau et al., 1993). This bolus release of GnRH occurs during positive E2 feedback, but data describing changes in GnRH mRNA levels have been equivocal (Gore and Roberts, 1997 and Sagrillo et al., 1996). The lack of an effect of E2 on GnRH mRNA was confirmed in the current study. Thus, an E2 regime that induces a LH surge had no significant effect on GnRH mRNA concentration (relative expression) at

ZT4–5 in comparison to mRNA expression at ZT11–12 on the day of induced proestrus (E2-treated morning, relative expression (RE) 1.02 ± 0.07; E2-treated evening, RE 0.84 ± 0.08 $p > 0.05$; $n = 5$). In addition, the GnRH mRNA expression in E2-treated as compared to oil-treated animals was not different at any time-point (oil morning, RE 1.03 ± 0.11, E2 morning, RE 1.05 ± 0.07; oil evening, RE 1.02 ± 0.06, E2 evening, RE 0.98 ± 0.09, $p > 0.05$, $n = 5$ in each group).

Similarly, the mRNA expression of GPR54 was analyzed at ZT4–5 (morning) and ZT11–12 (evening) in oil- and E2-treated animals. The analysis showed that the relative mRNA expression of GPR54 in GnRH neurons was not altered with E2-treatment at either time-point (oil morning, RE 1.02 ± 0.05, E2 morning, RE 0.91 ± 0.14; oil evening, RE 1.04 ± 0.08, E2 evening, RE 0.96 ± 0.12, $p > 0.05$, $n = 5$ in each group).

## C.5 Discussion

Presently we evaluated the mRNA expression and dominant subunits of numerous ion channels important for burst firing and transmitter (neuropeptide) release, including HCN, HVA, TRPC and SK channels, as well as their expression during E2 negative and positive feedback regulation of LH secretion. The salient findings were the following: (1) both HCN1 and HCN2 channel mRNAs were highly expressed in mouse GnRH neurons, but only the mRNA expression of HCN1 was regulated by E2. (2) The majority of HVA channel subtypes were expressed in GnRH neurons, and CaV1.3 (L), CaV2.2 (N) and CaV2.3 (R) transcripts were increased by E2 treatment. (3) TRPC4 mRNA in comparison to TRPC1 and TRPC5 was the most highly expressed in mouse GnRH neurons, and TRPC4 mRNA was increased in E2-treated mice. (4) Of the SK channel subtypes, only SK3 mRNA exhibited significant expression in GnRH neurons, and this channel subtype was decreased

in E2-treated animals. The increased expression of ion channels important for maintaining burst firing activity and decreased expression of channels attenuating this activity would help augment robust firing critical for the GnRH super secretion responsible for the LH surge.

For induction of the LH surge by ovarian steroids in mice, different models have been developed in which the animals are given E2-implants with and without surge-inducing treatment of E2 (Bronson and Vom Saal, 1979, Christian et al., 2005 and Gee et al., 1984). We have developed a two-step E2 injection procedure in which we used a priming dose followed by a surge-inducing dose of E2 in OVX mice. With this procedure we were consistently able to induce a LH surge in the CBB6 GFP-GnRH mice (Fig. 1). With a reliable model of E2-induced LH release in the evening (positive feedback) as well as inhibition of LH in the morning by E2 (negative feedback), we used this model to explore the corresponding changes in GnRH and GPR54 mRNAs as well as in ion channel expression in GnRH neurons.

In these studies we acutely dispersed, collected and analyzed individual GnRH neurons as well as pools of many neurons in order to assess the distribution and quantitative expression of transcripts. Initially, we found that the cellular mRNA expression of ion channels could not be precisely quantified in individual neurons or in pools of 2–4 neurons for most transcripts. However, pools of 5–10 neurons were sufficient for quantification of ion channel mRNA expression in GnRH neurons (see Fig. 2). Importantly, we have documented that with increasing number of cells, there is a linear increase in mRNA levels, which would suggest that cellular RNA is preserved during the pooling procedure.

According to most studies, GPR54 mRNA and the response to kisspeptin are present in the majority of GnRH neurons (Han et al., 2005, Irwig et al., 2004 and Zhang et al.,

2008), which was also confirmed in the current study. In addition, we found that the cellular mRNA expression of GPR54, although robust, was not altered by E2 treatment. Our findings may indicate that the cellular mRNA expression of GPR54 is not regulated by E2 in native GnRH neurons, which is different from findings reported in GT1–7 GnRH neuronal cell lines (Tonsfeldt et al., 2011).

It is well known that a bolus of GnRH is released into the portal vessels, which induces a surge of LH release from the pituitary (Caraty et al., 1989, Chappell and Levine, 2000, Levine and Ramirez, 1982 and Pau et al., 1993). In contrast, reported changes in GnRH transcripts during different physiological conditions including the afternoon of proestrus and lactation, have been more variable (Gore and Roberts, 1997 and Sagrillo et al., 1996). The previously reported lack of effect of E2 on GnRH mRNA levels (Kelly et al., 1989 and Marks et al., 1993) was confirmed in the current study using a sensitive qPCR assay. There was a tendency for a decrease in mRNA expression immediately prior to the surge, possibly due to increased translation to GnRH protein. However, overall there was no significant change in GnRH mRNA levels. These findings may indicate that the cellular expression of GnRH mRNA is not regulated by E2. Instead, E2 controls the expression and function of ion channels important for GnRH neuronal excitability and GnRH release (Chu et al., 2012, Kelly and Wagner, 2002, Rønnekleiv et al., 2011 and Zhang et al., 2009).

Numerous studies have documented the importance of HCN channels for induction of neuronal burst firing activities, and the h (pacemaker) current is expressed in GnRH neurons (Arroyo et al., 2006, Chu et al., 2010, Erickson et al., 1993a, Lüthi and McCormick, 1998 and Zhang et al., 2007). Our results that the HCN1 and also HCN2 subtypes were highly expressed in GnRH neurons in adult female mice are consistent with the electrophysiological data in adult males (Chu et al., 2010). Therefore, in contrast to results in

immature GnRH neurons in which HCN3 is the main HCN isoform (Constantin and Wray, 2008), in adult mice HCN1 and HCN2 are the main subtypes. Of the 4 different isoforms of HCN channels, HCN1 has the fastest kinetics and HCN4 the slowest. In addition, HCN2 and 4 are sensitive to cAMP, whereas HCN1 channels are less sensitive and HCN3 channels are insensitive to cyclic nucleotides (Biel et al., 2009). It is, therefore, interesting that the mRNA expression of HCN1 but not HCN2 was increased in E2-treated females (current findings), suggesting that HCN 1, but not HCN2, channel synthesis is regulated by E2. The effects of E2 on the h-current (Ih) have not been measured in females. But based on the increased HCN1 mRNA expression by E2, we would predict an E2-induced increase in Ih amplitude. A different regulation occurs in male GnRH neurons, where the Ih is increased in castrated as compared to intact animals, and E2-treatment reverses the effects of castration (Chu et al., 2010). The different steroid effects in female versus male mouse GnRH neurons could be due to a sex difference since males do not exhibit a GnRH or LH surge, and E2 is primarily inhibitory to male GnRH neurons (Pielecka and Moenter, 2006).

Consistent with published data in rat, we found that most of the HVA channel subtypes are expressed in mouse GnRH neurons with the R-type channel expression being the most prominent (Kato et al., 2003 and Tanaka et al., 2010). Moreover CaV1.3 (L), CaV2.2 (N) and CaV2.3 (R) mRNAs, were significantly increased in E2-treated animals. Interestingly, the HVA L- and N-type peak currents in GnRH neurons exhibit diurnal variation in E2-treated, but not in oil-treated mice, with reduced current amplitude in the morning and increased current amplitude in the evening (Sun et al., 2010). Although, we did not directly compare HVA channel mRNA expression in E2-treated animals during the morning and evening, we found no change in oil-treated animals. Therefore, our data that L- and R-type

channel mRNAs expression was increased with E2-treatment relative to oil-treatment irrespective of time of day, would indicate that the augmented HVA channel mRNA expression is dependent on E2 levels and not time of day in our animal model. Our previous results comparing T-type ion channel mRNA expression and current density in GnRH neurons and KCNQ channel mRNAs to M-current in NPY neurons, have found a close correlation between alterations in mRNA expression and function (Roepke et al., 2011 and Zhang et al., 2009). Numerous studies have illustrated that calcium entry through voltage-gated channels contributes to neuronal excitability and is important for GnRH neuronal excitability and GnRH release (Constantin et al., 2011, Constantin et al., 2010, Iremonger and Herbison, 2012, Kroll et al., 2011, Krsmanovic et al., 1992, Lee et al., 2010, Sun et al., 2010, Zhang et al., 2009 and Zhang and Spergel, 2012). However, more studies are needed to explore the correlation between HVA channel expression and HVA currents in GnRH neurons under different experimental conditions.

Our quantitative analysis of TRPC channel subtypes in GnRH neurons revealed that TRPC 1 and 4 mRNAs were the most highly expressed in mouse GnRH neurons, whereas TRPC 5 transcripts were expressed in significantly lower quantities. Interestingly, arcuate POMC cells express high levels of TRPC5 but low levels of TRPC4 transcripts (Qiu et al., 2010), suggesting a neuron-specific expression of TRPC channel subtypes. It is well known that the current–voltage relationship and mechanism of regulation of TRPC channels are dependent on the channel subunit composition (Clapham, 2003). The high expression of TRPC4 may help explain why kisspeptin activation of TRPC channels, underlying its robust depolarization, depends on phosphatidylinositol 4,5-biphosphate (PIP2) depletion and cSrc tyrosine kinase activation in GnRH neurons (Zhang et al., submitted

for publication; Odell et al., 2012 and Otsuguro et al., 2008). Moreover, the mRNA expression of TRPC4 channels was increased in E2-treated as compared to oil-treated mice. Interestingly, kisspeptin actions in GnRH neurons do not appear to be influenced by the estrous stage of the animals or E2-treatment (Pielecka-Fortuna et al., 2008 and Zhang et al., 2008). Rather, kisspeptin increases GABA-A and glutamate inputs to GnRH neurons in an E2-dependent manner (Pielecka-Fortuna and Moenter, 2010). However, to fully elucidate a potential E2 modulation of kisspeptin activation of TRPC current in GnRH neurons a dose response analysis is necessary, which has not yet been performed. Therefore, additional experiments are necessary to explore the functional significance of E2 modulation of TRPC4 mRNA expression in GnRH neurons.

Neuronal excitability and frequency of firing are also sculpted by the AHP that follows an action potential, and SK channels underlie a component of the medium AHP (mAHP) K+ currents in CA1 pyramidal cells and other neurons (Bond et al., 2004). SK channel subunits are expressed in GnRH neurons (Bosch et al., 2002 and Kato et al., 2006), and SK channel activation exerts a powerful influence on firing properties of GnRH neurons (Kato et al., 2006, Lee et al., 2010 and Liu and Herbison, 2008). Currently we have found that SK3 is the main subtype in GnRH neurons, and its mRNA expression is reduced in E2 treated mice. The mAHP current is inhibited by bath applied E2 in GnRH neurons (Chu et al., 2009). Therefore, these findings would indicate that E2 reduces the synthesis of SK channels and the expression of the AHP current in GnRH neurons. Since the apamine-sensitive AHP (SK) current regulates both intraburst and interburst neuronal firing (Lee et al., 2010), the E2-induced reduction of expression and current amplitude would play a significant role in modulating GnRH neuronal excitability and firing pattern.

For most, if not all, of the channel subtypes regulated by E2, the mRNA levels were increased (or decreased) in the morning during E2-inhibition of plasma LH levels (negative feedback?) and remained unchanged during the evening similar to that reported previously for T-type CaV3.3 calcium channels (Zhang et al., 2009). These findings would indicate that prolonged (>24 h) of surge levels of E2 lead to alteration in mRNA expression of a number of ion channel subunits in GnRH neurons already in the morning of induced proestrus. We hypothesize that surge levels of E2 alters the number of channels and thereby alters the excitability of GnRH neurons as we have shown for T-type calcium channels in GnRH neurons irrespective of time of day (Zhang et al., 2009). The precise mechanisms by which E2 maintains inhibition of GnRH neuronal activity and secretion until the afternoon (evening) of proestrus is currently not well understood. However, an E2-dependent circadian signal to GnRH neurons as well presynaptic neurons is clearly involved (Christian et al., 2005, Christian and Moenter, 2007 and Robertson et al., 2009).

In summary, our working hypothesis is that rising levels of E2 increase mRNA expression of multiple ion channels in GnRH neurons, including HCN channels, T-type and HVA calcium channels and TRPC channels, which would increase the overall excitability of GnRH neurons (Zhang et al., 2009, and current findings). At a hyperpolarized membrane potential due to the ATP-sensitive potassium (K-ATP) and G protein-activated inwardly rectifying K+ (GIRK) channel activity (Lagrange et al., 1995, Zhang et al., 2010 and Zhang et al., 2007), the hyperpolarization-activated pacemaker (h) current is triggered that drives the membrane potential towards a more depolarized level. This depolarization activates T-type channels, which were deinactivated during the preceding hyperpolarization. Rising E2 levels also increase kisspeptin excitatory drive to GnRH neurons, which inhibits K+ channel activity and activates TRPC channel inputs to depolarize GnRH (Liu

et al., 2008, Pielecka-Fortuna et al., 2008 and Zhang et al., 2008). E2 also decreases the expression (current findings) and function of SK channels, which underlie the medium afterhyperpolarization in GnRH neurons (Chu et al., 2009). Collectively, these actions of surging E2 levels in conjunction with the neural clock inputs, lead to an alteration in ion channel mRNA expression and GnRH neuronal burst firing sufficient for GnRH release, the LH surge and ovulation.

| Name | Accession no. | Sense primer (bp) | Antisense primer (bp) | Product length | Slope | Efficiency (%) | $r^2$ |
|---|---|---|---|---|---|---|---|
| HCN1 | NM_010408 | 1527-1546 | 1662-1641 | 136 | -3.25 | 100 | 0.96 |
| HCN2 | NM_008226 | 1664-1682 | 1763-1781 | 97 | -3.25 | 100 | 0.97 |
| HCN3 | NM_008227 | 1664–168 | 1781–1763 | 118 | -3.21 | 100 | 0.94 |
| HCN4 | NM_001081192 | 1929–1950 | 2051–2030 | 123 | -3.17 | 100 | 0.94 |
| TRPC1 | NM_011643 | 1387–1503 | 1503–1483 | 117 | -3.26 | 100 | 0.93 |
| TRPC4 | NM_016984 | 1841–1860 | 1956–1937 | 116 | -3.03 | 100 | 0.94 |
| TRPC5 | NM_009428 | 734–753 | 832–851 | 117 | -3.16 | 100 | 0.95 |
| SK1 | NM_032397 | 1035–1056 | 1194–1215 | 181 | | | |
| SK2 | NM_080465 | 1310–1327 | 1414–1433 | 124 | -3.16 | 100 | 0.94 |
| SK3 | NM_080466 | 2182–2203 | 2292–2273 | 111 | -3.46 | 95 | 0.98 |
| $Ca_v1.2$ | NM_009781 | 1642–1659 | 1750–1767 | 126 | -3.27 | 100 | 0.97 |
| $Ca_v1.3$ | NM_028981 | 775–796 | 890–869 | 116 | -3.15 | 100 | 0.90 |
| $Ca_v2.1$ | NM_007578 | 6035–6054 | 6109–6090 | 75 | -3.34 | 99 | 0.94 |
| $Ca_v2.2^a$ | NM_001042528 | 5134–5154 | 5284–5302 | 169 | | | |
| $Ca_v2.2^b$ | NM_001042528 | 5281–5302 | 5343–5364 | 84 | -3.32 | 100 | 0.99 |
| $Ca_v2.3$ | NM_009782 | 530–459 | 636–617 | 107 | -3.34 | 99 | 0.99 |
| GPR54[a] | NM_053244 | 1900–1917 | 2125–2144 | 245 | | | |
| GPR54[b] | NM_053244 | 1916–1934 | 1988–1968 | 73 | -3.24 | 100 | 0.98 |
| GnRH[a] | NM_008145 | 21–40 | 259–278 | 239 | | | |
| GnRH[b] | NM_008145 | 125–142 | 251–234 | 127 | -3.39 | 97 | 0.97 |
| β-actin | NM_007393 | 849–867 | 911-890 | 63 | -3.30 | 100 | 0.99 |

Table C.1: Primer sequences for PCR
[a]Primers used for single-cell PCR [b]Primers used for qPCR

| Channel | (n) | Morning (ZT 4) | Evening (ZT11) | Significance |
|---|---|---|---|---|
| $Ca_V1.3$ (L-type) | 3 | 1.098 ± 0.043 | 1.244 ± 0.171 | $p = 0.454$ |
| $Ca_V1.3$ (R-type) | 3 | 1.215 ± 0.175 | 1.243 ± 0.383 | $p = 0.951$ |
| TRPC4 | 3 | 1.122 ± 0.116 | 0.898 ± 0.147 | $p = 0.298$ |
| SK3 | 3 | 1.157 ± 0.206 | 1.382 ± 0.097 | $p = 0.378$ |
| HCN1 | 3 | 1.093 ± 0.102 | 1.599 ± 0.275 | $p = 0.160$ |

Table C.2: Ion channel mRNA expression in GnRH neurons from oil-treated animals.

Four pools of 5 cells were harvested from each of 3 animals at each time point. There were no differences in channel expression comparing evening versus morning samples.

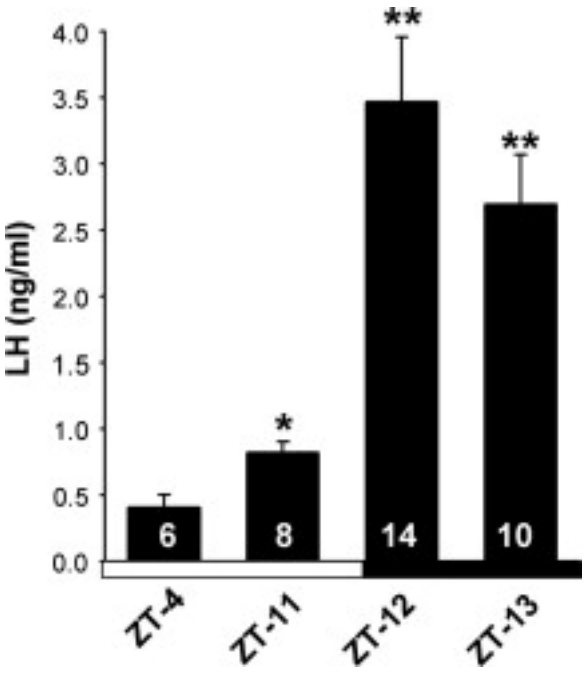


Figure C.1: Serum levels of LH

Mean serum levels of LH in OVX, E2-treated mice housed under 12 h light, 12 h dark lighting condition and killed at one of four time points, ZT4, ZT11, ZT12, ZT13. Lights were turned on at ZT0 and turned off at ZT12. Serum LH levels at ZT11, 12 and 13 were elevated compared to LH levels at ZT4; *$p < 0.05$, **$p < 0.01$, Student's t-test. The number of animals at each time point is indicated.

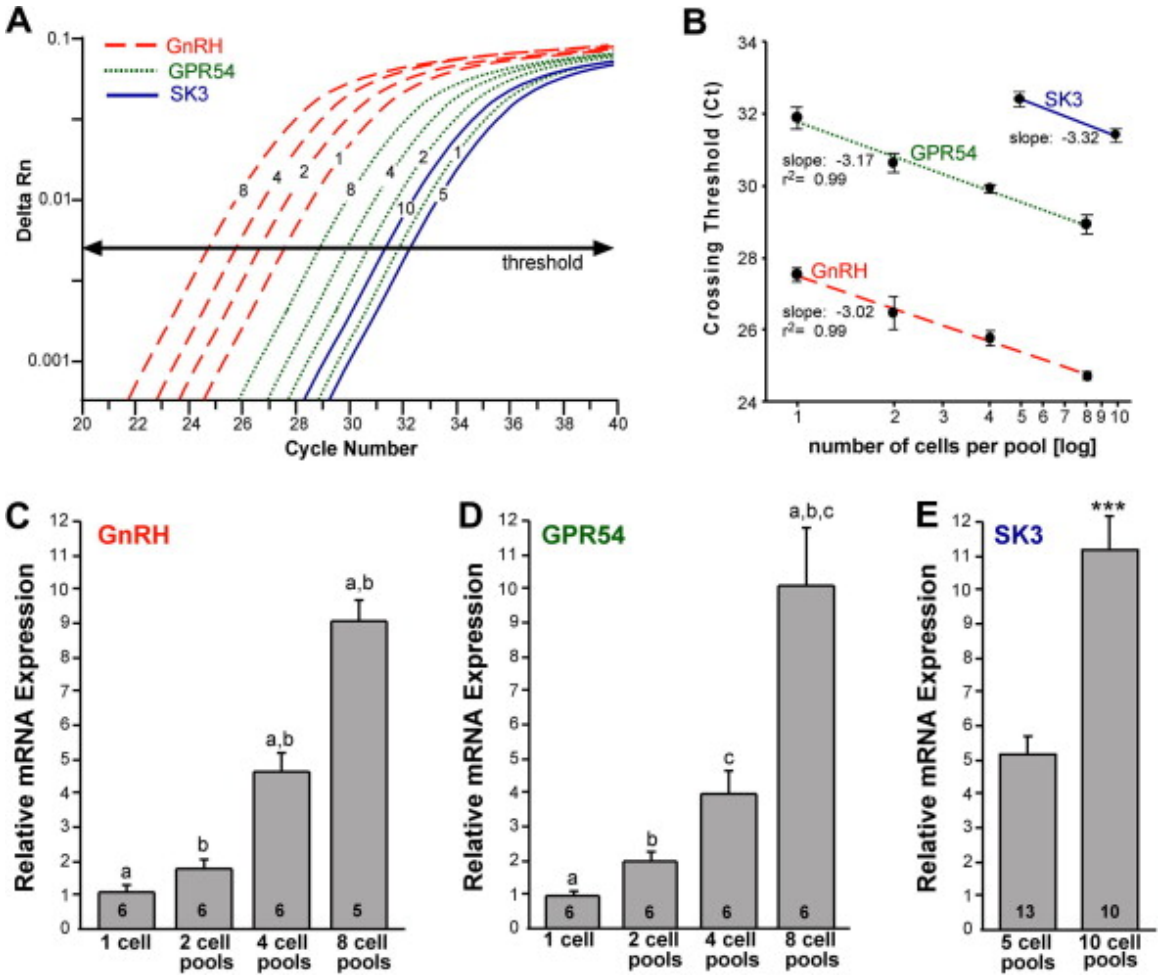


Figure C.2: qPCR amplification for GnRH, GPR54 and SK3 in GnRH neurons

Figure C.2 legend: Amplification of cDNA synthesized from differing amounts of RNA in individual GnRH neurons and pools of 2, 4, and 8 cells (GnRH and GPR54) as well as pools of 5 and 10 cells for SK3. cDNA from GnRH single cells and pools was diluted 1:10 for GnRH qPCR measurements. GPR54 and SK3 were quantified in full strength cDNA. (A) Cycle number was plotted against normalized fluorescence intensity (delta Rn) to visualize the PCR amplification. Cycle threshold (CT; line with arrows) is the point in the amplification at which the sample values were calculated. (B) Linear regression analysis plotting crossing threshold (CT) versus the log scale of number of cells collected in each pool (mean ± SEM;n = number of individual cells or pools of cells, which were 5–6 for GnRH and GPR54, and 10–13 for SK3. GnRH, GPR54 and SK3 produced slope values of −3.02, −3.17, and −3.23 respectively, which corresponds to a doubling between each cycle with high linearity (Pearson's coefficient r2 = 0.99). β-Actin showed a similar linear relationship between individual cells and cell pools (slope −3.00, r2 = 0.98; data not shown). The amplification efficiency for each primer pair is listed in Table 1. These efficiencies allowed us to use the $\Delta\Delta$CT method for quantification. (C) Bar graphs illustrating the quantitative analysis of relative mRNA expression of GnRH in individual GnRH neurons and in pools of 2, 4 and 8 cells (one-way ANOVA; a–a, b–b, $p < 0.001$; n = 6 individual cells and 5–6 pools). (D) Bar graphs illustrating the quantitative analysis of relative mRNA expression of GPR54 in individual GnRH neurons and in pools of 2, 4 and 8 cells (one-way ANOVA; a–a, b–b, c–c, $p < 0.001$; n = 6 individual cells and 6 pools). (E) Bar graphs illustrating the quantitative analysis of relative mRNA expression of SK3 in GnRH neuronal pools containing 5 and 10 cells (Student's t-test; ***$p < 0.001$, n = 10–13 pools).

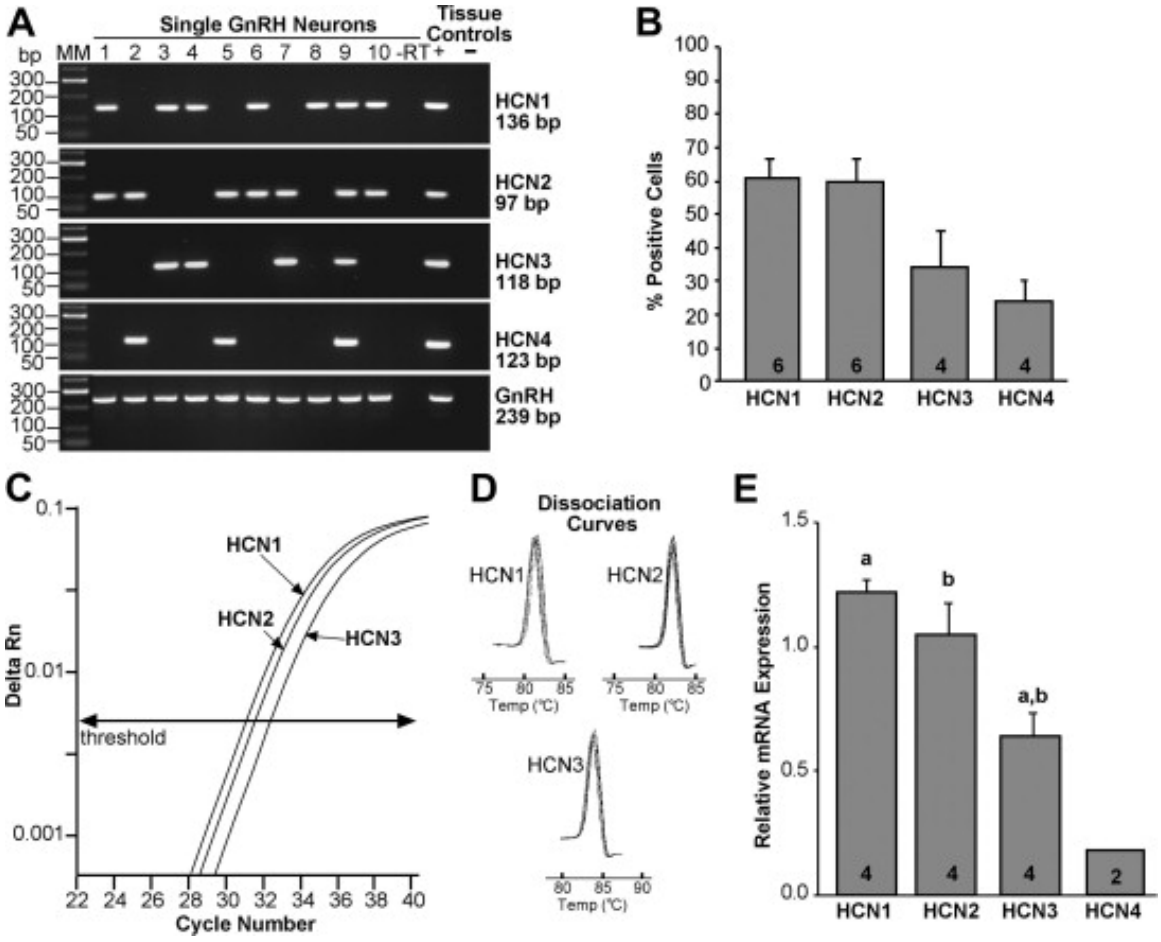


Figure C.3: Expression of HCN channels in GnRH neurons from intact proestrus/estrus EGFP-GnRH mice

Figure C.3 legend: (A) Representative gels illustrating the mRNA expression of HCN channel subtypes 1–4. The expected sizes for the PCR products are as follows: for HCN1, 136 bp; for HCN2, 97 bp; for HCN3, 118 bp; for HCN4, 123 bp; and for GnRH, 239 bp. As a negative control, a cell reacted without reverse transcriptase (−RT) did not express any of the transcripts. POA tissue RNA was also included as positive control (+, with RT) and negative control (−, without RT). MM, molecular markers. (B) Summary bar graphs of the percentage expression of HCN1, HCN2, HCN3, and HCN4. 12 cells/animal from 4 to 6 animals were analyzed by sc-PCR, and the mean number of neurons expressing HCN channel subtypes from each animal was determined. Bar graphs represent the mean ± SEM of the percentage of GnRH neurons expressing each HCN subtype per animal. (C) Quantitative real-time PCR assay with amplification curves for HCN1, HCN2 and HCN3 subunits. Cycle number was plotted against the normalized fluorescence intensity (delta Rn) to visualize the PCR amplification. The cycle threshold (CT, arrow) is the point in the amplification at which the sample values were calculated. The amplification efficiencies for each primer pair is listed in Table 1. These efficiencies allowed us to use the $\Delta\Delta$CT method for quantification. (D) The melting curves depict single-product melting at 82, 83 and 84 °C for HCN1, HCN2 and HCN3, respectively, illustrating that only one product was formed for each transcript in GnRH 5-cell pools. (E) Bar-graphs illustrating the relative mRNA expression of HCN1, HCN2, HCN3 and HCN4. a–a, $p < 0.01$, b–b, $p < 0.05$; Student's t-test. HCN4 was measured in 10-cell pools ($n = 2$) and was often below the level of detectability and was, therefore, not included in the statistical analysis. The number of animals is indicated.

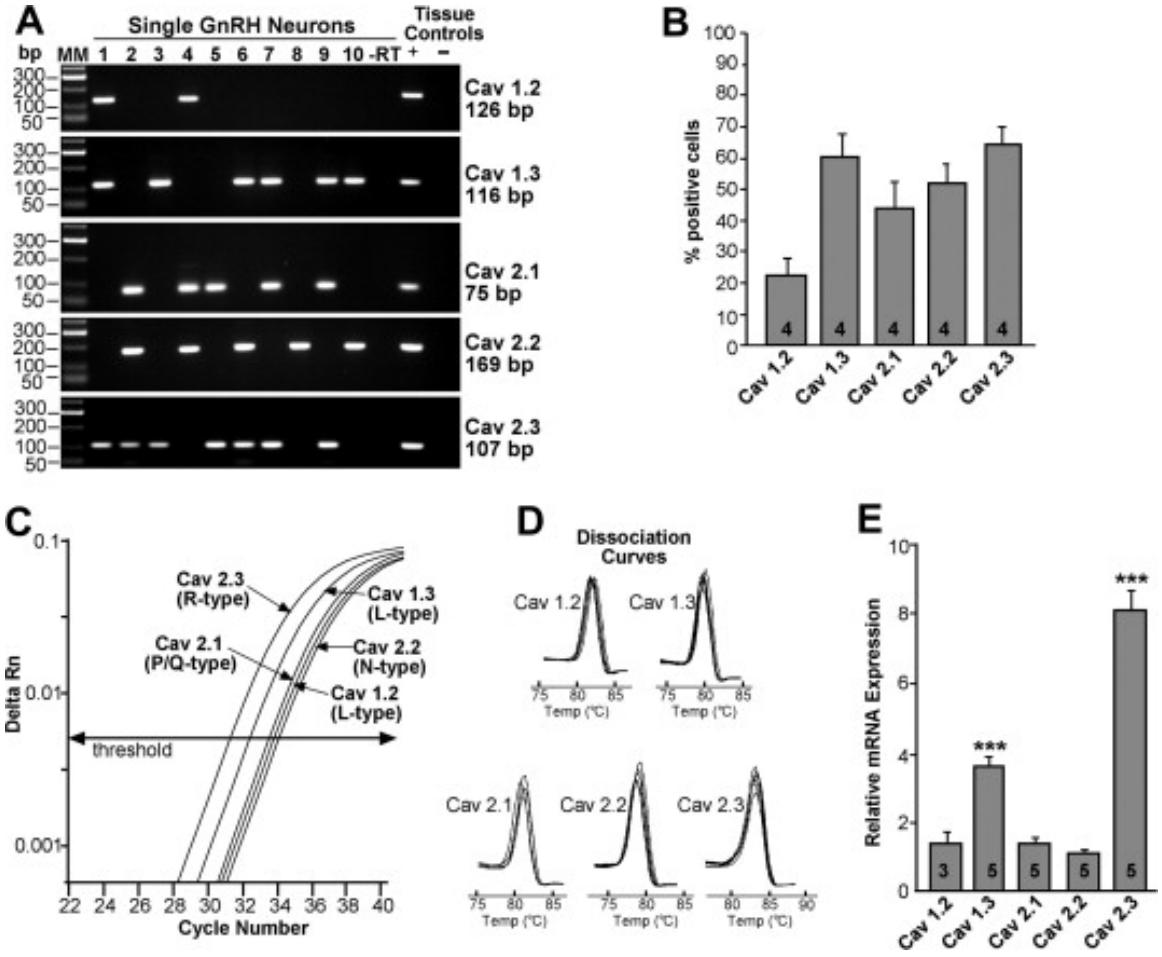


Figure C.4: Expression of HVA channels in GnRH neurons from intact proestrus/estrus EGFP-GnRH mice

Figure C.4 legend: (A) Representative gels illustrating the mRNA expression of HVA channel subtypes. The expected sizes for the PCR products are as follows: for CaV1.2 (L), 126 bp; CaV1.3 (L), 116 bp; CaV2.1 (P/Q), 75 bp; CaV2.2 (N), 169 bp; CaV2.3 (R), 107 bp. As a negative control, a cell reacted without reverse transcriptase (−RT) did not express any of the transcripts. POA tissue RNA was also included as positive control (+, with RT) and negative control (−, without RT). MM, molecular markers. (B) Summary bar graphs of the percentage expression of HVA channel subtypes in GnRH neurons. 12 cells/animal from 4 animals were analyzed by sc-PCR, and the mean number of neurons expressing HVA channel subtypes from each animal was determined. Bar graphs represent the mean ± SEM of the percentage of GnRH neurons expressing each HVA subtype per animal. (C) Quantitative real-time PCR assay with amplification curves for CaV2.3, CaV1.3, CaV2.1, CaV1.2, and CaV2.2. Cycle number was plotted against the normalized fluorescence intensity (delta Rn) to visualize the PCR amplification. The cycle threshold (CT, arrow) is the point in the amplification at which the sample values were calculated. The amplification efficiencies for each primer pair is listed in Table 1. (D) The melting curves depict single-product melting at 82, 80, 81, 80 and 83 °C for CaV1.2, 1.3, 2.1, 2.2 and 2.3, respectively, illustrating that only one product was formed for each transcript in GnRH 5- or 10-cell pools. (E) Bar-graphs illustrating the relative mRNA expression of the various CaV channel subtypes. R-type (CaV2.3) mRNA expression was significantly higher than that of the other channel subtypes (***$p < 0.001$; one-way ANOVA). L-type (CaV1.3) mRNA expression was significantly higher than CaV1.2, 2.1 and 2.2 mRNA levels (**$p < 0.01$; one way ANOVA). The number of animals is indicated.

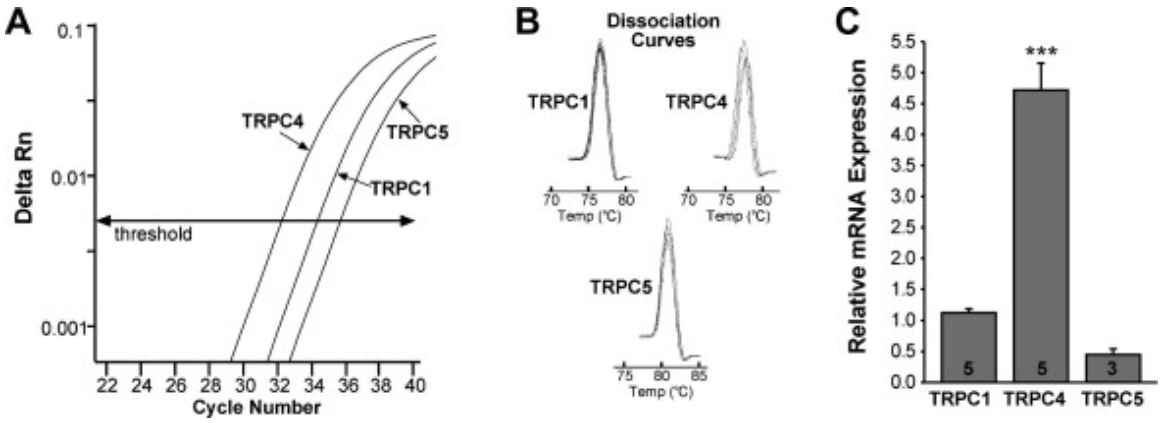


Figure C.5: TRPC channel subtype distribution by real-time PCR

(A) qPCR assay with amplification curves for TRPC1, TRPC4 and TRPC5 subunits. (TRPC1 and TRPC4 were analyzed in 5-cell pools and TRPC5 in 10-cell pools). Cycle number was plotted against the normalized fluorescence intensity (delta Rn) to visualize the PCR amplification. The cycle threshold (CT, arrow) is the point in the amplification at which the sample values were calculated. The amplification efficiencies for each primer pair is listed in Table 1. (B) Melting curves depict single-product melting at 77, 78, and 81 °C for TRPC1, TRPC4 and TRPC5, respectively, illustrating that only one product was formed for each transcript in GnRH neuronal pools. (C) Bar-graphs illustrating the relative mRNA expression of TRPC1, TRPC4 and TRPC5 (***$p < 0.001$, TRPC4 compared to TRPC1 and TRPC5). The number of animals is indicated.

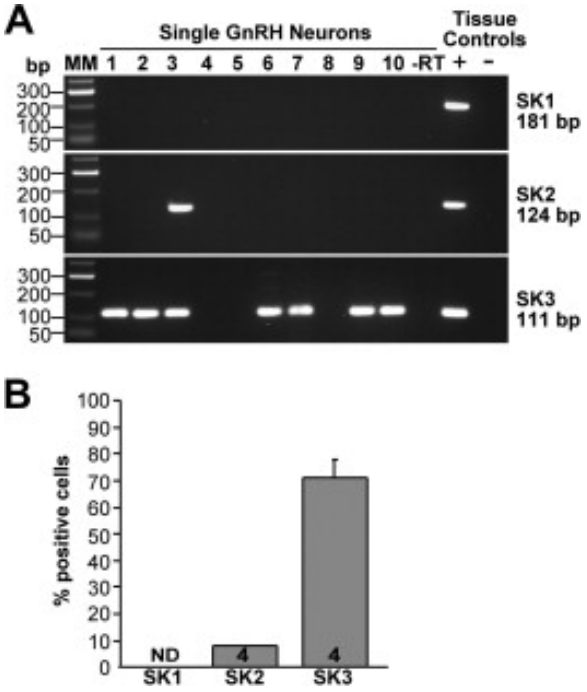


Figure C.6: SK channel subtype distribution in GnRH neurons

(A) Representative gels illustrating the mRNA expression of SK channel subtypes 1–3. The expected sizes for the PCR products are as follows: for SK1, 181 bp; for SK2, 124 bp; for SK3, 111 bp. As a negative control, a cell reacted without reverse transcriptase (−RT) did not express any of the transcripts. POA tissue RNA was also included as positive control (+, with RT) and negative control (−, without RT). MM, molecular markers. (B) Summary bar graphs of the percentage expression of SK1, SK2 and SK3 subunits. 12 cells/animal from 4 animals were analyzed by sc-PCR, and the mean number of neurons expressing SK channel subtypes from each animal was determined. Bar graphs represent the mean ± SEM of the percentage of GnRH neurons expressing each SK subtype per animal. Note SK1 was not detected in mouse GnRH neurons.

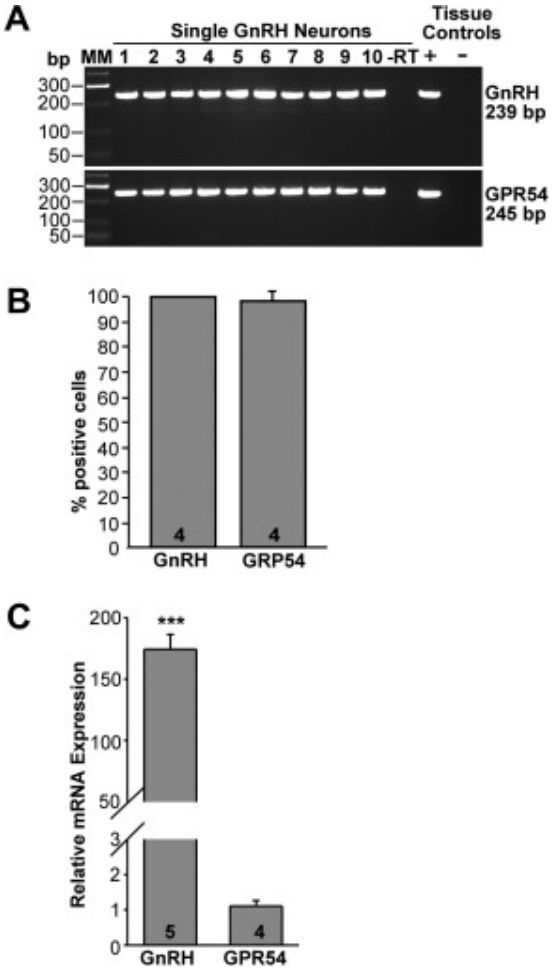


Figure C.7: Expression of GPR54 mRNA in GnRH neurons from intact proestrus/estrus EGFP-GnRH mice

(A) Representative gels illustrating the mRNA expression of GPR54 and GnRH in EGFP-GnRH mice. The expected sizes for the PCR products are as follows: for GnRH, 239 bp; for GPR54,245 bp; As a negative control, a cell reacted without reverse transcriptase (−RT) did not express any of the transcripts. POA tissue RNA was also included as positive control (+, with RT) and negative control (–, without RT). MM, molecular markers. (B) Summary bar graphs of the percentage expression of GnRH and GPR54 in EGFP-GnRH neurons. 12 cells/animal from 4 animals were analyzed by sc-PCR, and the mean number of neurons expressing GnRH and GPR54 mRNAs from each animal was determined. Bar graphs represent the mean ± SEM of the percentage of GnRH neurons expressing GnRH and GPR54 per animal. Essentially, all EGFP neurons harvested expressed GnRH and GPR54. (C) qPCR analysis of GnRH and GPR54 mRNA expression in GnRH neurons. Bar-graphs illustrating the relative mRNA expression of GnRH and GPR54 (***$p < 0.001$; Student's t-test; the number of animals is indicated).

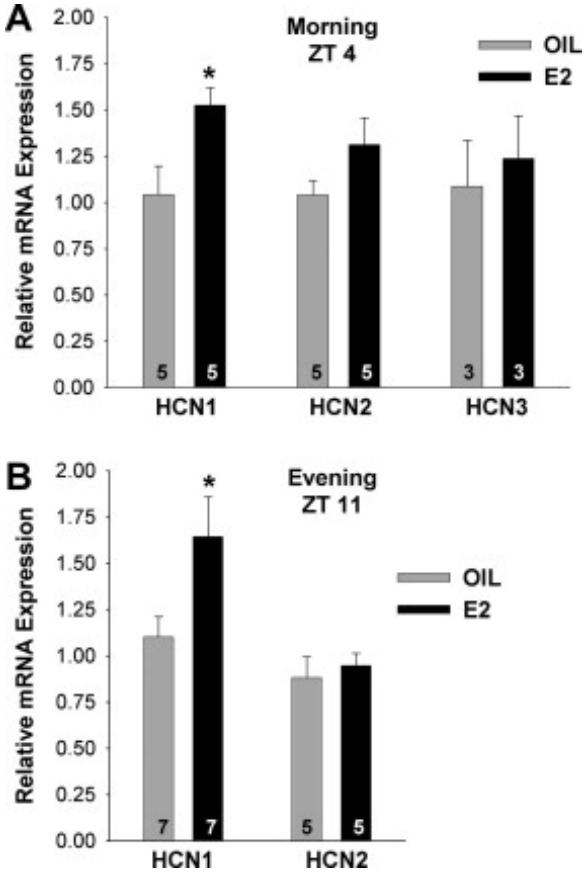


Figure C.8: E2 regulates HCN1 channel mRNA expression in GnRH neurons

(A and B) Quantitative real-time PCR measurements of HCN1, HCN2 and HCN3 mRNAs in GnRH neuronal pools (3–4 pools per animal) from oil- and E2-treated mice (n = 3–7 animals per group) obtained during the morning, ZT4 (A) or during the evening, ZT11 (B). The expression values were calculated via the $\Delta\Delta$CT method and normalized to the mean $\Delta$CT of the oil-treated samples. Bar graphs represent the mean ± SEM. *$p < 0.05$, oil versus E2.

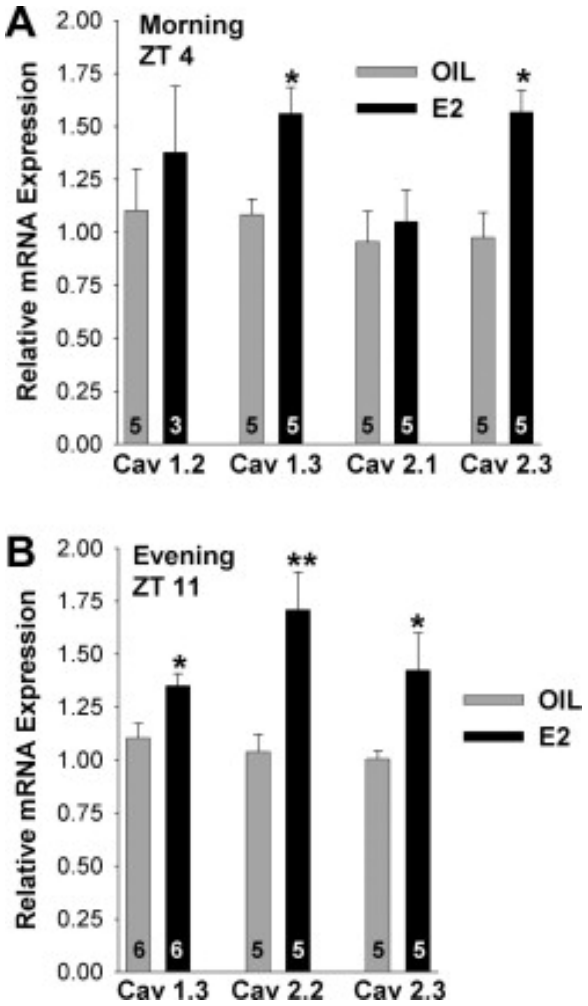


Figure C.9: E2 regulates HVA channel mRNAs in GnRH neurons.

(A and B) Quantitative real-time PCR measurements of CaV1.2, CaV1.3, CaV2.1 and CaV2.3 mRNAs during the morning, ZT4 (A) and CaV1.3, CaV2.2 and CaV2.3 mRNAs during the evening, ZT11 (B) in GnRH neuronal pools (3–4 pools of 5 or 10 (CaV1.2, CaV2.2) cells per animal) from oil- and E2-treated mice (n = 3–6 animals per group). The expression values were calculated via the $\Delta\Delta$CT method, normalized to $\beta$-actin and relative to the oil control values. Bar graphs represent the mean ± SEM. *$p < 0.05$, **$p < 0.01$, oil versus E2.

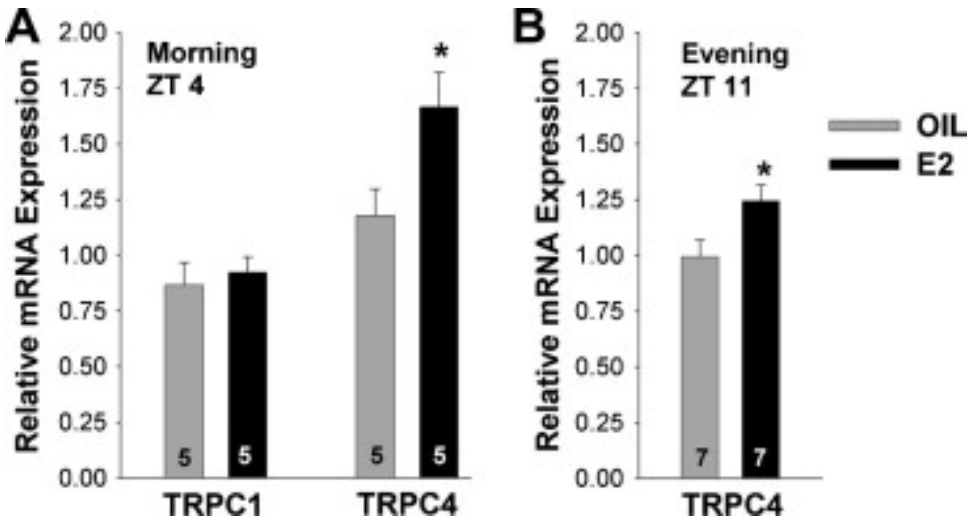


Figure C.10: E2 regulates TRPC4 mRNA in GnRH neurons

(A and B) Quantitative real-time PCR measurements of TRPC1 and TRPC4 mRNAs during the morning, ZT4 (A) and TRPC4 during the evening, ZT11 (B) in GnRH neuronal pools (3–4 pools of 5 cells per animal) from oil- and E2-treated mice (n = 5–7 animals per group). The expression values were calculated via the $\Delta\Delta$CT method, normalized to $\beta$-actin and relative to the oil control values. Bar graphs represent the mean ± SEM. *$p < 0.05$, oil versus E2.

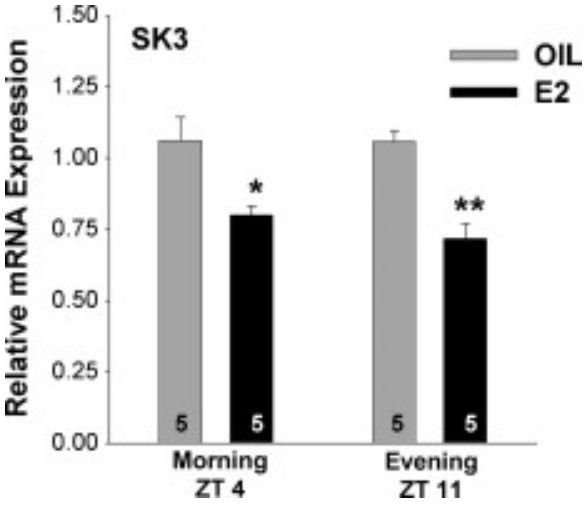


Figure C.11: E2 decreases SK3 mRNA in GnRH neurons

Quantitative real-time PCR measurements of SK3 mRNA during the morning, ZT4 and SK3 mRNA during the evening, ZT11 in GnRH neuronal pools (3–4 pools of 5 cells per animal) from oil- and E2-treated mice (n = 5 animals per group). The expression values were calculated via the $\Delta\Delta$CT method, normalized to $\beta$-actin and each E2 value was calculated relative to the respective oil control value. Bar graphs represent the mean ± SEM.*p $< 0.05$, **p $< 0.01$, oil versus E2.

## C.6 References


Arroyo, A., Kim, B., Rasmusson, R. L., Yeh, J., 2006. Hyperpolarization-activated cation channels are expressed in rat hypothalamic gonadotropin-releasing hormone (GnRH) neurons and immortalized GnRH neurons. J. Soc. Gyn. Invest. 13, 442-450.

Biel, M., Wahl-Schott, C., Michalakis, S., Zong, X., 2009. Hyperpolarization-activated cation channels: From genes to function. Physiol. Rev. 89, 847-885.

Bond, C. T., Herson, P. S., Strassmaier, T., Hammond, R., Stackman, R., Maylie, J., Adelman, J. P., 2004. Small conductance Ca2+-activated K+ channel knock-out mice reveal the identity of calcium-dependent afterhyperpolarization currents. J. Neurosci. 24, 5301-5306.

Bosch, M. A., Kelly, M. J., Rønnekleiv, O. K., 2002. Distribution, neuronal co-localization and 17$\beta$-E2 modulation of small conductance calcium-activated K+ channel (SK3) mRNA in the guinea pig brain. Endocrinology 143, 1097-1107.

Bronson, F. H., Vom Saal ,F.S., 1979. Control of the preovulatory release of luteinizing hormone by steroids in the mouse. Endocrinology 104, 1247-1255.

Bronson, F. H., Whitten, W. K., 1968. Oestrus-accelerating pheromone of mice: assay, androgen-dependency and presence in bladder urine. J. Reprod. Ferti.l 15, 131-134.

Caraty, A., Locatelli, A., Martin, G. B., 1989. Biphasic response in the secretion of gonadotrophin-releasing hormone in ovariectomized ewes injected with oestradiol. J. Endocrinol. 123, 375-382.

Catterall, W. A., Striessnig, J., Snutch, T. P., Perez-Reyes, E., 2003. International Union of Pharmacology.XXXIX. Compendium of voltage-gated ion channels: calcium channels. Pharmaco.l Rev. 55, 575-578.

Chappell, P. E., Goodall, C. P., Tonsfeldt, K. J., White, R. S., Bredeweg, E., Latham, K. L., 2009. Modulation of Gonadotropin-releasing hormone (GnRH) secretion by an endogenous circadian clock. J. Neuroendocrinol 21, 339-345.

Chappell, P. E., Levine, J. E., 2000. Stimulation of gonadotropin-releasing hormone surges by estrogen. I. Role of hypothalamic progesterone receptors. Endocrinology 141, 1477-1485.

Chemin, J., Monteil, A., Perez-Reyes, E., Bourinet, E., Nargeot, J., Lory, P., 2002. Specific contribution of human T-type calcium channel isotypes (alpha(1G), alpha(1H) and alpha(1I)) to neuronal excitability. J. Physiol. 540, 3-14.

Christian, C. A., Mobley, J. L., Moenter, S. M., 2005. Diurnal and estradiol-dependent changes in gonadotropin-releasing hormone neuron firing activity. Proc. Natl. Acad. Sci. USA 102, 15682-15687.

Christian, C. A., Moenter, S. M., 2007. Estradiol induces diurnal shifts in GABA transmission to gonadotropin-releasing hormone neurons to provide a neural signal for ovulation. J. Neurosci. 27, 1913-1921.

Christian, C. A., Moenter, S. M., 2008. Vasoactive intestinal polypeptide can excite gonadotropin-releasing hormone neurons in a manner dependent on estradiol and gated by time of day. Endocrinology 149, 3130-3136.

Chu, Z., Andrade, J., Shupnik, M. A., Moenter, S. M., 2009. Differential regulation of gonadotropin-releasing hormone neuron activity and membrane properties by acutely applied estradiol: dependence on dose and estrogen receptor subtype. J. Neurosci. 29, 5616-5627.

Chu, Z., Takagi, H., Moenter, S. M., 2010. Hyperpolarization-activated currents in gonadotropin-releasing hormones (GnRH) neurons contribute to intrinsic excitability and are regulated by gonadal steroid feedback. J.Neurosci. 30, 13373-13383.

Chu, Z., Tomaiuolo, M., Bertram, R., Moenter, S. M., 2012. Two types of burst firing in gonadotropin-releasing hormone neurones. J. Neuroendocrinol. 24, 1065-1077.

Clapham, D. E., 2003. TRP channels as cellular sensors. Nature 426, 517-524.

Clarkson, J., d'Anglemont de Tassigny, X., Moreno, A. S., Colledge, W. H., Herbison, A. E., 2008. Kisspeptin-GPR54 signaling is essential for preovulatory gonadotropin-releasing hormone neuron activation and the luteinizing hormone surge. J. Neurosci. 28, 8691-8697.

Constantin, S., Jasoni, C., Romano, N., Lee, K., Herbison, A. E., 2011. Understanding calcium homeostasis in postnatal gonadotropin-releasing hormone neurons using cell-specific Pericam transgenics. Cell Calcium 51, 267-276.

Constantin, S., Jasoni, C. L., Wadas, B., Herbison, A. E., 2010. $\gamma$-Aminobutyric acid and glutamate differentially regulate intracellular calcium concentrations in mouse

gonadotropin-releasing hormone neurons. Endocrinology. 151, 262-270.

Constantin, S., Wray, S., 2008. GnRH-1 neuronal activity in independent of HCN channels but is sensitive to PKA-dependent phosphorylation. Endocrinology1-24.

Dalal, S. J., Estep, J. S., Valentin-Bon, I. E., Jerse, A. E., 2001. Standardization of the Whitten Effect to induce susceptibility to Neisseria gonorrhoeae in female mice. Contemp. Top Lab Anim. Sci. 40, 13-17.

Erickson, K. R., Rønnekleiv, O. K., Kelly, M. J., 1993a. Electrophysiology of guinea-pig supraoptic neurones: Role of a hyperpolarization-activated cation current in phasic firing. J. Physiol. (Lond.) 460, 407-425.

Erickson, K. R., Rønnekleiv, O. K., Kelly, M. J., 1993b. Role of a T-type calcium current in supporting a depolarizing potential, damped oscillations, and phasic firing in vasopressinergic guinea pig supraoptic neurons. Neuroendo. 57, 789-800.

Gee, D. M., Flurkey, K., Mobbs, C. V., Sinha, Y. N., Finch, C. E., 1984. The regulation of luteinizing hormone and prolactin in C57BL/6J mice: effects of estradiol implant size, duration of ovariectomy, and aging. Endocrinology 114, 685-693.

Gore, A. C., Roberts, J. L., 1997. Regulation of gonadotropin-releasing hormone gene expression in vivo and in vitro. Front. Neuroendocrino.l 18, 209-245.

Han, S.-K., Gottsch, M. L., Lee, K. J., Popa, S. M., Smith, J. T., Jakawich, S. K., Clifton, D. K., Steiner, R. A., Herbison, A. E., 2005. Activation of gonadotropin-releasing hormone neurons by kisspeptin as a neuroendocrine switch for the onset of puberty. J. Neurosci. 25, 11349-11356.

Iremonger, K. J., Herbison, A. E., 2012. Initiation and propagation of action potentials in gonadotropin-releasing hormone neuron dendrites. J. Neurosci. 32, 151-158.

Irwig, M. S., Fraley, G. S., Smith, J. T., Acohido, B. V., Popa, S. M., Cunningham, M. J., Gottsch, M. L., Clifton, D. K., Steiner, R. A., 2004. Kisspeptin activation of gonadotropin releasing hormone neurons and regulation of KiSS-1 mRNA in the male rat. Neuronendocrinol. 80, 264-272.

Kato, M., Tanaka, N., Usui, S., Sakuma, Y., 2006. SK channel blocker apamin inhibits slow afterhyperpolarization currents in rat gonadotropin-releasing hormone neurones. J.

Physiol. 574.2, 431-442.

Kato, M., Ui-Tei, K., Watanabe, M., Sakuma, Y., 2003. Characterization of voltage-gated calcium currents in gonadotropin-releasing hormone neurons tagged with green fluorescent protein in rats. Endocrinology 144, 5118-5125.

Kelly, M. J., Garrett, J., Bosch, M. A., Roselli, C. E., Douglass, J., Adelman, J. P., Rønnekleiv, O. K., 1989. Effects of ovariectomy on GnRH mRNA, proGnRH and GnRH levels in the preoptic hypothalamus of the female rat. Neuroendocrinol. 49, 88-97.

Kelly, M. J., Rønnekleiv, O. K., 1994. Electrophysiological analysis of neuroendocrine neuronal activity in hypothalamic slices, in: Levine, J. E. (Ed.), Methods in Neurosciences: Pulsatility in Neuroendocrine Systems. Academic Press, Inc., San Diego, pp. 47-67.

Kelly, M. J., Wagner, E. J., 2002. GnRH neurons and episodic bursting activity. Trends Endocrinol. Metab. 13, 409-410.

Kim, D., Song, I., Keum, S., Lee, T., Jeong, M. J., Kim, S. S., McEnery, M. W., Shin, H. S., 2001. Lack of the burst firing of thalamocortical relay neurons and resistance to absence seizures in mice lacking alpha(1G) T-type Ca2+ channels. Neuron 31, 35-45.

Kroll, H., Bolsover, S., Hsu, J., Kim, S.-H., Bouloux, P.-M., 2011. Kisspeptin-evoked calcium signals in isolated primary rat gonadotropin-releasing hormone neurones. Neuroendocrinol. 93, 114-120.

Krsmanovic, L. Z., Stojikovic, S. S., Merelli, F., Dufour, S. M., Virmani, M. A., Catt, K. J., 1992. Calcium signaling and episodic secretion of gonadotropin-releasing hormone in hypothalamic neurons. Proc. Natl. Acad. Sci. USA 89, 8462-8466.

Lagrange, A. H., Rønnekleiv, O. K., Kelly, M. J., 1995. Estradiol-17$\beta$ and $\mu$-opioid peptides rapidly hyperpolarize GnRH neurons: A cellular mechanism of negative feedback? Endocrinology 136, 2341-2344.

Lee, K., Duan, W., Sneyd, J., Herbison, A. E., 2010. Two slow calcium-activated afterhyperpolarization currents control burst firing dynamics in gonadotropin-releasing hormone neurons. J. Neurosci. 30, 6214-6224.

Legan, S. J., Coon, G. A., Karsch, F. J., 1975. Role of estrogen as initiator of daily LH surges in the ovariectomized rat. Endocrinology 96, 50-56.

Levine, J. E., Ramirez, V. D., 1982. Luteinizing hormone-releasing hormone release during the rat estrous cycle and after ovariectomy, as estimated with push-pull cannulae. Endocrinology 111, 1439-1448.

Liu, X., Herbison, A. E., 2008. Small-conductance calcium-activated potassium channels control excitability and firing dynamics in gonadotropin-releasing hormone (GnRH) neurons. Endocrinology 149, 3598-3604.

Liu, X., Lee, K., Herbison, A. E., 2008. Kisspeptin excites gonadotropin-releasing hormone (GnRH) neurons through a phosphilipase C/calcium-dependent pathway regulating multiple ion channels. Endocrinology 149, 4605-4614.

Livak, K. J., Schmittgen, T. D., 2001. Analysis of relative gene expression data using real-time quantitative PCR and the 2(-delta-delta C(T)) method. Methods 25, 402-408.

Lüthi, A., McCormick, D. A., 1998. H-current: properties of a neuronal and network pacemaker. Neuron 21, 9-12.

Marks, D. L., Smith, S. M., Clifton, D. K., Steiner, R. A., 1993. Regulation of gonadotropin-releasing hormone (GnRH) and galanin gene expression in GnRH neurons during lactation in the rat. Endocrinology 133, 1450-1458.

Oakley, A. E., Clifton, D. K., Steiner, R. A., 2009. Kisspeptin signaling in the brain. Endocr. Rev. 30, 713-743.

Odell, A. F., Scott, J. L., Van Helden, D. F., 2012. Epidermal growth factor induces tyrosine phosphorylation, membrane insertion, and activation of transient receptor potential channel 4. J. Biol. Chem. 280, 37974-37987.

Otsuguro, K.-I., Tang, J., Tang, Y., Xiao, R., Freichel, M., Tsvilovskyy, V., Ito, S., Flockerzi, V., Zhu, M. X., Zholos, A. V., 2008. Isoform-specific inhibition of TRPC4 channel by phosphatidylinositol 4,5-bisphosphate. J. Biol. Chem. 283, 10026-10036.

Pau, K.-Y. F., Berria, M., Hess, D. L., Spies, H. G., 1993. Preovulatory gonadotropin-releasing hormone surge in ovarian-intact Rhesus Macaques. Endocrinology 133, 1650-1656.

Pau, K.-Y. F., Orstead, K. M., Hess, D. L., Spies, H. G., 1986. Feedback effects of ovarian steroids on the hypothalamic-hypophyseal axis in the rabbit. Biol. Repro. 35, 1009-1023.

Pfaffl, M. W., 2001. A new mathematical model for relative quantification in real-time RT-PCR. Nucleic Acid Res. 29, 2002-2007.

Pielecka, J., Moenter, S. M., 2006. Effect of steroid milieu on gonadotropin-releasing hormone-1 neuron firing pattern and luteinizing hormone levels in male mice. Biol. Reprod. 74, 931-937.

Pielecka-Fortuna, J., Chu, Z., Moenter, S. M., 2008. Kisspeptin acts directly and indirectly to increase gonadotropin-releasing hormone neuron activity and its effects are modulated by estradiol. Endocrinology 149, 1979-1986.

Pielecka-Fortuna, J., Moenter, S. M., 2010. Kisspeptin increases $\gamma$-aminobutyric acidergic and glutamatergic transmission directly to gonadotropin-releasing hormone neurons in an estradiol-dependent manner. Neuroendo. 151, 291-300.

Qiu, J., Fang, Y., Bosch, M. A., Rønnekleiv, O. K., Kelly, M. J., 2011. Guinea pig kisspeptin neurons are depolarized by leptin via activation of TRPC channels. Endocrinology 152, 1503-1514.

Qiu, J., Fang, Y., Rønnekleiv, O. K., Kelly, M. J., 2010. Leptin exceites proopiomelanocortin neurons via activation of TRPC channels. J. Neurosci. 30, 1560-1565.

Robertson, J. L., Clifton, D. K., de la Iglesia, H. O., Steiner, R. A., Kauffman, A. S., 2009. Circadian regulation of Kiss1 neurons: implications for timing the preovulatory gonadotropin-releasing hormone/luteninizing hormone surge. Neuroendocrinol.. 150, 3664-3671.

Roepke, T. A., Qiu, J., Smith, A. W., Rønnekleiv, O. K., Kelly, M. J., 2011. Fasting and 17$\beta$-estradiol differentially modulate the M-current in neuropeptide Y neurons. J. Neurosci. 17, 11825-11835.

Rønnekleiv, O. K., Bosch, M. A., Zhang, C., 2011. 17ß-Oestradiol regulation of gonadotrophin-releasing hormone neuronal excitability. J. Neuroendocrinol. 24, 122-130.

Sagrillo, C. A., Grattan, D. R., McCarthy, M. M., Selmanoff, M., 1996. Hormonal and neurotransmitter regulation of GnRH gene expression and related reproductive behaviors. Behav. Genet. 26, 241-277.

Spergel, D. J., 2007. Calcium and small-conductance calcium-activated potassium channels in gonadotropin-releasing hormone neurons before, during, and after puberty. Endocrinology 148, 2383-2390.

Sun, J., Chu, Z., Moenter, S. M., 2010. Diurnal in vivo and rapid in vitro effects of estadiol on voltage-gated calcium channels in gonadotropin-releasing hormone neurons. J. Neurosci. 30, 3912-3923.

Suter, K. J., Song, W. J., Sampson, T. L., Wuarin, J.-P., Saunders, J. T., Dudek, F. E., Moenter, S. M., 2000. Genetic targeting of green fluorscent protein to gonadotropin-releasing hormone neurons: Characterization of whole-cell electrophysiological properties and morphology. Endocrinology 141, 412-419.

Tanaka, N., Ishii, H., Yin, C., Koyama, M., Sakuma, Y., Kato, M., 2010. Voltage-gated Ca2+ channel mRNAs and T-type Ca2+ currents in rat gonadotropin-releasing hormone neurons. J. Physio.l Sci. 60, 195-204.

Tonsfeldt, K. J., Goodall, C. P., Latham, K. L., Chappell, P. E., 2011. Oestrogen induces rhythmic expression of the Kisspeptin-1 receptor GPR54 in hyopthalamic gonadotrophin-releasin hormone-secreting GT1-7 cells. J. Neuroendocrinol. 23, 823-830.

Vida, B., Deli, L., Hrabovszky, E., Kalamatianos, T., Caraty, A., Coen, C. W., Liposits, Z., Kalló, I., 2010. Evidence for suprachiasmatic vasopressin neurons innervating kisspeptin neurons in the rostral periventricular area of the mouse brain: regulation by oestrogen. J. Neuroendocrinol. 22, 1032-1039.

Wagner, E. J., Rønnekleiv, O. K., Kelly, M. J., 2001. The noradrenergic inhibition of an apamine-sensitive small conductance Ca2+ -activated K+ channel in hypothalamic $\gamma$-aminobutyric acid neurons: Pharmacology, estrogen sensitivity and relevance to the control of the reproductive axis. J. Pharmacol. Exp. Ther. 299, 21-30.

Ward, D. R., Dear, F. M., Ward, I. A., Anderson, S. I., Spergel, D. J., Smith, P. A., Ebling, F. J. P., 2009. Innervation of gonadotropin-releasing hormone neurons by peptidergic neurons conveying circadian or energy balance information in the mouse. PLos One 4, 1-8.

Wintermantel, T. M., Campbell, R. E., Porteous, R., Bock, D., Gröne, H.-J., Todman, M. G., Korach, K. S., Greiner, E., Perez, C. A., Schultz, G., Herbison, A. E., 2006. Definition of estrogen receptor pathway critical for estrogen positive feedback to gonadotropin-releasing hormone neurons and fertility. Neuron 52, 271-280.

Zhang, C., Bosch, M. A., Levine, J. E., Rønnekleiv, O. K., Kelly, M. J., 2007. Gonadotropin-releasing hormone neurons express KATP channels that are regulated by estrogen and responsive to glucose and metabolic inhibition. J. Neurosci. 27, 10153-10164.

Zhang, C., Bosch, M. A., Rick, E. A., Kelly, M. J., Rønnekleiv, O. K., 2009. 17β-estradiol regulation of T-type calcium channels in gonadotropin-releasing hormone neurons. J. Neurosci. 29, 10552-10562.

Zhang, C., Kelly, M. J., Rønnekleiv, O. K., 2010. 17β-estradiol rapidly increases adenosine 5'-triphosphate-sensitive potassium channel activity in gonadotropin-releasing hormone neurons via a protein kinase signaling pathway. Endocrinology 151, 4477-4484.

Zhang, C., Roepke, T. A., Kelly, M. J., Rønnekleiv, O. K., 2008. Kisspeptin depolarizes gonadotropin-releasing hormone neurons through activation of TRPC-like cationic channels. J Neurosci. 28, 4423-4434.

Zhang, X.-B., Spergel, D. J., 2012. Kisspeptin inhibits high-voltage activated Ca2+ channels in GnRH neurons via multiple Ca2+ influx and release pathways. Neuroendocrinol. 96, 68-80.